eman ta zabal zazu

Universidad
del País Vasco

Euskal Herriko
Unibertsitatea

BILBOKO
INGENIARITZA
ESKOLA
ESCUELA
DE INGENIERÍA
DE BILBAO

Universidad del País Vasco / Euskal Herriko Unibertsitatea

Doctoral thesis

Modelling and Control for the Oscillating Water Column in Wave Energy Conversion

François-Xavier Faÿ

Supervisors   Dr. Marga Marcos Muñoz
Dr. Eider Robles Sestafe

May, 2020

François-Xavier Faÿ

Modelling and Control for the Oscillating Water Column in Wave Energy Conversion

Doctoral thesis, May, 2020

Supervisors: Dr. Marga Marcos Muñoz and Dr. Eider Robles Sestafe

Universidad del País Vasco / Euskal Herriko Unibertsitatea

Automatics and System Engineering Department

Plaza Ingeniero Torres Quevedo.1

48013 and Bilbao

Abstract

Energy is what makes the world move. It is present in all human activities. Everywhere we are hearing the words 'energy transition'. What happened with our conventional way to consume energy for our day to day life ? International experts are unanimous: human activities are accelerating global warming and climate change. We know our appetite for energy. We also know that the main share of our energy consumption comes from the combustion of fossil fuels, one of the largest source of greenhouse gas emission. The world needs energy and the production of energy contributes to global warming.

So here we are, the world urges for a transition in the energy paradigm. Renewable energies are definitely part of the equation to limit our dependence to fossil fuels. Within this sector, ocean energies, and especially wave energy, represent a huge potential but is still a growing area. And like any new field, it is synonym to a high cost of energy production. Scale economy is out of scope at this stage, and there is not a clear and experienced value chain to drop down these costs. The technologies are effective but still need research and development to become affordable. In short, the levelised cost of energy is the ratio between the costs to produce it and the production, therefore its income. Increasing the energy production, while keeping the costs controlled, has the leverage to drop down the cost of energy produced by wave energy converters (WECs).

In this sense, the main objective of this thesis is to make progress on the understanding of the effect of advanced control algorithms in the improvement of the power produced by wave energy devices. For that purpose, several control strategies are designed, compared, and assessed. To support this analysis, numerical models representing the overall energy conversion chain of WECs are developed. The models are running in the time domain as there are transient events, imposed by the controllers behaviour, that must be carefully considered.

The Basque Country in Spain is fortunate enough to host the development and operation of two devices based on the Oscillating Water Column (OWC) principle. One is the Mutriku OWC plant, and the second is the floating buoy Marmok-A from Oceantec/IDOM. This technology is naturally the one selected to implement this work. Thanks to the opportunities represented by the European Commission funded project OPERA under the H2020 research and innovation program, both devices were made available for sea trials. Several control algorithms were then implemented to be tested in real environments. Among them was a non-linear predictive control algorithm. Its test in real conditions represent a world first in the area of control for OWC systems, and maybe for the whole WEC sector if comparing with publicly available information. An outstanding results of the thesis is undoubtedly to move forward the predictive control algorithm from TRL3 to TRL6 after successful implementation and operation in both devices under real environmental conditions. The experience gained is commented and the experimental results are gathered in this document.

Acknowledgement

I wish to address my sincere gratitude to my supervisors Dr. Marga Marcos (UPV) and Dr. Eider Robles (TECNALIA) for their guidance and high level of commitment throughout this journey. This thesis greatly benefited their high standard requirements which led me to provide the best work quality.

I am very grateful to the Offshore Renewable Energy department of Tecnalia, its director Jose Luis Villate for his right advice and careful listening, and the head of Ocean Energy Pablo Ruiz-Minguela. Even if he was not an official thesis supervisor, he guided me in the OceaNET project and, as coordinator of the OPERA project, he ensured the proper conditions were met for this thesis to go beyond the initial objectives. I am really thankful to my colleagues for their strong support in my many queries.

I am also grateful to those with whom I had the honnor to collaborate with. Citing the main ones, I wish to thank Eduardo F. Camacho and his research group from the University of Sevilla for the good advices on the development of the predictive algorithms. Thank you Oceantec (now part of IDOM) for accepting to host me during my OceaNET secondments and for its team who surely contributed to deepening my knowledge of the sector. An important outcome of the thesis is related to open sea testing. My thanks go the Ente

L'Homme et la Mer

Homme libre, toujours tu chériras la mer!
La mer est ton miroir; tu contemples ton âme
Dans le déroulement infini de sa lame,
Et ton esprit n'est pas un gouffre moins amer.
[...]

Man and the Sea

Free man, you will always cherish the sea!
The sea is your mirror; you contemplate your soul
In the infinite unrolling of its billows;
Your mind is an abyss that is no less bitter.
[...]

- Charles Baudelaire, Les Fleurs du mal, 1857.

Contents

List of Figures

List of Tables

Acronyms

Introduction

1

Summary: The introductory chapter provides the motivation and states the problematics of Wave Energy conversion. The objectives of the thesis are clearly raised in line with some of the challenges faced by the sector. They will tend to address some of the gaps identified in the literature review. Then, the main contributions to reach these goals are claimed before the structure of the document is presented.

1.1 Motivation and Problem Statement

For the past decades, a growing interest in energy extraction from renewable sources encourages Research and Development (R&D) activities of innovative technologies to produce clean energy in a sustainable way, without CO_2 emission. Nowadays, wind and solar energies are the most mature industries and their share in the power production is quickly increasing. The Bridge Scenario from the International Energy Agency (IEA) report [Int15] predicts an increase in the world electricity production from these sources of 4 to 14% between 2017 and 2030. In the Organisation for Economic Co-operation and Development (OECD) european zone, this share climbs from 9 to 25%. In 2017, 80% of the new european installed capacity was from renewable sources [Int17].

Offshore renewable energies wish to harvest the energy available in oceans and are still at their early stages of development. Among them, floating offshore wind, tidal, wave, ocean thermal energy conversion and salinity gradient are all innovative ways to produce electricity from the oceans. Ocean energy, which focuses mainly on wave and tidal energy, is said to have a global market potential of 337 GW of installed capacity in 2050 [DR19] and would power 10% of Europe's power consumption [Oce16]. In addition, public institutions are becoming more and more aware that this field brings new job opportunities and plays an important role in the security of power supply. The Ocean Energy Europe association says the sector would deliver 400,000 jobs by 2050 [DR19], taking the wind energy industry as a reference. From one side, wave energy accessible resource justifies the growing interest from governmental administrations who encourages its development. On the other side, the high number of existing concepts (several hundreds) to convert the energy from waves [Fal07; Fal10; Bab15] attest the concern of the scientific community and it is an indicator of the infancy of this sector. In the early years of wind energy history, many different concepts of turbines were experimented before the 3-bladed horizontal axis wind turbine, allying performance and cost effectiveness, became the reference design.

To become affordable, the wave energy sector requires innovations and breakthroughs in several disciplines in order to lower the Levelised Cost of Energy (LCOE). The main challenges faced by developers are related to the harsh environment where the devices are to be deployed. Indeed, a Wave

Energy Converter (WEC) has to survive storms, its structure is subjected to corrosion and biofouling and operation and maintenance activities are complex and costly processes in offshore installations. Many technological barriers have to be overcome in order to increase WEC's reliability and lower risks related to its development. The high costs related to the development of such technologies and the high perceived risk tend to slow down the emergence of a sustainable market for wave energy conversion. Today, wave energy is mainly dependant on public funds, the European Commission, Wave Energy Scotland (WES) programs and the Unites States of America Department of Energy (US DOE) Wave Energy Prize or ARPA-E programs are all funding innovative initiatives. Both WES and the US DOE are supporting the idea that in order to reach market readiness, technology developers have to follow a highly competitive stage gate process in order to drop down the production costs. WES illustrates their financing programs by aiming at impacting drastically the learning rate seeking high performance technologies, c.f. Fig. 1.1.
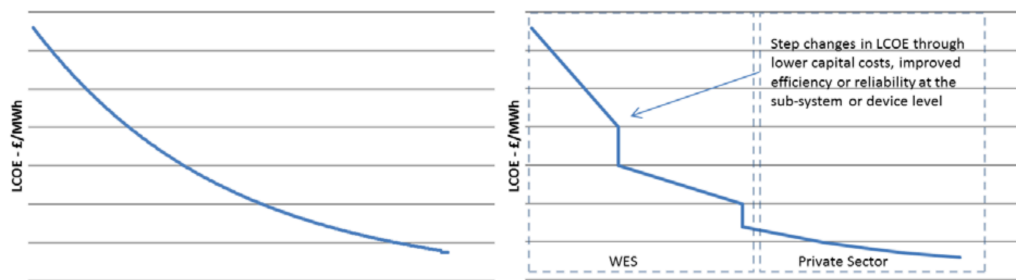
Fig. 1.1: Comparison of two learning curves over time and the effect of WES supports for faster decrease of production costs [Wav17]

Among the many existing concepts, the Oscillating Water Column (OWC) seems to provide a well-balanced solution aiming at reducing the complexity and thus the cost of a device. Its structure can be shoreline attached to a cliff or a breakwater, nearshore standing in shallow water, or even floating integrated into a buoy. The OWC relies on a simple principle: in a structure opened at both ends, the movement of an incoming wave where the sea water flow passes at the bottom of the structure, creates an oscillation of the water level in an air chamber and therefore a difference of pressure converting the energy from waves into pneumatic power. On top of the chamber, the air flows through a turbine converting the pneumatic energy into rotational mechanical one which is then converted into electricity thanks to a conventional electrical generator. Finally, the power converter assures the control for power conversion and grid compatibility.

The field of control applied to WEC offers many advantages. The first and obvious one being the optimisation of energy production, which directly increases the income by selling a higher amount of energy. An efficient control strategy allows the optimal conversion of the available energy and takes advantage of the full potential of wave energy. As well, control plays a fundamental role on the improvement of the device reliability and lengthen the useful life of the internal equipment. The high short term intermittent nature of the power extracted from waves represents a challenge in terms of grid compatibility. To be acceptable by the electrical grid, any production unit has to comply grid codes that set the rules so power can be injected into the network [Rob+19]. This is why it is sometimes relevant to implement an energy storage solution in correlation with the control strategy in order to improve power quality [Mur13].

Demonstrator plants have been built and tested in real sea environment, and only few prototypes are actually operating for several years. Still investigation on diverse areas is to be done to turn demonstrators into commercial devices that are cost-effective, energy efficient, reliable and that can withstand winter storms. The province of the Basque Country in Spain offers real opportunities for the development of such a technology. EVE (Ente Vasco de la Energía), the public local energy institution, manages the Biscay Marine Energy Platform (BiMEP) and its two test sites of the Basque Coast: the Mutriku OWC plant onshore and the offshore testing area in front of Armintza [BiM19]. The Mutriku wave power plant is feeding the grid since 2011 and, when commissioned, was the first WEC in Europe to be grid connected. It has generated over 2 GWh of clean electricity ever since. This demonstrator has a capacity of at most 300kW and is composed of 16 air chambers equipped by Wells turbines. The test area in Armintza was inaugurated in July 2015. It is an offshore test center with all the infrastructure (4 export cables of 5MW each) and services (24/7 surveillance) so developers of marine renewable devices can test full scale prototypes and advance in the Technology Readiness Level (TRL) of their solutions. In addition Oceantec, created by TECNALIA and Iberdrola and now part of the engineering consultancy IDOM, is developing a floating OWC spar-type buoy called Marmok [Oce19], named after the Basque word of the jellyfish. The Marmok-A-5 version is a reduced scale buoy in diameter and was deployed for a year and a half between October 2016 and July 2018 and redeployed in September 2018 in the framework of the European Commission funded project H2020 OPERA [OPE19], coordinated by TECNALIA. The objective of this project is to divide by 2 the cost of wave

energy technologies by integrating four major innovations to the Marmok-A-5. Previous to the installation in the buoy, two of them will be tested and validated in the Mutriku OWC plant.

Despite the growing interest in wave energy conversion, R&D activities are more than ever needed to boost the development of the sector, and at the same time bringing in new opportunities for technology development. Among them, the key is to be able to rely on sea testing experience which will open the way to develop more accurate numerical models replicating better the behaviours of such systems, and associated to them, further development on advanced control strategies. Consequently, the operation of a WEC in a real environment would be optimised and more robust. The increased Annual Energy Production (AEP) would contribute to reduce the LCOE and make this type of renewable energy conversion more competitive against other means to extract energy from renewable resources.

1.2 Objectives

The general goal of this thesis is to optimise energy production and lower the LCOE, the cost of energy production, by appropriate components sizing and advanced control strategies. This is also necessary to improve reliability and robustness to assure the device operation under any sea condition. It aims at improving the accuracy of Wave-to-Wire (W2W) numerical models of OWC systems and especially focusing on the Power Take-Off (PTO) side, from the air chamber to the electrical power conversion. Some tools covering certain aspects are already available in the literature to study the behaviour of such systems in the ocean but the air compressibility effects can be improved and the electrical components are often left aside. The work to be developed pretends to cover all the energy conversion chain by understanding the performance and limitations of each component (turbine, generator and power electronics) keeping in mind the general goal of proposing advanced control strategies that take into account their different constraints. The W2W provides useful information on detailed power production with concern on the quality of power sent to the grid. In addition, the field of control for WEC is nowadays quite well understood but a lack of practical applications is regrettable. Opportunities to improve the implementation of these advanced controllers in real environments will be explored, thanks to the ideal location of the Basque Country with the BiMEP test site and the Mutriku OWC plant.

In short, the thesis objectives are oriented to tackle four major aspects of the technology development of Wave Energy Converters:

- 1. Improve numerical models accuracy including more detailed non-linear effects of all the PTO components.

The first objective is the representation of the overall chain of energy conversion by developing full W2W numerical models in time domain which describe the WEC motion and the behaviour of the PTO. Modelling such systems require a multidisciplinary approach and the convergence of several scientific areas: hydrodynamics, aerodynamics, control, and electrical engineering. Existing methodologies to detail the motion of WECs in the frequency domain are well understood. However, these kind of models are limited as they rely on linear theory. Time domain models are more detailed and accurate as they include non-linearities which reside in all the energy conversion steps. This part of the research will include more detailed aspects on the numerical models including non-linearities of the air chamber, the turbine and the power conversion equipment. It will be designed in a way that it is modular enough to test several PTO configurations and be the common framework for testing the advanced control strategies.

- 2. Compare the performance of several PTO systems.

Thanks to the W2W model developed previously, several air turbines with a basic controller can be simulated. The study will focus here on the optimisation and comparison of the most relevant self-rectifying air turbines and the optimal sizing of the generator for a given device in a specific location.

- 3. Develop and assess several advanced control strategies both in performance and in terms of PTO components reliability.

The main objective of control systems is to optimise the electrical power output while assuring the safe and reliable operation of the PTO. Assessing the performance at different stages in the energy conversion can open ways for improvements. It would be relevant to take into account not only the increase in useful power produced but also in the power variation and peaks to carefully analyse the PTO limitations and study power quality needs in a more practical way. Recent developments in wave energy conversion demonstrate that the implementation of wave forecasting and predictive control algorithms

appear to bring a significant increase in the energy production. This approach is to be addressed to understand the pros and cons of such a predictive control framework.

- 4. Successfully implement and test the controllers in real sea environment.

The real time implementation of the studied control strategies will first be done at the TECNALIA's PTO test rig, in a dry and controllable environment. The implementation of control strategies in this facility offers a way to validate them, to study the behaviour from an electrical point of view and gives valuable information on its performance. Also, as mentioned in the introduction, the Basque region is a strategic place for the study of the OWC technology. This would offer an opportunity to validate the work done on control strategies in a practical way and in real conditions.

1.3 Contributions

1.3.1 Advances in W2W modelling

A methodology to develop W2W numerical models taking into account the dynamics of the whole energy conversion chain is proposed: first a linear one in the frequency domain; and another one in the time domain that is used to include non-linearities of the air chamber and the PTO system. The methodology is applied for two devices: a fixed onshore OWC plant with the example of the Mutriku OWC plant; and a floating OWC spar-type buoy. The models include the different stages of energy conversion from wave energy to electrical power including all the PTO components involved. The field tests at the Mutriku plant performed during the OPERA project offered the possibility to improve the accuracy of the W2W model based on operational data. The hydrodynamic model is adjusted and the air compressibility model improved for the air chamber using these experimental data. The process variables obtained by this model show a better match with operational data measured at the plant in comparison with the state of the art numerical models. In addition, the electrical power conversion is better represented by means of a novel generator loss model which also includes operation in

different regions and the effect of flux weakening when operating in ranges beyond the nominal values.

1.3.2 PTO configurations

The W2W of the fixed OWC is used to compare different turbine technologies along with a simple speed control strategy. The tool enables the optimisation of the sizing of PTO components such as the turbine type, its diameter and the size of the generator. The study includes the comparison of three Wells turbines and three impulse ones. The optimal turbine diameter is obtained for each turbine and this allows to select more accurately the generator nominal capacity. The results showed that the bi-plane Wells turbine installed in Mutriku was not necessarily the best choice when analysing the average mechanical output power. The results of this analysis are closely tied with the turbine characteristic curves used in the optimisation. Some curves may be obtained theoretically and can bias the outcomes while others are more accurate as they were obtained by experimentation. Nonetheless this methodology can be useful to select the optimal PTO components, if trusted turbine characteristic curves are used.

1.3.3 Development of advanced control strategies

Several turbine speed control strategies are developed, simulated and compared between each other and with the biradial turbine using the W2W model of Mutriku under several sea states. This common framework allows a quick and results-driven comparison between these algorithms that are:

- A fixed speed control using a PI controller;
- Several versions of variable speed controllers based on a torque law approach using tuned control parameters;
- One combining the benefits of the fixed and variable speed and using the pressure standard deviation to set the reference speed, followed by the PI-controller;
- Several versions of a non-linear receding horizon predictive controller using the torque law approach of the variable speed control law;

The obtained results are the base for a performance and reliability assessment that highlights the advantages and drawbacks of each. As a summary, when the controller tends to maximise the output power, it usually overloads the generator reducing de facto its reliability. It is highlighted that the controllers that operate best take into account in a balance manner the efficiency of both the turbine and the generator. Additional constraints imposed in a version of the predictive algorithm showed quite balanced results allying good performance and a more reliable operation.

A non-linear predictive controller applied to a latching control strategy in the floating OWC completes the analysis. The latching effect is brought by the implementation of high speed actuating valve located in series with the biradial turbine. Simulation results are obtained with and without latching, with the same turbine speed control law. The latching strategy increases the average mechanical power by 20 to 30% depending on the sea state, and between 10 to 25% in the average electrical power output.

1.3.4 Real time controllers implementation and test in real sea environment

The last contribution of the thesis addresses the issues related to the real time implementation of controllers and especially the non-linear MPC one, being the first of its kind to be tested in a scaled rotary test rig, in the Mutriku facility and in the Marmok-A-5 buoy. Challenges related to the estimation of the wave force prediction are overcome using real-time measurements of the wave elevation ahead of the plants. Another issue concerning the computation in real-time of the predictive optimisation is also solved without penalising the accuracy of the optimal solution. Comparing the results of the predictive controller in Mutriku with a simple torque law, an increased in the power production of around 30% is obtained. This is due to the fact the predictive law includes the overall PTO efficiency in the real-time optimisation whereas the other control law relies on off-line optimisation where the objective is to set only the turbine at its best efficiency point. Finally, the predictive algorithm is successfully implemented in the Marmok buoy when installed in BiMEP being the first of its kind to operate a WEC in real sea conditions. Unfortunately, no comparison with the state of the art control law is made.

1.4 Thesis Structure

Chapter 2 The context of the wave energy sector and state of the OWC technology

Chapter 2 sets the global context that pushed the scientists and inventors to imagine machines capable of converting the energy concentrated in ocean waves. First, an historical review is carried out to cover the very early developments made by the pioneers of the wave energy sector. The global wave resource in the oceans justifies to even consider this type of energy. The ocean waves are then detailed and the mathematical formulations to represent them are presented. Several WEC concepts are also described along with their main PTO systems. A focus is then set on OWC systems as it is the technology selected for this thesis. The OWC concepts which were actually put in the water are described, as well as the different components that constitute the PTO system.

Chapter 3 State of the art

In line with the thesis objectives, Chapter 3 highlights the state of the art that has to be performed to detect the gaps left aside by existing works. It focuses on reviewing some of the main aspects of wave energy conversion detailed on this thesis: numerical modelling and control strategies. First a brief review of the various approaches to model WECs is made, covering mainly the hydrodynamic issues and and detailing their motion due to sea waves. Then the focus is made on modelling techniques specific to OWC systems including the hydrodynamics in the frequency and in the time domain, the modelling of the air chamber and the PTO components. Finally a review of control strategies in all the energy conversion steps is performed where general considerations are made for WECs, and is followed by specifics of control for OWC systems.

Chapter 4 Modelling methodology for Wave-to-Wire OWC systems

The 4th Chapter develops a methodology to better define W2W numerical models for OWC systems. It details the various steps that constitute the development of full W2W models for both a fixed single-body device and a floating two-body one. The models are prepared to run in the time domain and for several sea states of the wave climate. The study of the hydrodynamic part made in this chapter is a synthesis on what it has been done so far but including new contributions on the Mutriku OWC plant. A detailed

analysis is performed on air compressibility models, key part on the energy conversion for the OWC, and a validation with experimental results obtained at the Mutriku is proposed. In what concerns the modelling of the PTO system, the electrical conversion is modelled in a more comprehensive manner compared with the existing research works. Finally, the W2W model is employed to optimise the PTO configurations by testing several combinations of turbines.

Chapter 5 Development of advanced control strategies for the OWC

In this Chapter, several control strategies are designed, developed, tested and compared using the W2W models developed in the previous chapter. For each one, a thorough analysis on their pros and cons is stated. First, the parallel is made with the fundamentals of PTO control in wave energy conversion to comprehend the effects on the buoy motion and the energy capture. Then the case of the Mutriku plant is taken to develop a number of turbine speed controllers for the PTO composed of the biradial turbine and analyse them in terms of power production and PTO reliability. Also, a latching controller is proposed for the floating device. This is achieved by acting on the shut-off valve at the inlet of the turbine, and a predictive controller optimises pressure thresholds to find the best instants to open and close the valve.

Chapter 6 Real-time control

Chapter 6 addresses several implementation issues related to testing control algorithms in real control environments. In particular, predictive controllers present many challenges to solve before successfully being implemented. Among them, the prediction and estimation of the wave forces, one of the main input and perturbation for the controller; the computation burden to run the online optimisation of the non linear model predictive control; and the aspects related to the I/O communications between the model and the real plant. These aspects are covered in this chapter. Also, the implantation validation of several controllers is made in a dry PTO test rig to prepare for the deployment in a physical system. An important added value of this thesis is the test of control algorithms during sea trials in Mutriku and in the Marmok-A-5 buoy during its operation at BiMEP test site. The testing experience and the analysis of operational results are gathered there.

Chapter 7 Conclusion and future works

The last chapter of the thesis sums up the thesis challenges and clearly states the main contributions made with respect to the state of the art previously

detailed. Then, the articles published during the thesis are listed. Finally, the aspects related with the thesis that could not be addressed in this document are raised and left aside for future works.

The context of the wave energy sector and state of the OWC technology

<div style="text-align: right">2</div>

> *Think of the motion of the waves, the ebb and flow of the tides and the coming and going of the waves. What is the ocean? An enormous lost strength. How is stupid not to make use of the ocean!*
>
> — **from Victor Hugo - Ninety-three, (1874), VII, 5**
> French writer 1802-1885

Summary: The idea of converting energy from the waves is not new, in fact the first concepts were imagined more than 200 years ago. This chapter sets the global context that motivated to imagine such devices to convert energy from ocean waves. First, an historical review is presented covering early developments. The global wave resource in the oceans justifies to even consider this type of energy. Several WEC concepts are also described along with their the main PTO types. A focus is then made on OWC systems treating the actual OWC concepts put in the water and detailing the different components that constitute the PTO system.

2.1 The pioneers of wave energy conversion

Actually, the idea consisting in converting the potential energy due to the oscillation of waves is not recent at all. As early as the end of XVIIIth, the first known patent for wave energy extraction was filed in Paris by Pierre-Simon Girard. In the second half of the XIXth century in the United States and in Europe, other patents appeared describing concepts using the force of waves to convert them to electricity. An early patent application attributed to the American Charles Buckner in 1873 details the utilisation of wave force for power generation. A buoy set in motion by the waves and connected to a system composed of pistons and water-engines is illustrated in Figure 2.1.
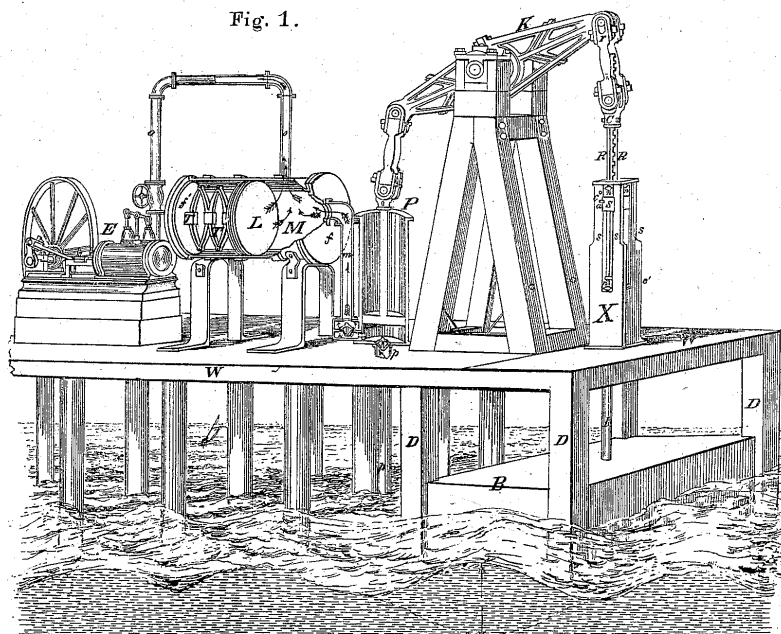
Fig. 2.1: Drawing of Charles Buckner's improvement in wave-powers from the patent *US138474A*

Pionneers in Spain also began to apply for their inventions, like José Barrufet y Veciana and its device called the Marmotor. It was actually built and presented to the public and the press in 1884. Fig. 2.2 presents drawings of its buoy and power extraction mechanism. He was applaused by the crowd but quickly passed into oblivion. Also to be named inventors like José Casanovas and its *new engine to use the driving force of the wind and the waves* in 1882, or José María Cienfuegos with its *machine for use as a driving force behind the waves of the sea* in 1897.
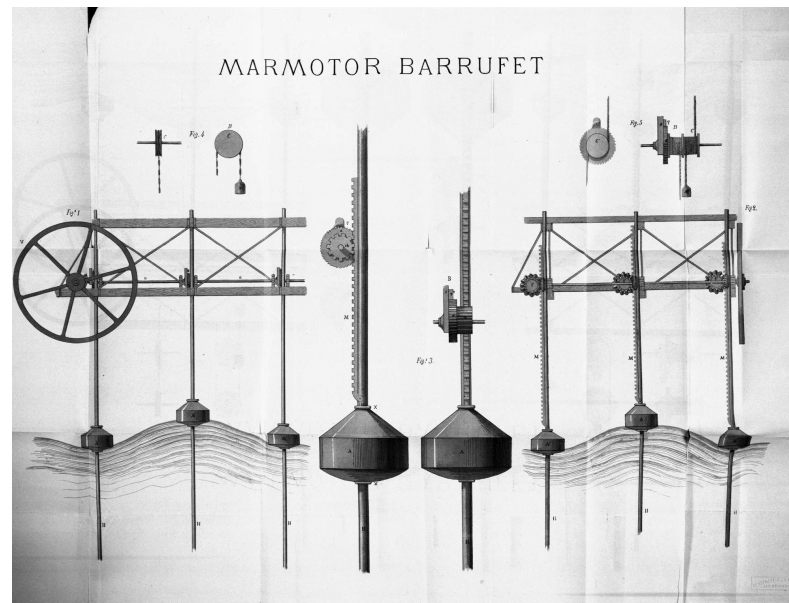
Fig. 2.2: Drawings of the Marmotor of Barrufet

One of the first significant inventions in wave energy conversion to be built is from the French engineer Paul Grasset. Evidence of the publication of his patent are found in France in 1925, in Spain, Great Britain and in the United States in 1929. It is simply called the *Bélier-siphon maritime à chambre barométrique* and can be traduced by marine ram with barometric chamber. The prototype was built in Biarritz just under the lighthouse (see Fig 2.3) thanks to private funds. The first part of the civil work was built until the 1929 worldwide crisis stopped the project. Later on, the beginning of World War II definitely put an end to the project and the wave power plant could never be completed.

Modern inventions like the one from Yoshio Masuda is the first OWC buoy to power marine navigation lights. They were actually commercialized and deployed along the Japanese coast (and later on in the USA) by Ryokuseisha company since 1965 [FH16]. The concept used a unidirectional turbine and a valve system to guide the air flow (see Fig. 2.4).

Cliché C. A. F.

Le Laboratoire hydrodynamique marin au phare de Biarritz

Cliché Mathieu.

La construction du Laboratoire

Fig. 2.3: Photographs of the prototype built in Biarritz at the end of the 30's [Arb12]

Fig. 2.4: The Uraga light buoy from Ryokuseisha [Hea12]

2.2 Ocean waves

Oceans worldwide cover around 70% of our planet. They concentrate a massive amount of energy, waiting to be harnessed. The global wave energy resource accessible along the globe coastlines is estimated to be between 0.5 and 2.2 TW [GS12]. Knowing the World installed generating power capacity is estimated to be between 5.25 to 5.7 TW, wave energy could supply between 10 to 40% of the World's needs [Mec13]. Wave energy is a derived form of solar energy. Indeed the Sun heats the Earth not uniformly inducing changes in temperature and thus changes of air pressure in the atmosphere. The masses of air flow from areas of high pressure to low pressure creating the wind. Waves are created by the friction of wind on a water surface. That is called the fetch. So by exerting a pressure on the ocean surface, the wind can produce two main forms of waves: swell waves and wind waves. Swell waves are related to a fetch exerting on a large surface area for a long time duration and far off the coasts. The waves travel a long distance along the open ocean and are characterised by long crested fully develop waves with high amplitudes and long wave periods. They concentrate a large amount of energy. On the opposite, wind waves are less energetic, created by a local wind blowing on a smaller water plane and are generally smaller in height, with shorter wave periods and reach the shore in a messier way.

At each conversion from solar to wind and finally to wave, the energy gets more and more concentrated for the same area. An average power from solar energy is typically 100 W/m^2, when converting into wave energy the power levels can be between 10 to 50 kW in average [Bro03]. Wave energy is not the most important form of energy present in the planet, but watching waves crashing on a breakwater in a winter storm, one can understand the density of energy liberated at that instant. In wave energy conversion, the challenge is to absorb this energy effectively and in a reliable manner in an environment that can be very harsh.

The resource

The annual wave resource of a test site is represented in the form of a scatter diagram and informs on the annual energy of waves per linear meter. It is a combination of the wave power and the frequency of the sea states over a year.

The wave climate is the annual frequency of occurence of each measured sea state. A sea state is usually defined by bins of 0.5 m of significant wave heights H_s and 1 s wave peak period T_p, considering unidirectional waves. Figure 2.5 represents the scatter diagram of the wave climate of BiMEP which is a test site situated in the North shore of Spain, off the coast of Armintza.

Tp [s]	Hs [m] - Significant wave height																						
	0,5	1	1,5	2	2,5	3	3,5	4	4,5	5	5,5	6	6,5	7	7,5	8	8,5	9	9,5	10	10,5	11	11,5
2	0	0	0	0	0	0	0	0	0	0	0	0	0	0	0	0	0	0	0	0	0	0	0
3	0	0	0	0	0	0	0	0	0	0	0	0	0	0	0	0	0	0	0	0	0	0	0
4	6,84E-04	2,28E-04	0	0	0	0	0	0	0	0	0	0	0	0	0	0	0	0	0	0	0	0	0
5	1,64E-02	9,16E-03	1,56E-03	0	0	0	0	0	0	0	0	0	0	0	0	0	0	0	0	0	0	0	0
6	2,27E-02	3,45E-02	1,11E-02	4,18E-03	5,70E-04	0	0	0	0	0	0	0	0	0	0	0	0	0	0	0	0	0	0
7	2,28E-02	5,18E-02	2,58E-02	1,11E-02	5,78E-03	1,41E-03	3,04E-04	0	0	0	0	0	0	0	0	0	0	0	0	0	0	0	0
8	1,63E-02	5,46E-02	6,23E-02	1,82E-02	6,46E-03	4,98E-03	3,04E-03	9,88E-04	7,60E-05	0	0	0	0	0	0	0	0	0	0	0	0	0	0
9	1,61E-02	3,54E-02	6,49E-02	4,11E-02	1,39E-02	8,29E-03	4,30E-03	4,37E-03	1,67E-03	1,90E-04	7,60E-05	0	0	0	0	0	0	0	0	0	0	0	0
10	6,65E-03	1,96E-02	2,68E-02	4,02E-02	3,38E-02	1,05E-02	5,51E-03	4,52E-03	3,38E-03	1,29E-03	4,18E-04	2,28E-04	3,80E-05	0	0	0	0	0	0	0	0	0	0
11	5,21E-03	9,88E-03	2,25E-02	2,11E-02	2,98E-02	2,22E-02	8,93E-03	2,13E-03	1,94E-03	1,86E-03	1,18E-03	7,22E-04	2,66E-04	3,80E-05	1,14E-04	7,60E-05	0	0	0	0	0	0	0
12	2,74E-03	3,08E-03	1,14E-02	9,31E-03	1,21E-02	1,57E-02	1,43E-02	6,61E-03	1,71E-03	1,56E-03	8,36E-04	1,56E-03	8,36E-04	5,32E-04	2,28E-04	7,60E-05	1,90E-04	7,60E-05	0	0	0	0	0
13	1,33E-03	2,05E-03	2,97E-03	4,87E-03	3,35E-03	6,50E-03	7,38E-03	4,75E-03	3,92E-03	1,44E-03	6,46E-04	9,88E-04	1,90E-04	1,90E-04	4,56E-04	3,80E-05	3,80E-05	1,52E-04	7,60E-05	3,80E-05	7,60E-05	3,80E-05	0
14	8,36E-04	4,94E-04	5,70E-04	6,46E-04	7,22E-04	1,48E-03	1,29E-03	1,98E-03	1,79E-03	1,29E-03	3,42E-03	9,50E-04	3,04E-04	2,28E-04	1,52E-04	1,14E-04	1,52E-04	0	0	0	0	0	0
15	7,60E-05	1,90E-04	2,66E-04	0	0	0	3,80E-05	1,90E-04	1,52E-04	5,70E-04	7,98E-04	4,94E-04	5,70E-04	3,04E-04	7,60E-05	7,60E-05	3,80E-05	0	0	0	0	0	0
16	3,80E-05	0	0	0	0	0	0	0	0	0	0	7,60E-05	0	0	0	0	0	0	0	0	0	0	0
17	0	0	0	0	0	0	0	0	0	0	0	0	0	0	0	0	0	0	0	0	0	0	0
18	0	0	0	0	0	0	0	0	0	0	0	0	0	0	0	0	0	0	0	0	0	0	0
Total	11%	22%	23%	15%	11%	7%	5%	3%	1%	1%	0%	1%	0%	0%	0%	0%	0%	0%	0%	0%	0%	0%	100%

Fig. 2.5: Scatter diagram of the annual wave climate in BiMEP

The power of the waves in presence during a sea state is defined per 1 meter of wavefront as the function of H_s and T_p following the formula (2.1). When multiplying the previous scatter diagram by a matrix of incident wave power, we obtain the site annual wave resource, which is the mean available power per meter of wave front at this specific site. For BiMEP the annual wave resource is shown in Fig. 2.6.

$$P_w = 0.42\, H_s^2\, T_p\ [kW/m], \tag{2.1}$$

Tp [s]	Hs [m] - Significant wave height																						
	0,5	1	1,5	2	2,5	3	3,5	4	4,5	5	5,5	6	6,5	7	7,5	8	8,5	9	9,5	10	10,5	11	11,5
2	0	0	0	0	0	0	0	0	0	0	0	0	0	0	0	0	0	0	0	0	0	0	0
3	0	0	0	0	0	0	0	0	0	0	0	0	0	0	0	0	0	0	0	0	0	0	0
4	0,00	0,00	0	0	0	0	0	0	0	0	0	0	0	0	0	0	0	0	0	0	0	0	0
5	0,01	0,02	0,01	0	0	0	0	0	0	0	0	0	0	0	0	0	0	0	0	0	0	0	0
6	0,01	0,09	0,06	0,04	0,01	0	0	0	0	0	0	0	0	0	0	0	0	0	0	0	0	0	0
7	0,02	0,15	0,17	0,13	0,11	0,04	0,01	0	0	0	0	0	0	0	0	0	0	0	0	0	0	0	0
8	0,01	0,18	0,47	0,25	0,14	0,15	0,13	0,05	0,01	0	0	0	0	0	0	0	0	0	0	0	0	0	0
9	0,02	0,13	0,55	0,62	0,33	0,28	0,20	0,26	0,13	0,02	0,01	0	0	0	0	0	0	0	0	0	0	0	0
10	0,01	0,08	0,25	0,68	0,89	0,40	0,28	0,30	0,29	0,14	0,05	0,03	0,01	0	0	0	0	0	0	0	0	0	0
11	0,01	0,05	0,23	0,39	0,86	0,92	0,51	0,16	0,18	0,22	0,16	0,12	0,05	0,01	0,03	0,02	0	0	0	0	0	0	0
12	0,00	0,02	0,13	0,19	0,38	0,71	0,88	0,53	0,17	0,20	0,13	0,28	0,18	0,13	0,06	0,02	0,07	0,03	0	0	0	0	0
13	0,00	0,01	0,04	0,11	0,11	0,32	0,49	0,42	0,43	0,20	0,11	0,19	0,04	0,05	0,14	0,01	0,01	0,07	0,04	0,02	0,05	0,03	0
14	0,00	0,00	0,01	0,02	0,03	0,08	0,09	0,19	0,21	0,19	0,06	0,20	0,08	0,07	0,05	0,04	0,06	0	0	0	0	0	0
15	0,00	0,00	0,00	0	0	0	0,00	0,02	0,02	0,09	0,15	0,11	0,15	0,09	0,03	0,03	0,02	0	0	0	0	0	0
16	0,00	0	0	0	0	0	0	0	0	0	0	0,02	0	0	0	0	0	0	0	0	0	0	0
17	0	0	0	0	0	0	0	0	0	0	0	0	0	0	0	0	0	0	0	0	0	0	0
18	0	0	0	0	0	0	0	0	0	0	0	0	0	0	0	0	0	0	0	0	0	0	0
Total	0,09	0,73	1,93	2,41	2,85	2,89	2,59	1,93	1,44	1,04	0,67	0,96	0,51	0,35	0,31	0,13	0,17	0,10	0,04	0,02	0,05	0,03	21,26

Fig. 2.6: Scatter diagram of the annual wave resource in BiMEP

The mean annual wave power available at BiMEP is the sum of all the sea states values, here $P_{\text{bimep}} = 21.26\,kW/m$. These data are essential for the conception of the WEC because it strongly influences the structural design of

a WEC. Its shape will be optimised so the natural frequency falls within the range where there is the best resource.

Ocean wave theory and spectral analysis

There exists several models to represent numerically irregular ocean waves [JW01]. Depending on the water depth and the sea state, one should select the most appropriate model as defined by DNV's environmental conditions [DNV07] in Fig. 2.7.
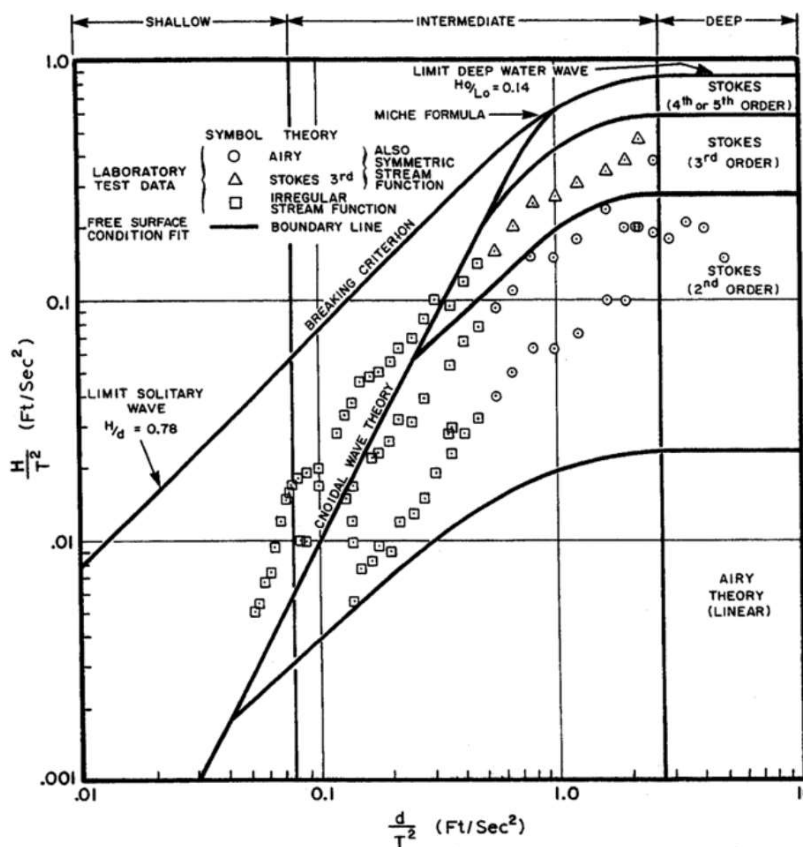
Fig. 2.7: Validity of ocean wave theories - taken from [DNV07]

The linear water wave theory is often used when developing a W2W model of a WEC. Although it is limited to low steepness waves in flat bathymetry and considering an irrotational flow, it is a fairly good approximation. The profile of the water sea level is simplified as the sum of several sinusoidal waves with different amplitudes and phases. Let's take an example of the superposition of 4 unidirectional regular waves, each of them being characterised by its wave

height H [m] (amplitude $a = H/2$) and its period T [s] (cyclic frequency $\omega = 2\pi/T$ [rad/s]). The superposition of the wave elevations is:

$$\eta_{\mathrm{w}}(t) = \sum_{i=1}^{4} a_i \cos(\omega_i t + \varphi_i)\,[m] \tag{2.2}$$

With the phase φ randomly varies from $[0 : 2\pi]$.
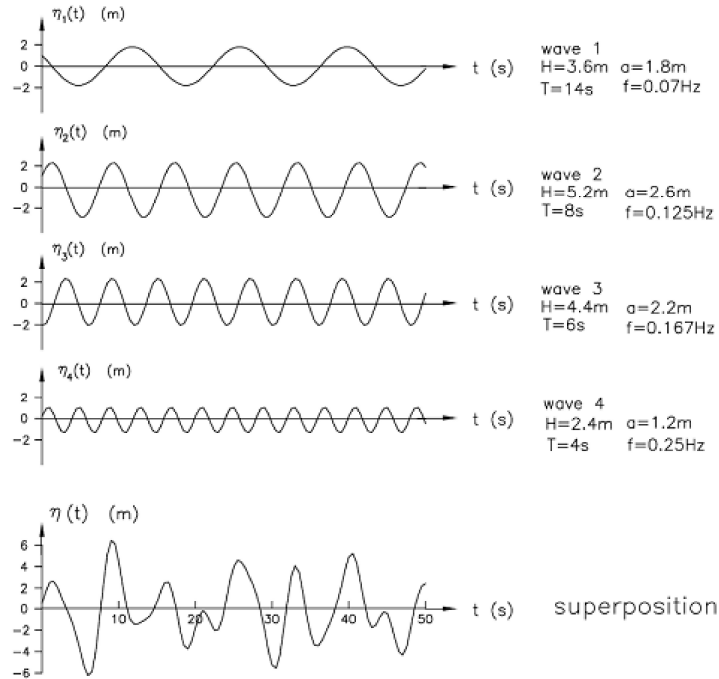
Fig. 2.8: Irregular ocean waves, superposition of wave elevations [Kof15]

The associated spectrum in frequency domain $f_i = \omega_i/2\pi$ [Hz] is such as:
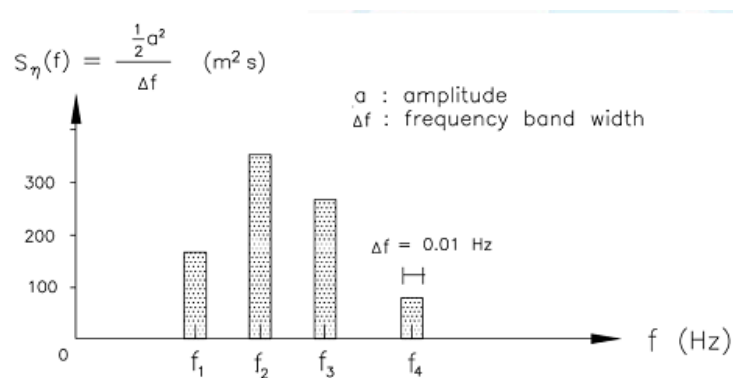
Fig. 2.9: Spectrum of the superposed wave elevation [Kof15]

In reality, during a sea state, there is an infinite number of frequencies (and amplitudes) where the energy is represented in a wave spectrum. The

spectrum of a wave elevation is built using a fast Fourier transform over the discrete signal of the wave elevation to obtain the Fourier coefficient a and b. The spectral density of the simplified wave elevation: $\eta_w(t) = \sum_{i=0}^{N-1} c_i cos(\omega_i t + \phi_i)$, being N the number of superposed waves, is then defined as:

$$S_\eta(\omega_i) = \frac{1/2\, c_i^2}{\Delta\omega} \tag{2.3}$$

with $c_i = \sqrt{a_i^2 + b_i^2}$
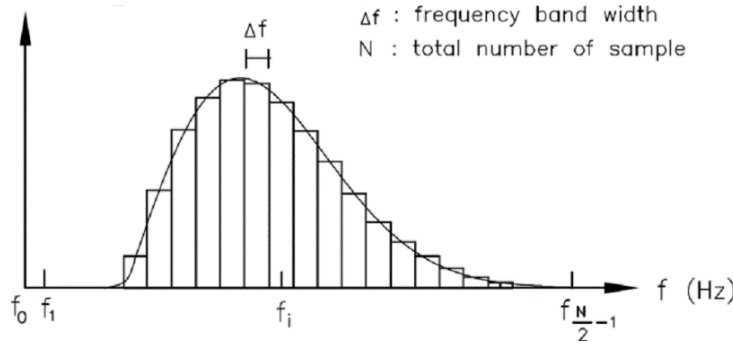
Fig. 2.10: Polychromatic wave spectrum [Kof15]

To represent ocean waves more accurately, several approaches have been developed and the most commonly used ones being the Pierson-Moskowitz (1964), Bretschneider (1978) and the Jonswap (1984) spectra. They are based on the observation of the wind blowing upon a large area of sea water of the North Atlantic Ocean. All of them have been validated by the International Towing Tank Conference. The Pierson-Moskowitz spectra was defined with an empirical relationship describing the distribution of energy in the ocean:

$$S_{\text{PM}}(\omega) = \frac{\alpha\, g^2}{\omega^5} \exp\left(-\beta\left(\frac{\omega_{\text{p}}}{\omega}\right)^4 \right) \tag{2.4}$$

With the parameters $\alpha = 0.0081$, $\beta = 1.25$, g the gravitational acceleration and $\omega_{\text{p}} = 1/T_{\text{p}}$.

The Bretschneider spectrum, suitable for open sea areas, is a modification of the PM spectrum and the formulation in function of a sea state, defined by its significant wave height H_{s} and the mean centroid wave period T_1, is then:

$$S_{\text{B}}(\omega) = k_1 \frac{H_{\text{s}}^2}{T_1^4\, \omega^5} \exp\left(-\frac{k_2}{T_1^4\, \omega^4} \right) \tag{2.5}$$

Where parameters $k_1 = 173$ and $k_2 = 692$ and $T_{\text{p}} = T_1/0.772$ [JW01].

Later on, the Joint North Sea Wave Project (JONSWAP) was conducted during which a new empirical law has been defined to describe the wave spectrum by adding the γ parameter to the $S_{\mathrm{PM}}(\omega)$, that represents the sharpness of the spectrum peak's frequency:

$$S_{\mathrm{J}}(\omega) = \frac{\alpha\, g^2}{\omega^5} exp\Big(- \beta \Big(\frac{\omega_{\mathrm{p}}}{\omega}\Big)^4\Big)\gamma^{\mathrm{a}} \tag{2.6}$$

And defined by a $= exp\Big(- \frac{\omega - \omega_{\mathrm{p}}}{2\,\omega_{\mathrm{p}}^2\,\sigma^2}\Big)$ and $\sigma = \begin{cases} 0.07 & \text{if } \omega \leq \omega_{\mathrm{p}} \\ 0.09 & \text{if } \omega \geq \omega_{\mathrm{p}} \end{cases}$ [JW01].

To better understand the different shape of ocean wave spectra, Fig. 2.11 shows a comparison of different wave spectra.
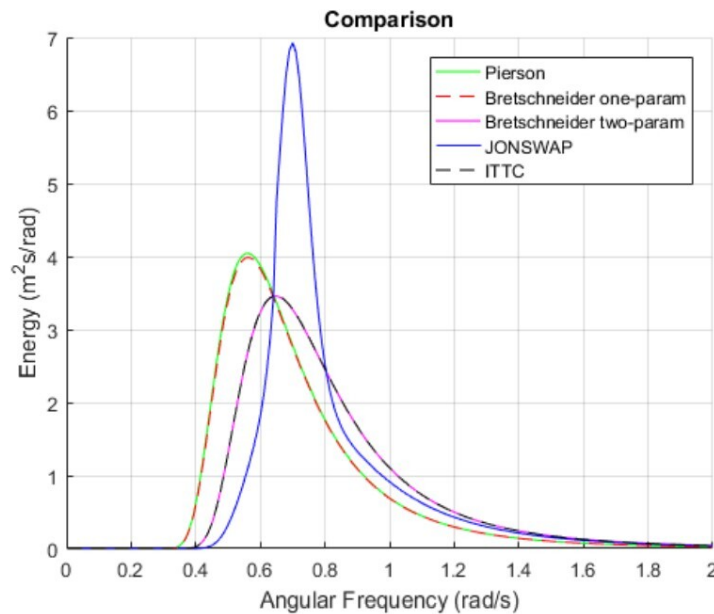
Fig. 2.11: Comparison of wave spectra - taken from [Ram17]

Numerical modelling of waves in time domain

Illustrating the previous explanation on wave spectra analysis, the example of the BiMEP test site is taken for ocean waves modelling in time domain. The temporal domain is used to represent the transient effects in non-linear numercial models. Let us use a JONSWAP spectrum with a $\gamma = 2.8$, more accurate for this wave climate, and consider unidirectional irregular waves. The purpose here is to generate time series of wave elevation and will serve

to compute the excitation forces exerted on a WEC in the following section. To do so, a script is run to initialise the frequency domain quantities of amplitude and phase and then traduced in time domain. Specifically, the spectral density is:

$$S(\omega) = 320 \frac{H_s^2}{T_p^4 \, \omega^5} \exp\left(- \frac{1950}{T_p^4 \, \omega^4} \right) \gamma^a \tag{2.7}$$

Figure 2.12 is the JONSWAP spectrum for a sea state $H_s = 2.16$ m and $T_p = 11$ s:
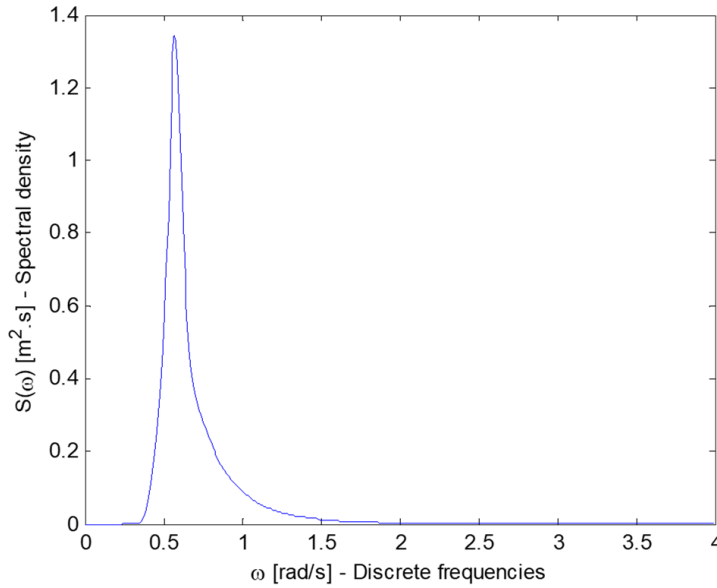
Fig. 2.12: JONSWAP spectrum for a sea state $H_s = 2.16$ m and $T_p = 11$ s in BiMEP

In order to generate times series of the wave elevation η_w the following formulation has been used:

$$\eta_w(t) = \sum_{i=1}^{N} a_i(\omega_i) \, cos(\omega_i t + \varphi_i) \, [m] \tag{2.8}$$

Where $a(\omega) = 2 \sqrt{S(\omega) \, \Delta\omega}$, and φ is randomly generated with uniform distribution from 0 to 2π. To be able to run simulations longer than $T_sim = 2\pi 100$ s, the spectrum discretisation is done with a randomly variable interval between in the $\Delta\omega$. Also, the same seed is used for the random generation of the discretisation interval and the phase. That way the time series of the wave elevation and forces are always the same for a selected sea state. This allows a repeatability of tests and a better results comparison. Fig. 2.13 shows the wave elevation over time from the wave spectrum defined previously.
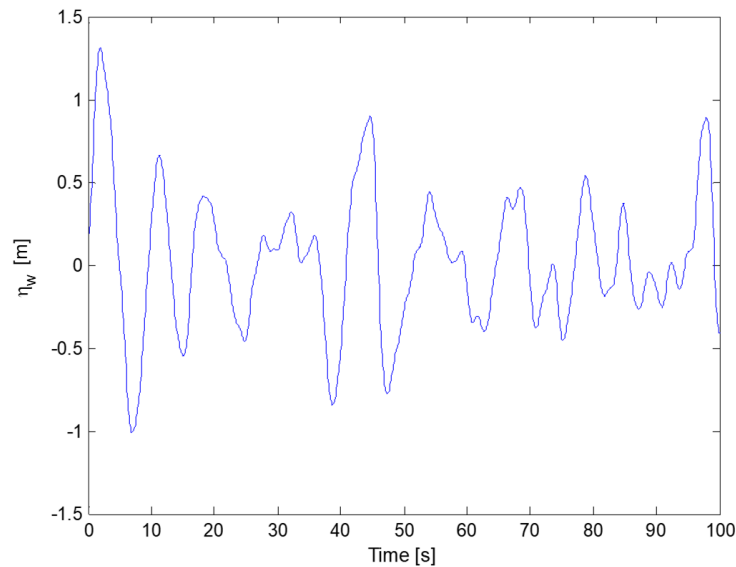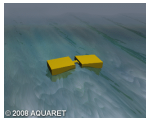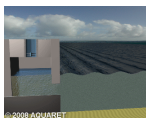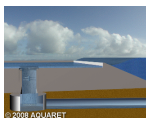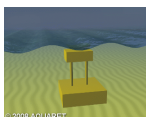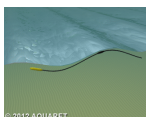
Fig. 2.13: Wave elevation for the sea state $H_s = 2.16$ m and $T_p = 11$ s

2.3 Various WEC concepts and PTO systems

The most recent history of wave energy resumed when the worldwide oil crisis stroke the world in 1973. Priority was to find alternative ways to produce power diversifying from fossil fuels. A new generation of scientist focused their work into finding alternative ways of producing power from renewable sources and especially from waves. In the UK, professor Stephen Salter of the University of Edinburgh invented what was later called the Salter's duck. At that time he was under the spotlight in the scientific community for publishing its work in the prestigious journal *Nature* in 1974. Since then, scientists have developed hundreds of concepts to convert potential energy from the waves into electricity [Fal07; DPS09; Fal10; Bab15]. A classification of the various technologies was proposed by [Aqu12], reported on Table 2.1. Among these WECs, only a small number have reached sea trials and today a few prototypes have or are being tested in real environment conditions. During the past 10 years, technology developers do not seem to have converged through a particular type of WEC as it was the case in wind energy where the 3-bladed horizontal-axis turbine is now the reference in the sector. A segmentation showing the various forms of converting the captured hydrodynamic energy into grid power, PTO systems, is shown in Fig. 2.14. Each PTO type is detailed as follows:

Tab. 2.1: WEC classification according to [Aqu12]

Name	Illustration	WEC developers	Working principle
Attenuator		Pelamis, Mocean	Floating WEC operating parallel to the wave direction Energy is captured from the relative motion of the two arms as the wave passes through them.
Point absorber (PA)		SeaBased, CETO FredOlsen, OPT, Oscilla Power, CorPower, Wave4Wave	Floating WEC absorbing energy from all directions through its movements at/near the water surface. It converts the motion of the buoyant top relative to the base into useful energy.
Oscillating Wave Surge Converter (OWSC)		WaveRoller, Langlee, Resolute Marine, PolyGEN,	OWSCs extract energy from wave surges and the movement of water particles within them. The arm oscillates as a pendulum mounted on a pivoted joint in response to the movement of water in the waves.
Oscillating Water Column (OWC)		OE buoy, Mutriku, Oceantec, Oceanlinx	An OWC is a partially submerged, hollow structure. It is open to the sea below the water line, enclosing a column of air on top of a column of water. Waves cause the water column to rise and fall, which in turn compresses and decompresses the air column.
Overtopping or Terminator		WaveDragon, WaveCAT,	Overtopping WECs capture water as waves break into a storage reservoir which can, in turn, drive a PTO. An overtopping device may use collectors to concentrate the wave energy.
Submerged Pressure Differential (SPD)		AWS, Symphony	SPD WECs are typically located near shore and attached to the seabed. The motion of the waves causes the sea level to rise and fall above the WEC, inducing an differential internal pressure . The alternating pressure pumps fluid through a system to convert into useful energy.
Bulge wave		S3, Anaconda, WaveTube S3 Vigor AB	Bulge wave technology consists of a flexible tube filled with a fluid, moored to the seabed heading into the waves. With the wave passing along the length of the tube, it exerts a pressure at different section creating a "bulge" in the fluid. As the bulge travels through the tube it grows, gathering energy.
Rotating mass mass		Wello, ISWEC	Two forms of rotation are used to capture energy by the movement of the device pitching and rolling in the waves. This motion drives either an eccentric weight or a gyroscope.

- Hydraulic systems rely on the waves large forces and slow speeds moving a hydraulic cylinder which pressurises a fluid over several stages until flowing through an hydraulic motor driving a conventional generator. The presence of pressure accumulators allows a smoothed output power and the hydraulic motor can be reversed in a pump to perform reactive control as it has been done in the Wavestar prototype [HKV13]. The device, which has been extensively tested in real environment until the project shut down in 2016, was composed of two floaters who shared a common hydraulic system. The floating attenuator Pelamis where the PTO is situated at each joint between two segments was capable of capturing the energy from several degrees of motion. The Pelamis P2 machine reached 1.5 years of sea trial after three deployments including a pre-commercial full-scale device until the company Ocean Power Delivery bankrupted. Yet the performance was high for a WEC and the efficiency of the device was raised to 80%, although penalised by the valves [Hen06]. This issue can be overcome when a proper control strategy is used [Gas+16]. Both devices are compared in a techno-economic assessment in the paper [OLD13], and in the operational experience in the scientific report [Quo16].

- Air turbines convert pneumatic power into mechanical rotational one and are connected to an electrical generator, sometimes coupled with a flywheel, to produce electricity. The pressure variation due to the
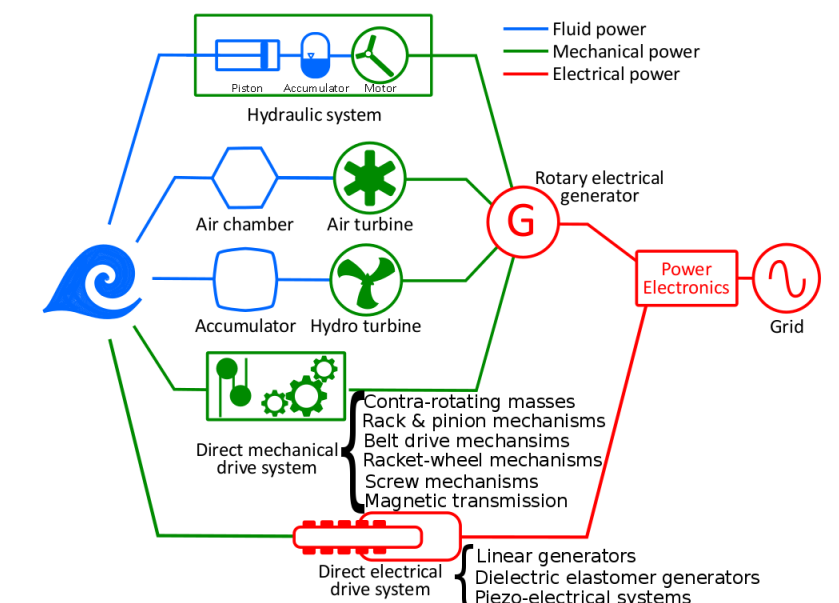
Fig. 2.14: Different power-flow paths for wave energy to electricity conversion adapted from [PK17]

motion of the OWC in an air chamber creates a reciprocal air flow driving the turbine. The most popular, which is as well the most simpler one, is the Wells turbine which can be found in the operating plants of Pico [Fal00] and Mutriku [TML10], the decommissioned LIMPET [Whi+02], or the recently installed floating spar from IDOM/Oceantec [Mig18]. The major drawback is the associated stall occurring when the flow separates around the blade profile. In addition to a rapid loss of efficiency, it creates noise and vibration which can potentially cause failures if an appropriate control is not implemented [VSR15]. In order to overcome the stall and aiming at higher efficiencies, the impulse and the Dennis-Auld turbines were developed. The first one was tested in the OE buoy during the CORES project [LK11; Thi+11; Kel+14]. The presence of moveable guided vanes (GV) actuated by an hydraulic system added complexity and raised reliability issues in addition to the power consumption needed for the vanes' actuation [COR11]. The Denniss-Auld turbine relied on fast pitching blades and was installed in the Oceanlinx MK3.

- Hydro turbines are often used in overtopping devices, the objective is to concentrate the waves into a ramp forcing them to break and so the sea water fills a reservoir higher than the sea-level. The water is flushed through an inward flow low-head turbine. The most famous prototype is the Tapchan - for TAPered CHANnel - installed in 1986 [Meh86] and equipped with a Kaplan turbine, conventional setup for hydroelectric power generation. In the floating Wavedragon 1/4.5th scale prototype, several Kaplan arrangements have been tested at sea during a year and a half [Kof+04; Ted07; Dra14]. The turbines coupled to permanent magnet generators could adapt to operation conditions thanks to movable guide vanes and pitching blades. Still this type of turbine can be subjected to cavitation reducing its performance. Another application of hydro turbines was made in the first generation of the Oyster where a bottom-hinged flap type device pumped water onto a station on-shore and where the pressurised flow drove a Pelton turbine [WF12]. Due to the complexity of this PTO, the next Oysters used an hydraulic setup.

- Direct mechanical drive systems are all types of mechanisms converting mechanical motion (most of the time from heave) into a rotational one that can fit a conventional generator. It exists many different PTO

concepts: contra-rotating mass, magnetic transmission, rack & pinion, belt drive, racket-wheel, and screw mechanisms.

- Linear generators use directly the wave oscillation to set in motion a buoy tethered to a translator, composed of magnets, in front of a stator made of coils; both are situated in a sealed hull. This concept was firstly used in the nearshore devices Archimedes Wave Swing who suffered two unfruitful intents before being installed in 2004 [Fal10]. The SeaBased is another nearshore device in test at sea [Lei+08]. The principle issue of this technology is to assure perfect sealing of the hull while being able to follow the changing tides to avoid reaching the dead ends.

2.4 OWC technologies

2.4.1 Working principle

One of the key advantages of the OWC over the other WEC types is its simplicity and robustness due to its intrinsic working principle. Many of the existing concepts convert the slow motion of waves into mechanical energy and produce huge torque magnitudes when absorbing wave energy. The mechanical structure and components need to be thought out to withstand these forces and can result in costly designs. In the OWC, the air trapped in a chamber adds another conversion step between the potential energy from the wave to the mechanical one at the turbine. This pneumatic power induced by the compression and expansion of air in the chamber creates an air flow that drives an air turbine rotating at high rotational speed and relatively low torque. The torque produced by the so-called self-rectifying turbines is unidirectional regardless of the flow direction and thus off-the-shelf generators are suited for this type of turbines. The energy conversion chain of the OWC is displayed in Fig. 2.15.

The OWC is one of the simplest and most widely studied technology for wave energy conversion. This technology can be divided into two types of devices: shoreline or bottom-fixed devices, and offshore floating structures. On the case of a fixed OWC, the device comprises a partly submerged hollow shell structure opened below the water surface, inside which air is trapped in
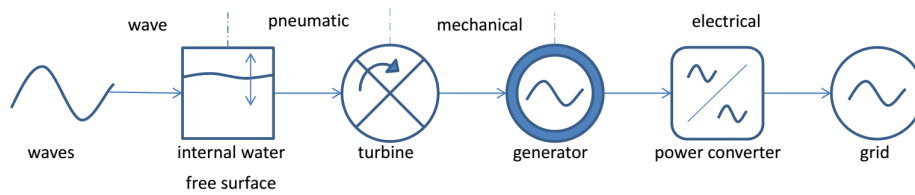
Fig. 2.15: Power-flow paths for energy transformation from the OWC

the air chamber above the water free surface. The oscillating motion of the internal free surface produced by the incident waves generates a bidirectional flow of air through the turbine that drives the electric generator. Even if the wave resource is less energetic and the device is sensitive to tides and wave orientation, it is easier to install, maintain and perform research activities. A cross-section of the chamber of a fixed OWC plant equipped with the biradial turbine is illustrated in Fig. 2.16.
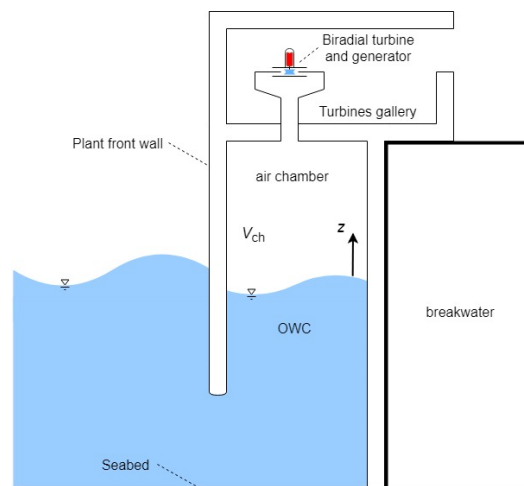
Fig. 2.16: Cross-section of one chamber of a fixed OWC power plant

The extensive exploitation of wave energy resource is not compatible with the specific characteristics and constraints of shoreline power plants. It is necessary to deploy large arrays of buoys to make this type of ocean energy conversion commercially viable. It also brings diversity in the electrical production mix in the marine renewable energy sector. The OWC spar-buoy is an axisymmetric device and so, insensitive to wave direction. It consists essentially of a submerged vertical tube (open at both ends) fixed to a floater whose upper part forms an air chamber. The incident waves excite both the floating structure and the internal water surface at different magnitudes an frequencies. This relative motion produces a reciprocating air-flow that drives the turbine mounted on the top of the buoy. Fig. 2.17 shows the cross-
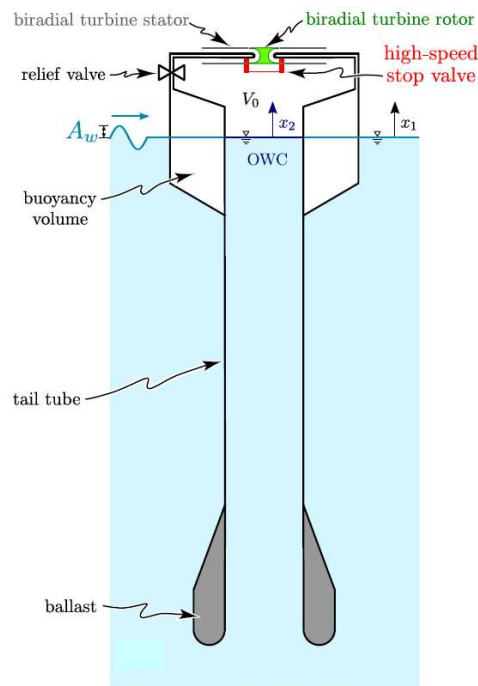
Fig. 2.17: Cross-section of a floating OWC spar type buoy

section of the floating OWC spar-type. Another floating OWC technology is the BBDB, for Backward Bent Duct Buoy, and uses not only heave but also pitch motion. It has an internal water channel opened at the opposite of the wave travel direction. In comparison with the shoreline structures, offshore buoys benefit more energetic waves and by nature no heavy civil work for the structure construction is needed. However they suffer costly steel structure and offshore equipment (mooring lines, dynamic and static underwater power cables, cable hubs) and represent significant costs related to Operation & Maintenance (O&M).

2.4.2 Relevant OWC devices

Among the many existing concepts, the OWC benefits a significant interest studied in several technology reviews [Hea12; Del+15; FH16]. First applications of the oscillating water column principle were dedicated to supporting marine navigation. The first patent recording the use of an OWC to the whistle navigation buoy was proposed in 1885 by J. M. Courtney. The buoy would produce a sound to warn the vessels of a nearby danger. Later in 1950, Masuda created and installed several hundreds of OWC buoys to power navigation lights, each one hosting an unidirectional turbine, air flow

rectifying valves and combined with an induction generator. Then the Kaimei was developed, it was an 80-meter-long floating barge hosting 8 chambers for a rated power of 125 kW [Fal10].

Since, few prototypes were built and have been or are actually in operation. They are reported in Table 2.2 along with details on their PTO systems and the references to the figures of the OWC prototypes presented below. To cite only the latest developments: the Pico plant [Bri+01; Mon+13; MWL18; Fal+19], the Mutriku plant [TLH07; Tor+09b], the BBDB from Ocean Energy [LK11; Kel+14; She19] and the Oceantec/Idom Marmok-A5 spar-type buoy [Wel+; Mig18]. The Mutriku OWC plant, situated in the North shore of Spain in the Bay of Biscay, is a shoreline device integrated into a breakwater. The total capacity totalises 296 kW thanks to 16 air chambers, upon which 14 are operational. Each one is equipped with a set of Wells turbine and generator with 18.5 kW of nominal power [Tor+09b]. A picture of the plant is presented in Fig. 2.25. In operation since 2011, the plant is connected to the grid where it has delivered more than 2 GWh of wave energy in March 2020.
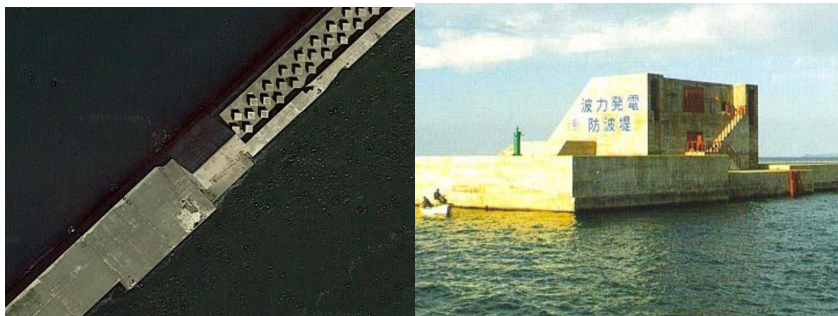
Fig. 2.18: Sakata port OWC power plant from [The05]

Fig. 2.19: Vizhinjam near-shore OWC plant from [The05]

Tab. 2.2: Relevant OWC prototypes

Name	Type	Description	Turbine	Date	Location	Generator	Fig.	Ref.
Kaimei	Floating	13 air chambers	various turbine arrangements unidirectional and self-rect turbines	1978	Western coast, Japan	500 kW		[FH16]
Kvaemer-Brug	Shoreline	Multi-resonant OWC	N/A	1987	Toftestallen, Norway	60 kW		[Bro03; FH16]
Sakata Port	Shoreline	5 air chambers	Twin Monoplane Wells with GV 1.337m	1989	Sakata, Japan	75 kW	2.18	[Bro03; The05; FG12]
Islay OWC	Shoreline		Biplane Wells 1.2m	1991	Island of Islay, UK	150 kW SCIG		[Bro03; FG12]
Vizhinjam	Near-shore		1x Monoplane Wells 2.0m SCIG then Wells then 2x impulse turbines	1991	Vizhinjam, India	Slip-ring generator 2x 55 kW slip-ring IG	2.19	[Bro03; The05; FH16]
OSPREY	Near-shore		4x Contra-rotating Wells 3m	1995	Dounrey, UK	4x 500 kW	2.20	[Bro03; Tho95]
Mighty Whale	Floating	BBDB	3x Wells	1998	Gokasho Bay, Japan	10 kW, 2x 30 kW, 50 kW		[Bro03; FH16]
Pico plant	Shoreline		Monoplane Wells with GV 2.3m	1999	Pico Island, Portugal	400 kW	2.21	[Bri+01; Bro03; The05] [Mon+13; Mon15] [VSR15; FH16; MWL18; Fal+19]
LIMPET 500	Shoreline	3 air chambers	2x Contra-rotating Wells 2.6m	2000	Island of Islay, UK	2x 250 kW	2.22	[Boa+02; Whi+02; Bro03] [The05; Hod+08; Cas10]
Oceanlinx	Near-shore		Denniss-Auld variable-pitch blades 1.6m	2005	Port Kembla, Australia	200 kW SCIG	2.23	[TD03; Fin04; Bro03] [The05; FG12]
OceanEnergy	Floating	1:4th scale BBDB	Wells Impulse moveable GV	2008	Galway bay, Ireland	N/A 11 kW SCIG	2.24	[Rea+11; LK11; Kel+14]
Oceanlinx Mk3	Floating	1:3rd scale, 2 chambers	HydroAir concept, pat. Wells turbine	2010	Port Kembla, Australia	N/A full scale 2.5 MW		[FH16]
Mutriku OWC	Shoreline	16 air chambers	14x Biplane Wells 0.75m Biradial turbine 0.5m 2017-2018	2011	Mutriku, Spain	14x 18.5 kW 30 kW SCIG	2.25	[Tor+09a; TML10]
REWEC3	Shoreline	Multi-resonant OWC	N/A	2014	Civitavecchia, Italy	N/A	2.26	[MA13; Are+18; MA19]
PW-OWC Sakata Port	Shoreline	Multi-resonant OWC	Impulse turbine fixed GV	2015	Sakata, Japan	2x 250 kW	2.27	[Kih+; Shi+17; Kih+16]
Yongsoo OWC	Near-shore	2 air chambers	2x Impulse turbines	2015	Jeju Island, South Korea	2x 15 kW SCIG	2.28	[FH16]
Marmok A5	Floating	Spar type buoy	2x Monoplane Wells 0.75m Biradial turbine in 2019	2016	Arminza, Spain	30 kW SCIG	2.29	[Mig18; Gat+17]
OceanEnergy	Floating	Full scale BBDB	HydroAir concept	2019	Hawaii, USA	500 kW	2.30	[mar17]

Fig. 2.20: OSPREY bottom-standing OWC from [The05]

Fig. 2.21: Pico Plant in the Pico Island of Azores, photo credit *pico-owc.net*

Fig. 2.22: The LIMPET 500 on the Island of Islay from [The05]

Fig. 2.23: The wrecked Oceanlinx off Port Kembla from [Joh15]

Fig. 2.24: The OE buoy floating in Galway bay, photo credit *oceanenergy.ie*

Fig. 2.25: Aerial view of the Mutriku Wave power plant, courtesy of EVE

Fig. 2.26: The caissons of the REWEC3 in the port of Rome, photo credit *duomi.it*

Fig. 2.27: Another OWC project at Sakata port from [Kih+]

Fig. 2.28: The Yongsoo OWC in the western coast of Jeju Island, photo credit *ocean-energy-systems.org*

Fig. 2.29: The Marmok-A-5 spar buoy installed at BiMEP, photo credit *opera-h2020.eu*

Fig. 2.30: The OE buoy construction in Portland shipyard for installation in Hawaii, photo credit *oceanenergy.ie*

2.4.3 Components of OWC systems

This section presents the components of an OWC system: the air turbine, the valves, the electrical generator and the electronic power converter.

1) Air turbines:

The air turbine is a main component of the PTO of an OWC and converts the pneumatic energy gathered inside the chamber into a mechanical rotary one. At first, unidirectional turbines were employed and had to rely on complex rectifying valve systems. This design was suitable for small scale buoys like the Masuda lightning buoy [Fal10], but not suitable for larger devices with higher air flow velocities [FG12]. The specific principle of the OWC implies the use of a self-rectifying air turbine that can rotate in the same direction, and produce a unidirectional torque, regardless the bi-directional airflow. The most common self-rectifying turbines rely on axial airflow. The first self-rectifying air turbine designed for the OWC, the **Wells turbine**, was created by professor Alan Wells from the Queen's University Belfast in 1976. It is the simplest design of that kind of turbine, also the most economic one, and presents a symmetrical blade profile, like the NACA0012. It is the most largely studied and it has been installed in power plants such as the LIMPET [Whi+02], the Pico plant [Fal+19], and the Mutriku OWC plant [Tor+09a]. It relies on a high rotational speed for low air flow velocity and the peak efficiency ranges from 0.5 to 0.8. The major drawback of this turbine is a large efficiency drop above a certain flow coefficient. This effect is the result of blade stall due to a high angle of attack of the relative flow. The flow separation causes an abrupt decrease in performance, noise and undesired fatigue. As a matter of fact, it stimulated research on newer designs. To increase its performance, researchers developed several versions of the Wells turbine such as installing some GV at each side of the rotor as shown in Fig. 2.31, letting the rotor blade tilt a bit to adjust the angle of attack as in the pitching blade Wells turbine. Also setting another stage of blades as in the biplane Wells turbine of the Mutriku OWC plant (see Fig 2.32), or even with contra-rotating rotors as the McCormick turbine built for the OSPREY site [RB96], increases the solidity and thus the performance.
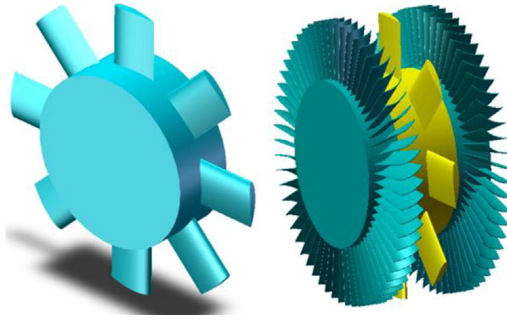
Fig. 2.31: Wells turbines: without and with guide vanes [FHG18]

Fig. 2.32: The Wells turbine of Mutriku #3 (photo taken at the power plant)

Similarly to the pitching blade Wells turbine, the **Dennis-Auld turbine** presents a wider pitching range, so a higher solidity, and an increased efficiency [Lóp+13]. It was developed to be installed in the OceanLinx prototype in Australia [TD03]. The blades are symmetrical in a vertical plane, the leading edge is identical to the trailing edge, and are able to rotate along an axis at the center of the blade. When the air flows in one direction the blade rotates to optimise the angle of attack in function of the air speed and when the flow changes direction, the blade rotates and the trailing edge becomes the leading edge, see Fig. 2.33.

The **impulse air turbine** is an alternative to the Wells and is less present in real applications of OWC systems. Unlike the Wells turbines where the airflow is axial, the impulse type is radial and operates in a larger range of air flow. A schematic view is presented in Fig. 2.34. An interesting concept of impulse turbine is the Variable Radius Turbine (VRT) of the **HydroAir**

Fig. 2.33: The Dennis-Auld turbine with a schematics of the pitching blades at the top, from [TD03]
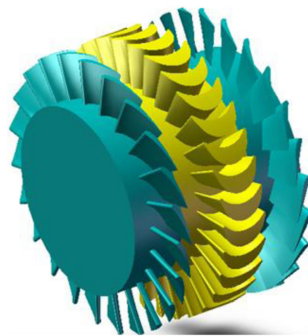
Fig. 2.34: The axial impulse turbine with its guide vanes, #4 has fixed and #5 switching guide vanes

concept by Dresser-Rand with its two ducts looking like a sandglass, see Fig. 2.35. It is equiped with fixed guide vanes at the outer parts with the largest diameter of the ducts and forces the flow to swirl while accelerating. It equipped the Oceanlinx Mk3 deployed in Australia [Dre15]. The most recent, and more compact, version of 500 kW of this HydroAir concept was manufactured to be deployed in the Ocean Energy BBDB device for the future tests in the Wave Energy Test Site (WETS), Hawaii USA [Lai17].

Another concept, developed by the IDMEC/IST Wave Energy Group, is the **biradial turbine** presented in [FGN13]. With a bit of imagination, it is
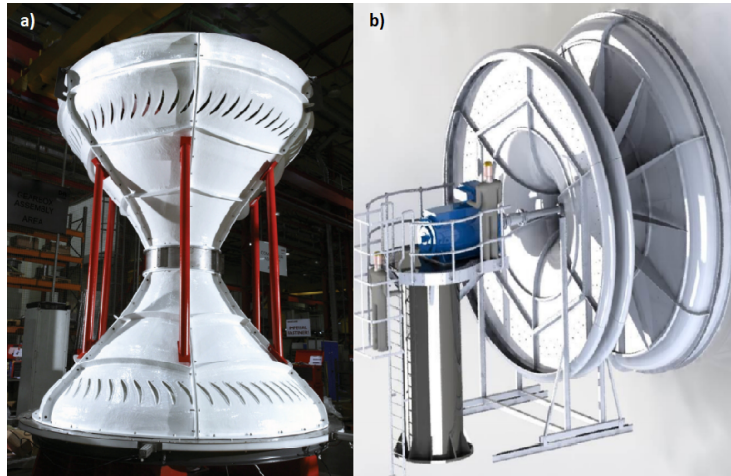
Fig. 2.35: The HydroAir turbine by Dresser-Rand: a) version for the OceanLinx and b) for the OE BBDB [Dre15; Lai17]

similar to the HydroAir but shrinked and lighter. It has a wider operating range and an increased peak efficiency in comparison with the other impulse turbines. A 0.50 m diameter biradial turbine was manufactured by Kymaner and tested in the IST aerodynamic test bench before being installed for one year in one of the chamber of the Mutriku plant in the framework of the OPERA project, see Fig. 2.36. Here it has a conic adapter duct to fit the diameter of the chamber hole.

Fig. 2.36: The biradial turbine installed in the Mutriku OWC plant and a schematic of the turbine with guide vanes at the stator outer rim [Hen+16d]

2) Valves:

Typically, three valve configurations are considered to regulate the pressure in the chamber: a relief valve, a butterfly valve and an high-speed stop valve. The relief valve is mounted in parallel with the turbine and connects the chamber with the outside air at atmospheric pressure, as in the Pico plant [Mon+13]. The butterfly valve, as the one installed in front of each turbine of the Mutriku plant [Tor+09a], is essential to prevent the Wells from stalling. It can be partially closed to reduce the air flow and add pneumatic losses. Both valve systems are especially useful in high energetic sea states to control the turbine rotational speed. The high-speed stop valve is installed in series with the turbine and can be used to perform latching or to prevent green water to reach the turbine. However, in the case of axial turbines the design of such a valve for latching purposes is quite complex due to the large area of the turbine ducts and the actuation times required to close it, typically of the order of 1/10 s. Salter and Taylor [ST96] proposed an adaptation for the axial Wells turbine to close the 1.7 m inlet diameter and has been tested for the Pico plant [HG01]. In the case of the biradial turbine, a sliding mechanism operates the high-speed stop valve for a typical excursion of less than 10 cm [Hen+16a].

3) Generators:

The goal of the generator coupled to the turbine is to transform the rotational mechanical energy into electricity. The turbine operation typically ranges around 500 to 3000 rpm. As a consequence, gearboxes are not necessary in this type of application as it matches conventional generators operation ranges. Gearboxes are not recommended since they increase the risks of failure. O'Sullivan [OL11] compared several generators for OWC applications and rated them according to their efficiency, cost, grid integration capability and suitability to offshore environment. López et al. in [Lóp+13] exposed several PTO components including the power conversion parts and electrical generators. Hodgins' thesis [Hod10] studies the different type of generators for OWC systems, including the power losses and heat transfer. It appears that the most common types of generators for OWC systems are three-phase electrical machines using alternative current (AC) such as:

- the SCIG - Squirrel Cage Induction Generator: it is an induction machine with three copper windings in the rotor and three in the stator. The magnetic field generated in the air gap between them is the origin of the electromotive force. It is necessary to magnetise the windings by injecting current in order to generate that force. This constitutes a consumption of reactive power. It needs to be connected to a full power converter to condition the produced power to the electrical grid requirements. It admits a good ratio of maximal torque versus its nominal torque and thus can absorb high power peaks for a short period of time. It is one of the most robust, simplest and economic type of generator.

- the DFIG - Doubly Fed Induction Generator: it is part of the wound rotor electrical machine family. The name comes from the fact that the current at the stator is directly fed to the grid while the rotor current passes through a back-to-back power converter of about 30 to 40%. It uses slip rings and brushes to extract the rotor current. There are mechanical parts that have to be changed regularly, which is not convenient for remote application in an offshore environment.

- the PMSG - Permanent Magnet Synchronous Generator: it is nowadays the most common generator type for wind turbine applications due to its higher efficiency and the possibility of working at low speeds, avoiding the use of gearboxes. It is self-excited and does not use reactive power to magnetise the rotor windings, because it uses a magnetic material in the rotor. It is more sensitive to temperature and thus admits less peaks of power in comparison with the induction generators because of the risk of demagnetisation of its core. They are also generally more complex mechanically and more expensive. The magnetic material, mainly Neodymium magnets which is a rare earth element, raise the issue of supply and price volatility due to its high demand.

Setting the requirements for the use of a generator in the power conversion equipment of the OWC is relevant to define the challenges of offshore energy production. The choice of a generator is motivated by both environmental and electrical conditions. In terms of environmental aspects, the high motion amplitude of a buoy during storms can cause mechanical stresses leading to shaft misalignment (important axial and radial forces), unbalance, and a reduction of the air gap between the rotor and the stator for all the generator

types. The generator's lifetime and performance may be reduced because cracks can appear in the magnetic core in the case of the PMSG. The cost associated to replace the magnets has to be taken into account in the selection of a generator. Because of the high salinity of the offshore environment, corrosion issues have to be monitored. In the case of axial flow turbines like the Wells for example, the generator is directly situated in the air flow where there is a high level of humidity and important concentration of salt (salty water vaporisation) as can attest the picture of a 18.5 kW generator taken at Mutriku in Fig. 2.37. This would require the use of special coating to prevent the rust from corroding the metal frame. To remove salt deposition in the most exposed parts of the PTO components, each turbo-gen set of the Mutriku OWC plant is equipped with a fresh water cleaning system vaporising water regularly.

Fig. 2.37: Picture of the corrosion around a generator frame at Mutriku

Concerning the electrical aspects, a generator is subjected to losses that are mostly related to the conductive material that are employed, copper losses, the iron core losses and mechanical losses due to bearing frictions (see Fig. 2.38). The quantification of these losses will be detailed in Section 4.18. The performance of a generator is tightened to these losses especially at partial load. The sizing and selection of the generator has to be carefully advised and the control of the system adapted to avoid low efficiency regimes. During low and regular/normal energetic sea states the production tends to be maximised by the control strategy. Still some power peaks provided by the turbine can be transmitted to the generator depending on the control algorithm employed. At high energetic sea states it is most likely that these

peaks overshoot the generator rated power causing an overcurrent and an abnormal temperature raise. The thermal behaviour of the generator has to be carefully studied because if not controlled, an excessive temperature can melt coil insulation of the windings and provoke a shortcut between two phases. The supervisory control has to avoid this operating range and the generator requires an effective cooling system.
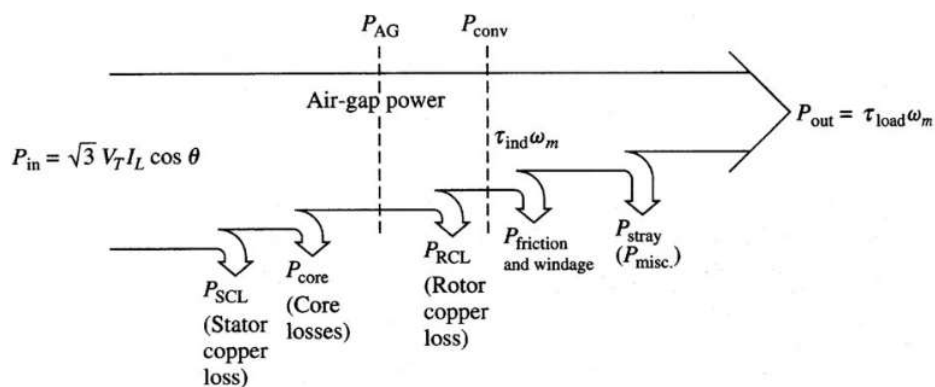
Fig. 2.38: Power losses in electrical machines

Tedeschi [Ted+11b] studied the influence of the power conversion losses. It is clear that the performance of the generator and the power converter rapidly decreases below a 50% load factor. The author developed a comparison between passive loading and optimum control in order to highlight the effect of the electrical components. Although the study was applied to a point absorber with a mechanical PTO, the conclusions can be adapted to the case of the OWC. When considering the losses and saturation due to the generator and power electronics, it is said that passive loading results in a higher average power generation and even lower requirements in the power equipment. Clearly, the research of an optimum control solution should consider the WEC as a full system equipped with electrical parts.

4) Electronic power converters:

The power converter is the electrical equipment in the power conversion chain that isolates the production unit and the electrical grid. It is often called a Back-to-Back (B2B) converter because it consists in two power converters sharing the same DC bus. Both parts are composed of electronic transistors, mainly IGBTs (Insulated-Gate Bipolar Transistors) and Pulse Width Modulation (PWM). In the rectifier, when switching the controlled gate at very high frequency, they transform the current alternative wave forms from the generator into direct current - AC to DC - and vice versa for the inverter. The three main sections are detailed below and illustrated in Fig. 2.39:

- The generator side converter converts the power of the generator from AC to DC. It hosts the generator side controller that follows the reference torque/speed of the generator.

- The DC bus decouples the generation unit and the grid with its capacitor.

- The grid side converter converts the power in the bus from DC to AC. It hosts the grid side controller that keep stable the voltage of the DC bus, and conditions the power to fit the grid requirements in terms of voltage and frequency.
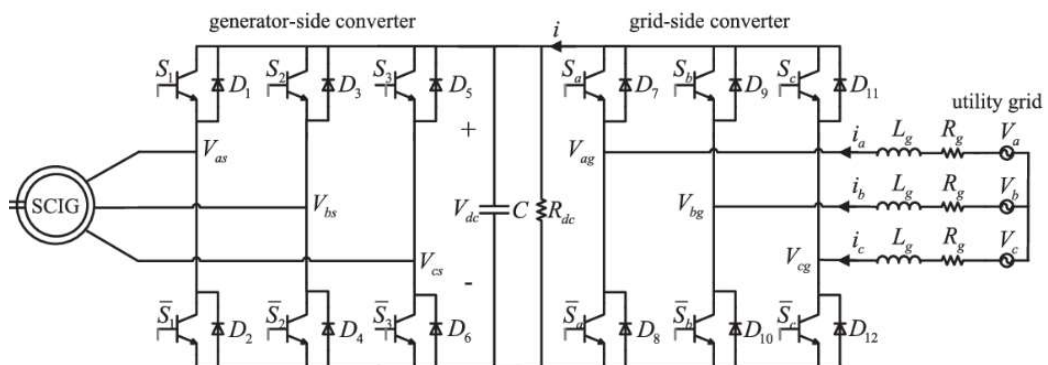
Fig. 2.39: Schematic of a power conversion chain with an SCIG and a B2B converter [KA14]

2.5 Chapter conclusion

The power concentrated in ocean waves has always fascinating men and women. This chapter illustrated that by evoking the pioneers of the wave energy conversion who invented, and even built prototypes, the early WEC concepts. A scientific approach to ocean waves is also described to understand this type of energy and how it can be modelled numerically. Then several WEC concepts associated to their PTO systems are mentioned followed by the OWC systems that were built until now. Finally, this section discussed the main components of the PTO system in an OWC plant. They are the several equipment parts to consider, including there restrictions, to capture all the energy conversion phases and control the power extraction.

State of the art

<div style="text-align:right">3</div>

> *The breaking of a wave cannot explain the whole sea*

— **Vladimir Nabokov**
Russian writer 1899-1977

Summary: In line with the thesis objectives, a state of the art has to be performed to detect the gaps left aside by existing works. This section focuses on reviewing three aspects of wave energy conversion. First a brief review of numerical modelling approaches of WECs is made, covering mainly the hydrodynamic issues and detailing their motion due to sea waves. Then the focus is made on modelling techniques of OWC systems including the hydrodynamics in the frequency and time domains, the modelling of the air chamber and the PTO components. Finally, a review of control strategies in all the energy conversion steps is performed. First general considerations are made for WECs, and then specifics of control for OWC systems are highlighted.

3.1 Review of WEC hydrodynamics modelling

Scientific considerations and interests for wave energy conversion started to become more and more relevant after the 1973 oil crisis. A research community began to arise with the 'fathers' of the modern wave energy conversion. They stated the necessity to develop WEC W2W models to describe devices' motion and their capacity to capture wave energy. As early as 1974, Salter [Sal74] presented what will be later called the Salter's duck, a pitching floater capable of converting wave power into mechanical power. It started a new era of scientific developments for the sector. Budal and Falnes [BF77] from Norway, followed by French [Fre79] in England, discovered that resonant point absorbers would be capable of absorbing a significant amount of power from the waves. The Norwegian scientists started to develop one of the firsts simple linear numerical models of a heaving point absorber controlled through latching [Bud82], already setting the requirement of prediction of incoming waves for optimal power absorption. The models did take into account all the components of the PTO system. In the reference book *Ocean Waves and Oscillating systems*, Falnes presented a detailed approach on wave power extraction covering all the linear wave theory for modelling W2W systems [Fal02b]. Many concepts of the following sections are inspired from this book.

3.1.1 Equation of motion of a WEC

Structures moving in the water are subjected to hydrostatic and hydrodynamic effects and can be considered as mechanical oscillating bodies. In order to describe their motion, the Cummin's equation – derived from Newton's 2nd law – applies. For the specific application of wave energy conversion of a single-body point absorber, being $\ddot{z}$ its heave acceleration, the equation of motion is:

$$M\,\ddot{z} = F_{\text{exc}} - F_{\text{rad}} - F_{\text{hyd}} - F_{\text{PTO}} - F_{\text{others}} \tag{3.1}$$

Where M is the mass of the floating body. The excitation force F_{exc} is the force exerted by an incoming wave on the floating body forced to stay in a fixed position. F_{rad} is the radiation force due to the proper buoy's motion on a still water surface (without waves). The typical illustration of this force is

the concentric circles created by a floater that oscillates in the water. The hydrostatic force is noted F_{hyd}. It is the force proportional to the buoy's position and the hydrostatic stiffness. It is mechanically equivalent to a spring where the force increases when the structure is moved away from its equilibrium position. The PTO force is the one applied by the PTO system to extract energy. Finally, the WEC is subjected to other non-linear forces like viscous and drag forces and the one related to the mooring lines.

A simple linear model can be defined in the Frequency Domain (FD) over a set of frequencies ω for linear forces, to calculate the WEC heave motion: its position z, velocity $\dot{z}$, and acceleration $\ddot{z}$.

$$M \, \ddot{z}(\omega) = F_{\text{exc}}(\omega) - \underbrace{A(\omega) \, \ddot{z}(\omega) - B(\omega) \, \dot{z}(\omega)}_{F_{\text{rad}}(\omega)} - \underbrace{K_{\text{H}} \, z(\omega)}_{F_{\text{hyd}}(\omega)}$$
$$- \underbrace{C_{\text{PTO}} \, \dot{z}(\omega) - K_{\text{PTO}} \, z(\omega)}_{F_{\text{PTO}}(\omega)} \quad (3.2)$$

Which gives, after reordering, the following differential equation describing the device motion:

$$\ddot{z}(\omega) = \frac{F_{\text{exc}}(\omega) - \left(B(\omega) + C_{\text{PTO}}\right) \dot{z}(\omega) - \left(K_{\text{H}} + K_{\text{PTO}}\right) z(\omega)}{M + A(\omega)} \quad (3.3)$$

being the hydrodynamic coefficients of $A(\omega)$, the added mass (or inertial component), and $B(\omega)$, the radiation damping. The excitation force is also characterised by frequency components with magnitude and phase responses upon incident waves. This will be explained in the next section 3.1.2 with the time domain model analysis. These frequency coefficients are obtained using a hydrodynamic solver based on potential flow theory and Boundary Element Method (BEM) codes, such as WAMIT [WAM16], ANSYS AQWA [ANS19] or NEMOH [Nan19; PG16]. An example is illustrated in Section 4.2.1 where the FD analysis is detailed for the Mutriku OWC plant. As a result of the FD analysis, the WEC motion subjected to all the forces can be expressed in a Response Amplitude Operator (RAO).

Finally, the PTO force is the one that allows the device to extract the useful energy from the waves. It has a damping coefficient C_{PTO} and a PTO stiffness K_{PTO}. These are the parameters to control and maximise the output power of the WEC. While the amplitude control is provided by the C_{PTO} coefficient, the phase control is achieved with the K_{PTO} one. Not all the PTO types include

both parameters. Although, it is the case of rigid PTOs such as mechanical or hydraulic PTOs, the OWC only relies on a PTO damping for wave energy extraction.

3.1.2 W2W time domain model

A Time Domain (TD) model is employed to further detail the W2W numerical model. This is more complete than the FD model because it can include the non-linear forces exerted on the WEC, especially the PTO force which converts the energy captured into useful energy. Let us now consider Eq. (3.2) expressed in time domain:

$$
M\,\ddot{z}(t) = \underbrace{\sum_{i=1}^{N}\Big(\Gamma_i(\omega)\,a_i(\omega)\,cos(\omega t + \varphi_i + \epsilon_i(\omega))\Big)}_{F_{\text{exc}}(t)}
$$

$$
\underbrace{-A_\infty\,\ddot{z}(t) - \int_0^t K(t-\tau)\,\dot{z}(t)\mathrm{d}\tau}_{F_{\text{rad}}(t)} \underbrace{-\rho g S\,z(t)}_{F_{\text{hyd}}(t)} - F_{\text{PTO}} \quad (3.4)
$$

The excitation force is expressed as the sum of the N wave components of the incident wave elevation as in (2.8) knowing for each frequency the wave amplitudes a_i and phases φ_i, and given the excitation amplitudes Γ and phases ϵ.

The radiation response is composed of the added mass at infinity A_∞ and the convolution integral expressed with the radiation impulse function $K(t)$. To solve this in TD, a frequency identification is necessary. There are several methods to do so, being the most popular ones the PRONY method [R P95; DCC01] or the Frequency Domain Identification (FDI) [PF07]. Both are valid for the approximation of the radiation force, and their use is illustrated in Chapter 4 for different OWC devices.

The PRONY method approximates the radiation term with the coefficients α and β, representing the matrices of the complex radiation approximation coefficients:

$$
K(t) \approx \sum_{i=1}^{N}\alpha_i\,exp(\beta_i t) \quad (3.5)
$$

The convolution integral function can therefore be approximated by $\sum_{i=1}^{N} I_i$ and mathematically solved by the differential equation:

$$\dot{I}_i = \beta_i I_i + \alpha_i \dot{z} \tag{3.6}$$

The FDI method consists in a state-space approach to approximate the radiation term. Let us consider:

$$R = \int_0^t K(t-\tau)\,\dot{z}(t)\mathrm{d}\tau \tag{3.7}$$

Using the transfer function:

$$K(s) \approx \frac{P(s)}{Q(s)} = \frac{p_r s^r + p_{r-1} s^{r-1} + ... + p_0}{s^n + q_{n-1} s^{n-1} + ... + q_0} \tag{3.8}$$

The complex polynomials P and Q are defined by fitting the continuous transfer function to a frequency domain response. The transfer function is then associated to a state-space system defined as:

$$\begin{aligned} \dot{X} &= A_{\mathrm{r}} X + B_{\mathrm{r}} \dot{z}(t) \\ R &= C_{\mathrm{r}} X + D_{\mathrm{r}} \dot{z}(t) \end{aligned} \tag{3.9}$$

The parameters $A_{\mathrm{r,mxm}}$, $B_{\mathrm{r,mxn}}$ and $C_{\mathrm{r,mxm}}$ ($D_{\mathrm{r,mxn}} = 0$) are state-space matrices corresponding to the transfer function $K(s)$. They are defined by the FDI method with a m-degree of approximation of the radiation terms and for $n = 1$, the order of the state input of the heave velocity $\dot{z}$. The convolution problem resolution can be included in an extended state-space for simulation purposes. This extended system describes all the system dynamics.

3.2 Review of W2W modelling for OWC systems

As commented above, numerical models in the frequency domain solve a set of differential equations describing the hydrodynamic motion of the structure and the water column. Complete W2W time domain models are more complex and should also include the non-linear effects of the various steps of energy conversion:

- The dynamics of the air chamber, including air compressibility models;

- The aerodynamic conversion through the air turbine;
- The electrical conversion via the electrical generator and power electronics;
- The algorithm to control the energy conversion.

Also, sometimes numerical models include other existing non-linear forces damping the device motion. It is the case of the viscous drag forces of the structure or the mooring lines forces but whose coefficients are challenging to obtain. Indeed, they may need experimental scale tests to be estimated.

Full or partial W2W models of shoreline OWC devices are well represented in the literature. The Queen University of Belfast published the design process of the device installed in the Isle of Islay. Curran et al. [CWS98] focused on the aerodynamic conversion where the optimisation of the absorbed power supported the sizing of the PTO. The maximum absorbed power is obtained varying the damping induced by the turbine during scaled tank testing at $1/40^{th}$. The process included the optimal selection of the turbine diameter, solidity and rotational speed by an iterative process. They concluded that the plant, taking into account the pneumatic power optimised by the best turbine characteristics, would have an electrical output of 500 kW by two equal units of 250 kW. These conclusions were too ambitious and the plant had to be downsized to one unit of 250 kW as it was producing below its rated capacity [Whi+02; Del+15]. The depreciation of the pneumatic power also penalised the electrical conversion as it was producing in regions where the generator had higher losses. Sea trials showed that the models did not take into account non-linear effects of wave theory in shallow water. Also, additional turbine losses appeared in real seas. They were not foreseen during the dry testing where the turbine was subjected to unidirectional flow whereas in real operation oscillating flow is witnessed.

Another well studied device is the Pico plant where many research works were produced by prof. Falcão and his team from Portugal. He brought details on the design of the plant and the choice of a PTO rated at 400 kW [Fal00]. This choice was justified by tank testing and PTO optimisation using numerical model simulations. The results highlighted a plant rated pneumatic power of 700 kW. Falcão and Justino discussed the spring-like effect produced by the air compressed in the chamber in W2W models in [FJ99]. They concluded that this non-linearity had strong incidence on the absorbed power and should be included in time domain models for a

better approximation. A hydrodynamic study of the plant based on a 3D radiation-diffraction BEM and including the complex topography of the site was made by Brito-Melo et al. [Bri+01]. The paper shows the hydrodynamic coefficients of the plant and the effect of varying the bathymetry and the shape of the coastline. The authors alerted on the necessity for FD and TD numerical models to include the bathymetry and nearby coastline in the hydrodynamic analysis. No study on the energy conversion by the PTO was done in this work. Here, the authors resulted in an electrical nominal capacity of 115 kW. A more advanced methodology for modelling shoreline OWC is made by Josset and Clément in [JC07], and applied to the Pico plant. It shows the coupling of the hydrodynamic model of the outside flow potential with the aerodynamics of the internal air flow variation. Including this coupling in the time domain model offered a way to take into account the non-linear effects of both the air compressibility and the turbine on the pressure inside the chamber. The authors estimated a mean annual pneumatic power to 67 kW. This shows a strong disparity in comparison with the initial design of 700 kW which was beased on studies made 20 years earlier. Sea trials experience was collected by Monk et al. in [MWL18]. The study concluded that the plant was oversized when analysing the actual power production. The model developed here used a flow variation method and was calibrated with experimental data. The performance curves of the turbine from the dry testing experiment prior the installation and the operational results were compared. The real mechanical power was half the expected one. The model was finally validated with operational data readjusting the turbine theoretical curves. The adjusted model was used to design a passive valve system which resulted in a gain of power production of 30%.

In what concerns the Mutriku OWC plant, very little scientific work is publicly available. This may be due to its commercial application as it was developed by a company named Wavegen. However, theoretical developments giving indication on the PTO sizing are published by Tease et al. [TLH07] and Heath [Hea07].

Apart from these fixed-structure OWC, floating ones with 2 degrees of freedom or more have also presented some interests in the literature. Alves et al. [Alv+11] demonstrated that the method used to develop the radiation estimation of the TD model was accurate when compared with the FD model for a floating theoretical OWC of cylinder shape. The authors relied on the approach consisting in describing the OWC motion with the Cummins'

equation. The radiation problem was approximated by the FDI method. The air compressibility model used an ideal gas under an isentropic process and variations of air density in the computation of the pressure variations. The PTO included a Wells turbine, the model of a relief valve and the generator. Although the generator torque and its losses are mentioned, the paper lacks a mathematical formulation of the electrical energy conversion. The paper highlights though the device motion validation between the TD - in free dynamics (without PTO force) - and the FD models. The TD W2W model is simulated in regular waves for a set of wave frequencies, and the position and velocity are obtained for both bodies. Only the cylinder motion is compared against the FD model and it shows good agreement. The paper could have revealed the following conversion steps including the pressure variations in the air chamber and PTO behaviour. Indeed, the mathematical equations are given but no results on the power produced is made.

The floating sparbuoy developed by the Instituto Superior Tecnico in Portugal is studied in [Gom+12], and used to optimise the shape of the device. The same kind of model was used to develop more advanced control strategies for better power performance by Henriques et al. [Hen+12b]. The sparbuoy was further used by Falcão et al. in [Fal+14] in a stochastic model to support the selection of air turbines in a wave-to-mechanical model. Stochastic models are well suited when applied to linear models or when non-linearities are linearised. For example, here it is done for non-linear turbines. In [Hen+16c], Henriques et al. presented a more complete model of the sparbuoy from the wave power to the electrical power of the generator. The Cummin's equations are solved for the relative motion of the 2-body device (structure and internal water surface), the radiation problem was solved by the FDI method and isentropic air chamber model was used. The non-linear biradial turbine was also modelled and the electrical power was obtained after applying several variable speed control laws. Nonetheless no generator losses were considered.

Another floating time domain model is presented by Bailey et al. [BRB16] to describe the BBDB of Ocean Energy. The development included the computation of the frequency dependant hydrodynamic parameters using the solver WAMIT. The Cummin's equation is used to describe the motion of the structure and the internal water surface, each in three degrees of freedom of heave, surge and pitch. In addition to previous publications, in this review the balance of forces included the forces exerted by the mooring lines and the

viscous drag forces of the structure against the water. The air chamber model followed the isentropic assumptions of air as an ideal gas. It used the biradial impulse turbine for the aerodynamic conversion and an optimisation of the turbine size and rotational speed was also included. An electrical efficiency comprising both the generator and the power converter was considered by a very simple interpolation of 3 points at 2, 20 and 100% of the rated power and no overload was allowed. The control strategy used was a simple fixed speed law based on the optimum speed defined during the turbine sizing.

A partial W2W model was used by Ceballos et al. [Ceb+13; Ceb+15] for the development of advanced control strategies for increasing the performance of the Wells turbine. The authors relied on pneumatic power profiles obtained in tank testing with a certain induced damping represented by an orifice in the scaled physical model. While the model did not take many considerations on the hydrodynamic part, it focused more on a detailed electrical conversion, the development of control strategies and their validation on a dry test rig.

Also, there are works that used partial models assumed they describe the Mutriku OWC plant for the development of control strategies to a Wells turbine coupled to a DFIG [Amu+10a; Amu+10b; Alb+11a]. The choice of the electrical conversion was done for research purposes as it is not the installed configuration in the plant. Although the controllers allowed to avoid stall behaviour of the turbine and improve its efficiency, the model did not include the hydrodynamics of the plant meaning that the effect of the control on the internal pressure and the device motion are not explored. The pneumatic power was simply obtained by generating a sinusoidal regular wave form of the pressure drop which is far from realistic conditions. Although more centered into electrical aspects and grid integration issues, Alberdi et al. used the same approach in [Alb+11a; Alb+11c; Alb+11b; Alb+12b]. The main drawback of such pneumatic-to-wire models is that they cannot take into account the effect of the control, i.e. change of turbine speed, on the pressure of the air inside the chamber and thus neither on the hydrodynamics. The lack of inter-relation between the hydrodynamics, aerodynamics and effect of control can bring to inaccurate conclusions in comparison with full W2W models.

An attempt to develop a more accurate model of the Mutriku OWC plant based on operational values coupled with wave data resource is presented in [Gar+15]. Although it is said that the 20 min average pressures are

similar between the real and theoretical pressure drop, the time series of the pressure drop do not coincide in instantaneous values because of the smoothing effect of the approach. The model needs improvement to better represent the fast changes and all the dynamics of the real plant that is a very complex system where linear water wave theory hardly applies in a shallow water OWC plant.

Concerning PTO systems, Setogushi and Takao [ST06] reviewed the performance of the existing self-rectifying turbines available at that time: Wells and axial impulse turbines with and without guided vanes, the biplane Wells turbine, turbines equipped with self-pitched-controlled blades and the contra-rotating versions of each. In addition, a complete review about air turbines for OWCs is made by Falcão and Gato [FG12], and an extensive review of OWC devices and air turbines is presented in [FH16]. Pereiras et al. analysed the differences of an axial and a radial flow impulse turbines [Per+15]. The optimal sizing of the turbines and the control algotihm permitted to reach the maximum theoretical mean aerodynamic efficiency in both cases which rounded 45% for the axial impulse turbine and 35% for the radial impulse one.

The aerodynamic characteristics of the turbines used in the models can be represented by the relation $\Phi = f(\Psi)$, $\Pi = f(\Psi)$ and $\eta_t = f(\Psi)$ with Ψ the dimensionless pressure head, Φ the dimensionless flow coefficient, Π the dimensionless power coefficient and η_t the aerodynamic efficiency.

In order to understand the different performance of turbines, a selection of 6 turbines is made and their characteristics are compared. They consist of 3 Wells and 3 impulse type turbines:

- 1 - Monoplane Wells turbine without guide vanes c.f. Fig. 2.31, curves are taken from [FHG18].

- 2 - Monoplane Wells turbine with guide vanes c.f. Fig. 2.31, curves are taken from [FHG18].

- 3 - Biplane Wells turbine installed in Mutriku c.f. Fig. 2.32, curves are taken from [TLH07].

- 4 - Axial impulse turbine with fixed guide vanes c.f. Fig. 2.34, curves are taken from [FHG18].

- 5 - Axial impulse turbine with movable guide vanes c.f. Fig. 2.34, curves are taken from [FHG18].

- 6 - Biradial impulse turbine with guide vanes c.f. Fig. 2.36, curves are taken from [Gat+17] and performance were obtained testing the 0.5m diameter turbine built for OPERA in IST aerodynamic test rig.

Their aerodynamic characteristics of dimensionless flow rate versus normalised pressure head are plotted in Fig. 3.1. One can observe that Wells turbines have a linear relation whereas the impulse ones are non-linear. Moreover, the Wells relies on low pressure high flow rate, being the contrary for the impulse turbines. The efficiency curves in function of the normalised pressure head offers a clear way to compare their performance, see Fig. 3.2. Although they are quite alike in terms of blade profile and solidity, the Wells #2 shows a greater peak efficiency than the #1. This better performance is made possible by the installation of the guide vanes that orientate the flow in the blades at a better angle of attack. The counterpart is that the stall appears at pressure head lower for #2 when compared with #1. Turbine #3, the biplane Wells turbine, highlights poorer efficiencies than the other Wells. This may be due to the fact that the flow between the first and the second stage of rotors is more turbulent than the monoplane turbines. Another reason is that the curves can be more realistic because obtained experimentally whereas it is not the case of the turbine #1 and #2. In what concerns the impulse turbines, they do not present stall and thus can operate in a wider range of pressure head and higher energetic sea states. There is an obvious gain of performance of the turbine #5 over #4. The guide vanes can be controlled so the airflow is always optimal to the blades. The main drawback is the need for an actuator and many moveable pieces which represents a higher risk of failure in the long term. The turbine #6 does not present this drawback and thanks to its unique design presents the higher performance when compared with the other impulse turbines.

O'Sullivan and Lewis [OL11] reviewed electrical generator technologies for the use in OWC systems. Tedeschi and Molinas [TM10; TM12a] studied the effect of various controller strategies on the sizing of PTO components for a generic WEC. The model did include consideration for the electrical
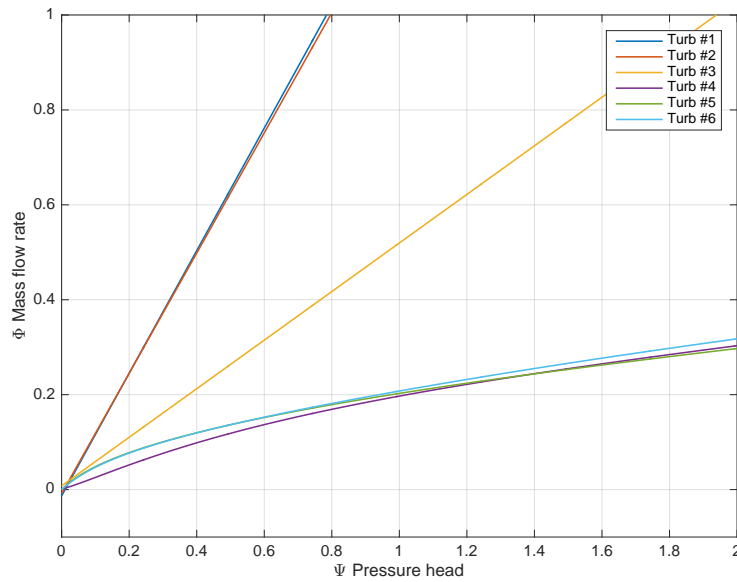
Fig. 3.1: Compared dimensionless pressure-flow characteristics of the six turbines, adapted from [FHG18; TLH07; Gat+17].
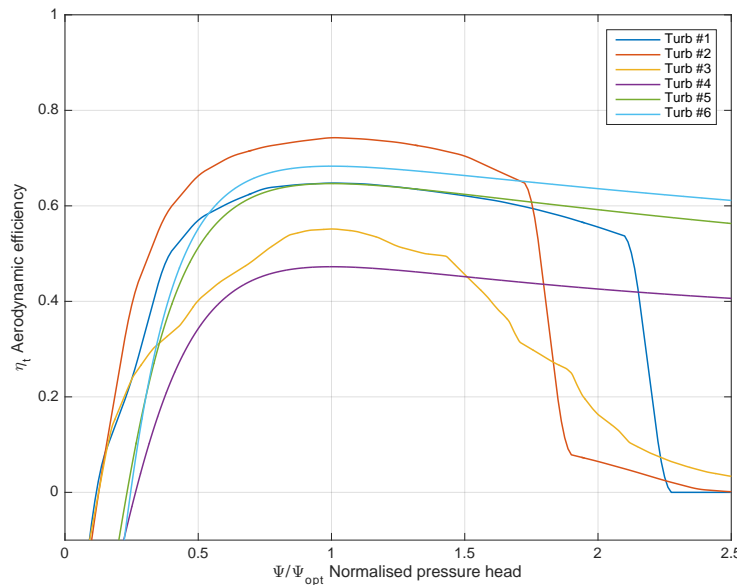
Fig. 3.2: Compared efficiency of the six turbines versus normalised flow rate coefficient, adapted from [FHG18; TLH07; Gat+17].

generator even if it was represented as simplified efficiency curve. Apart form these works and as far as the author knows, there are no works in the literature that include generator losses in OWC application and even less in full W2W models.

A methodology developed by Henriques et al. in [Hen+16d] defines the design process of a OWC project. It includes three main phases: the preliminary design, the detailed design, and model testing. The development

and validation of an accurate W2W numerical model takes place in the preliminary phase. As it was seen before, numerical models can support the choice and selection of the main PTO components and can result in oversized systems. This phase is therefore crucial and should draw specific attention at the begining of an OWC project.

3.3 Review of control strategies for wave energy systems

3.3.1 Generalities about WEC control

The energy concentrated in ocean waves represents a considerable potential that justifies the need to investigate a way to harvest it [Mor+10]. Many concepts have been formulated and the large number of developed devices attests the motivation for this topic. As it is often the case in relatively recent research fields, some developments were unable to prove the viability and cost effectiveness of their designs. In order to accelerate the technology development, device developers have to find cost-effective and robust solutions to achieve competitiveness. PTO tuning and control can result in significant increases in energy production. Indeed, as exposed by [BF77], optimum control aims to maximise the power absorption by acting on the device motion in order to force resonance between the WEC structure and the incoming waves. For a point absorber oscillating as a mechanical body due to a regular excitation force, one can easily understand that by tuning the PTO, it is possible to match the phase between the excitation and the body velocity. It results an amplification of the motion and a substantial amount of power can be extracted.

Theoretically, this tuning is described in the literature as 'impedance matching' (when referring to an electric equivalent circuit in general), or 'complex conjugate control'. The controllable PTO force has to fit the optimal phase and the amplitude conditions of the hydrodynamic forces acting on the device, adapting the PTO components K_{PTO} and C_{PTO}. From a conceptual point of view it results in a series of engineering issues [RBF14a]:

- Although the energy absorption is maximised in monochromatic waves, it is actually frequency dependant so the PTO tuning is sub-optimal in irregular waves.

- This scheme requires excitation force prediction (non-causal function) and this leads to uncertain and inaccurate solutions.

- The system becomes more complex since it requires a PTO able to supply energy to act on the WEC motion, equivalent to reactive power. That is why this type of strategy is often called reactive control. In practice, the gain in performance in reactive phase control are smaller since there is significant energy loss by dissipation inherent to the back-and-forth energy exchange. In most cases, this exchanged energy can have an order of magnitude similar to the mean absorbed energy.

- This approach does not take into account the design limitations of the PTO components or even the structural constraints of the WEC.

The most promising phase control strategy is known as latching. It is a more practical approach as it does not imply a bi-directional energy flow. The latching control technique, first proposed by Falnes and Budal [FB78] for single body systems, consists in locking the body so it is motionless and releasing it to force the velocity to become in phase with the excitation force when the WEC is unlatch. A significant increase in power extraction can be achieved when compared to a non-controlled case as proposed by French [Fre79]. This strategy can be adapted to the relative motion of two-body systems, using the relative velocity as a reference. Babarit and Clément [BC06] presented a study of latching implementation for a heaving point absorbers in irregular waves .

Other advanced (adaptive) control strategies have been applied to wave energy conversion to overcome some practical issues previously exposed. The idea is to provide optimal energy absorption by involving wave force prediction and the handling of physical constraints. A comparison of several adaptive control strategies for real-time control is done by Hals et al. [HFM11] and include: resistive loading, complex-conjugate, optimal velocity tracking, model predictive control (MPC), latching and clutching. The MPC strategy was the most efficient. Its advantage is the ability to maximise the energy absorption over a finite receding horizon while taking into account

physical limitations (i.e. device motion and PTO force) and introducing model-based predictive controllers. Another strategy based on MPC was developed by Cretel in [Cre10], as an application of this controller for a single body WEC. The study highlights that the maximum theoretical energy extraction was reached for an ideal unconstrained case with regular waves. The control showed extreme power flow values in irregular waves. This was then improved by penalising the aggressiveness of the control and offered a more suitable approach for practical application. Ringwood et al. [RBF14b] give a detailed review of control for the general field of wave energy conversion, including farm control and wave prediction.

3.3.2 Control of an OWC

Most of the previous studies focused on heaving bodies and implemented a theoretical approach to WEC control. The main reason to control is to assure the safe operation of the device while optimising the absorption of wave energy and maximising the generated electrical power. Controlling the electrical output also provides an acceptable quality of power sent to the grid. This is why the control framework must include every different stages of energy conversion. Among all the research areas designated to reduce the cost of electrical production from wave energy sources, the discipline of control theory focuses on optimising the energy production. In the meantime, it requires very little additional investments apart from the additional sensors, the process instrumentation and the control unit. The interest given to the OWC technology resulted in a number of publications oriented to its control and gathered in a number of review publications [Del+15; OA17]. The following subsections present a collection of the control strategies studied so far to ensure the optimisation of power production in OWC systems with three main approaches:

- To maximise the power captures between the waves and the structure
- To optimise the power production from the captured energy to the electrical useful one through the PTO
- To condition the power for better grid integration

Maximising power absorption

Basically, tuning the hydrodynamic parameters of the device changes its response to the wave excitation. In order to maximise power absorption, it is necessary to create a resonant condition in the buoy oscillation by controlling its motion. The two main approaches are the average sea state control and the wave-by-wave control, referred as slow tuning and fast tuning respectively. A wave-by-wave control is most efficient as it changes the buoy response to match the characteristics of the incoming waves (response in seconds), while the other applies for the average sea state which varies in dozens of minutes or hours. In the following sub-sections, the WEC motion control is introduced as well as the issues related to latching control and also the contribution of control in device survivability.

Device motion control:

For the case of the OWC, the most common way to match the phase of the buoy velocity with the excitation force is by implementing a latching control strategy. The device motion is adapted by opening or closing an high-speed stop valve blocking the air flow. The sudden change in pressure can therefore tune the velocity of the oscillating bodies. Hoskin et al. [HN86] were the first to consider phase control for an OWC system explaining the existence of an optimal solution when tuning only a damping coefficient as a proportional gain applied to the device velocity. But at that time in 1986, the means at the researchers disposal could not lead to accurate studies. Mathematical development concerning a fixed OWC was made for the first time by Nichols et al. [Nic96]. In this research, optimal control techniques based on the projected gradient method were used for several strategies (pressure difference, flow rate and relief valve) to maximise the energy produced by the turbine. They used the Pontryagin's Maximum Principle (PMP) in three control strategies. A pressure difference control was developed actuated by a stop valve affecting turbine power. The control variable for this valve is inside [0,1] representing the fast switch of the valve position (open/close). This is the definition of a bang-bang control. When the valve is opened, the turbine produces energy normally; otherwise the turbine stops producing power while the pressure increases. The optimal moment to open the valve, or unlatch, is decided by the control algorithm. Reactive control was also achieved by controlling the flow rate across the turbine and pumping energy from the system during some parts of the wave cycle. Numerical

results were obtained with a simplified model approximating the Pico plant applying optimal control to a simplified PTO model. Improvements were seen to be within few percent to 35%. It arose phenomena to be taken into account but leading to unrealistic applications: chattering in valve operation, turbine acting as a compressor, the constrained pressure control was getting closer to the uncontrolled case while reducing the critical pressure.

An air flow control was then implemented by Falcão and Justino [FJ99] in a more complex numerical model of the plant including air compressibility, equivalent to a spring-like effect of the air chamber. Both the by-pass valve and series throttle valve were investigated and the effect on the production analysed for various turbine dampings. The benefits were quite substantial especially in avoiding the stalling behaviour of the Wells turbine. Falcão [FR02] developed a stochastic modelling approach for the optimisation of the plant performance of the fixed OWC at the Pico Island. It was equipped with a Wells turbine and simulations were performed for a variety of realistic sea states. The aim was to optimise the turbine diameter and its optimal constant rotational speed that maximised the annual plant average efficiency with and without air flow control. The best improvement in terms of performance was obtained when optimising the turbine speed under flow control.

Nunes et al. [Nun+11] proposed to control the pitch angle of the Wells turbine's blades to acheive the phase and amplitude conditions. An additional variable in the mass flow equation representing the pitch angle is included. The reference was followed by a simple PID in the implementation. It was found that for regular waves the energy was more than three times higher compared to a non-controlled case. However the study concluded that is was impractical to apply it for irregular waves. This approach is not advised in practice as self-rectifying air turbines are not designed to operate as compressors. Also, the low reliability of such pitching blades makes the approach not suitable as it increases the risk of failures. A relief valve control was developed to avoid reaching the turbine maximal speed.

The experimental work presented by Lopes et al. in [Lop+09] presents the benefits of latching using a shut-off valve in series with the turbine and applied to a fixed OWC. Several unlatching times were tested with thresholds set when the value of the excitation force crosses the zero value. The estimation of this excitation force was done with measurements of the wave elevation close to the device. The wave excitation power dissipated

by the PTO, the viscous losses and the radiation damping was measured with and without latching. The result shows a clear increase of the absorbed power by a factor of 2.5. This control strategy was inspired by a similar zero-crossing threshold method was used in [Fal08] for the definition of the unlatching moments in hydraulic PTO.

Lately, research on latching control for the sparbuoy OWC was performed by Henriques et al. The article presented in [Hen+14] is an extended work of [Hen+12a] adding the case of irregular waves. Two latching strategies were considered for the stop valve operation: one tracking the zero-crossings of the excitation force and the other based on the measurement of the internal pressure and the turbine speed. For the first one, the computation burden of the excitation force estimation was avoided by predicting the wave elevation for the next zero-crossing of the excitation force. The captured energy was enhanced around 25% for most of the tested sea conditions. The second strategy avoided the use of prediction by measuring the chamber pressure and the turbine rotational speed. It is a more practical solution since these quantities are easily accessible with sensors but, on the other hand, it is less efficient (around 10-15% increase). Also the issues revealed in [Lop+09], regarding the effect of air burst in the pressure measurements, limit this strategy. The authors included model prediction combined to the PMP to further develop latching using the biradial turbine in the sparbuoy in [Hen+16a].

Issues related to latching control:

Based on the bibliographical study, it appears that phase control in a floating OWC results in a significant improvement in the power capture. However, one should be aware of certain side effects of latching for practical applications. As this strategy intends to reproduce resonant condition, the motion of the device, the pressure and the forces are amplified. The risks related are the slamming produced when the buoy jumps out of the water and hits the water surface, as well as higher stress on the moorings. Additionally, the water will possibly flood the turbine. The latching mechanism has to be very fast to respect real-time operation and of moderate size to withstand peak pressure. Cretel [Cre+11] warned about these undesired phenomenon in wave energy conversion where it is a serious issue in some WEC designs such as tight-moored ones. Thus in the case of the OWC, the air compressibility in the air chamber offers an advantage as it absorbs part of these negative

impacts. Finally, while the overall power output is increased, so is the power fluctuation, resulting in a high average-to-peak ratio and poor power quality.

Survivability issues:

An important issue to consider in the development of a floating OWC is its ability to survive high energetic sea states. The best way to do so is to force the buoy to stop its operation and let the device move freely without converting any energy. One way to achieve this is to block the valve at the turbine inlet preventing the water from entering the turbine. At the same time, the relief valve is opened to avoid overpressure in the chamber. Recent WEC concepts are taking the survivability criteria more and more seriously, some WECs are equipped with mechanisms to submerge below the area of wave influence. Others are able to de-tune the control parameters so the motion response is transparent to some wave frequencies during storm. The natural frequency of the WEC is moved away from the ones of the storm and therefore the buoy does not oscillate as much.

Optimisating the generated power

The PTO design is made considering the system to be able to work on a wider range of sea states. Hydrodynamics and aerodynamics have to be studied as a whole to control the turbine. The power pressure induced by the water column oscillation is transferred to the turbine. But the effect of the turbine rotation also affects the dynamics of the water column. The relation is even stronger in a floating OWC where the relative motion of the buoy and the water column is of interest.

There exists two main types of PTO control for the OWC:

- Fixed Speed control (FS): the W2W model is simulated to compute the power turbine for a range of fixed speeds of the turbine-generator set. It is done for every sea states of the wave climate at the deployment site. An optimal speed is computed for each sea state, being the one corresponding to the maximum mechanical average power $\bar{P}_t$ along the simulation. The optimal speed is then the reference speed for the rotational speed controller. The control variable is the electromagnetic

torque to be applied at the generator which is calculated from the speed error. This control strategy is efficient but sea state dependant and does not benefit from the natural kinetic energy storage of the drive train.

- Variable Speed control (VS): With the knowledge of the optimal speeds in the range of sea states, a Maximum Power Point (MPP) curve is obtained by fitting the points as demonstrated in [Fal00]. Knowing that power depends on the torque T and the rotational speed, $P = T\Omega$, the following formulation is stated:

$$\bar{T}_t = \frac{\bar{P}_t}{\Omega} \qquad (3.10)$$

  with $P_t = a\,\Omega^3$, a being a constant characteristic of the turbine.

  Assuming a lossless PTO with no energy storage capability, in average the turbine power is the same as the generator power $\bar{P}_t = \bar{P}_{\text{gen}}$. The torque law for the controller is then derived at each time instant in function of the rotational speed:

$$T_{\text{gen}} = a\Omega^b \qquad (3.11)$$

  where the coefficient b should be equal to 2 if only the turbine efficiency is taken into account and slightly higher if optimized considering also the hydrodynamics of the device and the wave climate of the deployment site.

Both controllers will be detailed later on in Section 5 and their performance assessed with simulation results based on W2W model simulations.

The VS control approach was applied by Falcão [Fal02a] for the Pico plant assuming 44 sea states. A comparison was made on the electrical output power obtained applying different torque laws. In addition, the effect of a relief valve in the system was proposed by the author. It was observed an increase of 37% in the annual energy production using such a valve in comparison with the case without the valve. The stalling behaviour of the Wells could be avoided by releasing pressure inside the chamber. For the specific case of the Wells turbine, control is crucial to avoid stalling. In this context, an efficient control law is proposed by Ceballos in [Ceb+13] to optimize the efficiency of the turbine. The law is a modified version of a

torque-law and considers various ranges of speed to apply the torque control: no torque at low speed to let the turbine gain speed; optimal speed with turbine torque estimation at normal speed; and a ramp at high speed to break the turbine and avoid overspeeds. This modification of the theoretical torque curbe provided a gain of 10% of generated power.

The FP7 european project CORES [Kel+14; COR11] led to experimental development of speed control algorithms for a Wells turbine and an impulse turbine with movable guide vanes. They were tested in the $1/4^{th}$ scale prototype of the OE buoy [Thi+11; Ceb+13; Ceb+15]. In total five algorithms were developed and implemented in a Hardware-In-the-Loop (HIL) electrical infrastructure. They were based on either pressure or turbine speed measurements to compute the control torque to be applied by the generator.

Henriques et al. [Hen+16c] developed several torque laws to control the biradial turbine installed in an OWC sparbuoy. They included a peak-power control to avoid generator overloads [Hen+16b]. Again, the turbine speed was controlled by applying an electromagnetic torque to the generator and these strategies were validated by HIL experiments.

In [Mon+13] the Pico plant was used as a laboratory to develop and implement several algorithms to control the Wells turbine linked to the 200 kW generator. A flow control was applied by actuating on a relief valve to avoid stalling issues produced at high flow rates. An Artificial Neural Network algorithm estimated future potential turbine stall events enabling the valve operation to prevent the turbine from stalling. Several control strategies were tested on site and the performance analysis stated that the generator was oversized and the Wells turbine poorly characterised. It was found that besides the many assumptions used in the numerical simulations, the turbine characteristic curves were unrealistic.

Other publications cite the Mutriku Wave power plant installation for the numerical development of control algorithms [Alb+11b; Alb+12a; Amu+10a; Amu+11; Gar+13] to control the Wells turbine coupled to a DFIG. Although they permitted to avoid stall behaviour of the turbine and improve its efficiency the model did not include the hydrodynamics of the plant meaning that the effect of the control on the internal pressure was not explored.

Power integration into grid

The short-term intermittent nature of the wave energy resource induces fluctuations in power production from OWC. The peak to average power ratio is usually used as an indicator of the significant variation of the power extracted from the sea. To mitigate the effect of wave energy penetration into the grid, smoothing solutions are now being explored. Including energy storage reduces the power variability making it more suitable for grid integration. The most obvious way to store energy in the OWC is to use the turbine inertia, or a flywheel, to store mechanical energy [VGA14]. Low inertia systems offer faster response to variation of pneumatic power, thus the best average power is obtained as the turbine starts at lower sea states. However, this configuration results in high peak-to-average power ratios. In contrast, high inertia systems smooth turbine power and absorb the power peaks but the system is slow to respond at low sea states so speed control cannot operate the turbine at optimum speed on a wave-by-wave basis.Having knowledge of the turbine peak power is valuable for optimising the generator and power electronics ratings. In addition, other options are being investigated such as batteries, supercapacitors [Mur+12] and superconducting magnetic energy storage [NM10]. Whereas a short-term storage (seconds) solution is enough to cope with power quality issues, long- term storage (hours/months) would be required for energy scheduling.

Power quality is an issue to be managed locally at the point of connection [Bol03] and based on the characteristic of voltage or current injected into the grid. The WEC affects the quality of the power delivery at this point causing voltage drops, power factor decrease or frequency variations for all the users connected to the same point [Bla+12]. Thus, WECs should comply with the strict requirements imposed by local grid codes, as all the other power generators. A review comparison of the latest European grid codes is presented by Robles in [Rob+19]. In order to achieve full flexibility of the device a fully controlled power electronics interface is strongly advised. The back-to-back converter assures this condition both on the WEC side, to improve power generated from the waves; and on the grid side, to cope with power quality issues.

Another important aspect to ease the grid integration of any WEC is their voltage ride through capability. Nowadays, regulations require the production unit to stay connected to the grid for a specified time during faults. In case

of high renewable penetration, this is done to avoid the loss of a significant amount of production during large voltage dips and insure grid stability. For variable speed systems with a doubly fed induction generator, special measures might be necessary [Alb+11c]. The OWC is equipped with a full converter where the control forces the stator to stay connected while the rotor windings are short circuited activating a crowbar. It supports the grid during faults, thus reducing the criticality of the event.

The integration of a 20 MW wave farm in the BiMEP test centre is proposed by Tedeschi in [Ted+11a] and the effect of control both on the WEC and on the grid side is analysed. The aim is to understand how control strategies coupled with energy storage compensate for power fluctuation and improve grid connection issues for different generator types with fully controllable power electronics (as is the configuration of an OWC). The impact of wave farms will not only depend on the technology itself but also on the strength of the grid. A weaker grid will suffer larger voltage variations at the connection point than a stronger one.

3.4 Chapter conclusion

Based on observations made on this chapter, the W2W models for OWC systems usually do not, or poorly include the full conversion from the wave power to electrical power. Some of the works found in the literature detail pretty well the hydrodynamic and aerodynamic parts for the optimal choice and sizing of the air turbines but they do not consider the electrical conversion. This side of the PTO is essential in the development of control algorithms since speed control strategies for the OWC are actually applied to the generator by the power electronics. In other publications, little consideration is done on the wave to pneumatic conversion where the focus is more on the electrical power conversion and the control of the PTO. Thus, there is a lack of numerical models taking into account the whole energy conversion chain, known as full W2W models.

The review of control strategies for OWC systems that were highlighted in this section led to a conference publication presented in the EWTEC 2015 [FX +15]. The controllers assessments present in this work eventually analyse the electrical output power, that is the true meaning of Wave-to-Wire models. In terms of control, fixed turbine speed approach to fit the optimal turbine

damping and size is often looked at but there is no practical implementation on following the reference optimal speed. Otherwise, there exist variable speed controllers based on torque-speed curves designed to optimise the mechanical power conversion, but do not include the generator and so leave aside the full PTO efficiency. MPC algorithms applied to wave energy conversion present a number of benefits: the adaptability to different sea states, and the possibility to include the effects of the different PTO components. When talking about control in OWC no development of predictive algorithms are found.

Another key observation on previous research is that there is a lack of evidence of field testing of the control algorithms. Performance assessments that are based on operational data bring a realistic approach that is, in most cases, missing in the wave energy sector. These are essential to better assess the controllers and adjust them to real environment.

The next chapters will tend to provide novel approaches to cover the gaps detected in this chapter.

Modelling methodology for Wave-to-Wire OWC systems

<div style="text-align:right">

4

</div>

> " *All models are wrong, but some are useful*
>
> — **George E. P. Box**

Summary: This section develops a methodology to better define W2W numerical models for OWC systems. It details the various steps that constitute the development of full W2W models for both a fixed single-body device and a floating two-body one. The models are prepared to run in the time domain. It is the only way to consider the non-linearities of air compressibility and the behaviour of the PTO. Moreover, the control design needs to analyse the transients which is not possible in the frequency domain. As it has been detailed in Section 3.2, W2W models of OWC systems until now usually considered either the hydro and aerodynamic side, or the aerodynamic and electrical side but did not include the full energy conversion chain as in full W2W models. In this section, the study of the hydrodynamic part is a synthesis on what it has been done so far, but including new contributions on the Mutriku OWC plant. It also proposes additional details on the modelling of air chambers, with the comparison of several air compressibility models. In what concerns the electrical part of the PTO, the novelty resides in the development of an improved loss model. The numerical model is conceived so it is easy to assess different PTO configurations. It can be used as a decision support for the sizing of the PTO components.

4.1 Introduction

The methodology developed in this chapter is applied for one chamber of the Mutriku OWC plant and the spar-type floating OWC. These numerical models are used in Chapter 5 for the development and assessment of controllers: the one of Mutriku for the development and simulation of several turbine speed controllers in Section 5.3; and the sparbuoy is used for the development of a latching control strategy in Section 5.4. In addition, open-sea testing are planned within the framework of the OPERA project both at the Mutriku plant and at BiMEP with the IDOM/Oceantec buoy. The experimental results are reported respectively in Section 6.4 and Section 6.5 to test in real sea some of the controllers developed in Section 5.

An advanced analysis is made on several air compressibility models, key part on the energy conversion for the OWC. A validation of the most accurate one is made with experimental results obtained at the Mutriku plant. In what concerns the modelling of the PTO system, the electrical conversion is modelled in a more comprehensive manner compared with the existing research works. This includes a detailed generator loss model and the dynamic variation of power extraction subjected to the flux weakening region of operation of electrical generators. Finally, the W2W model is employed to optimise the PTO configurations by testing several combinations of turbines and associated generators.

4.2 Hydrodynamics of OWC devices

The methodology to describe mathematically the motion of devices is presented in this section. First of all, the hydrodynamic coefficients specific to each device are obtained using an hydrodynamic solver. These are fed into a Frequency Domain (FD) analysis and later on included into the more complex Time Domain (TD) model. The Response Amplitude Operators (RAO) are obtained for each of the selected degrees of freedom. As mentioned by Alves in [Alv+11], the TD model is validated against the FD in free dynamics. It is a required step to prove the correct implementation of the radiation force approximation. The use of a TD model is justified by the fact that it can include non-linear terms and thus better describe the behaviour of the whole system.

4.2.1 The fixed OWC: the case of Mutriku

Mutriku OWC plant is located on the North shore of Spain in the province of the Basque Country. It is operational and grid connected since 2011 [TML10]. Additionally, it is nowadays open to researchers for testing innovative solutions. The plant has a total of 16 air chambers, each one having a PTO composed of a biplane Wells and an induction generator. This section presents the W2W model for one chamber. It is an important requirement for the present work in order to prepare for the test campaign. The biradial turbine was installed for one year on top of the chamber #9 as planned in the OPERA project. Some experimental results of its operation under different controllers are presented later on in Section 6.4. A schematic side-view of one of the chambers can be seen in Figure 2.16.

Frequency domain analysis

The frequency dependant hydrodynamic coefficients are obtained using the boundary element method solver WAMIT [WAM16] which is based on potential flow theory. It is applied to the geometry of the OWC chamber of the real plant associated with the corresponding seabed slope in front of the breakwater wall. Following the approach of the rigid piston modelling of the onshore OWC at Pico [Bri+01], the Internal Water Free Surface (IWFS) is considered a massless oscillating body, which is the commonly agreed approach [Eva82]. The IWFS motion is simplified to take into account only the heave displacement and the chamber walls is set as the second fixed body. During the hydrodynamic characterization it was found that both the seabed geometry and the length of the dike considered in the model would significantly affect the results obtained. This was already observed in [Bri+01], where the effects in the plant capture width were analyzed. For the case of Mutriku, and without detailed bathymetric information, the seabed geometry is simplified to a constant slope starting 50 m ahead of the plant with a 15 meter water depth. The total length of the dike is 100m (c.f. Fig. 4.1), where air chamber #9 would fall right in the centre. This results in a quite realistic assumption given the real plant layout. The RAO in FD is obtained by calculating the displacement of the OWC using Eq. (3.3) without any PTO force.
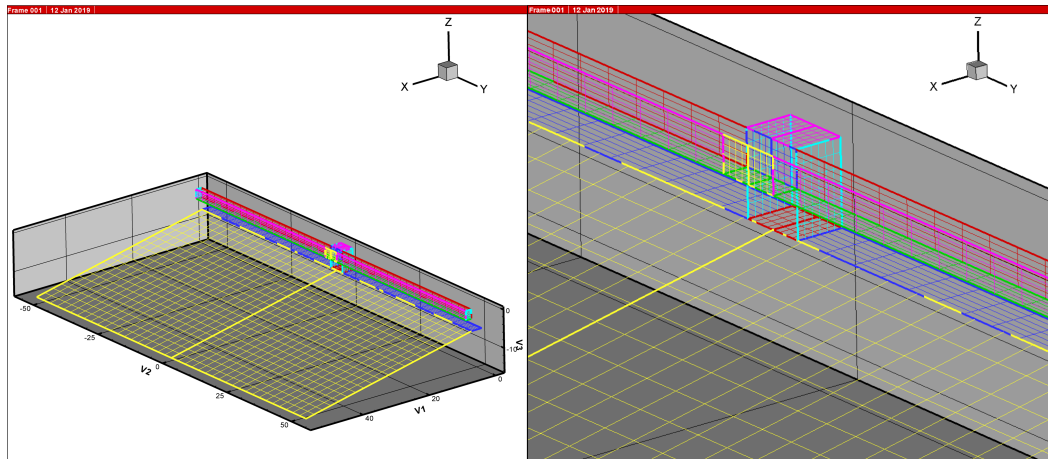
Fig. 4.1: WAMIT model of Mutriku and detailed view of chamber 9

The hydrodynamic coefficients of excitation force $F_{exc}(\omega)$, radiation damping $F_{rad}(\omega)$ and added mass at infinite frequency $A(\omega)$ for each angular frequency ω, obtained from the hydrodynamic solver are represented in Fig. 4.2.
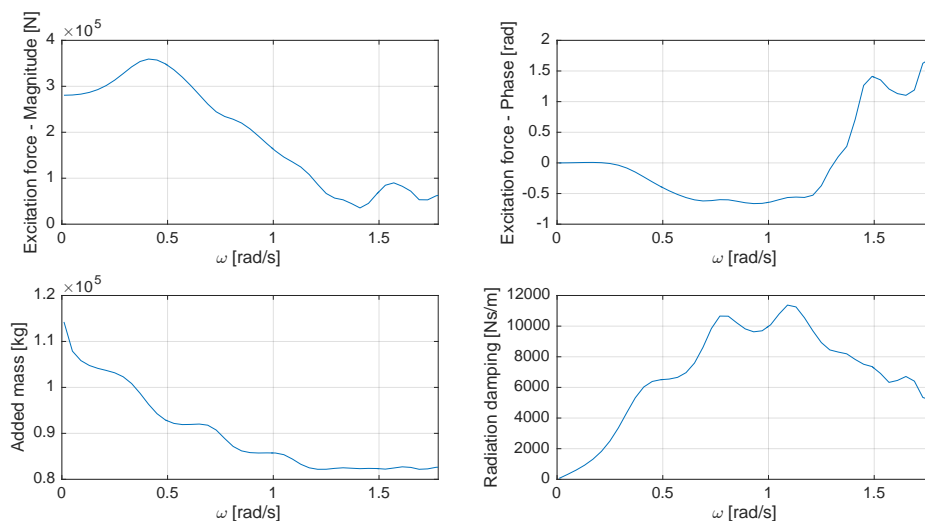
Fig. 4.2: Hydrodynamic coefficients of the modelled chamber 9 of the Mutriku plant

The effect of the seabed on the excitation force is concentrated in the low frequency range, where a maximum in force coefficients is observed around $\omega = 0.4$ rad/s. In addition, the inclusion of a long dike in the model introduces high frequency ripples in the excitation force, that otherwise would not be captured with a shorter dike. In a short dike, or without a dike, the effect of the slope would not be captured. There is an influence of the surroundings of the device on the IWFS motion, which confirms the work of Brito-Melo et al. [Bri+01] which included the chaotic seabed shape in front of the Pico plant due to the presence of boulders. Considering both the seabed slope and the

length of the dike led to more realistic results in modelling the Mutriku OWC chamber. The results obtained are checked with both the Haskind relations and the pressure integration method (c.f. WAMIT manual [WAM16]), and are quite consistent. The FD RAO of heave displacement z is obtained for all the studied frequency in Figure 4.3 where they serve as reference to compare with the displacement of the TD model, also represented on the same graphic.
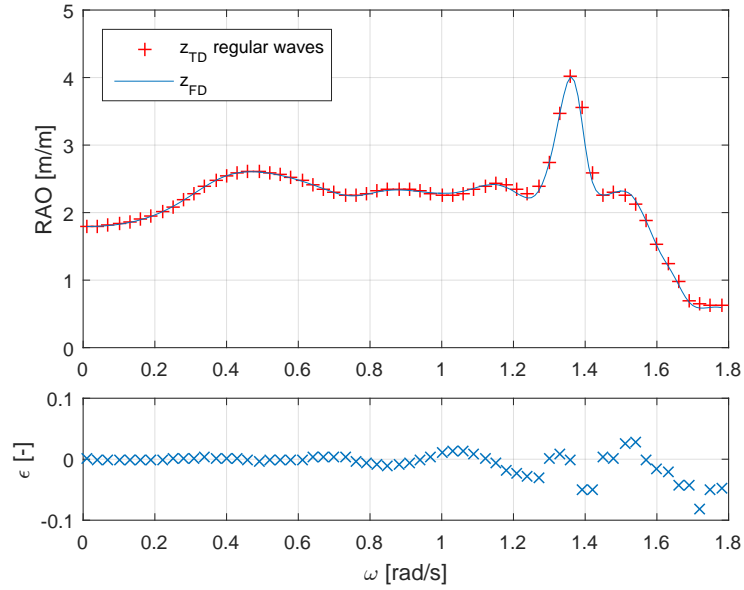
Fig. 4.3: Validation of the IWS motion in time domain using Prony method at order 5

Time domain model and validation

The W2W model in time domain, t being time, solves the differential equation of motion in heave z of the IWFS following the 2nd law of Newton:

$$A_\infty \, \ddot{z}(t) = F_{\text{exc}}(t) + F_{\text{rad}}(t) + F_{\text{h}}(t) + F_{\text{p}}(t) \tag{4.1}$$

where A_∞ is the added mass at infinite frequency of the OWC, $\ddot{z}(t)$ the heave acceleration, $F_{\text{exc}}(t)$ the excitation force from the waves, $F_{\text{rad}}(t)$ is the radiation force, and finally $F_{\text{p}}(t)$ is the force of the air pressure.

The excitation force of the incoming waves on the IWFS is expressed as:

$$F_{\text{exc}}(t) = \sum_{i=1}^{N} \Gamma_i(\omega_i)\, a_i(\omega_i) cos(\omega_i t + \varphi_i + \epsilon_i) \tag{4.2}$$

that is the sum of N wave components each one described as the product of $\Gamma_i(\omega)$, the excitation force from the frequency domain analysis, with the individual wave amplitude $a_i(\omega)$ and phase φ. Lastly ϵ is a random phase from $[0{:}2\pi]$.

The radiation force is the damping component due to the motion of the free surface over still water outside the wall and is obtained by solving the convolution integral equation:

$$F_{\text{rad}}(t) = -\int_0^t K(t-\tau)\dot{z}(\tau)d\tau \tag{4.3}$$

K is the impulse function that is approximated using the PRONY method [DCC01] (see Fig. 4.4) and is formulated as:

$$K(t) \approx \sum_{i=1}^{N} \alpha_i\, exp(\beta_i t) \tag{4.4}$$

where the coefficients α and β representing the matrices of the complex radiation approximation coefficients at the ith order. The convolution integral equation can therefore be approximated by $\sum_{i=1}^{N} I_i$ and mathematically solved by the differential equation in function of the heave velocity $\dot{z}$:

$$\dot{I}_i = \beta_i I_i + \alpha_i \dot{z} \tag{4.5}$$
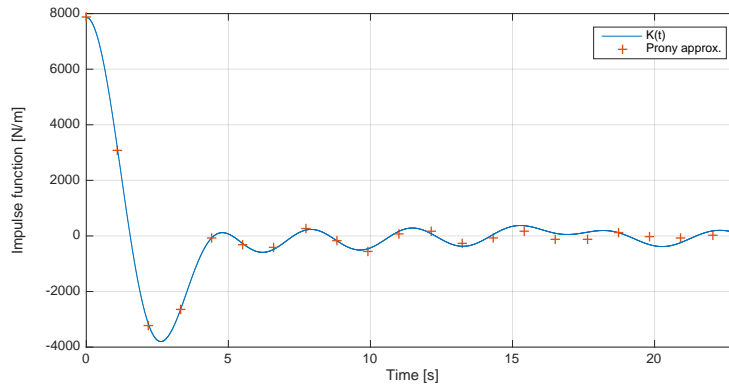
Fig. 4.4: Impulse function approximation using Prony method at order 5

A 5th order Prony approximation was found to be accurate enough as seen in Fig. 4.3 and F_{rad} is then:

$$\dot{I}_i = A_r I_i + B_r \dot{z}$$
$$F_{rad} = C_r I_i + D_r \dot{z}$$

(4.6)

The hydrostatic force is composed of the water density ρ_w, the gravitational constant g, and S_{IWFS} the area of the IWFS.

$$F_h(t) = -\rho_w g S_{iwfs} z(t)$$

(4.7)

The differential equation is solved in time domain using monochromatic (regular) waves for each angular frequency. This is done in free dynamics, without the pressure forces F_p. The RAO of the heave motion is compared against the FD model in order to validate numerical implementation of the TD model. In Fig. 4.3, the difference between the two models is shown. It proves the accuracy of the time domain model as the error is relatively small and falls in the range [5% to -10%]. The largest errors occur only in the high frequencies which represent wave components with short periods. These periods have very little influence on the IWFS motion. An ideal reflection coefficient (=1) is used when modelling the walls of the chamber and waves are assumed to be totally reflected. This fact leads to a RAO starting in a value above 1 for very low angular frequencies. Further work on the hydrodynamic model should consider more realistic values, where some reflections losses are allowed.

The force F_p, is the resultant of the pressure forces on the IWFS. It is associated to the PTO power extraction and is detailed in the subsection 4.3, where different air compressibility models are developed.

4.2.2 The floating OWC sparbuoy

The floating spar-type buoy is a two-body system composed of the structure (floater, tube and ballast), and the water column oscillating inside the tube. A schematic side-view of one of the chambers can be seen in Figure 2.17. It has a circular shape that makes it indifferent to the wave direction. The difference with respect to the fixed OWC resides in the fact that each body has its own response to the incident waves and each body has an influence on the other. It is the relative motion that creates the pressure variation. Note

that the hydrodynamic coefficients were generously provided by IST-IDMEC during a short course within the OceaNET project. The modelling part is detailed in the following section as well as the FD-TD validation methodology, similar as the one used for Mutriku, but this time using the Frequency Domain Identification (FDI) method developed by Perez and Fossen [PF07]. This allows a comparison of both methods, the PRONY method and the FDI approximation respectively.

Frequency domain analysis

As any structure moving in the water, the floating OWC is subjected to hydrostatic and hydrodynamic effects. It is considered as an oscillating system composed of two mechanical bodies ($k = 1, 2$). The buoy structure includes the floater and the steal tube, body 1. The warping of the inner free surface is neglected, which seems an acceptable assumption due to the large length and small diameter of the tube compared to a typical wavelength. This allows the IWFS to be represented as an imaginary thick rigid piston of small length, named body 2, which has the density of the water. In the model described in this section, the bodies masses are denoted m_k and their plane surface area S_k. As any rigid body both can move in all the 6 degrees of freedom (DoF). The DoF of the body 1 are given by (j=1,2,...,6), corresponding to motions of surge, sway, heave, roll, pitch and yaw respectively, and the motion modes of the second body are given as (j=7, 8,..., 12). The motion of each body will described only with heave and denoted z_j, the vertical coordinate defining the position of the bodies. Indeed, this DoF is the most relevant one for this type of floating structure, when comparing all the RAOs. The hydrodynamic coefficients will follow the conventional annotation related to their DoF and their interactions. These are obtained using the hydrodynamic solver WAMIT and the IWFS is considered this time a weighted piston [Gom+12; SRA14]. The excitation force magnitudes and phases for each body are plotted in Fig. 4.5, the added masses for each DoF are in Fig. 4.6, and the radiation damping coefficients for each DoF are in Fig. 4.7.
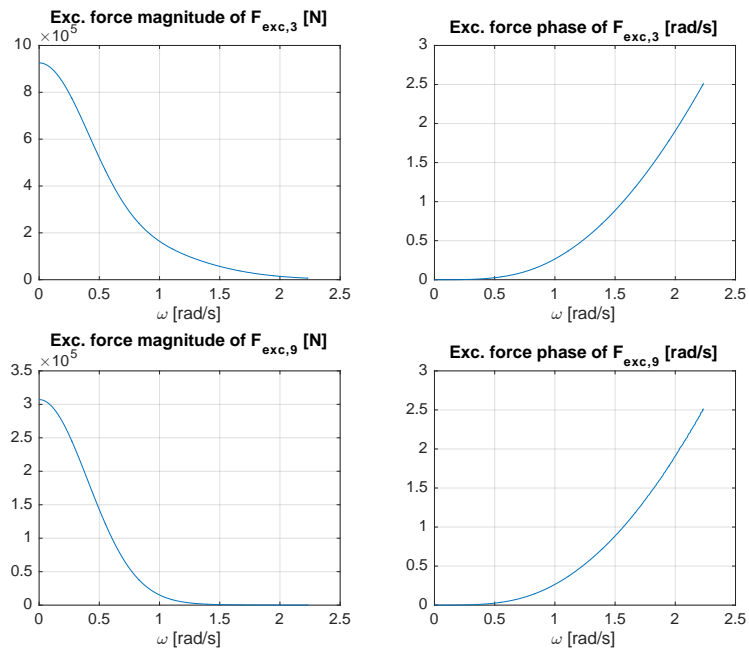
Fig. 4.5: Excitation forces for the sparbuoy
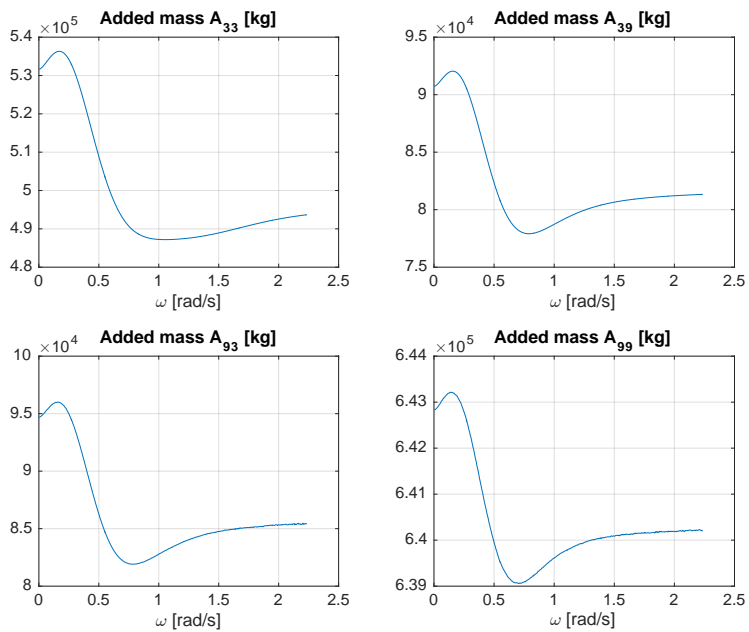
Fig. 4.6: Added masses for the sparbuoy
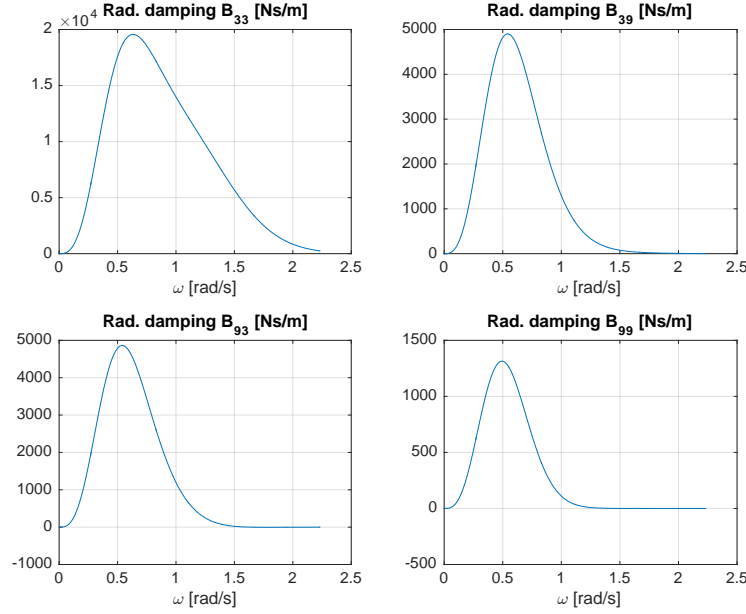
Fig. 4.7: Radiation damping coefficients for the sparbuoy

Time domain model and validation

In order to describe its motion, the Cummin's equation applies – derived from Newton's 2nd law. The equations of motion of this two-body system in the time-domain considering the cross terms can be written as Eq. (4.8a) for the floater and Eq. (4.8b) for the IWFS.

$$m_1\, \ddot{z}_3(t) = F_{\text{exc},3}(t) \underbrace{-A_{33}^\infty\, \ddot{z}_3(t) - R_{33}}_{F_{\text{rad},33}(t)} \underbrace{-A_{39}^\infty\, \ddot{z}_9(t) - R_{39}}_{F_{\text{rad},39}(t)}$$

$$\underbrace{-\rho_{\text{w}}gS_1\, z_3(t)}_{F_{\text{h},3}(t)} + F_{\text{nl}}(t) \quad (4.8a)$$

$$m_2\, \ddot{z}_9(t) = F_{\text{exc},9}(t) \underbrace{-A_{39}^\infty\, \ddot{z}_3(t) - R_{93}}_{F_{\text{rad},93}(t)} \underbrace{-A_{99}^\infty\, \ddot{z}_9(t) - R_{99}}_{F_{\text{rad},99}(t)}$$

$$\underbrace{-\rho_{\text{w}}gS_2\, z_9(t)}_{F_{\text{h},9}(t)} + F_{\text{nl}}(t) \quad (4.8b)$$

The force noted F_{nl} represents all the non-linear forces of a W2W model. This includes the internal air chamber pressure F_{p}, similar to the PTO force. In other advanced models, it can also comprise viscous forces or mooring lines forces but these considerations are out of the scope of this research.

Rearranging Eq. (4.8a) and Eq. (4.8b), the state-space representation can obtained with the following system of equations, being the mass matrices $M_j = m_j + A_{jj}^\infty$:

$$\begin{pmatrix} \ddot{z}_3(t) \\ \ddot{z}_9(t) \end{pmatrix} = \begin{bmatrix} M_1 & A_{12}^\infty \\ A_{12}^\infty & M_2 \end{bmatrix}^{-1} \times \begin{pmatrix} F_{\text{exc},3}(t) - R_{33} - R_{39} - \rho_{\text{w}}gS_1\,z_3(t) + F_{\text{p}}(t) \\ F_{\text{exc},9}(t) - R_{93} - R_{99} - \rho_{\text{w}}gS_2\,z_9(t) - F_{\text{p}}(t) \end{pmatrix} \tag{4.9}$$

The ocean waves exert forces on each body independently. As seen in Fig. 4.5, each of them has its own response represented by the two frequency dependant excitation force magnitudes $\Gamma_j(\omega)$ and phases $\epsilon_j(\omega)$. Then, the formulation is similar to Eq. (4.2) but including the DoF $j = 3, 9$ for each i wave component:

$$F_{\text{exc},j}(t) = \sum_{i=1}^{N} \Gamma_{ij}(\omega_i)\,a_i(\omega_i)cos(\omega_i t + \varphi_i + \epsilon_{ij}) \tag{4.10}$$

The radiation damping forces are defined by the convolution integrals for each body affected by the other body having the four cases $jj = 33$, $jj = 39$, $jj = 93$, and $jj = 99$.

$$R_{jj} = \int_0^t K_{jj}(t - s)\,\dot{z}_j(s)\,\mathrm{d}s. \tag{4.11}$$

which will be approximated by a state-space approach

$$\begin{aligned} \dot{\mathbf{I}}_{jj} &= \mathbf{A}_{jj}^r\mathbf{I}_{jj} + \mathbf{B}_{jj}^r\dot{z}_j \\ R_{jj} &\approx \mathbf{C}_{jj}^r\mathbf{I}_{jj} \end{aligned} \tag{4.12}$$

where $\mathbf{A}_{jj}^r$, $\mathbf{B}_{jj}^r$ and $\mathbf{C}_{jj}^r$ are the matrices obtained using the FDI method described in 3.1.1 and using the matlab toolbox described in [PF09]. Different orders of approximation are found to be more accurate for the radiation terms:

- Figure 4.8 shows the FDI approximation of the buoy on the sea surface (DoF 33) for an approximation at order 7;

- Figure 4.9 shows the FDI approximation of the buoy on the IWFS (DoF 39) for an approximation at order 7;

- Figure 4.10 shows the FDI approximation of the IWFS on the buoy (DoF 93) for an approximation at order 4;

- Figure 4.11 shows the FDI approximation of the IWFS on the sea surface (DoF 99) for an approximation at order 4;
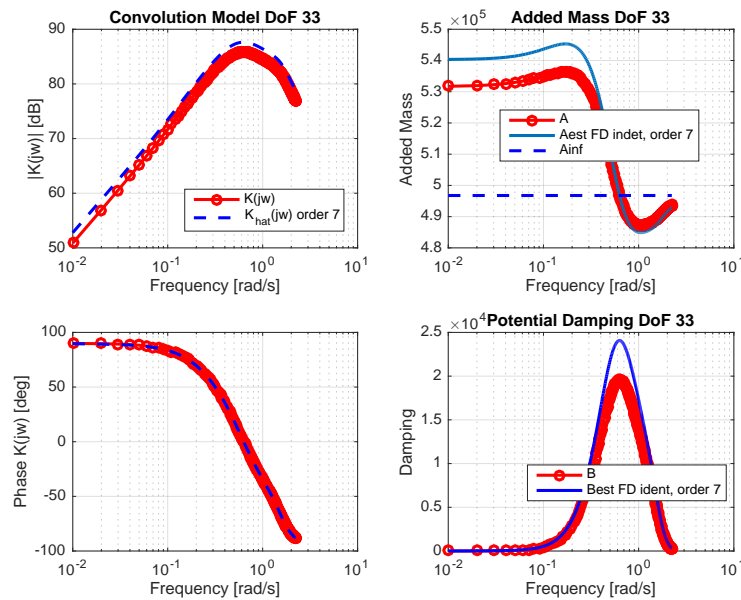
Fig. 4.8: FDI approximation for DoF 33
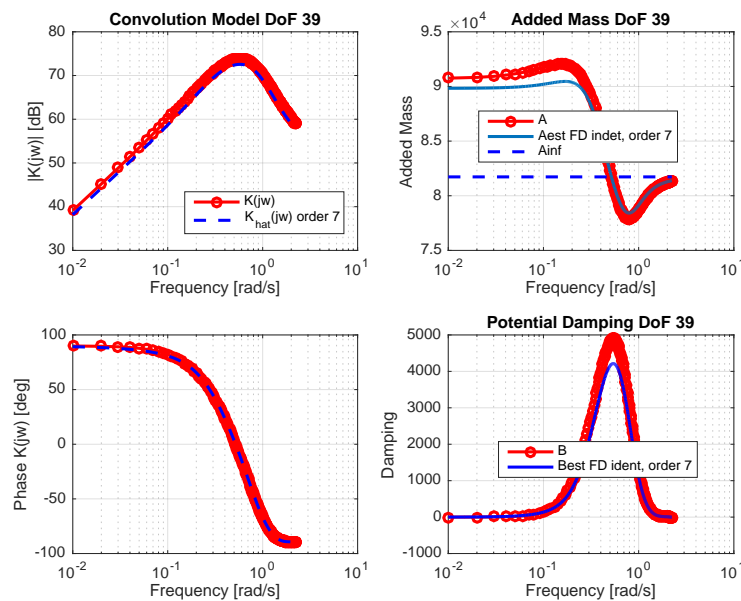
Fig. 4.9: FDI approximation for DoF 39

To validate the correct implementation of the radiation approximation in TD, the same simulation as for the case of Mutriku is run. For regular waves defined for all the frequencies, the time domain model comprising only the linear forces is simulated in free motion to get the position of both bodies
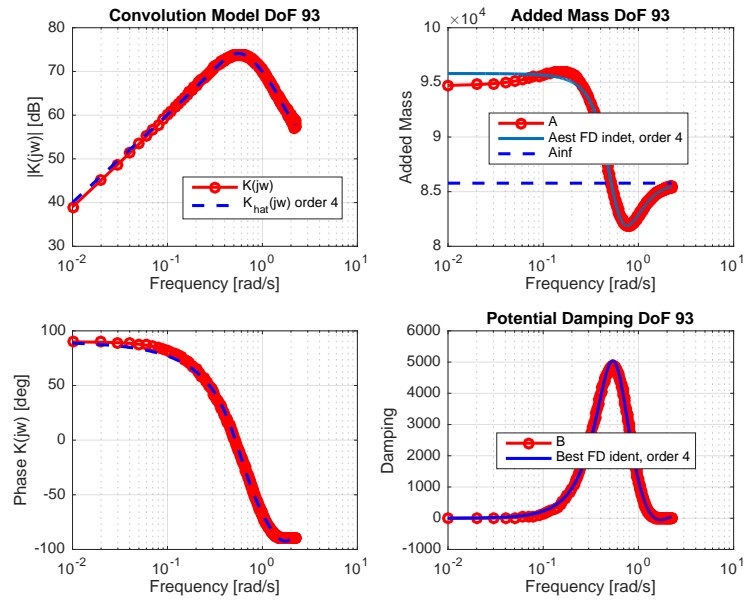
Fig. 4.10: FDI approximation for DoF 93
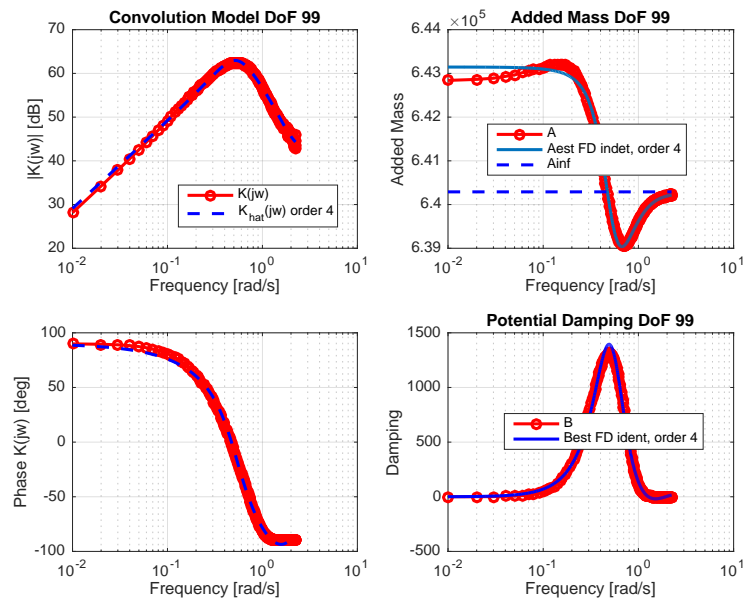
Fig. 4.11: FDI approximation for DoF 99

without the effect of the PTO force. The comparison of the displacements found for the FD and the TD are presented in the RAOs of Figure 4.12. The RAOs from the two models are quite alike, although the difference between them, highlighted by the error, is a bit higher when comparing the case of Mutriku, especially in frequencies higher than the natural frequency of the floating buoy. It means that the model may not properly represent the buoy motion response at wave periods lower than 8.9 s.
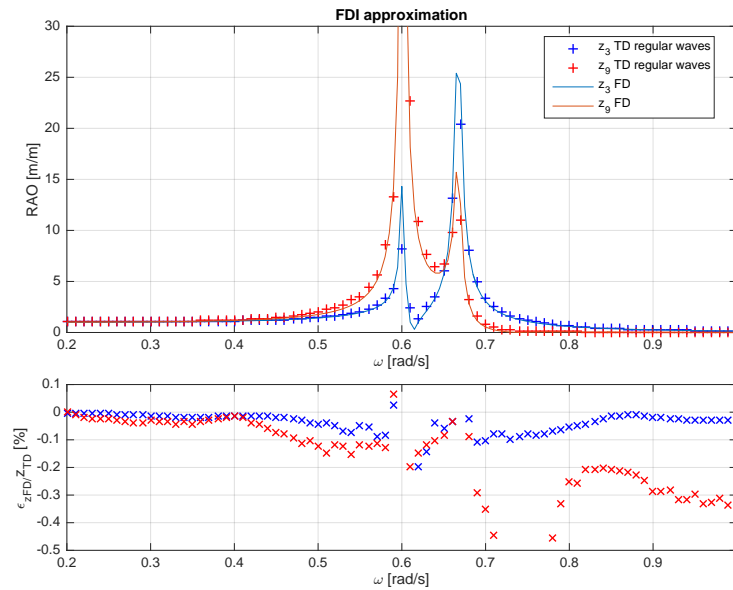
Fig. 4.12: Validation of the TD against the FD for the radiation approximation using FDI

4.3 Air chamber models

The hydrodynamic power captured by an OWC is represented as the pneumatic power inside the air chamber. It comes from the variation of pressure due to the IWFS motion (or relative motion between the two bodies), and also from the damping induced by the turbine when the air flows across. In fact, two different processes come into play in the pressure variations: a compression, or exhalation, when the air is pushed out of the chamber; and an expansion, or inhalation, when the air is sucked back inside the chamber. Complex thermodynamic effects are involved coming from the fact that air is a compressible gas having its own pressure p, temperature T and density ρ. Depending on the air chamber models, for example considering air as incompressible or compressible, the magnitudes of pressure can be overestimated up to 15% [Sim+18]. This effect can have an impact on the output power between 10-30% [Kuo+17]. In [FH18] the incompressible, unrealistic, air model overestimated the output power by a factor of 1.7 with respect to a model including air compressibility. The pressure variation has a non-linear spring-like effect on the internal water surface that has to be taken into account in the W2W model. To simplify the formulation in this section, the equations are presented for the case of the fixed OWC.

In order to define the force extracted by the PTO, the pressure force F_{p} (see Eq. (4.1) in the case of the OWC), it is convenient to develop an approach to model the air inside the chamber. Given p the pressure variation, the equation of that force is:

$$F_{\mathrm{p}} = -p\, S_{\mathrm{IWFS}} \tag{4.13}$$

4.3.1 Formulation of air compressibility models

Let us define the pressure variation between the internal pressure p_{c} and the outside atmospheric pressure p_{at} as $p = p_{\mathrm{c}} - p_{\mathrm{at}}$. The subscript 'at' denotes atmospheric conditions, while 'c' refers to the chamber. Considering p^* the dimensionless relative pressure normalised with p_{at}, the formulation is then:

$$p^* = p_{\mathrm{c}}/p_{\mathrm{at}} - 1 \tag{4.14}$$

The air in the chamber is also assumed to be an ideal gas of density ρ_c. The mass of the inside air is time dependant and is expressed in function of the chamber volume V as:

$$m_{\mathrm{c}} = \rho_{\mathrm{c}}\, V \tag{4.15}$$

where V is the chamber air volume at each time instant and is written as:

$$V_{\mathrm{c}} = (h_0 - z)S_{\mathrm{IWFS}} \tag{4.16}$$

given that $V_0 = h_0\, S_{\mathrm{IWFS}}$ is the air chamber volume at equilibrium assuming that the chamber height at rest is h_0. The volumetric flow rate driven by the water surface is simply $Q = -\dot{V}_{\mathrm{c}}$. Differentiating in time Eq. (4.15) gives the mass flow rate of air:

$$\dot{m}_{\mathrm{c}} = \rho_{\mathrm{c}}\dot{V}_{\mathrm{c}} + V_{\mathrm{c}}\dot{\rho}_{\mathrm{c}} \tag{4.17}$$

During the exhalation and inhalation, there is a change of air density - internal density of air ρ_{c} and the air at atmospheric conditions ρ_{at} - and therefore the flow rate across the turbine is:

$$Q = \begin{cases} -\frac{\dot{m}}{\rho_{\mathrm{c}}}, & \text{for exhalation} \\ -\frac{\dot{m}}{\rho_{\mathrm{at}}}, & \text{for inhalation} \end{cases} \tag{4.18}$$

Incompressible air model

When considering the air as an incompressible ideal gas, the density is constant and therefore $\rho_c = \rho_{at}$. The volumetric flow rate is then, for both compression and expansion, linked to the variation of volume in the air chamber subjected to the motion of the IWFS. Given k_t the turbine pressure-flow characteristics, d_t its diameter, and Ω the rotational speed, the pressure in the incompressible air model is proportional to the volumetric flow rate and is defined such that:

$$p_c = \frac{\Omega\, k_t}{d_t} Q \tag{4.19}$$

Air compressibility models

As OWC systems rely on pneumatic power from the pressure variations in an air chamber, it is very important that the W2W model takes into account the compressibility effect of air. In the literature, air chamber models considering the compressibility of air are most of the time referred to follow an isentropic process [FJ99; Hen+12a; Hen+16a]. In this case, the process is assumed to be adiabatic and so the heat exchange through the wall is null. In fact, the isentropic process is a particular case of the polytropic process. The difference resides in the fact that in the isentropic process there is no heat transfer and the system is assumed frictionless. On the contrary, in the polytropic process heat transfer is taken into account as detailed later on.

Assuming air is compressible during the inhalation and exhalation phases under polytropic process, the following relation between pressures and densities can be stated:

$$\frac{p_c}{\rho_c^\kappa} = \frac{p_{at}}{\rho_{at}^\kappa}, \tag{4.20}$$

where κ is the polytropic exponent which depends on the turbine efficiency η_t [DH14] and is defined as:

$$\kappa = \frac{1}{1 - \frac{\gamma-1}{\gamma}\eta_t} \tag{4.21}$$

The turbine efficiency η_t (see Eq. (4.31)) is needed to compute the polytropic exponent. In the isentropic process, the coefficient κ is simply equal to γ that

is the specific heats ratio for air. It is the ratio of the heat capacity at constant pressure c_p to heat capacity at constant volume c_p, which gives:

$$\gamma = c_p/c_v = 1.4 \tag{4.22}$$

Taking the logarithmic derivative of Eq. (4.20) and introducing p^* from Eq. (4.14) and after simplifying, we obtain:

$$\frac{\dot{\rho}_c}{\rho_c} = \frac{\dot{p}^*}{\kappa(p^* + 1)}. \tag{4.23}$$

Using the mass balance of air of Eq. (4.17) and Eq. (4.15), we can state that:

$$-\frac{\dot{m}_c}{m_c} = \frac{\dot{V}_c}{V_c} + \frac{\dot{\rho}_c}{\rho_c} \tag{4.24}$$

where $V_c = S_{\text{iws}}(h_{\text{ch}} + z)$ is the instantaneous volume of the chamber, $m_c = \rho_c V_c$ denotes the mass of air inside the chamber, and $\dot{m}_t$ is the turbine flow rate (positive for exhalation). Replacing Eq. (4.20) in Eq. (4.24) gives

$$\frac{\dot{p}^*}{p^* + 1} = -\kappa \left(\frac{\dot{V}_c}{V_c} + \frac{\dot{m}_t}{m_c} \right). \tag{4.25}$$

To solve Eq. (4.25) in time, the density ρ_c is computed using Eq. (4.20). The computation of the turbine mass flow rate is described in the next section.

The pressure variation is expressed as:

$$\dot{p}^* = -\kappa \frac{\dot{V}_c}{V_c}(p^* + 1) - \kappa \frac{\dot{m}_t}{\rho_c V_c}(p^* + 1)^{(\kappa - 1)/\kappa} \tag{4.26}$$

During a wave cycle, there is a cycle of compression and expansion of air inside the chamber. This implies a change in the air density ρ_c at the turbine inlet as explained in Eq. (4.18). During compression the density is computed as:

$$\rho_c = \rho_{\text{at}}(p^* + 1)^{\gamma - 1/\gamma} \tag{4.27}$$

During the expansion phase, the air comes from outside the chamber at atmospheric conditions and is naturally $\rho_c = \rho_{\text{at}}$.
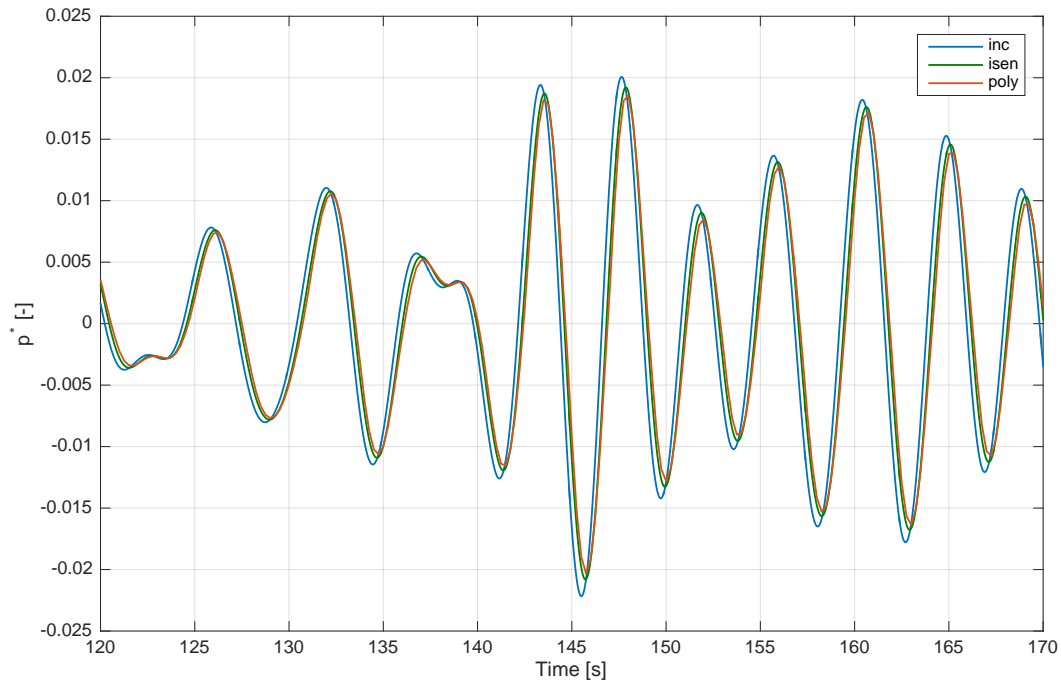
Fig. 4.13: Comparison of the dimensionless pressures from the different air chamber models for the Mutriku W2W model with the installed PTO: incompressible, isentropic and polytropic

4.3.2 Analysis of the influence of air compressibility models

The W2W model of Mutriku with the Wells turbine is used to compare the three air chamber models: the incompressible one and the two compressible ones (isentropic and polytropic). The dimensionless pressures are compared in Fig. 4.13. When air compressibility is considered, a reduction of the magnitude of pressures is observed and a phase shift occurs. This is explained by the fact the air compressibility induces a spring-like effect (a small K_{PTO}) and some losses in comparison with the case when air is considered incompressible. As a matter of fact, the pneumatic power is less when considering air as compressible, and in the end, the output useful power is expected to be reduced.

Now, let us focus on the two air compressibility models: one considering the isentropic process ($\kappa = \gamma$) and the other, is the polytropic one. The effect of the selection of the compressibility models on the power production is not negligible. When comparing the ranges of pressure the polytropic model shows lower amplitudes as illustrates Fig. 4.14, which seems more

realistic. Eventually, the pressure variation differences have an impact on the power outputs given by Fig. 4.15 where the pneumatic, the turbine and the generator powers are displayed. Note that both figures refer to simulations results of SS10 using the W2W model detailed in 4.2.1.

The power quantities are explained in Section 4.4 and the control method employed is the control law CL2.2 developed in Section 5.3.3 for this study. When comparing the mean power production between the polytropic model developed here and the isentropic one, as often used in the literature, it presents a decrease in electrical output power higher than 15%. In a variety of sea states, the difference of the three powers between the polytropic and the isentropic model can be seen in Fig. 4.16 and oscillates around -15%. The figure only presents the first 11 SS. Above, the sea states are too energetic and the safety valve begins to operate, which makes it impossible to compare the cases.
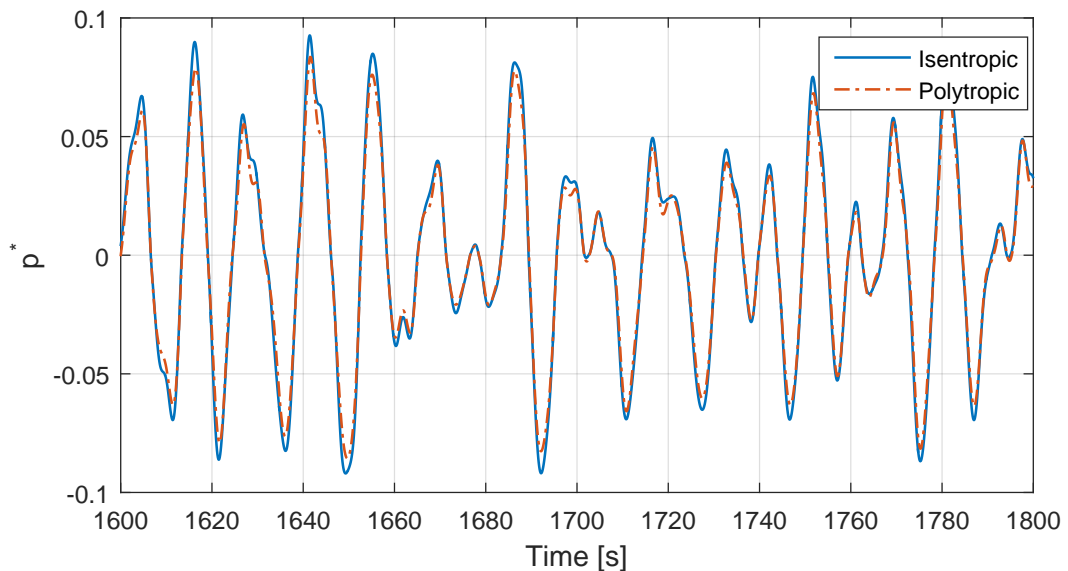
Fig. 4.14: Relative dimensionless pressure using an isentropic and a polytropic model during SS10 with CL2.2

4.3.3 Experimental validation of the polytropic model

The validation of the model based on the polytropic process is done with real data measured at the Mutriku OWC plant. The validation methodology consists in isolating the pressure variation. The numerical model takes as input the plant data of water surface elevation position and velocity, and the
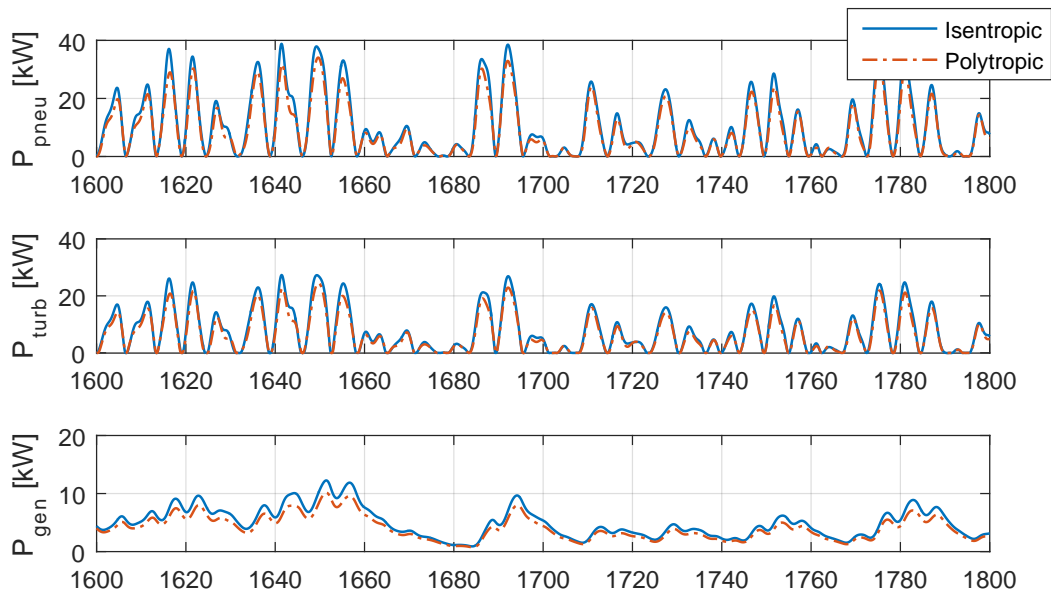
Fig. 4.15: Comparison of powers using an isentropic and a polytropic model during SS10 with CL1
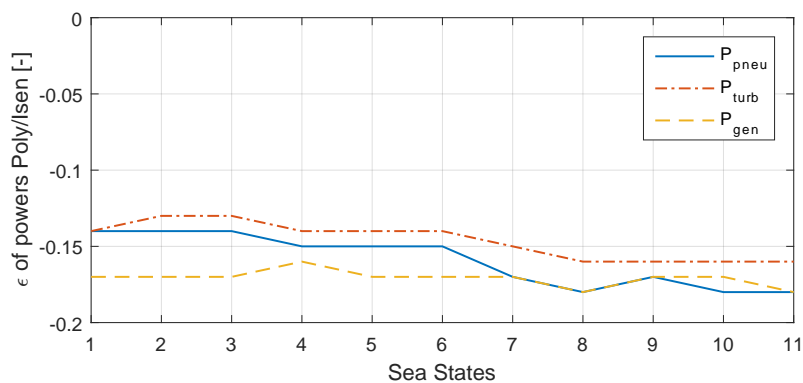
Fig. 4.16: Relative error of the pneumatic, turbine and generator powers using the polytropic process versus the isentropic one

turbine rotational speed. The pressure variation obtained with the polytropic model is then compared with the measured pressure values. Fig. 4.17 shows the comparison of a modelled and a measured relative dimensionless pressure for a medium energetic sea state. The model overestimates the pressure around 4% and the errors are more visible in frequencies lower to 0.8 rad/s. Following the same methodology for a range of realistic sea states, the error is in the range of +15% to -5%.
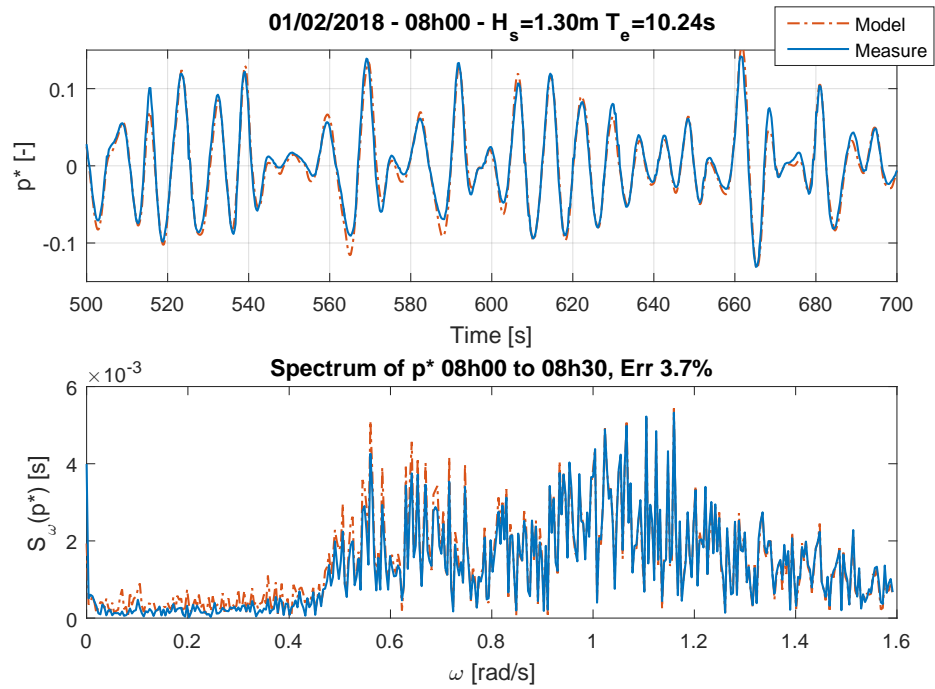
Fig. 4.17: Comparison of p^* in time and frequency domains, from plant measured data and using the polytropic model

4.4 Power Take-Off system

The PTO system represents the set of components that transform the pneumatic power of the chamber into useful electrical power. It is composed of a self-rectifying air turbine, sometimes with a safety valve, an electrical generator and the power electronics. In the W2W developed here, the focus is made on the energy conversion from the turbine taking into account its characteristics of pressure, flow rate and mechanical power. A shut-off valve, installed in series with the turbine, is included for safety reasons to protect the PTO components. The generator is modelled so that it includes a loss model and the different operation ranges. The losses of the power electronics are not explored here.

4.4.1 Air turbine model

In turbomachinery, it is common to define turbines according to the dimensionless aerodynamic parameters of pressure head Ψ, mass flow rate Φ,

power coefficient Π and the turbine aerodynamic efficiency η_t expressed as in [FR02].

$$\Psi = u_v \, \frac{p^* p_{at}}{\rho_{in} \, \Omega^2 \, d_t^2} \tag{4.28}$$

$$\Phi = \frac{Q}{\Omega \, d_t^3} \tag{4.29}$$

$$\Pi = \frac{P_t}{\rho_{in} \, \Omega^3 \, d_t^5} \tag{4.30}$$

$$\eta_t = \frac{\Pi}{\Psi \Phi} \tag{4.31}$$

Let us recall Q is the volumetric flow rate, Ω is the rotational speed in radians per unit of time, d_t is the turbine rotor diameter and P_t is the mechanical power at the drive-train shaft.

4.4.2 Valve system

As commented above, for safety reasons, the turbine is equipped with a shut-off valve. It blocks the flow rate when the rotational speed reaches a certain threshold, avoiding damages in the moving parts of the PTO. From one side, at high speed, the generator looses its capacity to extract torque and so cannot break the turbine. From the other side, there is a risk of damaging the turbine if the maximum speed is exceeded due to the increase of mechanical vibrations and centrifugal forces. The valve position (closed-0, or open-1) is determined by the associated control variable u_v introduced in Eq. (4.28).

$$u_v = \begin{cases} 0, & \text{if } \Omega > \Omega_{th,up}, \\ & \text{stays closed until the turbine slows down to } \Omega_{th,lo}, \\ 1, & \text{otherwise.} \end{cases} \tag{4.32}$$

In practice, the thresholds of speed - $\Omega_{th,up}$ for the upper threshold and $\Omega_{th,lo}$ the lower threshold - are defined depending on the PTO components.

4.4.3 Advanced electrical power conversion model

Generator loss model

In this section, the loss model of an induction generator as the one used in the W2W model is detailed. This consideration is usually not included in the literature, but there are direct effects on both the power conversion and on the control system. The mechanical to electrical power conversion is subjected to losses coming from the generator operation. Its efficiency is defined by the amount of power at the generator input and the sum of its power losses that include:

- Mechanical losses P_{ml},
- Iron losses P_{il},
- Winding losses P_{wl}.

The **mechanical losses** P_{ml} are mainly due to bearing friction and depend on the diameter shaft and its number of poles, or nominal speed. The friction losses are estimated with catalogue data of the manufacturer of electrical machines in [ABB04].

The **iron core losses** are related to Eddy currents flowing in the laminated steel plates.

$$P_{il} = B^2 \left(\sigma_h \frac{f_{hz}}{100} + \sigma_h \left(\frac{d_{ip} f_{hz}}{100} \right)^2 \right) w_{gen} \qquad (4.33)$$

They depend on the magnetic field B. σ_h and σ_e are respectively the hysteresis and the Eddy current loss coefficients. Their values are estimated through the generator presented in [WL13]. The steel plate thickness d_{ip} is taken from [Ste07].

The **winding losses** stand for the resistive heating mainly from the copper wires in the stator. They are calculated with the instantaneous RMS stator current I_{rms} and their resistance R_{st} which is function of the diameter and length of the wires:

$$P_{wl} = I_{rms}^2 R_{st} \qquad (4.34)$$

Finally the generator efficiency is $\eta_g = P_g/P_{in}$ where the electrical power at the output of the generator is:

$$P_g = P_{in} - (P_{ml} + P_{il} + P_{wl}) \qquad (4.35)$$

Operation ranges

The induction generator can extract energy in two regimes, the steady one and the flux weakening one. In the steady region the generator operates normally and the current and voltage increase until reaching the nominal ratings. The flux weakening region appears when the rotational speed reaches the rated one, the voltage is maximum and cannot be overshot. If the turbine spins faster than the nominal, the frequency rises above the nominal. Torque can still be extracted until the current reaches its maximum capacity. This available torque decreases as the speed gets higher. That type of operation regime is represented in Fig. 4.18 with an example of the main parameters of the electrical equipment shown in Table 4.1. In that specific case, the electrical generator is connected to a power converter whose voltage rating is higher and its nominal power oversized in comparison with the generator ones. It means that the system will operate normally until reaching the overspeed value N_{os}. The voltage limitation is then the one of the power electronics V_{pe} and so this overspeed is greater than the generator nominal speed by a factor of V_{pe}/V_g. Note that we denote the rotational speed in rpm by N while Ω is in rad/s.

$$N_{os} = V_{pe}/V_g \ N_{nom} = 1.725 \ N_{nom} \qquad (4.36)$$

In both the steady and the flux weakening regions, the generator is allowed to operate over its rated capacity for short periods of time. The maximal torque that can be extracted depends on the generator. It is represented by the gain M_{mn} that is the ratio between the maximal over the nominal torque. In induction generators, this ratio can reasonably be higher than 2 [ABB04].

$$T_{max} = M_{mn}T_{nom} \qquad (4.37)$$

Oversizing the power electronics allows to overload the generator close to three times the generator rated power during short periods of time. This is a challenging operation mode for the generator and thus requires a good

ventilation and insulation class in practice. In this condition, the temperature inside the generator rises and there is a risk of melting the winding insulation material with a risk of shortcut between phases. The model does take into account the maximal power extraction but does not include a heat model.
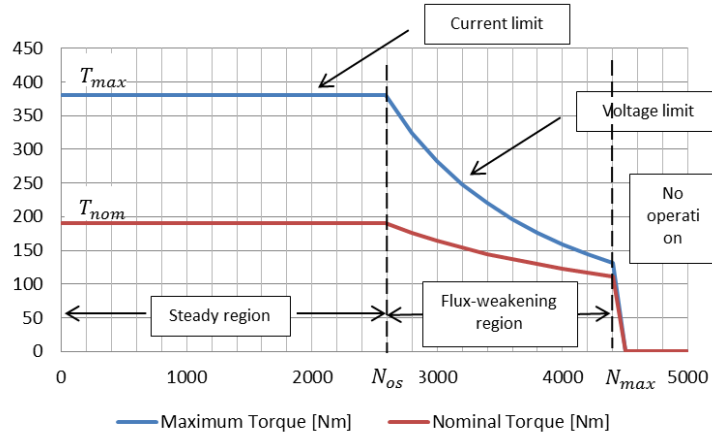
Fig. 4.18: Possible generator operation regions

Tab. 4.1: Main specifications of the electrical generator and power electronics

Parameters	Symbol	Value	Unit
Rated power	$P_{g,nom}$	30	kW
Rated torque	$T_{g,nom}$	191	Nm
Rated speed	N_{nom}	1500	rpm
Ratio max/nom torque	M_{mn}	2	-
Frequency	f_{hz}	50	Hz
Generator voltage	V_g	400	V
Power elec. power	P_{pe}	90	kW
Power elec. voltage	V_{pe}	690	V
Overspeed	N_{os}	2650	-
Weight	w_{gen}	250	kg

4.4.4 Drive train model

Following the $2^n d$ law of Newton, the angular acceleration is the sum of the torques over the inertia of the turbo-generator set and is described such as:

$$\dot{\Omega} = \frac{T_t - T_g - T_{loss}}{I_{PTO}} \tag{4.38}$$

where T_t is the torque provided by the turbine and given by $T_t = P_t/\Omega$, T_g is the resistive control torque applied by the generator and T_{loss} represents the generator losses.

4.5 Optimising the PTO configuration

The main goal in this section is to prove that the W2W model is a useful tool for a technology developer aiming at selecting the main components of the PTO based on specific evidence. This section focuses on the optimisation of the key parameters that constitute the turbine specifications in order to guide their selection and sizing for the specific site of Mutriku. Among the parameters to be optimised, there are the turbine type, the rotational speed and the diameter. The objective of the optimisation is to extract the highest average mechanical turbine power. That analysis offers quantitative advice for the generator type selection and its sizing.

An example is proposed for the case of Mutriku. The optimisation of the turbine diameter and the optimal rotational speed is done for the set of 6 turbines presented in the section 3.2. They consist in 3 Wells and 3 impulse turbines and their characteristic curves are displayed in 4.19.:

- 1 - Monoplane Wells turbine without guide vanes (see Fig. 2.31). The characteristic curves are taken from [FHG18].

- 2 - Monoplane Wells turbine with fixed guide vanes (see Fig. 2.31). The characteristic curves are taken from [FHG18].

- 3 - Biplane Wells turbine installed in Mutriku (see Fig. 2.32). The characteristic curves are taken from [TLH07].

- 4 - Axial impulse turbine with fixed guide vanes (see Fig. 2.34). The characteristic curves are taken from [FHG18].

- 5 - Axial impulse turbine with moveable guide vanes (see Fig. 2.34). The characteristic curves are taken from [FHG18].

- 6 - Biradial impulse turbine with fixed guide vanes (see Fig. 2.36, curves are taken from [Gat+17]. In this case, the performance was obtained during testing the 0.5 m diameter turbine built for the OPERA project in the IST aerodynamic test rig.
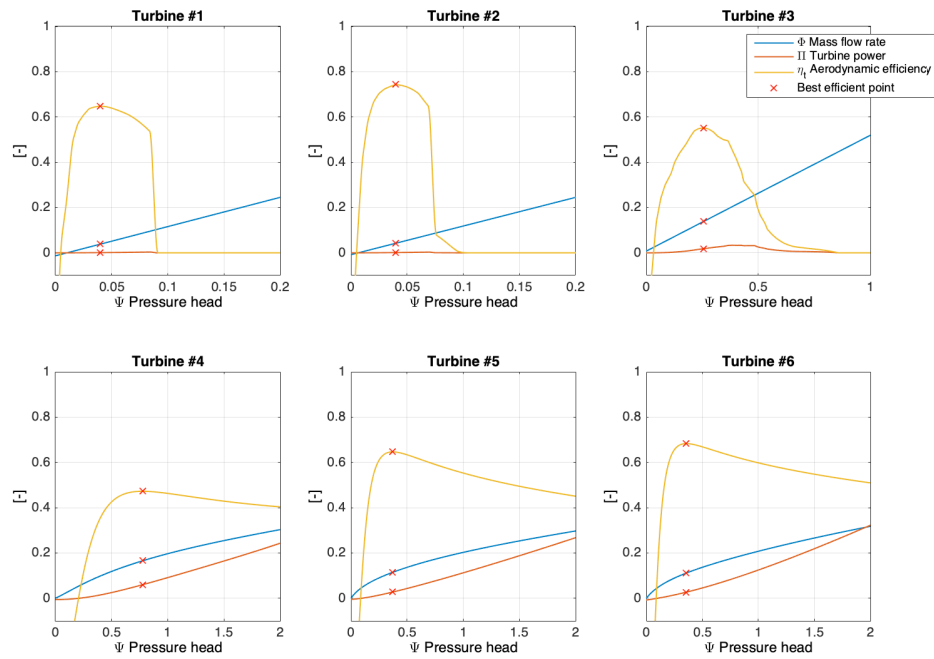
Fig. 4.19: Characteristic curves of the six turbines, adapted from [FHG18; TLH07; Gat+17].

The sea states composing the wave climate of Mutriku are presented in Figure 5.5. Among them, the most energetic sea state is SS10, characterised by $H_s = 2.0$ m and $T_p = 14$ s. That sea state is not the most powerful in terms of kW/m but the most energetic one in kWh/m, considering its frequency of occurrence over a year.

The results of the turbine parameters optimisation using this SS are presented in Figures 4.20 and 4.21. Note that the turbine curves from the biplane Wells #3 and the biradial #6 are obtained experimentally and are more likely to be trusted than the Wells turbines #1 and #2 and the impulse ones #4 and #5. As a general comment, the Wells turbines (upper line of the figures) usually rotate faster than the impulse ones. The explanation comes from the aerodynamic stall in the Wells. The turbine rotates faster in presence of high flow rates to move away from the stalling region. Focusing on the Wells, the first two ones show the highest average turbine power output but the counterpart is that for a specific turbine diameter, the operation range is quite narrow in comparison with the biplane Wells of Mutriku. In the Mutriku OWC plant, the turbine rotor diameter is 0.75 m. The optimisation highlights an optimal diameter between 0.65 to 0.75 m, which is quite close to the one that was selected by the technology developers at the time the plant was

conceptualised. In addition, the generator composing the PTO in the power plant is a 18.5 kW induction generator of one pair of poles, equivalent to 3000 rpm nominal speed. This is quite in line with the results of *Turbine #3* in Figures 4.21 and 4.20. They highlight an optimal speed for SS10 of around 200 and 300 rad/s for a maximal average power of over 15 kW. It means that peaks of power higher than that value can arise and the 18.5 kW generator seems to be a good choice.

In what concerns the impulse turbines - *Turbine #4 to #6* in the Figures 4.21 and 4.20 - the biradial exerts the best performance with a maximal average power output close to 20 kW which ranks it third in respect to the other turbines. Its optimal diameter obtained from this simulation is between 0.7 to 0.8 m and its optimal rotational speeds oscillates around 150 rad/s. To complete this PTO selection and sizing, that study should include results on a series of representative sea states of the entire wave climate at Mutriku. Nonetheless, the main aim of this analysis was to provide a practical explanation on the benefits of using W2W models to support the PTO selection and sizing.
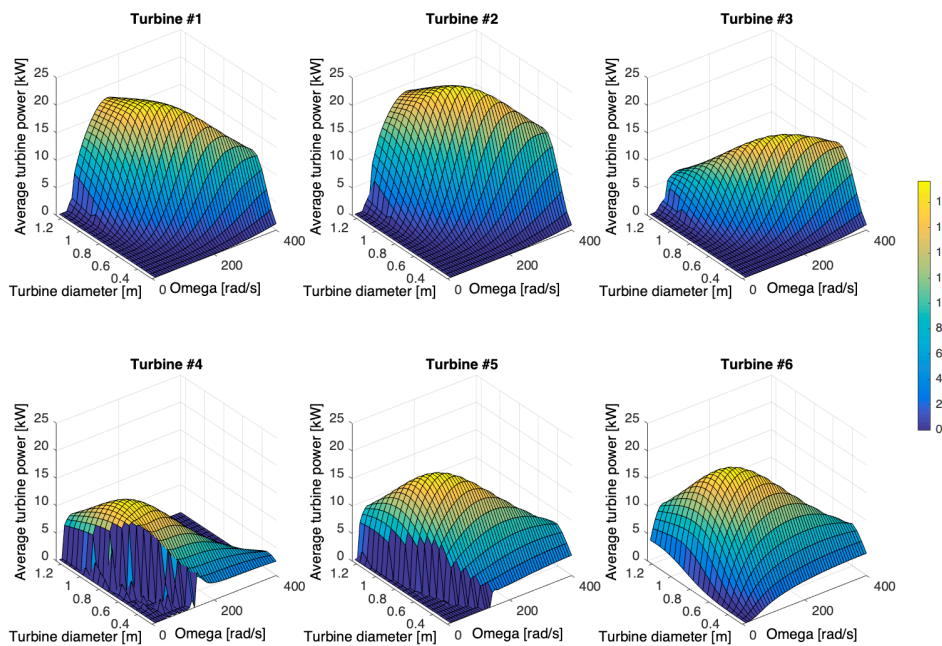
Fig. 4.20: Optimal sizing of the PTO key parameters for the Mutriku OWC plant

Within the OPERA project, the PTO components - biradial diameter and induction generator - were sized using a similar methodology but applied
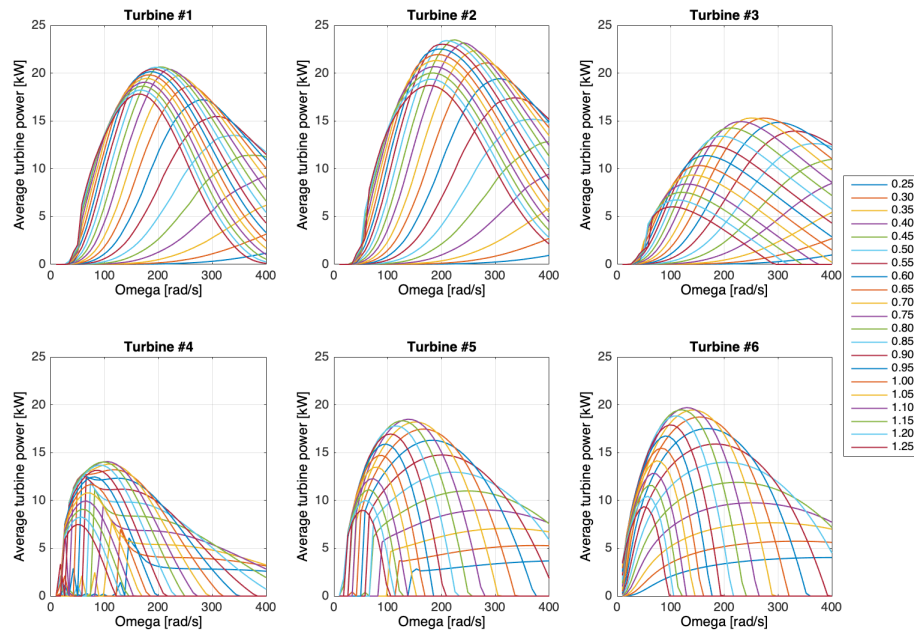
Fig. 4.21: Another view of the optimal sizing of the PTO for the Mutriku OWC plant

to the Marmok-A-5 buoy. The optimal diameter was found to be 0.5 m and in the same ranges of speeds and powers as the initial configuration. The selected generator was a 2-pair of poles rotating close to 1500 rpm with 30 kW of rated capacity. In terms of rated speed and nominal power, the PTO selected for the buoy fits the conditions of Mutriku. Besides, the optimal diameter of the biradial at Mutriku is quite higher than the one of the buoy (0.75 compared to 0.5 m).

4.6 Chapter conclusion

This chapter covered up the main considerations for W2W modelling of the entire energy conversion chain for OWC systems by highlighting two examples: the fixed OWC, like the one in Mutriku; and the floating spar-type one like the IST sparbuoy or the IDOM/Oceantec Marmok buoy. The proposed methodology first presented the analysis in the frequency domain followed by the one in time domain, including explanations on how to deal with the radiation terms. The RAOs presented for both models proved the validation of the TD against the FD in free motion, especially the radiation approximation.

In the full W2W numerical model, the air compressibility effect implies to add non-linearities to the system which supports the use of a time domain model. A comparison was made on several air compressibility models, including one considering air as incompressible, another one where air was subjected to an isentropic process and the last one to a polytropic process. The impact of the compressibility effect on the pressure variations and the power transformations from the pneumatic one to the electrical one were analysed. An experimental validation was then proposed to compare the polytropic model with real data obtained in one of the chambers of the Mutriku OWC plant. The full W2W model and the air chamber model were published in the peer review journal article [Faÿ+20b] as part of the thesis results.

To complete the W2W models, the main equations describing the PTO components (turbine, valve, generator) were also presented resulting in full W2W models coupling hydrodynamics, aerodynamics and electrical concerns. Finally, the numerical model of Mutriku was employed to highlight the possibility it offers in providing evidence for the selection of the main PTO components of OWC systems. These full W2W models are prepared for the development, design and test of the advanced control strategies detailed in the next chapter.

Development of advanced control strategies for the OWC

5

> *Power is nothing without control.*

— **Pirelli's slogan**

Summary: The time domain numerical models prepared in last chapter offer the possibility to deeply study control strategies. In the present chapter, several of them are designed, developed, tested and compared using these W2W models to understand their pros and cons. First, the fundamentals of PTO control in wave energy conversion are illustrated with the model of Mutriku. This section explains the effects of changing the control parameters on the buoy motion and the energy capture. Then the case of the Mutriku plant is taken to develop a number of turbine speed controllers for the PTO composed of the biradial turbine. An analysis assesses them in terms of power production and reliability of the components of the PTO. It focuses mainly on 2 speed controllers: Fixed Speed (FS) controllers and Variable Speed (VS) ones. The FS is first proposed because it is the one most related to the analysis of optimal damping in control theory. The VS are developed because they offer a better balance in terms of power production and component reliability. Several algorithms are developed to apply these controllers such as: Proportional-Integral (PI) controllers, Torque-Speed curves, Non-Linear Model Predictive Controllers (NL-MPC). In comparison with the other algorithms, the MPC one offers the advantage to include the components limitations in an on-line optimisation, and this in function of the coming incident waves. In total 4 main families of controllers are detailed, sometimes having several versions of each. Finally, a latching controller is proposed for the floating device. The aim of a latching control strategy is to tune the device motion to force resonance and extract more energy. Its presence in this chapter is to evaluate these hypothesis with numerical models. This is achieved by acting on the shut-off valve at the inlet of the turbine, and the predictive controller optimises pressure thresholds to find the best instants to open and close the valve.

5.1 Introduction

Control in wave energy conversion is essential for optimising power extraction while ensuring the components reliability, avoid failures, and extend their service life. In this section several control strategies are proposed and their overall performance assessed. In the literature (see Section 3.3.1), the basics of control are often explained in the frequency domain applying optimum control of oscillating bodies to a heaving point absorber. The fundamentals of control are explained later on to understand its effects in terms of wave energy absorption. For this purpose, the W2W model of Mutriku in the frequency domain is used.

Then, the control strategies are all developed using the time domain W2W models to offer a practical approach of the control issues. Here, the time domain is crucial to capture transient events and design/adjust the controllers in a more realistic manner. These are categorised in two main families: the turbine speed controllers which tend to focus on the PTO and transform the captured energy into useful power; and the latching strategy that aims at increasing the power captured by a WEC.

In what concerns the PTO controllers, four main Control Laws (CL) are developed and compared:

- CL1 is the only sea state dependant control strategy. It is based on a Fixed Speed control using a PI-controller to follow the optimal reference speed for a given sea state. FS controllers are the ones that fit better the power absorption from the waves because they represent a constant PTO damping. This parameter is usually the first to be optimised in the design of the device. They offer little flexibility because the parameters are optimised depending on the sea states, which is not optimal in practice. Also, they tend to produce high peaks of power in the electrical conversion if the components are not oversized. It causes the most demanding operation for the electrical parts in high energetic sea states.

- CL2, and versions, uses the well-known approach of Torque-Speed (T-Ω) curves. A torque is applied in function of a rotational speed. These curves can be characterised in function of two control parameters:

a slope and an exponent. The philosophy behind the selection of these parameters defines the different versions of this CL: optimise the captured power, the mechanical one, and/or the electrical one.

- CL3 is a trade-off between the FS and VS approaches. The speed varies but not as much as in CL2, that is why it is named Quasi-FS. The objective is to be as close as possible to the optimal PTO damping while offering some variations of speed. The operation is not as harsh as the FS because, like any VS controllers, it can benefit from the kinetic energy storage offered by the turbine-generator inertia.

- CL4 is the most advanced controller because it can perform an online optimisation in function of the system external and internal conditions. Indeed, it constantly adapts the T-Ω coefficients depending on the incident wave forces, the efficiencies and limitations of the components. In addition, the algorithm can include restrictions to better consider the reliability of these components.

In total, with the different versions of the four groups, 7 control laws are presented and their performance assessed, see Table 5.1. CL2 to CL4 are considered as **adaptive controllers** because they rely on measurable process variables to apply the control action regardless of the sea state. Simulations are made using the full TD W2W model of Mutriku presented in Section 4 associated with the PTO developed for the OPERA project, that is to say the biradial turbine with a 30 kW generator.

Tab. 5.1: Turbine speed control strategies developed and tested

Family	FS	VS	Quasi-FS	VS
Id	CL1	CL2.1 CL2.2 CL2.3	CL3	CL4.1 CL4.2
Algorithm	PI controls turbine speed based on ref. and feedback speeds	Torque-Speed Laws control torque based on rot. speed	PI controls speed calculating ref. speed based on pressure variations	NL-MPC controls torque knowing incident wave force, numerical model and rot. speed
Note	Adapted from existing studies [COR11]	These are conventional in wind turbine control. CL2.1 is an adapted version of [Ceb+13] CL2.2 is adapted from [Fal02a; Thi+11; Hen+16c] CL2.3 is a new approach	New contribution	New contribution

Finally, the latching control strategy is detailed using the full TD W2W model of the sparbuoy. This one uses the fast actuating valve of the biradial to open and close the turbine inlet. When the valve is closed, the pressure inside the chamber rises and changes the relative motion between the structure

and the water column. The actuation of the valve depends on the optimally calculated pressure thresholds. The algorithm used for that purpose is an adaptation of the CL4 developed earlier but instead of optimising the T-Ω law parameters, the predictive algorithm optimises the pressure thresholds. Results are presented both for regular and irregular waves.

5.2 Control fundamentals

Let us consider a WEC as a mechanical mass-spring-damper system restricted to a simple degree of freedom. The PTO system is theoretically capable of adapting its coefficients of damping C_{PTO} and stiffness K_{PTO}. The force of the PTO is noted:

$$F_{PTO} = C_{\text{PTO}} \, \dot{z} + K_{\text{PTO}} \, z \tag{5.1}$$

In the case of the OWC, the turbine-generator set can extract energy captured in the chamber and is associated to a damper mechanism. The RAO of the studied chamber of Mutriku in free motion, without PTO system, is represented by the dark blue line of Figure 5.1. Note that in that case, the power P_{PTO} is null. The force introduced by the PTO, here only considering the damping coefficient C_{PTO}, has the effect of reducing the WEC motion while extracting energy. If the system is underdamped, the power extraction is less and the displacement higher. In the opposite, an overdamped system will not allow the device to move enough and sacrifices the power capture. Therefore, there exists an optimal value of the damping coefficient. The optimisation of the C_{PTO} coefficient as presented in Figure 5.1 allows to understand that phenomenon. There is an optimal damping coefficient that extracts more energy, i.e. the integral of the power over all the frequencies (red dotted line in bold).

Adapting the stiffness would be equivalent to changing the phase of the device motion and force resonance conditions, when the oscillating body velocity is in phase with the excitation force. This is referred as phase control in the literature. The practical principle of a negative spring is difficult to comprehend because it leads to an unstable system and requires that the PTO feeds back energy to the system to actuate on the motion. Nevertheless, Figure 5.2 shows a theoretical approach with an optimisation of the PTO stiffness. The first observation to be made is that the motion is amplified drastically. As the stiffness gets closer to the optimal, the energy extraction
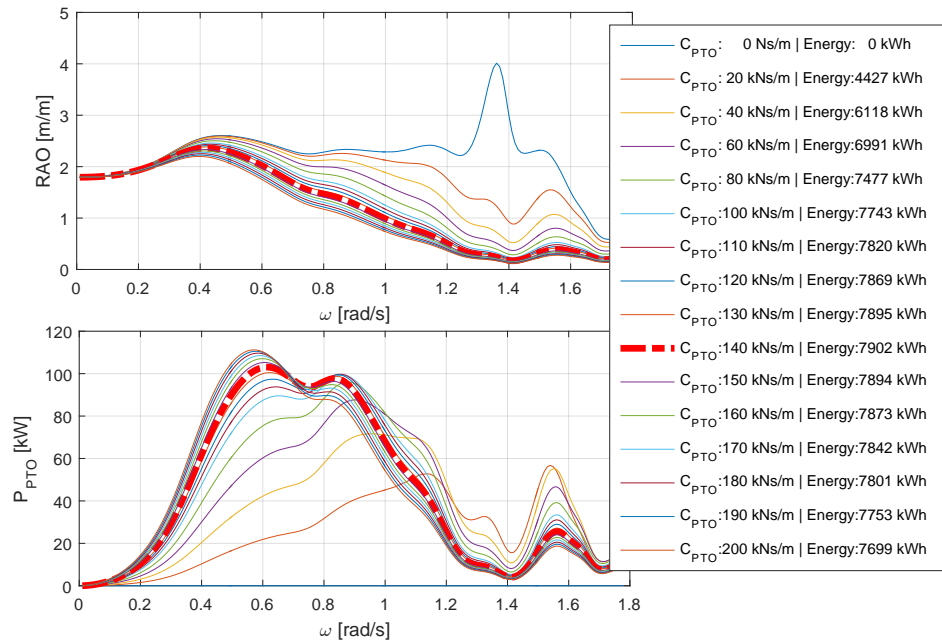
Fig. 5.1: Optimisation of the damping coefficient C_{PTO} in the Mutriku W2W model in FD

is greatly improved until reaching more than 3 times the one of the optimal C_{PTO} only. The case where $K_{\text{PTO}} = -160$ kN/m is not considered as the motion goes to infinity at a frequency close to 0. The figure informs about the resonant frequency that is close to $\omega = 0.4$ rad/s, this is equivalent to the frequency where the amplitude of the excitation force is the highest (see Figure 4.2).

Finally, Figure 5.3 shows the case where both the damping and stiffness are optimally tuned and illustrates the great increase in power capture made by this combination of control parameters. In the literature, this is known as optimum control. Note that apart from the fact it is a challenge to design a mechanism to introduce this component on the PTO force, the motion is so amplified it is difficult to conceive a WEC able to oscillate with these levels of displacement. This study should therefore only support the theoretical explanation of optimum control in wave energy as it was detailed in the state of the art on control exposed in Section 3.3.1.
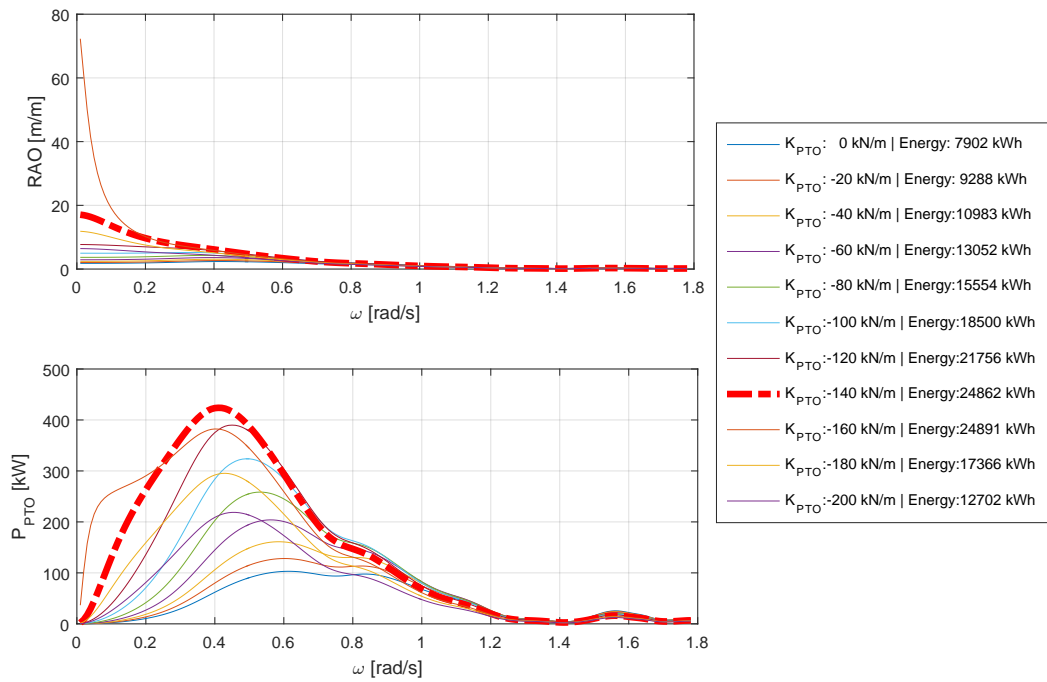
Fig. 5.2: Optimisation of the stiffness coefficient K_{PTO} in the Mutriku W2W model in FD
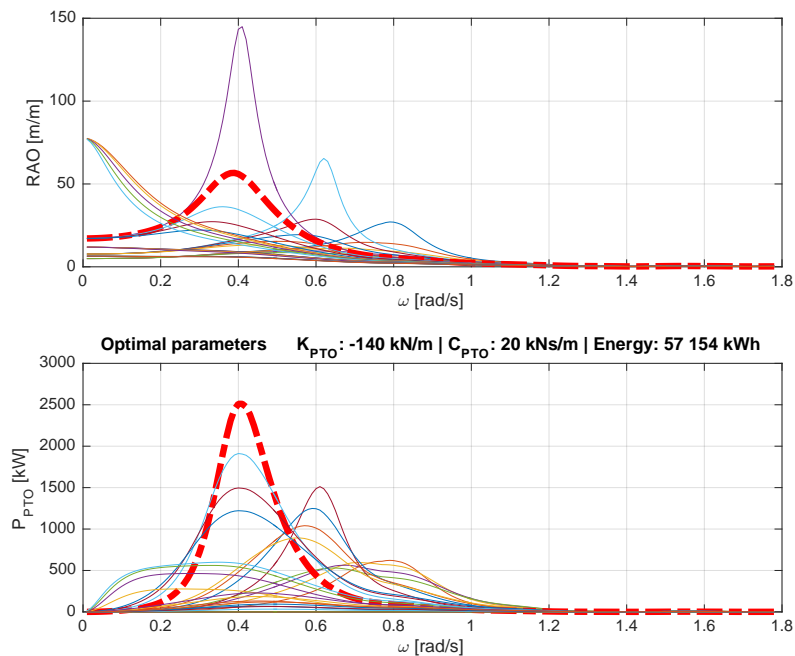
Fig. 5.3: Optimisation of both C_{PTO} and K_{PTO} in the Mutriku W2W model in FD

5.3 Turbine speed control in Mutriku for the biradial turbine

The effect of tuning the control parameters on the power capture has been presented using the FD W2W model of Mutriku, and with it, the challenges and unrealistic concerns brought by optimum control. This section presents the development of several control strategies applied to the PTO, whose objective is to optimise the power transformation from the captured energy into electrical power at the output of the generator. This analysis uses the full TD W2W model of Mutriku which includes all the non-linearities detailed in Section 4. In the present section, the 4 main types of controllers are described and listed in Table 5.1, 7 in total when including their versions. The performance of each controller is analysed along with some concerns on the components reliability. The PTO is composed of the biradial turbine of 0.5 m diameter coupled to the induction generator of 30 kW and connected to a B2B power converter of 90 kW rated capacity. Its characteristic curves are the ones of Turbine #6 in Figure 4.19.

5.3.1 Common framework for the analysis of the control laws

For each control law, simulation results are obtained for 14 realistic sea states picked out of the wave climate at Mutriku as seen in Figure 5.5. The numerical model is implemented in Matlab/Simulink illustrated in Figure 5.4.
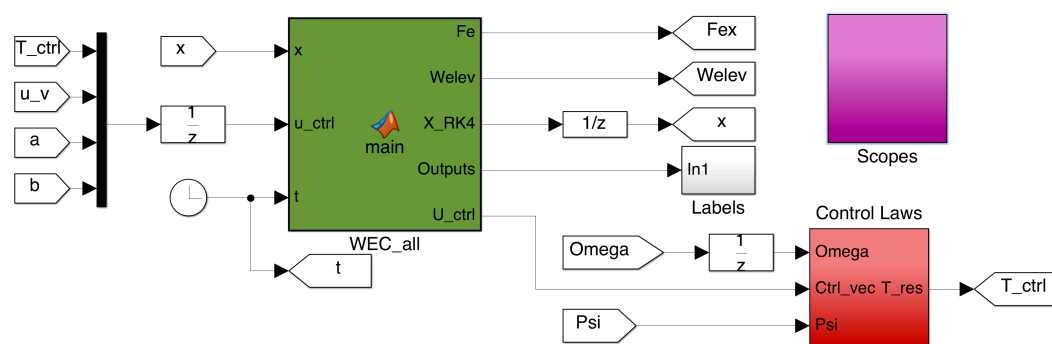
Fig. 5.4: Simulink diagram used to describe the Mutriku W2W model including the control laws

The wave climate was measured at Mutriku thanks to the installation of a pressure sensor disposed at the sea bottom in front of the plant during the period February to April 2018. Although there are uncertainties related to the measurements of the wave elevation using hydrostatic pressure variations [Faÿ+18b], this equipment was the best trade-off between accuracy, reliability and cost. The wave elevation time series measured at 2Hz were then used to obtain the hourly sea states. These statistical wave data are available online on Zenodo [Ber18], and have been used to compute the wave statistics such as the significant wave height H_s, and energy period T_e. The selection of the 14 SS is done over the compromise of high occurrence for a large variety of sea states. Both the wave climate and the selected sea states are presented in Fig. 5.5. Each bin is characterised by 0.5 m of H_s and 1 s of T_e. Each of the 14 wave spectra used in the simulations comes from all the real wave spectra falling inside the sea state bin, and averaged over all the angular frequencies. Fig. 5.6 highlights the averaged spectra for all the SS. For example, Figure 5.7 shows the wave spectrum of SS10 (orange bold line) as the average of 90 real spectra measured in front of the plant. Following the DNV recommendations [DNV07], each sea state lasts 30 min in the simulation.

SS	H_s [m]	T_e [s]	%	Pow. [kW/m]	Ener. [kWh/m]
1	0,50	10	3,14	1,05	283
2	0,50	11	5,95	1,16	591
3	0,50	12	6,06	1,26	657
4	1,00	9	1,24	3,78	405
5	1,00	12	4,87	5,04	2111
6	1,00	13	4,17	5,46	1957
7	1,50	14	6,49	13,23	7388
8	1,50	15	3,25	14,18	3958
9	1,50	18	0,65	17,01	950
10	**2,00**	**14**	**4,87**	**23,52**	**9851**
11	2,00	15	2,22	25,20	4808
12	2,50	15	2,27	39,38	7696
13	3,00	15	0,81	56,70	3958
14	4,00	18	0,49	120,96	5066
	Tot. Occ.		46,48		
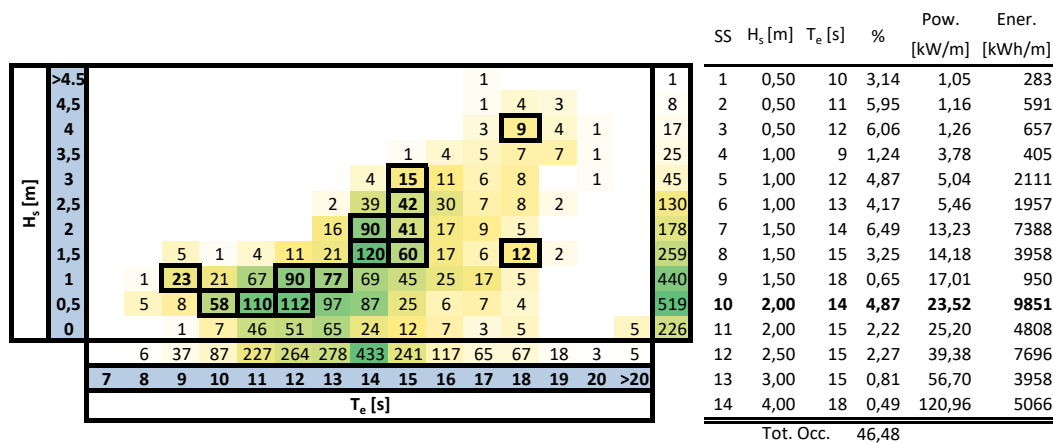
Fig. 5.5: Wave climate measured at Mutriku and the selected 14 SS

5.3.2 Sea state control - Fixed reference speed

The first control law, **CL1**, is sea state dependant which means the control parameters are optimised for each sea state. In this case, the rotational speed is set as reference for a PI-controller. The optimisation method consists in searching for each sea state the optimal speed that provides the highest average turbine power. To do so, the full W2W model is used but considering
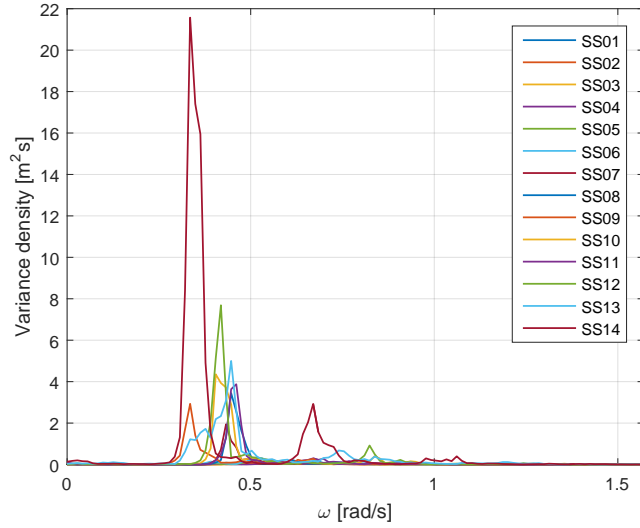
Fig. 5.6: Wave spectra of the 14 SS used in the numerical simulation
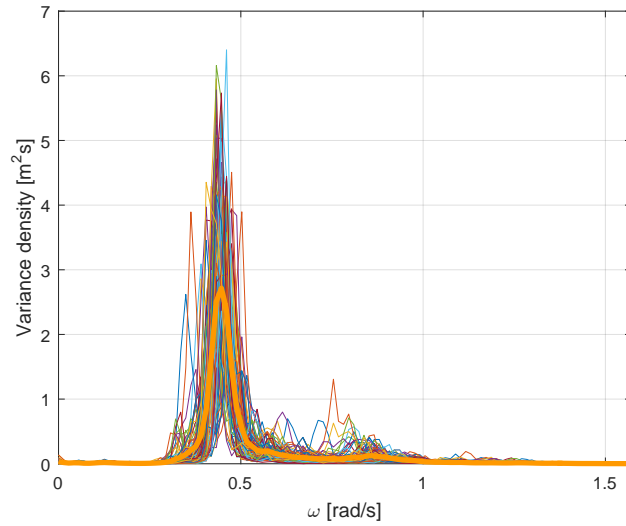
Fig. 5.7: Wave spectra of SS10 and the average spectrum taken for the simulation

there is no acceleration, i.e. in the drive train equation (4.38) $\dot{\Omega} = 0$. Therefore, there is an equality between the torques $T_{\mathrm{t}} = T_{\mathrm{g}} + T_{\mathrm{loss}} = T_{\mathrm{res}}$ at each time instant. It is similar to assume a system with infinite inertia. Figure 5.8 shows the optimisation process where each line represents a sea state. For each one of them, there exists an optimal reference speed giving the maximum average turbine power. To implement the control law in the TD W2W model, a control block that includes the PI-controller is added. Ω^* is the rotational speed reference for each sea state, the error ϵ is calculated and set as the input of the PI-controller block. The controlled variable is the generator resistive torque T_{g} applied to minimise the speed error ϵ, see Figure 5.9. It is restricted to compute only positive control torques to avoid reverting the generator in motor mode.
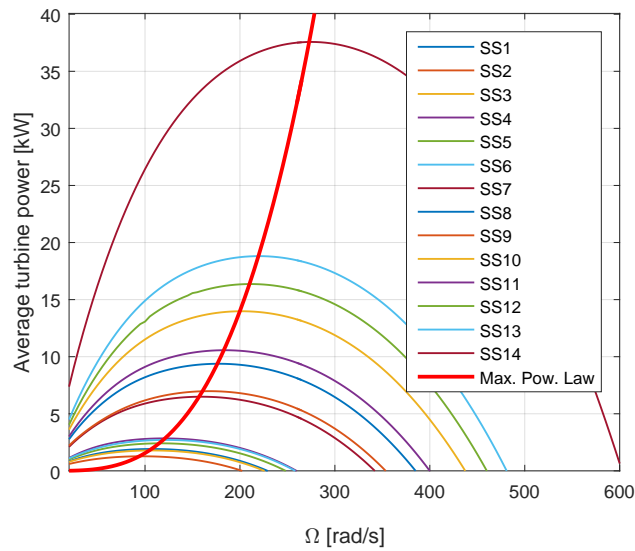
Fig. 5.8: Optimisation of turbine operation to design CL1
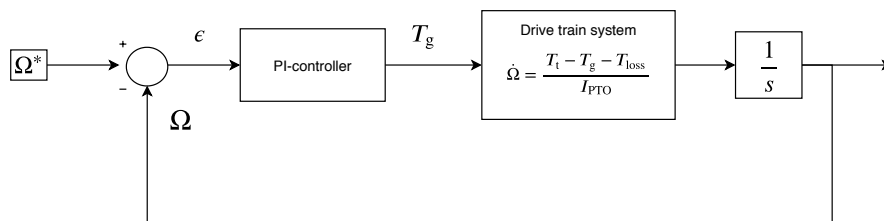
Fig. 5.9: Control loop of CL1
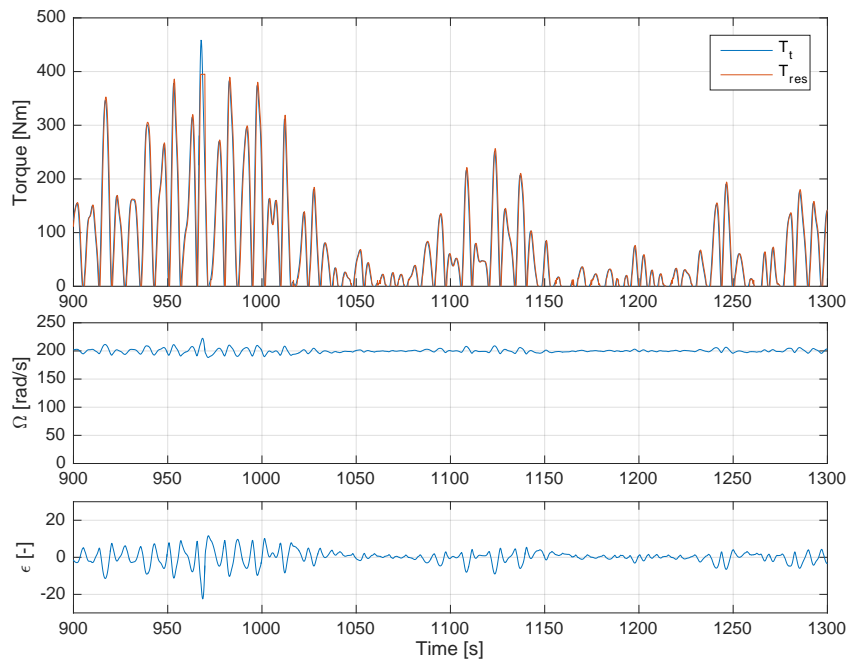
Fig. 5.10: Time series of the turbine and generator torques, rotational speed and speed error during operation of CL1 in SS10

The proportional and integral coefficients of the PI-controller were tuned so the feedback speed is almost constant, allowing small oscillations due to pertubations caused by the sudden changes of turbine torque. This can be seen in the example of SS10 presented in Figure 5.10. The oscillations are also due to the fact the PI-controller cannot compute a negative control torque, which means acting as a motor. In this figure, the torques, the rotational speed and the PI error ϵ are plotted. The rotational speed rounds the reference speed for this SS, $\Omega^* = 200$ rad/s with an error in the range [-20:+10] rad/s. The highest value being when the maximum torque allowed by the generator is reached.

5.3.3 Adaptive controllers

The main drawback of **CL1** is its dependence to sea states. Adaptive controllers are designed to be valid for every sea conditions without the need to change the control parameters when the sea state changes. The characteristics of an adaptive controller is that it applies for any sea state and adapt to the changing conditions of the environment. The ones controllers developed here are all VS controllers and present the advantage of reducing the stress on the electrical conversion components because the drive train inertia can store kinetic energy for short periods of time which was not the case for CL1. Here two adaptive controllers are developed. They compute the control action in function of measurable process variables: the rotational speed for CL2 and the air pressure inside the chamber for CL3.

CL2 enters the category of the torque-speed curves, also known as T-Ω curves, or torque laws. The objective of T-Ω laws is to apply a generator torque in function of the rotational speed. Three versions are designed where each one corresponds to a different design point:

- CL2.1 maximises the turbine efficiency. It relies on known efficiency turbine curves and the controller's objective is to operate the turbine closest to the highest operation point. It is one of the simplest one because there is no need for any kind of optimisation using a W2W model but only takes into account the efficiency of the turbine and not the overall PTO one.

- CL2.2 maximises the average mechanical power. It is based on an offline optimisation process where the W2W model runs and finds the best operation point that maximises the turbine power and generalises it for all the sea states. This controller is more advanced as it considers the turbine operation as part of a system with the dynamics of the device. Thus, there is a need for a reliable W2W model to perform the optimisation. Still there is no consideration for the electrical conversion.

- CL2.3 tends to maximise the average generator power considering both the turbine and the generator in the torque law. The curve is adjusted in function of the generator rated values as a priority criteria but also includes the turbine behaviour. There is no need for an offline optimisation, the design parameters only rely on known values.

The other adaptive control law - **CL3** - tends to optimise the absorbed power like CL1 but allowing some speed variations on the drive train. As such it benefits from the power smoothing effect brought by the drive train inertia. It uses the statistical value of standard deviation of pressure to obtain a reference speed which is then followed by a PI-controller like in CL1. The reference point is obtained by an offline optimisation like in CL1 and CL2.2. The approach is systemic and has to rely on an accurate W2W model.

CL2.1 - Theoretical turbine torque estimation

A simple variable speed control strategy is designed to operate the turbine at its best operation point, see Turbine #6 of Figure 4.19. This T-Ω law only requires the turbine characteristics to compute the required design point. There is an operational condition for which the turbine is at its best efficiency point that corresponds to optimal values of Ψ_{opt}, Φ_{opt} and Π_{opt}. By rearranging equations (4.28) to (4.31), this corresponds to an optimal estimated turbine torque as highlighted in [Ceb+13]:

$$\eta_{\text{t,max}} = \frac{\Pi_{\text{opt}}}{\Psi_{\text{opt}}\Phi_{\text{opt}}} \equiv T_{\text{t,opt}} = \underbrace{\eta_{\text{max}}\Psi_{\text{opt}}\Phi_{\text{opt}}\rho_{\text{in}}d_{\text{t}}^5}_{K_{\text{t}}} \, \Omega^2 \qquad (5.2)$$

The value of the turbine gain is $K_{\text{t}} = 1.1\text{x}10^{-3}$. The objective is to control the turbine speed to reach the turbine operation point where the efficiency is maximum by applying the generator torque T_g. This control variable then

affects the rotational acceleration of Eq. (4.38). Let us consider a lossless power conversion system, the powers in the turbine and the generator side are equal in average for a simulation time long enough. This means that, similarly to an optimal estimated turbine torque, there is an optimal torque at the generator side controller, defined by a quadratic law in function of the rotational speed.

$$T_g = K_t \, \Omega^2 \qquad (5.3)$$

The gain for the curve slope is selected for this specific design point offering the best turbine efficiency. It will serve as the base case to compare the simulation results of the control laws. CL2.1 torque law is represented in Fig. 5.11 by the solid blue line. It appears that at the highest speeds, the controlled torque is only half of the nominal generator one. This control law presents the advantage to perform fair enough independently of the sea state. However it does not take into account the global dynamics of the plant nor the generator operation.

CL2.2 - Optimum turbine operating region

This control strategy uses Eq. (5.3) but formulates it in a more general manner by introducing as control parameters a slope a and an exponent b to the T-Ω curve:

$$T_g = a \, \Omega^b \qquad (5.4)$$

The control parameters can be tuned in function of the control objective. It was employed in a number of publications [Fal02a; Thi+11; Hen+16c]. The principle resides in finding the parameters best suited for a specific OWC operation in a certain wave climate and with a specific air turbine. Based on the optimisation done in CL1 which resulted in Fig. 5.8, for each sea state there is an optimal speed associated to a maximum turbine average power. By performing a power law regression of each optimal operation point, a curve representing the maximum achievable mechanical power is obtained, represented by the red curve named "Max. Pow. Law" in Fig. 5.8. This curve is characterised by the a and b parameters resulting from the curve fitting process. The main difference with CL2.1 is that the offline optimisation process, where CL2.2 is based on, includes the hydrodynamics of the WEC and the turbine behaviour to obtain the highest average mechanical power, whereas the other CL only relies on the turbine characteristic curves. In the present case, the torque law of CL2.2, being associated to these operation

conditions, is defined by the two control parameters of the T-Ω curve slope $a = 7\text{x}10^{-4}$ and its exponent $b = 2.1731$. As for CL2.1, CL2.2 torque law is represented by the red dotted line in Fig. 5.11.

CL2.3 - Optimal generator operation

The last torque law is designed to include considerations on the PTO as a whole with both the generator and the turbine. The electrical conversion at the generator's side is optimised thanks to the choice of appropriate coefficients for the curve slope and exponent. They are selected to reach the generator nominal values of torque and speed. This is the operation point where the generator efficiency is the highest. The curve is defined by a quadratic shape, instead of a linear one, to allow the turbine to speed up at low speeds. For this case, the T-Ω parameters are the slope $a = 6\text{x}10^{-5}$ and its exponent $b = 3$. CL2.3 torque law is represented by the black dotted line in Fig. 5.11.

In summary, the three torque laws of CL2 are represented in Figure 5.11. The behaviour of these three versions can be compared in Figure 5.12 where the time series of the torques from the turbine and the generator, and the rotational speeds are plotted during operation of SS10. It appears CL2.1 and CL2.2 are somehow similar with slightly higher values of both torques for CL2.2 and an average speed a bit lower. CL2.3 contrasts in comparison with the two others. The torque levels induced by this third torque law are significantly higher and as a consequence the speed oscillates in values closer to the nominal (around 150 rad/s). In addition, there are events when the safety valve actuates, between 920-1100 s for example. The valve position is not present in the figure so one can only see the effects of a valve closing. During the time it is closed, the air does not flow through the turbine and the mechanical torque is null. The generator continues to apply the torque laws and the turbine slows down until the speed threshold is reached so the valve can be opened again and the system operates normally. This is what happens for CL2.1 and CL2.2 between this time interval when the turbine torque falls suddenly from >250 Nm to 0 several times. The rotational speed slows down from 250 rad/s, the closing threshold, to 190 rad/s, the opening threshold. At the same time, the torques applied using CL2.3 are sometimes beyond the nominal, which signifies a higher production. The speed stayed far from the safety valve actuation and, therefore, it did not need to be operated.

Figure 5.11 shows that the torque levels imposed by CL2.3 are much larger than the other CLs. Furthermore, this control law does not allow the drive train to speed up as much as the two other cases. The counterpart is that it operates more often in regions above the nominal torque/power. Let us take the example of the set of highly energetic waves in the time interval 900-1050 s. There are 11 events when the generator operates higher than the 191 Nm of nominal torque, and one event where the maximum torque is reached (the saturation near the 400 Nm). In this kind of operation, the induction generator shall withstand short time period power peaks but the reliability would be impacted.
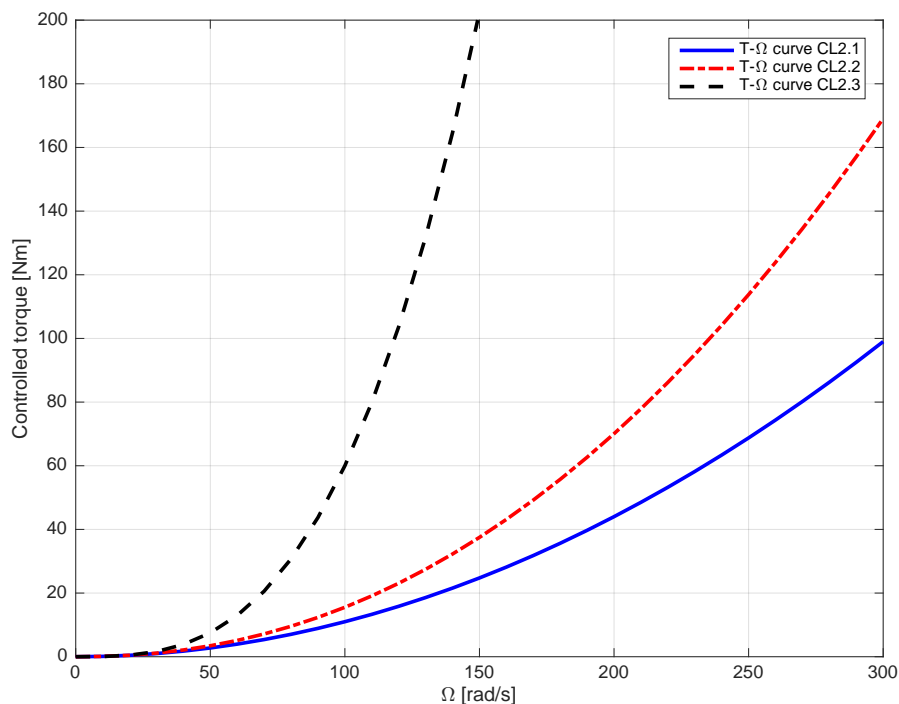
Fig. 5.11: Torque laws for the different versions of CL2

CL3 - Quasi-fixed speed

This other adaptive controller takes advantage from the evidence given by the optimisation done in CL1. There are optimal operational conditions where the power absorbed is best under a specific turbine damping. In practice, it means that there is an optimal average speed for each sea state. As a consequence, the levels of pressure inside the chamber are optimal under that conditions. The variable that relates the rotational speed and the pressure is the dimensionless pressure head Ψ (see Eq. (4.28)). For the
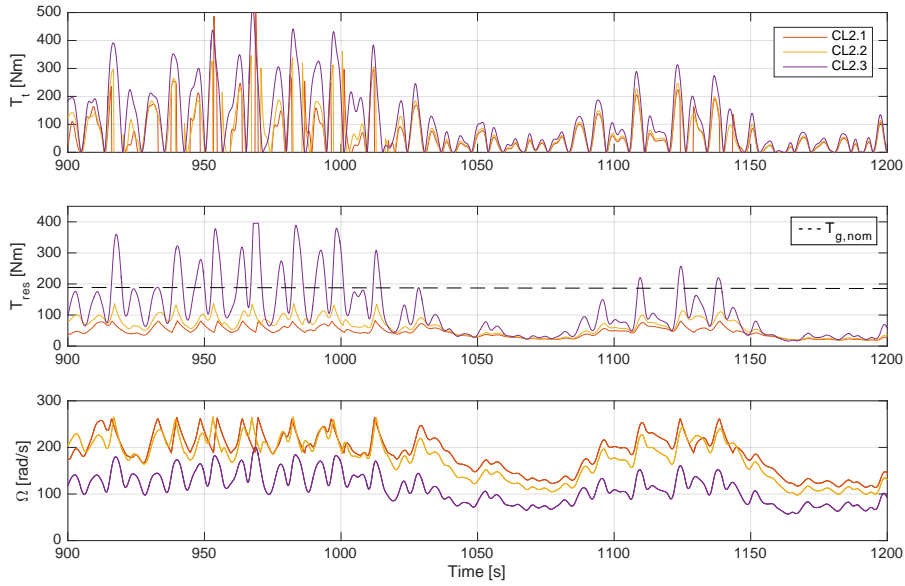
Fig. 5.12: Time series of the turbine and generator torques, and the rotational speeds for the three versions of CL2 in SS10

optimal conditions of CL1, the time series of Ψ are obtained and the standard deviation deduced. This statistical value indicates the levels of pressure that are optimal for each sea state. In Table 5.2 the values of $\sigma(\Psi)$ are collected. It appears quite stable with variations around 0.31-0.34 (if SS12 and SS14 are out of range, it is surely due to the valve actuation). The philosophy around CL3 is to try to adapt the turbine speed at each instant in order to be as close as possible to this reference point of operation. To do so, let us introduce the gain relating the $\sigma(\Psi)$ and the average speed $\bar{\Omega}$:

$$K_{\sigma(\Psi),SS} = \frac{\bar{\Omega}}{\sigma(\Psi)} \tag{5.5}$$

The average of the valid $K_{\sigma(\Psi),SS}$ done in Table 5.2 gives the common gain to be used by the controller. Taking the average value makes it independent to sea states. The control algorithm then traduces the variations of Ψ during the simulation into a reference speed, see Eq. (5.5), which is controlled thanks to the same PI-controller as used in CL1. The diagram of the controller is presented in Figure 5.13. The standard deviation is computed with a sliding window of 180 s. The duration of the sliding window has to be large enough to consider enough variations of Ψ but not too long to allow enough

Tab. 5.2: Definition of $K_{\sigma(\Psi)}$ with process variables from CL1 simulation

SS	$\sigma(\Psi)$	$\bar{\Omega}$	$K_{\sigma(\Psi),SS}$
1	0.33	110	334
2	0.33	95	284
3	0.33	105	322
4	0.34	120	350
5	0.33	115	344
6	0.33	120	366
7	0.31	160	517
8	0.31	180	590
9	0.31	170	555
10	0.33	200	610
11	0.31	185	599
~~12~~	~~0.24~~	~~250~~	~~1041~~
13	0.32	220	694
~~14~~	~~0.36~~	~~249~~	~~701~~
		Average	**464**
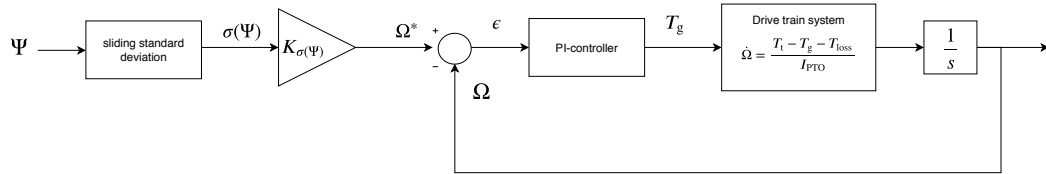
Fig. 5.13: Control diagram of CL3

variations of speed. The length of the sliding window was defined by an offline optimisation.

$$\Omega^* = K_{\sigma(\Psi)}\, \sigma_{180}(\Psi) \tag{5.6}$$

Similarly to the other controllers, the main control variables are shown in Figure 5.14 where the system operates during the same SS10. The variation of the speed reference and the speed feedback can be observed. This controller acts similarly to CL1 in terms of torque variations but with the important advantage that it is not dependent on sea states. It can be seen as a generalisation of CL1 for any SS and make it more practically implementable.
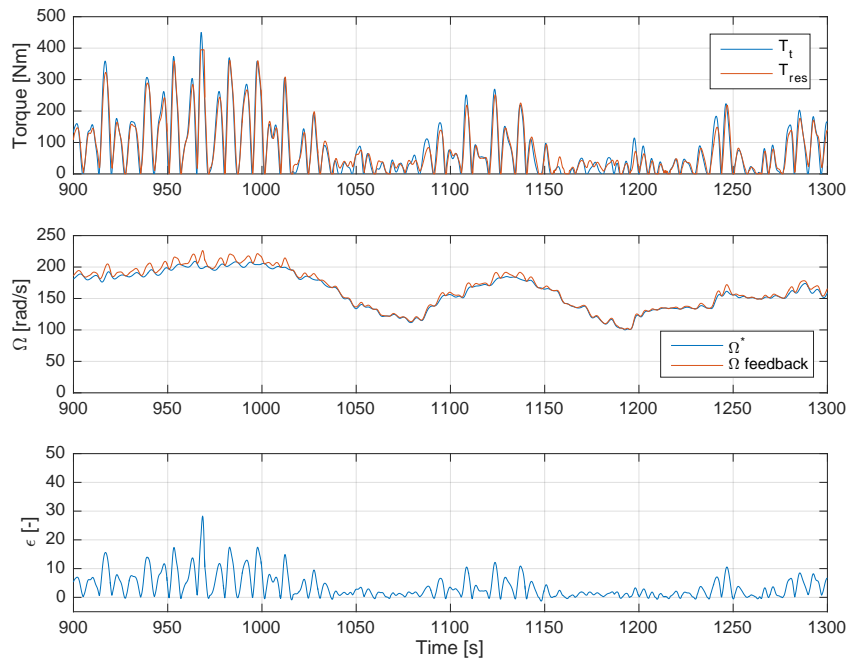
Fig. 5.14: Time series of the torques, reference and feedback speeds and speed error during operation of CL3 in SS10

5.3.4 Non-linear constrained model predictive control

The aim of this non-linear model predictive control, nammed **CL4**, is to maximise the electrical output power based on a variable speed controller. The torque laws proposed in CL2.1 and CL2.2 rely on a lossless drivetrain and on the perfect characterisation of the turbine and CL2.3 simply uses generator nominal values for the design of control setpoint. In comparison, the proposed strategy takes into consideration the overall power conversion of the PTO, and includes in the optimisation process the efficiencies of both the turbine and the generator. Eventually it includes all the numerical model non linearities. At each sampling time, the torque law in Eq. (5.4) is used to compute the control torque, but with the curve slope a and its exponent b optimised online by the controller. At the beginning of the control horizon, called replanning period, the best configuration of a and b is calculated for the prediction horizon T_{ph}, and constitutes the new control vector $u_{\text{c}} = [a, b]$. These parameters are now updated and applied by the torque law at each sampling time during the replanning time, until a new control vector is computed at the beginning of the next replanning period. Fig. 5.15 depicts the timings of the controller.
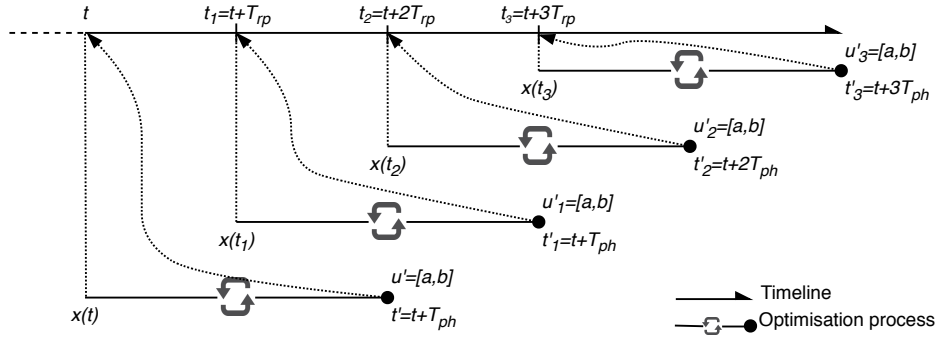
Fig. 5.15: Global process of the controller

In Section 5.3.1, the wave resource at Mutriku was described. The sea states were obtained thanks to an underwater pressure sensor capable of measuring the wave elevation. This data is fundamental for the predictive controller because it is mandatory to know in advance the charateristics of an incoming set of waves. The predictive horizon time is constrained by the wave travel time from the real-time wave elevation sensor to the plant. Assuming shallow water conditions, the constant wave travel speed for all frequencies depends on the water depth d_w, the theoretical wave celerity is defined as $c_\mathrm{w} = \sqrt{g d_\mathrm{w}}$ [DNV07]. Because the sensor is installed at $d_\mathrm{s} = 200\mathrm{m}$ ahead of the chamber wall at a mean tide depth around $d_\mathrm{w} \approx 10\mathrm{m}$, the average prediction time is

$$T_\mathrm{ph} = d_\mathrm{s}/c_\mathrm{w} \approx 20\mathrm{s} \tag{5.7}$$

This gives sufficient time to consider between one and two wave periods for the prediction. A replanning time of half the prediction time is appropriate in this case. As the optimisation takes into account average values of power, it is not so sensitive to synchronisation between the wave measured and the one actually hitting the plant. In fact in real conditions, the waves are not cylindrical and do not always travel in the same direction, adding uncertainty in the wave prediction.

The optimisation algorithm of **CL4.1** tends to minimise the cost function in Eq. (5.8). It includes the turbine and the generator power in order to integrate both efficiencies and intrinsic constraints. Restriction on the generator maximum torque and the turbine threshold speed for the valve actuation are considered in the numerical model during the optimisation.

$$J = \min - \frac{1}{T_\mathrm{ph}} \int_t^{t+T_\mathrm{ph}} (\alpha_\mathrm{J}\, P_\mathrm{t} + \beta_\mathrm{J}\, P_\mathrm{g})\, \mathrm{d}t \tag{5.8}$$

The parameters α_J and β_J are weighting parameters that allow setting priority to power transformation at the turbine or power conversion into electricity. During the online optimisation, the parameters a and b are able to evolve within a bounded vector centered to there initial values (from the previous optimisation). A multi-parametric optimisation resulted that a maximum increment of +/-25% for a and +/-5% for b leaded to the best increase in power production (see Fig 5.16). This allows to guide the search of the optimal parameters during the optimisation. The variations of b are more constrained because the torque law exponent has an impact much more significant than the slope.
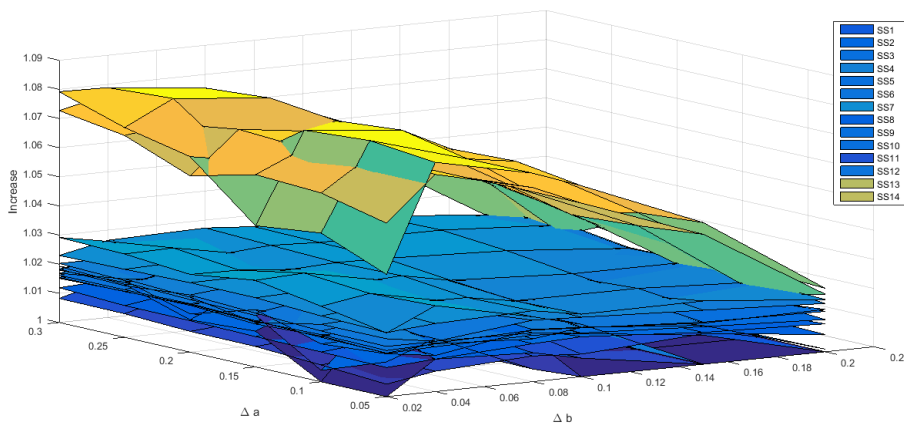
Fig. 5.16: Sensitivity analysis for the increments of a and b
to evaluate the increase in power production

Another version of this NL-MPC, **CL4.2**, considers additional constraints during the optimisation process. The aim is to benefit from the performance gain brought by the predictive algorithm while adding a concern on the generator reliability. Indeed, although it is known that induction generators like the one used in this study can operate beyond the nominal capacity, it increases the probability of failure associated with an operation in these ranges of powers and as a matter of fact can impact the equipment reliability. The objective function is then subjected to the constraint condition that the predicted peak generator power is limited to a value proportional to the nominal power K_{lim}:

$$\hat{P}_g < K_{lim}\, P_{\text{nom}} \tag{5.9}$$

In this application, $K_{lim} = 2$ was selected.

Similarly to the other control laws, time series of the main control variables are presented in Figure 5.17 to understand the operation of both CL4 versions during SS10. These results shows they are wrking as expected: the variables are strictly the same except when operating during the highly energetic set of waves. CL4.1 simply aims at taking full potential of the generator, the resistive torque is higher in that episode which slows down the turbine and avoids the operation of the valve, i.e. the turbine continues providing torque. On the contrary, because it includes the additional constraint on the generator power, CL4.2 selects the control parameters more appropriate to lower the electrical power peaks. The effect is then quite obvious, the turbine speeds up, reaches the upper threshold ordering the valve to shut off and the turbine stops producing during the 4 events when the valve is closed, at t = [953, 968, 983, 998] s. The evolution of the control parameters are in the bottom graphic. They are strictly the same for both CL4 versions before and after the set of highly energetic waves. They only differ during that episode. In brief, while CL4.1 optimises the power production within the design operations ranges, CL4.2 adds another concern on the generator reliability. The production is expected to be higher on CL4.1 and the reliability score better for CL4.2.
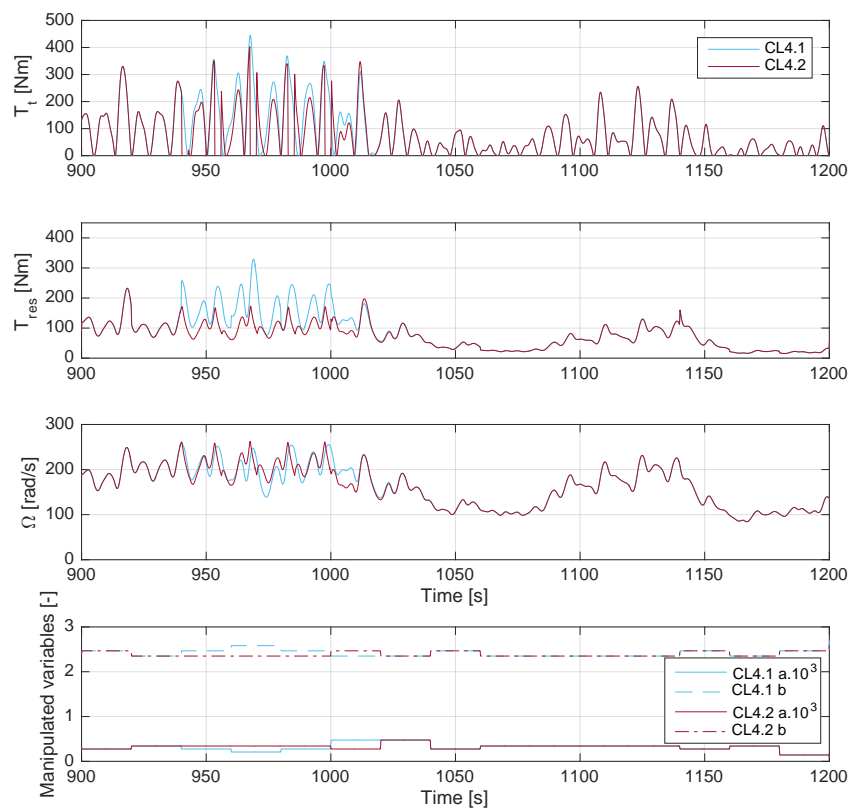
Fig. 5.17: Time series of the main control variables for both CL4 versions during SS10 operation

5.3.5 Comparative assessment of the controllers

This section presents an assessment and quantitative comparison of the controllers performance in terms of power production and reliability concerns. The numerical results are obtained running the W2W model with the 7 CLs controlling the biradial turbine and generator for the 14 realistic sea states. The duration of each simulation lasts 1/2 hour with a sampling time of 0.1 second.

Production performance

In this section the performance of the 7 control laws are compared focusing on the indicators like Annual Energy Production (AEP), power levels for each conversion steps and efficiencies of the PTO components. Figure 5.18 shows the equivalent AEP of every CL as the sum of the energy produced during the 14 SS. It is computed by multiplying the average electrical output power of a SS by the number of hours during which it operated, upon its occurrence during a year, see Fig. 5.5 and assuming a 100% availability of the plant.

$$AEP_{\mathrm{CL}} = \sum_{\mathrm{SS}=1}^{14} \bar{P}_{\mathrm{g,SS}} \, 8760 \, Occ_{\mathrm{SS}} \, 10^{-6} \; [MWh] \qquad (5.10)$$
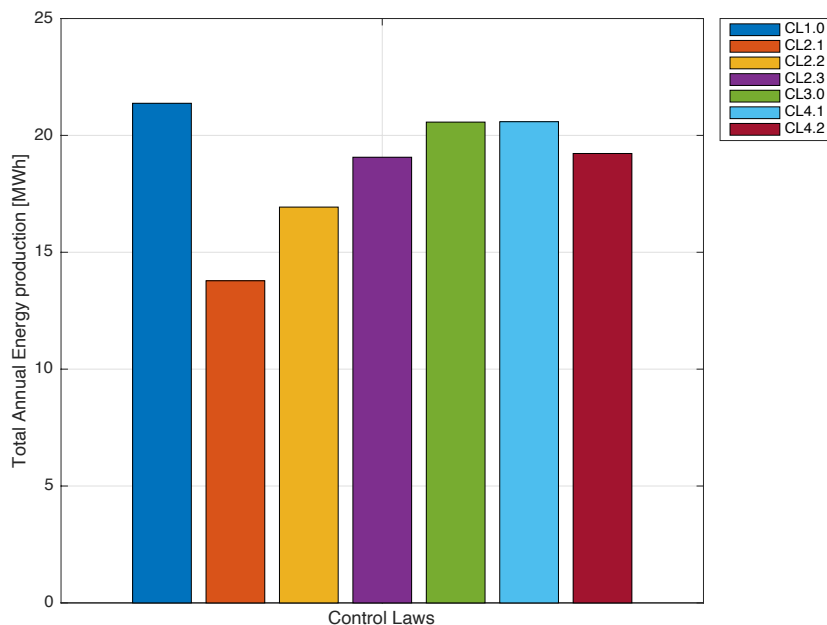
Fig. 5.18: Total energy production during the 14 SS for every controller

The AEP gives a general view of the global production performance. As illustrated in Figure 5.18, CL1 is the one producing more energy. It is the only control law that is sea state dependant and thus is the less easily implementable. It would require either an accurate sea state estimator or to receive the instantaneous sea state by a measurement buoy moored in the area. If the sea state is not properly estimated/measured, the power output may not be as good as expected. In addition, the optimal reference speeds for the PI-controller were computed offline with the numerical model which may not always represent accurately the real WEC behaviour.

For the performance comparison, CL2.1 is taken as the base case because it is the controller requiring less knowledge on the global system. It is designed based on the simple observation of the turbine characteristic curves, independent to the generator selection. Obviously, it is a variable speed control non sea state dependent. Table 5.3 lists the increase of annual energy production compared to that base line. Focusing on the CL2 versions, they vary from +23% (CL2.2) to +38% (CL2.3). There is a very similar score for CL3 and CL4.1 reaching almost an AEP increase of +50%. The MPC version including the additional constraints CL4.2 produces 10% less than the MPC case without this constraint, but still 40% more energy in comparison with the base case, which is better than the CL2 versions, although quite close to CL2.3.

Tab. 5.3: Difference of total AEP of all controllers with respect to CL2.1

CL1	CL2.1	CL2.2	CL2.3	CL3	CL4.1	CL4.2
1.5510	1	1.2287	1.3835	1.4926	1.4938	1.3951

For a deeper analysis of the energy production, Figure 5.19 depicts the AEP divided by sea states. With a sea state of 1 m of wave height and below, from SS1 to SS6, there is not much difference in energy production between the control algorithms. The same trend is witnessed when focusing on the power along the conversion chain, see Fig. 5.20 for the performance of each CL per SS. The pneumatic captured power and the turbine one appear quite similar for every CL. Only the generator powers in CL1, and thus the AEP, are slightly higher. This is explained by the fact that the generator torque levels are higher, for similar average speeds and implies a higher efficiency of this component during these low energetic sea states, see Fig. 5.21.
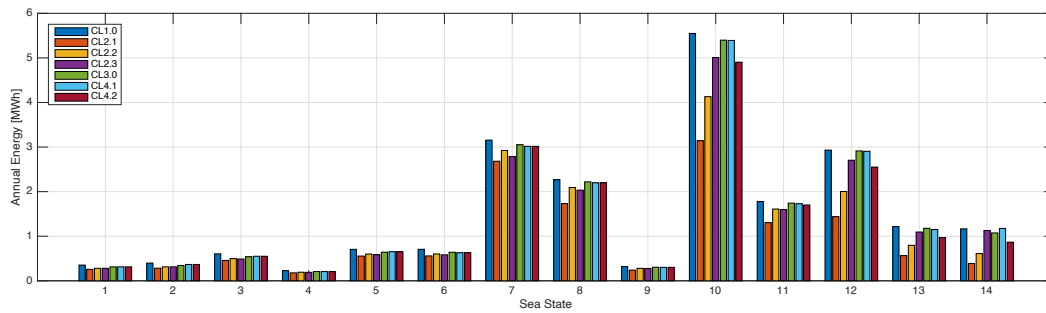
Fig. 5.19: Energy production breakdown by SS for every controller
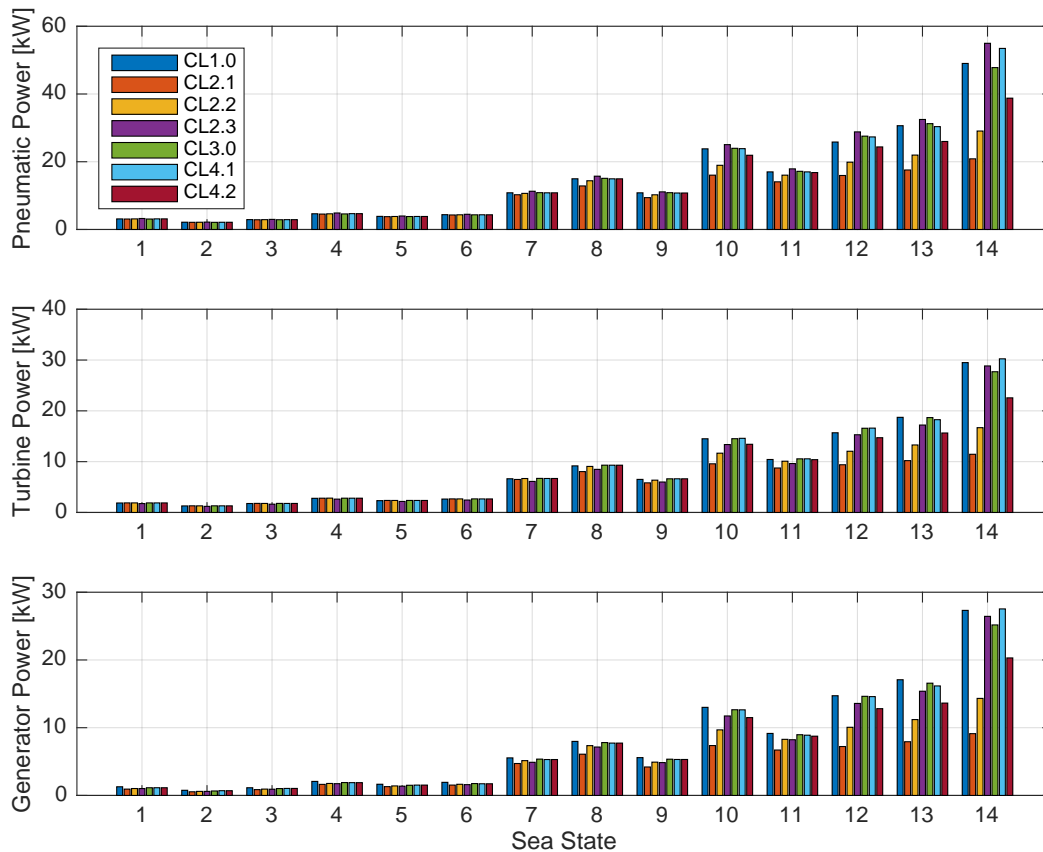
Fig. 5.20: Average pneumatic, turbine and generator powers for all the SS and every controller

From more powerful sea states, from SS7 and above (besides SS9 that rarely occurs), that is where the most quantity of energy is produced. During these mid-energetic sea states of around 1.50 m of wave height, differences begin to appear. Besides, although SS9 is more energetic because the wave period is higher for the same wave height, the period is further away from the natural frequency of the WEC so the captured power is less. There are some fluctuations in the CL2 versions, CL2.2 operates best in comparison with the others. The explanation for the poorer performance of CL2.3 is found in the average speeds quite below the nominal values. CL2.1 exerts

less performance because the torque applied is not high enough letting the turbine speeding up.

Table 5.4 shows the time duration of the safety valve closure. And it is clear that during these sea conditions, its actuation begins to affect the production. CL3 and both CL4 versions are strictly identical.
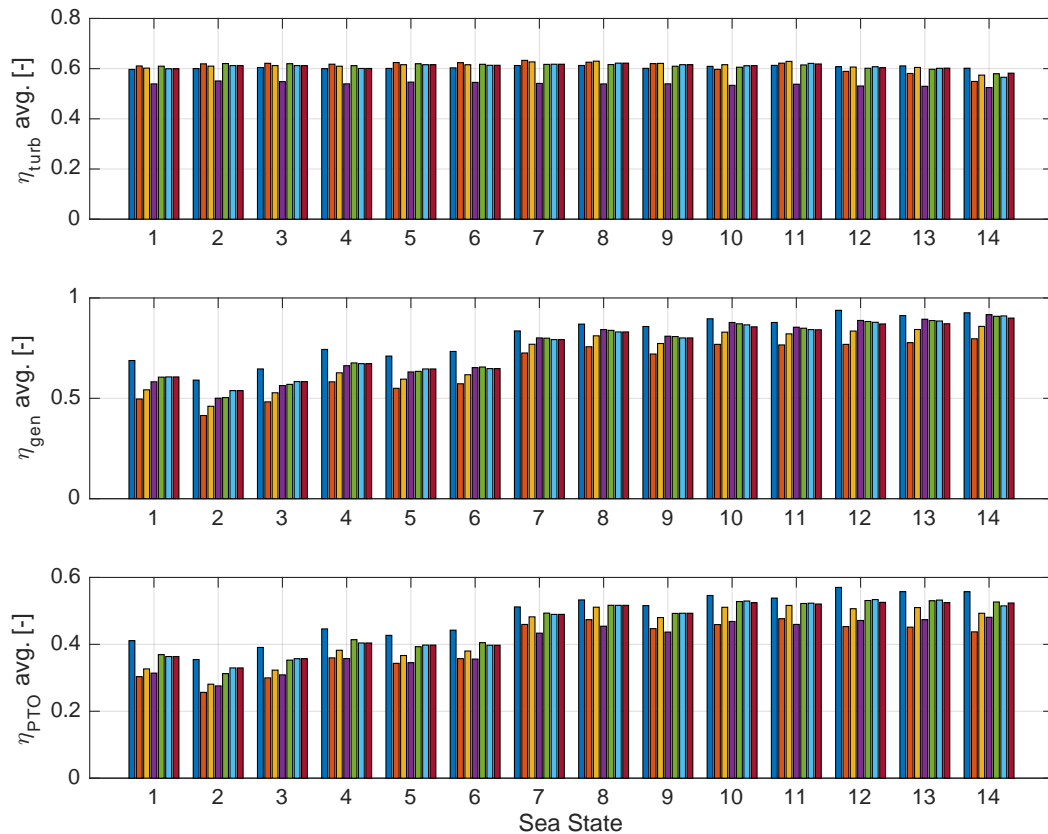
Fig. 5.21: Average efficiencies of Turbine, Generator and overall PTO

At the higher energetic sea states SS10 to SS14, where the wave heights are 2 m and beyond, the differences of performance are much more noticeable. Comparing the CL2 versions, it appears that the turnpoint begins at SS10 and the improvements of CL2.3. In the best cases, CL2.1 is somehow clamped at an average power of a quarter to a third of the generator rated capacity and a third to a half in the case of CL2.2. Again, the explanation comes from the safety valve operation, the torque laws of CL2.1 and CL2.2 are too weak at higher rotational speeds. CL2.3 implies harder torque levels which keeps the velocity lower. It induces more damping as can be seen in the pneumatic power. Although the turbine efficiency for this case is globally lower, see Fig. 5.21. The power capure increases and the operation of the generator is close

Tab. 5.4: Valve closing duration in sec.

SS	CL1	CL2.1	CL2.2	CL2.3	CL3	CL4.1	CL4.2
6	0	0	0	0	1	0	0
7	0	10	3	0	0	0	0
8	0	78	13	0	0	3	3
9	0	49	10	0	2	4	4
10	0	236	76	0	2	6	12
11	0	108	20	0	0	0	0
12	64	287	127	0	2	11	31
13	1	348	146	1	1	11	57
14	126	625	399	31	171	66	219

to its nominal values. As a matter of fact, more energy is produced. As a summary, CL2.3 sacrifices part of the turbine efficiency to keep the generator at high operation ranges and prevents the valve from actuating. If the focus is only on the energy production, this is an advantage and the performance is close to the best controllers, CL3 and CL4.1. CL1 stays the best for energy production and average output power. CL3 and CL4.1 are similar except for SS14 where the predictive algorithm manages to keep the valve less often closed, around 3 times less. CL4.2 results in lower energy and power in comparison with CL2.3, CL3 and CL4.1, reaching average electrical power levels of half to two third of the rated capacity. According to Figure 5.21, the average PTO efficiency for CL3 and both of the CL4 is quite good with values above 50%. Because CL4.2 prevents heavy operation of the generator, the average speeds are higher and the valve closing time almost 4 times longer than the other predictive controller.
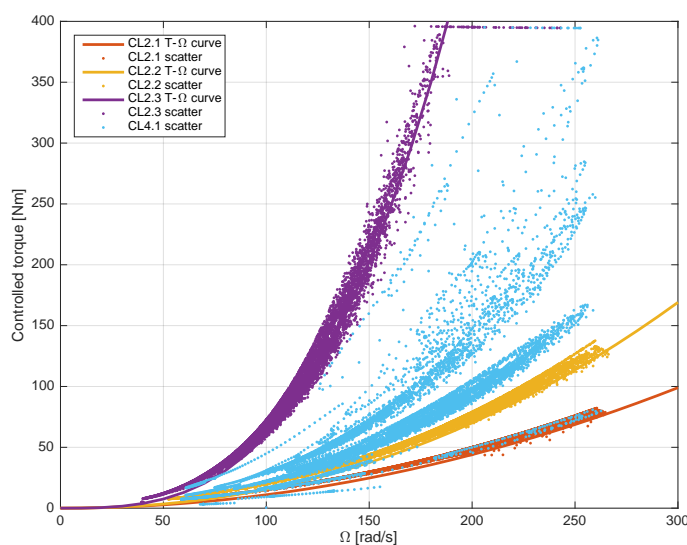
Fig. 5.22: Torque laws for all CL2 versions and CL4.1

For the speed controllers relying on torque laws, the Figure 5.22 shows the same figure as in Fig. 5.11 representing the CL torque laws but adding the scatter plots of the simulated $T_g = f(\Omega)$ of SS10 associating the controlled torque to the rotational speed. This highlights the capacity of the predictive controller to adjust the torque law to the wave and plant conditions in a more dynamic manner. It is very versatile and can act as the CL2.1 for calm wave groups, and also apply a harder torque at high speeds like in CL2.3 to avoid turbine overspeeds and thus prevent the valve from staying closed during large time duration. Still, the generator limitations in terms of maximum torque are respected (see Fig. 4.18). Table 5.4 shows the valve closing times for every control algorithm during sea states from 6 to 14. Obviously, the longer the valve stays closed, the higher the losses of absorbed power.

When referring to the control fundamentals, it is the one closer to the optimal PTO damping. Due to the non-linearities of the entire system, C_{PTO}, the PTO damping, is also by extension non-linear. The damping coefficient is calculated knowing the equations (5.1) and (4.13) that:

$$F_{PTO} = -C_{PTO}\dot{z} = p\,S_{IWFS} \equiv C_{PTO} = \frac{p}{\dot{z}}\,S_{IWFS} \tag{5.11}$$

So in order to know how the turbine's operation damps the system, it is necessary to know the relation between the pressure and the velocity of the OWC. In the present case, there are strong non-linearities related to the air compressibility and the biradial turbine so an equivalent C_{pto} is defined by a linear regression. This is far from following the theory but it offers a way to understand how the controllers act on the power capture. In Figure 5.23 the unscaled (not taking into account the IWFS area) linearised damping coefficient is calculated for CL1, CL2.1, CL2.3 and CL3 during SS10. All these controllers are compared to CL1 to highlight the effect of the damping on the energy capture. It appears CL2.1 is underdamped while the others are quite close the CL1. The poor performance of CL2.1 can also find an explanation through this analysis.

Quality of power and PTO reliability

This part highlights simulation results of the power fluctuations affecting the quality of power injected to the grid and the reliability of the PTO components. The amplitude of power profiles are likely to create disturbances in the grid
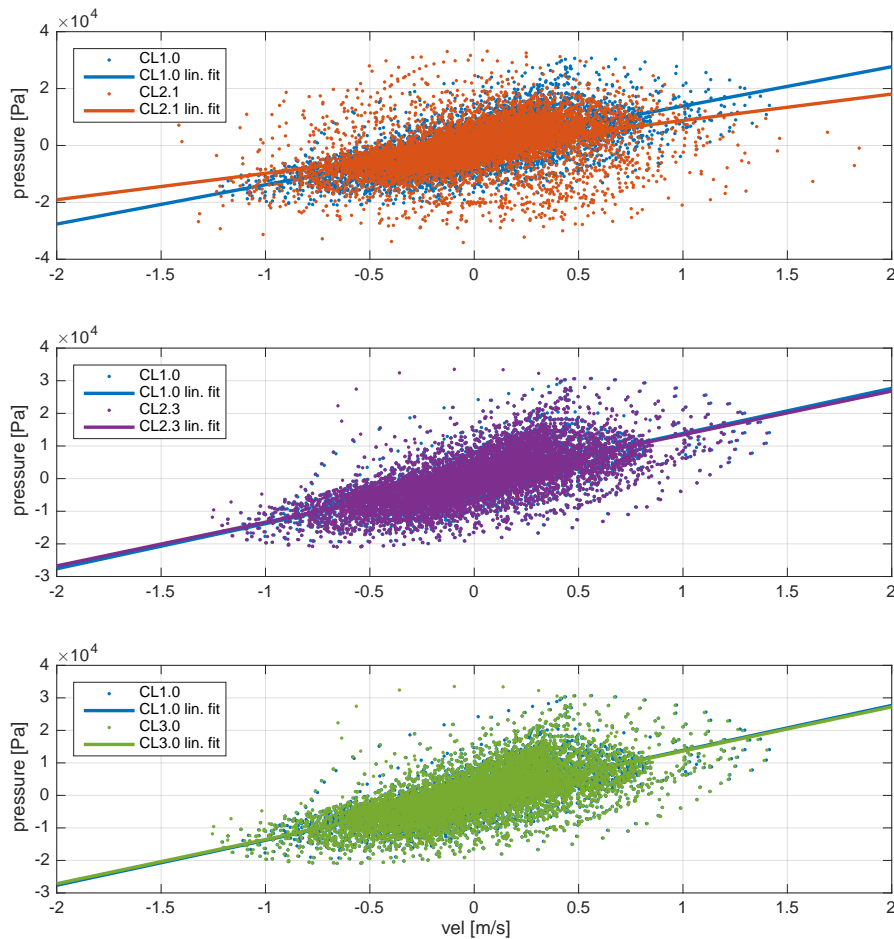
Fig. 5.23: Comparison of unscaled equivalent linearised C_{pto} of CL2.1, CL2.3 and CL3 in comparison with CL1

in larger production units or to affect the useful life of the WEC electrical components. Although at the scale of a 30 kW generator the impact of a poor power quality into the grid is low, this study allows to understand how the controllers apprehend the peaks of electrical power production. The impacts and the stresses of power peaks on the electrical equipment caused by control strategies is out of the scope of this work but has been analysed in [TM12b]. The peak-to-nominal power ratio (Pk2nom) is the ratio of the maximum value of electrical power from the generator over its nominal capacity. Also, the standard deviation shows how far from the average electrical production the extreme events are situated. Both of values quantify the variation of power during a sea state. A high value represents a poorer quality of power injected into the grid and a generator operating in higher ranges.

In the upper graphic of Figure 5.24 the peak-to-nominal power ratio of all CL for every SS is represented. Globally, while the sea conditions get
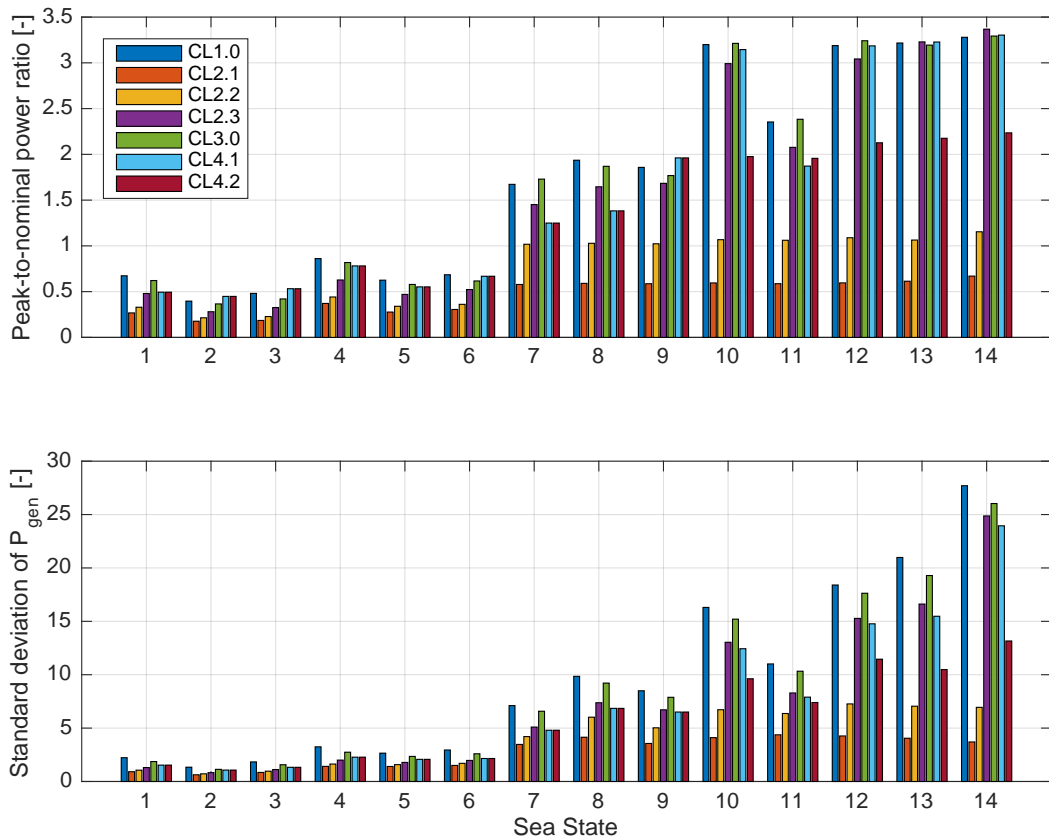
Fig. 5.24: Generator reliability indicators by SS for every controller

higher, the peak-to-nominal power ratio increases. The figure reveals a much higher peak-to-nominal power ratio for the fixed speed CL1, the adaptive controllers CL2.3 and CL3 and the predictive law CL4.1. In the most extreme cases, the peaks of power can reach 3 times the nominal power. In contrast with the good score of power production, these control laws induce larger standard deviation and highest power peaks, that are most likely to reduce the generator life if it is often operated at these values. Induction generators can withstand, for short periods of time, high power peaks as long as the temperature of the windings does not overshoot a certain threshold. In a continuous overloaded operation the insulation of the copper windings can melt, cause a shortcut and seriously damage the generator. Although this operation represents a little percentage of the annual wave climate, in practice the control framework should include safe temperature thresholds that trigger alarms and allow adapting the power production in consequence. CL2.1 gets the best score when focusing on this indicator. Indeed, in the most energetic sea states the power peaks are always under the nominal power with maximums of 70%. Similarly CL2.2 can present power peaks slightly higher than the nominal power. Finally, the predictive law CL4.2 provides
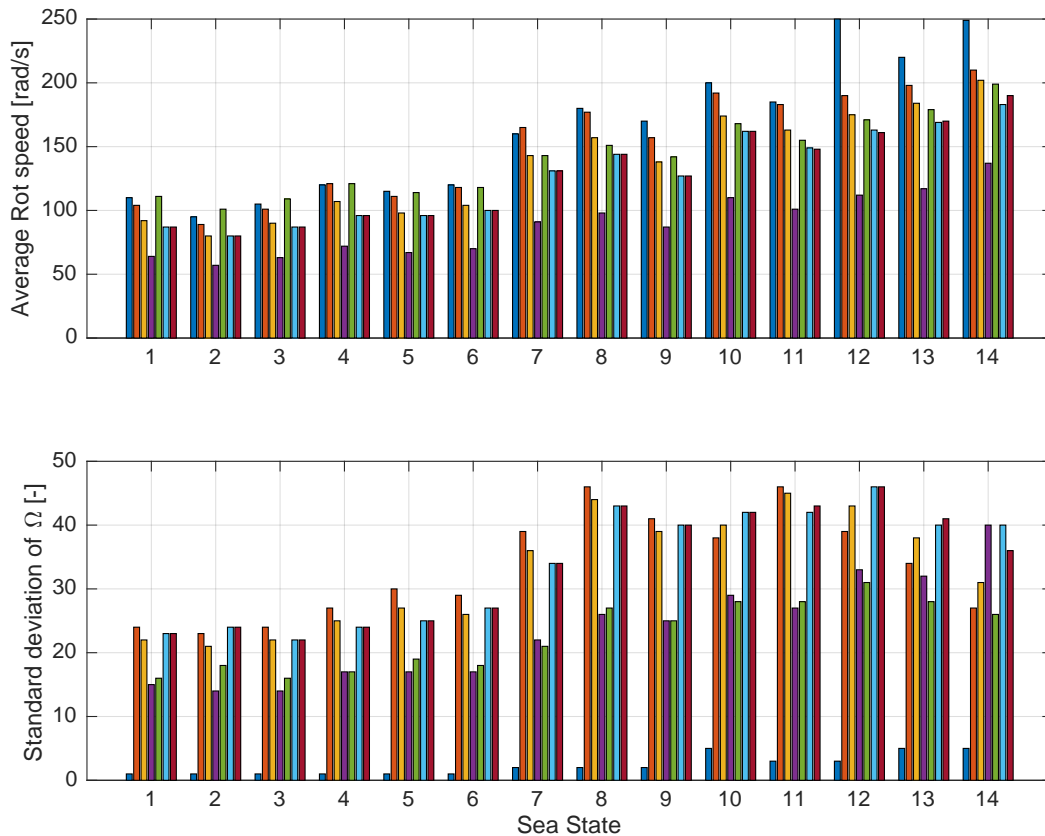
Fig. 5.25: Evaluation of the speed ranges by SS for every controller

here a real added value in comparison with the original CL4.1. Until SS9 there is no change between the two versions of the MPC. Starting from SS10, the power peaks in CL4.2 are clearly reduced at around twice the generator rated power. Instead, CL4.1 produces peaks 3 times higher than the nominal power.

Another way to value these concerns is proposed by the lower graphic of Figure 5.24 where the standard deviations of the generator power are highlighted. The same trends are observed in general, the difference being that the fixed speed CL1 and CL3 present the largest standard deviations, meaning even poorer quality of power. Both controllers rely respectively on a fixed or quasi fixed speed reference. On the one hand, because the speed allows no to little variations (see the lower graphic of Fig. 5.25), the fluctuations of the turbine power are directly transmitted to the generator. On the other hand, there is very few power smoothing effect from the drive train inertia. In the variable speed controllers, the power levels have less standard deviation because they benefit from the storage of kinetic energy. CL2.3 also presents high standard deviation of power, one can understand that the shape of

the curve implies to induce higher torque levels than the other torque laws for speeds around the nominal value (see Fig. 5.22). In what concerns the predictive law CL4.2, the benefits of the additional constraints to avoid power peaks are clearly visible.

5.3.6 Observations on controllers selection

From this comparison analysis, the pros and cons of each controller were clearly exposed. Selecting the best controller between the 7 candidates can be tricky and depends on well defined criteria. CL1 would not be a right choice due to its dependence to sea states which makes it not very autonomous. If the deployment site includes a measurement buoy able to send real-time wave measurement data autonomously and the control setup able to run the predictive algorithm, CL4.2 seems to be the perfect trade-off between performance and reliability in all sea states. However, it needs a very accurate W2W model representing quite well the real plant. A thorough model validation is thus highly required. On the contrary, a hybrid control strategy can include CL3 during sea conditions until SS9 and then CL2.2 takes over. This would allow the optimal power extraction from low to mid-energetic sea states and when the conditions are being too high and the CL3 begins to present reliability challenges to the PTO components, the control framework shifts to CL2.2 which offers a lower production extraction but has a better reliability score.

5.4 Latching control in the OWC sparbuoy

In the literature it has been seen that a latching kind of controller is the only way to apply optimum control for OWC systems. In particular phase control by latching can perform quite well for an OWC point absorber, the challenge is to design a controller capable of opening and closing a latching valve at the perfect time instants. The shut-off valve, has to be fast enough to block the air flow at the best moment. Thanks to its design, the biradial turbine has a quite small inlet (around 10 cm) which facilitates the conception of a High Speed Shut-off Valve (HSSV). Such a valve has been integrated in the biradial turbine designed and built for the OPERA project. The valve

is able to fully actuate in a time close to 1/5 s which complies with the requirement of fast actuation stated earlier. A first attempt to develop a latching control algorithm based on the predictive controller CL4 was made for the Mutriku OWC plant but this study revealed very marginal increase in power capture. Indeed, when looking at the RAO of the plant (see Fig. 4.3), it was understood that the IWS motion was already amplified by the proper design of the chamber and that this strategy would not be relevant in that case. That is the reason why this section details a latching control approach using the W2W model of the floating OWC developed in Section 4.2.2.

5.4.1 The control law

The objective of this predictive control strategy based on pressure threshold is to act on the buoy motion to force near resonance condition with the incident waves and thus increase the energy capture on the waves-WEC interaction. When the valve closes, it exerts an over-compression and changes the buoy motion. The issue here is to find the optimal condition for the shut-off valve to actuate. In the case of this latching control, the optimisation is applied by the predictive algorithm CL4 but modified to optimally compute the four pressure thresholds of the control vector $u_{th} = [p_{\text{Th1}}\, p_{\text{Th2}}\, p_{\text{Th3}}\, p_{\text{Th4}}]$. Depending on these ones, the algorithm actuates on the HSSV at the best instants which maximises the energy absorption. Remembering from Section 4.4.2 that u_{v} is the variable defining the valve position. The control law designed to open/close the valve depending on the pressure thresholds is such that:

$$\text{In compression } p^* > 0 \begin{cases} \text{if } p^* > p_{\text{Th1}}, u_v = 0 \\ \text{if } p^* > p_{\text{Th2}}, u_v = 1 \end{cases} \tag{5.12}$$

$$\text{In expansion } \ p^* < 0 \begin{cases} \text{if } p^* < p_{\text{Th3}}, u_v = 0 \\ \text{if } p^* < p_{\text{Th4}}, u_v = 1 \end{cases} \tag{5.13}$$

It is important to state that the control law applies the pressure thresholds sequentially, meaning that, for example, the valve will close when the pressure reaches threshold 3 only if opened by threshold 2. This was required to avoid valve chattering (repeated fast switching).

As an illustration and aiming at understanding the effects of latching, a case in regular waves is presented. In order to draw conclusions only on the effect of latching, an optimal turbine damping is represented by a fixed turbine

speed. The effect on the dimensionless pressure is visible in Fig. 5.26 which compares the case with (solid line) and without latching (doted line). The pressure thresholds and the resulting valve actuation are also visible. When the thresholds are applied starting at $t = 450s$, the dimensionless pressure (solid line) in expansion reaches Th1, the valve closes instantaneously. As a result, the pressure gets higher then passes over Th2 where it opens, and so on for all the thresholds followed sequentially by the control law.

The consequence of such a behaviour is presented on the device motion with respect to the excitation forces in Fig. 5.27. The relative velocity between the floater and the water column is shifted due to the valve actuation until entering in phase with the relative excitation force. This results in an amplification of motion when comparing the case with (solid line) and without (doted line) the valve actuation. This condition fulfills the phase condition of latching control.
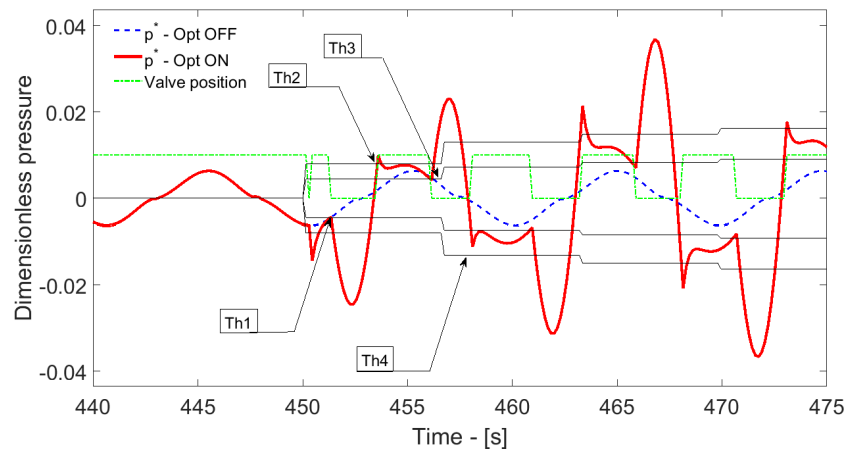
Fig. 5.26: Effect of latching on the dimensionless pressure compared to the case without latching

A non-linear predictive control which would optimise the valve position for each time step and over a prediction horizon requires a very significant computational resources penalizing its practicability. Following the algorithm CL4 developed in Section 5.3.4, the strategy proposed here relies on the optimisation of only few key control parameters during the prediction horizon, that are the pressure thresholds instead of the torque law parameters. Similarly, the control law then applies them during the re-planning time.
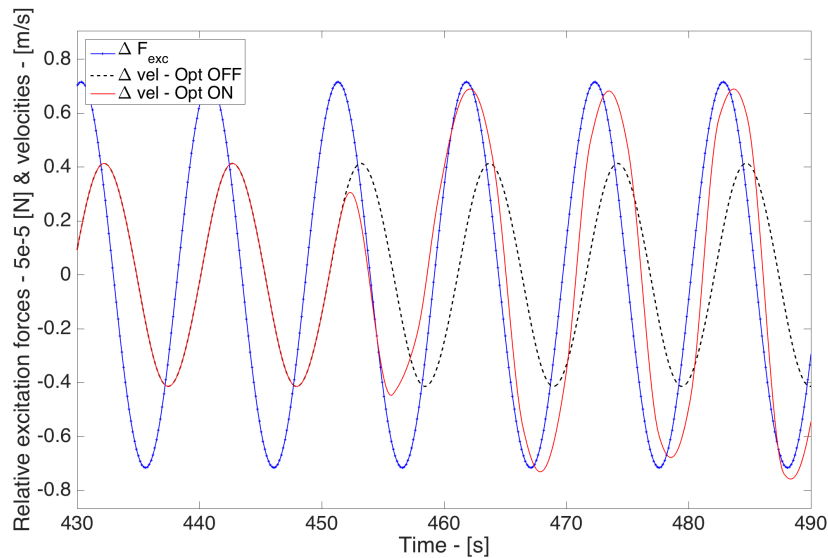
Fig. 5.27: Effect of latching on the relative velocity compared to the case without latching

5.4.2 Simulation results

The simulation results are obtained in a set of 12 realistic sea states (see Table 5.5) for a test duration of half an hour which statistically represents the duration of a sea state in the ocean. The PTO components include a 1.5 m diameter biradial turbine of inertia 200 kgm^2 and a 90 kW induction generator of 4 pairs of pole selected from a manufacturer catalog [ABB04]. Its nominal torque is 1159 Nm at 741 rpm of nominal speed. The ratio between maximum and nominal torque is 1.8 and the nominal voltage is 400 V. It is connected to a back-to-back power converter of 690 V allowing an overspeed of $\Omega_{os} = V_{B2B}/V_{gen} = 1.725$ which permits higher rotational speeds while shifting the flux-weakening region. Each sea state is simulated first with the variable speed control only in order to set the base case and then the predictive algorithm is applied combined with the speed control. The optimisation algorithm used to obtain the vector of thresholds is performed with the *fmincon* function of Matlab. Using a typical desktop computer equipped with an i5 Intel processor, the real simulation time of a half hour simulation is around 40 s by sea state.

The results of the increase of power both at the turbine and the generator side thanks to the predictive threshold latching compared to case without latching are presented in Fig. 5.28. Let us recall that the same variable speed controller is used on both cases to highlight only the effects of the

SS	H_s - m	T_p - s
1	1.5	7.5
2	1.5	9.5
3	1.3	12
4	1.3	14
5	1.5	11
6	2	12
7	2	13
8	2	14
9	2.5	12
10	2.5	13
11	2.5	14
12	3	14

latching strategy. Globally the controller shows good performance bringing an improvement on the turbine power between 20 to 30 %. Following the conversion chain, the electrical power at the generator is increased from 7 to 25 %. The difference of power increase on the generator side compared to the turbine side in lower sea state (from 1 to 6) can be explained by the fact that in these conditions, the generator operates at low efficiency range. In higher sea states, the improvements in the output power tend to stabilise around 20 %.
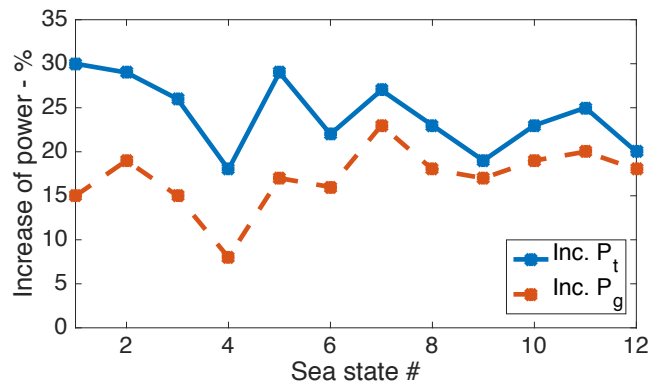
Fig. 5.28: Power increase due to latching

Looking more carefully at the time series of the electrical power in the highest sea state, it is possible to see the effects of the predictive control in the power variation. Both cases, with (solid line) and without (doted line) latching, are illustrated by Fig. 5.29. Indeed, peaks of power are higher but still respecting

the generator limitations because they are included as constraints in the optimisation. As a consequence the power quality is poorer. To highlight this effect, the standard deviation of the electrical power is showed in Fig. 5.30 along with the power peak for the entire simulation.
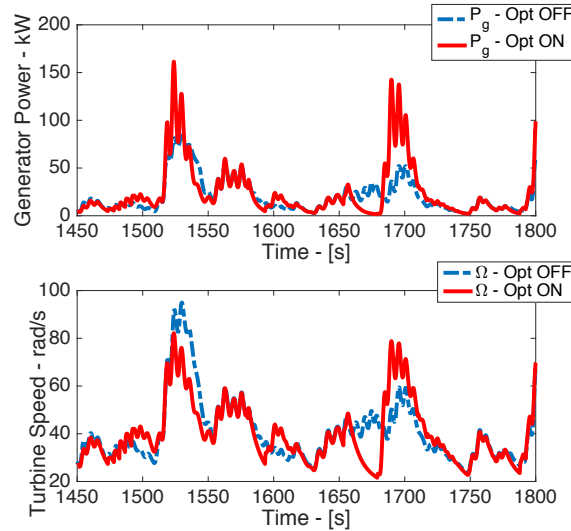
Fig. 5.29: Comparison of power production and turbine speed for SS12
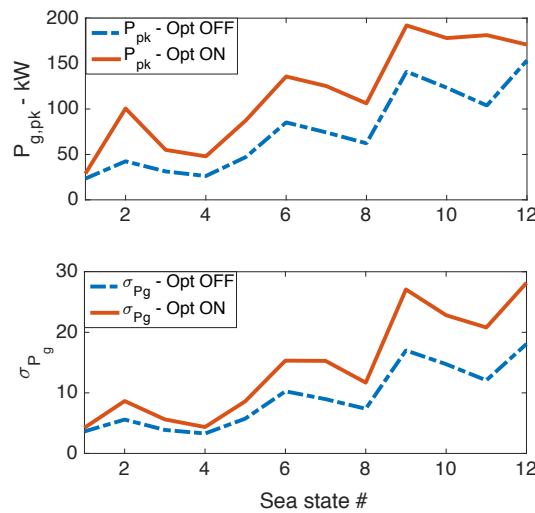
Fig. 5.30: Comparison of peaks and standard deviations of electrical power output for each SS

5.4.3 Discussion points

It is clear that strong benefits are brought by latching control in a floating OWC device when associated to a predictive algorithm. Although the proposed strategy performs fast and effectively, some important considerations are needed and should be kept in mind before any practical implementation.

First of all, the algorithm is based on a numerical model, meaning that the optimisation is as good as the accuracy of the WEC model. Also the ideal prediction of the excitation force is not realistic and an accurate wave forecasting has to be developed and integrated into the whole model. Besides, each time the valve opens, it creates an air burst and the phenomenon of air flow reconstruction is not captured in this study. In addition, real time implementation of such a control strategy is a challenge. Although the predictive algorithm is performing fast in a desktop computer, the integration in a Programable Logic Controller, in charge of monitoring and controlling the WEC and all the sub-systems, can be a complex task. If the end of the optimisation is delayed with respect to the actual actuation of the valve, the controller can loose its target and actuate the valve at the wrong instants and thus penalising the power extraction. In CL4 where the predictive algorithm was developed for controlling the turbine speed, this limitation was less disturbing because there was not the same hard constraint on the accuracy of actuation. In real operation, the repetitive fast switching of the valve can affect the reliability not only of the turbine as a sub-system but also to the whole system. In terms of quality of power, it has been shown that peaks of power injected into the grid are higher with the latching strategy.

5.5 Chapter conclusion

In this chapter dedicated to control strategies for OWC systems, applications of control fundamentals in the frequency domain are made on the W2W model of Mutriku to understand how the control parameters of damping and stiffness are tuned and their effect on the device motion and the power capture. With the concern of providing a more practical approach to control the PTO of the fixed OWC plant, the development of several speed control laws is then proposed using the full time domain W2W model including all non-linearities such as the air compressibility effect of the chamber, the biradial turbine and the electrical power conversion. A common framework is setup to compare simulation results of the 4 main controllers and their different versions. In total, 7 control laws are developed and simulation results are obtained during the plant operating under 14 realistic sea states. The wave spectra were obtained from real wave elevation measurements during a deployment campaign on site of a pressure sensor. Among the control strategies considered, one was a sea state dependant controller based on an optimal fixed speed reference followed by a PI-controller, and several adap-

tive variable speed controllers that presented the advantage of being more practically implementable on a real plant. Among the adaptive controllers, 3 different torque laws were considered where the design specifications were detailed. Also a quasi-fixed speed control scheme was highlighted whose advantage is to take the benefits of high power production like in the fixed speed control law but rendering it untied to sea state dependence. Finally, 2 versions of a non-linear model predictive control were developed based on the torque law approach, one being more focused on PTO components reliability as it included additional constraints on the power generation.

An intensive comparative assessment of the controllers concluded on their production performance taking both energy, power production and efficiency at each conversion step, quality of power injected to the grid and component reliability issues. While the fixed speed control law was the one producing more AEP, it was also the one penalised by the lowest score on the two other issues. The quasi-fixed speed and the version of the first predictive law (the one without the additional constraints) did produce a substantial amount of energy. They also provided more stresses on the generator and higher output power peaks especially on high energetic sea states. The same conclusions are drawn for third version of the torque laws (the one considering the entire PTO in the design) in what concerns poor reliability and quality of power issues. The main benefit of the second predictive algorithm (including constraints on the electrical power during the online optimisation) was to still produce a fair amount of energy while reducing significantly the peaks of power, and thus increasing the reliability score. While the first two versions of the torque laws offered a more reasonable approach related to peaks of power, they were the ones generating less energy, especially the first one.

In brief, technology developers should be aware that there is a balance to consider in the attempt to optimise the energy production while ensuring proper quality of power sent to the grid and keeping the PTO components inside reasonable operation ranges. A general recommendation is to select the best controller depending on specific criteria. The second predictive control law seems a good trade-off considering both the performance and reliability indicators. However, for the implementation of a predictive controller one should consider certain aspects such as:

- The deployment site and its capacity to measure and transmit the wave resource in real time;

- The way to manage algorithm complexity in the control unit;
- The sensitivity of the controller to modeling inaccuracy for the estimation of the wave force and the full W2W model.

Another way to select the best controller can be to hybrid them. It was seen that the quasi fixed speed control law was one of the best performing ones but when the sea conditions were starting to increase, the reliability score dropped down significantly. In these sea states, it would be a good practice to change the controller for one of the torque laws, for example the second one, which is one the best in terms of components reliability and still showing a reasonable energy output during high-energetic sea states.

In what concerns the latching strategy for the floating OWC, the study presented the predictive control strategy firstly developped for controlling the turbine speed and then modified to apply pressure threshold latching the OWC buoy. The mathematical development has been stated and simulation results were presented, highlighting the benefits of this control strategy in terms of power production. Indeed, the electrical power output was increased by 10 to 25% in comparison to the case without latching. The controller was developed so that the prediction of only few key control parameters are optimised and applied by the control law during a re-planning period. It brought fast computation and an implementation in a real time controller can be foreseen. A critical assessment has been stated with the undesired impact of a latching strategy applied to the OWC. Still improvements can be done especially if combining the predictive latching with the predictive turbine speed control. It would be quite interesting to evaluate the gain in performance from a control strategy able to take the best of each controller.

Part of the results presented in this chapter were published in several articles such as [Faÿ+18a; Faÿ+20a] for the comparison of adaptive controllers for the Mutriku plant, a deeper analysis of the MPC in [Faÿ+20b] and the latching control strategy in [FMR17]. These analysis do not include a complete reliability study with the effect on component failure rates due to controllers allowing heavy PTO working conditions. It would be interesting to know the impact of the controllers on the components useful life and on the operation and maintenance plans, including the consequence on the operational expenditure (OPEX). A complete LCOE analysis would be very relevant taking into account the increase of AEP, and thus incomes, and a possible decrease of OPEX.

The development, tuning and test of control algorithms in a simulation environment is an important step to capture their behaviour, performance and requirements in numerical systems. However, a controller can only be fully assessed once implemented and tested in a real environment during sea trials. The intermediate step is the validation of the correct implementation in a dry testing laboratory with physical equipment similar to those that are to be used in the device at sea.

Real time control

6

> *The proper method for inquiring after the properties of things is to deduce them from experiments.*

— **from Isaac Newton 1643-1727**

Summary: The present chapter addresses several implementation issues related to testing control algorithms in the real control environment embedded in a prototype. In particular, predictive controllers, whose relevance has been proved in Chapter 5, present many challenges to solve before successfully being implemented. Among them, the prediction and estimation of the wave forces, one of the main input and disturbance for the controller; the computation burden to run the online optimisation of the NL-MPC; and the aspects related to the I/O communications between the model and the real plant. These aspects are covered in this chapter. Also, the validation of several controllers is made in a dry PTO test rig prior to their deployment in a physical system. An important added value of this work is the test of control algorithms during sea trials in Mutriku and in the Marmok-A-5 buoy in BiMEP. The testing experience and the analysis of operational results are gathered in this chapter.

6.1 Introduction

The renewable energy sector benefits constant growth and conventional renewable energies are nowadays mature industries. However, marine renewable energies still need to improve confidence in order to success. A key point towards building trust in the industry is the ability to provide reliability through a power generation unit that is cost-effective and optimally performing. The sector of Wave Energy conversion lacks of real implementations and sea trial campaigns providing experimental data. This section is dedicated to the real time testing of some control algorithms developed in Chapter 5. In particular model predictive algorithms present several challenges related to their practical implementation as it requires the knowledge of the future wave excitation force, an accurate numerical model, and represent a computational burden for the real time optimisation. The approach to overcome these technological barriers is explained along the development phases from the model adaptations for real time testing using HIL dry test rigs, to sea trials both in the Mutriku plant and the Marmok-A-5 buoy when installed in BiMEP test site. Along the developments made during the OPERA project, an outstanding result of this research is that these control algorithms advanced from TRL3 to TRL6.

In model-based controllers, it is required to run the model to compute the control action. It is hardly possible to measure the wave excitation force with sensors installed in the WEC. It is the main input required to run the W2W model and to compute the control action. For MPC algorithms, this quantity has to be known in advance. A methodology to obtain the wave excitation forces from incoming waves consists in using wave elevation measurements from a sensor located in front of the plant. The estimated excitation force is then propagated in time to the plant and is the input to the MPC algorithm.

Dry testing using HIL test rigs is the required step previous to any deployment of the algorithms in the control framework of a WEC at sea. The algorithms presented here were successfully tested in a controlled and dry environment and the implementation issues have been solved, certifying their readiness for implementation in the Mutriku OWC Plant. However, test bench limitations were brought to light and did not allow testing in the most extreme case scenarios to understand the effects of the CL algorithms on the power conversion equipment. To complete extreme case scenarios, it is better to

test all of them with the full scale real PTO components and not in scaled experiments. A dedicated section in this chapter details the methodology to be employed to perform prototype scaled testing in HIL test rigs and is applied to validate control strategies to be deployed at the Mutriku plant as well as the spar-type buoy.

A test campaign at the Mutriku OWC plant took place under the framework of the OPERA project. Several control algorithms could be tested in real environment for the biradial turbine and measurement data collected. The implementation of the MPC was validated and the performance of the controllers was assessed in an extensive manner. The excitation force was estimated thanks to a sensor installed in front of the plant and connected to the control unit onshore.

Following this test campaign, the PTO was decommissioned from Mutriku and installed in the IDOM/Oceantec buoy before being towed back to BiMEP. Another set of tests allowed to gather significant sea trial data from this new deployment and further confirmed the correct implementation of the MPC algorithm. In this specific case, a wave measurement buoy, the Triaxys from Axys Technologies [Tec], was moored in the BiMEP area in front of the Marmok-A-5. It was able to send the wave elevation measurement to the control system which calculated the estimation of the excitation forces and send them to the predictive algorithm.

6.2 Approximation of the future excitation force

One of the greatest challenges of using predictive control algorithms for the real time control of wave energy devices is the estimation of the excitation forces of the incoming waves. This issue has been raised in a number of publications [FR10; Kra13; NT18; Li+18]. These forces were assumed to be known in the previous simulations for the predictive speed control in Section 5.3.4 and the predictive latching strategy in Section 5.4. This is not a realistic assumption for the real implementation of such controllers. This chapter details the sea trials of the predictive algorithms in the Mutriku OWC and the Marmok-A-5 buoy. One requirement for these algorithms is the knowledge of the excitation forces. In practice, one way to anticipate the excitation forces

is by measuring in advance the waves coming to the WEC and use the process presented here to approximate them. The travel time of the set of waves between the wave measurement point and the WEC gives the maximum prediction time.

The approach developed here is inspired from the methodology introduced by Falnes [Fal02b; Guo+18]. It consists in computing the excitation forces knowing the wave elevation. More precisely, the approach considers resolving the convolution between the Excitation Impulse Response Function (EIRF) K_{exc} and the known wave elevation η_{w} such that:

$$F_{\text{exc}}(t) = K_{\text{exc}}(t) * \eta_{\text{w}}(t) = \int_{-\infty}^{\infty} K_{\text{exc}}(t - \tau)\, \eta_{\text{w}}(\tau)d\tau \qquad (6.1)$$

and knowing the complex EIRF:

$$K_{\text{exc}}(t) = \frac{1}{2\pi} \int_{-\infty}^{\infty} \Gamma(j\omega)\, e^{j\omega t}d\omega \qquad (6.2)$$

Similarly to solving the radiation problem when modelling the hydrodynamic response of a WEC (see Section 4.2), the EIRF is approximated using the Prony method. The real and imaginary parts of the EIRF are considered by finding complex Prony matrices. That way both amplitudes and phases are maintained during the computation of the excitation force from the wave elevation.

Taking the example of the **Mutriku W2W model**, the Prony approximation at order 5 gives fair results and is illustrated in Figure 6.1. The complex Prony matrices are integrated in a state-space system. The approximation of this excitation force is done resolving this system having the wave elevation in input.

The validation process is done by generating the excitation force and wave elevation respectively from the Eq. (4.2) and (6.3) with the one estimated using the present method.

$$\eta_{\text{w}}(t) = \sum_{j=1}^{N} A_{\text{w}}(\omega_j) \sin(\omega_j t + \varphi_j), \qquad (6.3)$$

Figure 6.2 shows the comparison of a wave excitation force and its respective wave elevation calculated from a wave spectrum, versus the estimated one computed this time using the wave elevation. The sea state in the figure
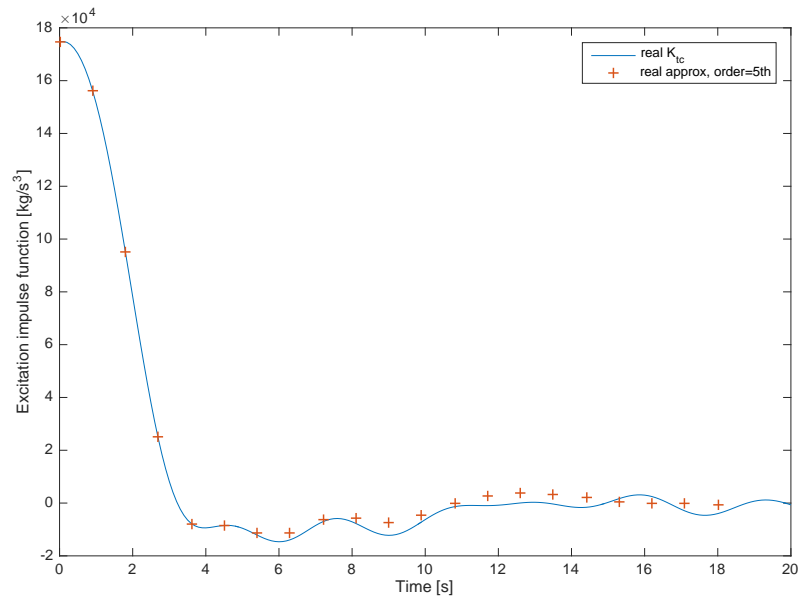
Fig. 6.1: Prony approximation of the real part of the EIRF for Mutriku

is characterised by $H_s = 2$ m and $T_p = 14.5$ s. An error inside the range of +/-10% is obtained by comparing the two excitation forces modelled and estimated. At first sight, the estimation looks rather good, but a spectral representation allows to compare the magnitudes for several frequencies. A Fourier transform of these time series is illustrated in Figure 6.3 to further compare the quality of the approximation. For frequencies until 0.5-0.6 rad/s the estimation is fine, and above there is a slight overestimation meaning that the estimation will be less accurate for wave periods lower than 10 s. This methodology has been validated for several other sea states, where similar results were found. The approach will be the one used in the implementation of the predictive controllers for the sea trials in Mutriku in Section 6.4.

The same methodology is applied for the **Marmok buoy** considering that they are two excitation forces, one for the floater structure and the other one for the IWS. The convolution is resolved in the time domain by approximating the EIRF with the Prony method at 5th order for each body and calculated by a state-space system. The approximation of the impulse functions will not be displayed to respect confidentiality terms agreed with the WEC developer.

To assess the accuracy of the methodology for this case, the same approach as the one of Mutriku is used. The sea state here is $H_s = 2.78$ m and $T_p = 15.88$ s. In the present case, Figure 6.4 shows a comparison in simulation of the excitation forces and their estimates for both bodies from the same wave elevation η_w. The estimation for the structure is not precisely accurate
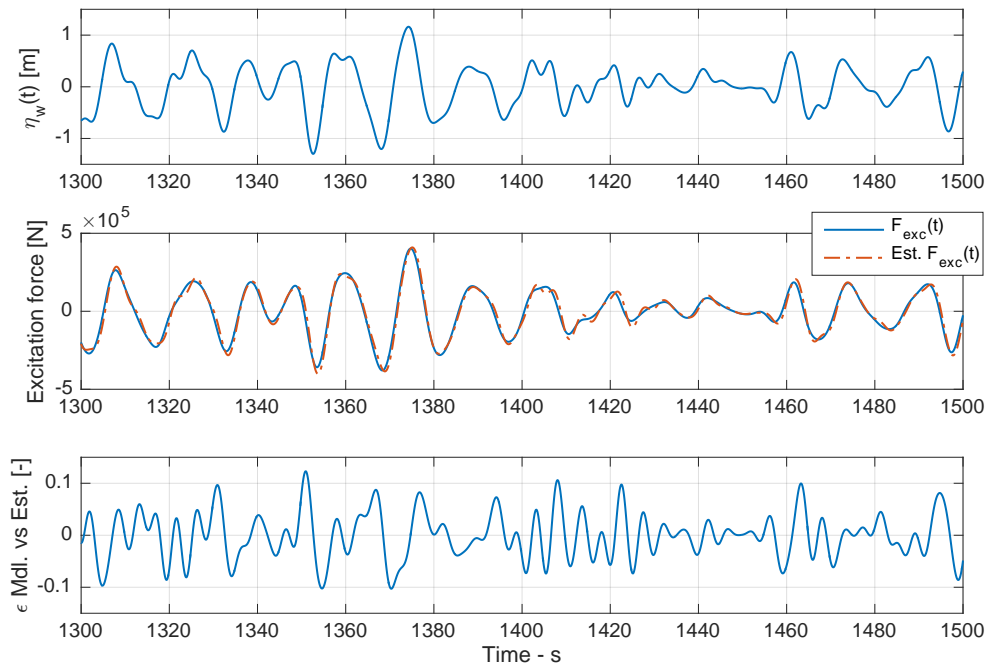
Fig. 6.2: Validation of the estimated excitation forces
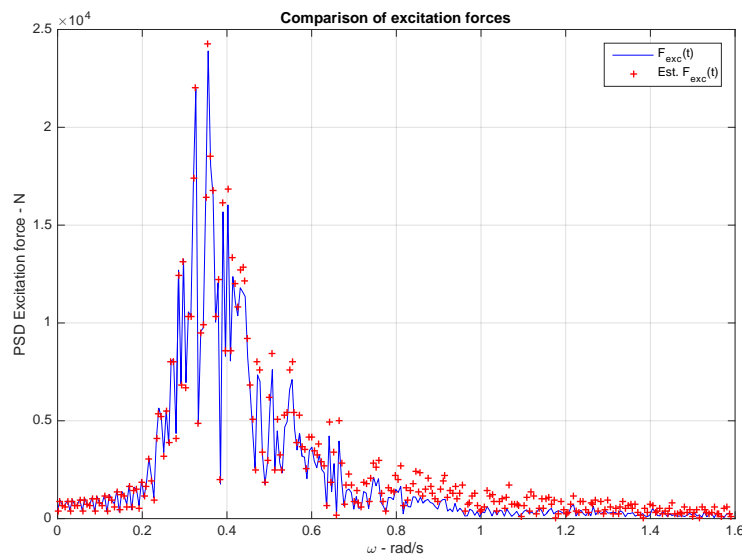
Fig. 6.3: Fourier analysis of the time series of excitation force and its estimate

and slightly underestimated. The estimated force for the water column overlaps better. The Fourier analysis reveals in Figure 6.5 the estimation starts to be less accurate at frequencies around 0.4 rad/s and above. However, this estimation was deemed satisfactory to include in the predictive model implemented in Section 6.5.
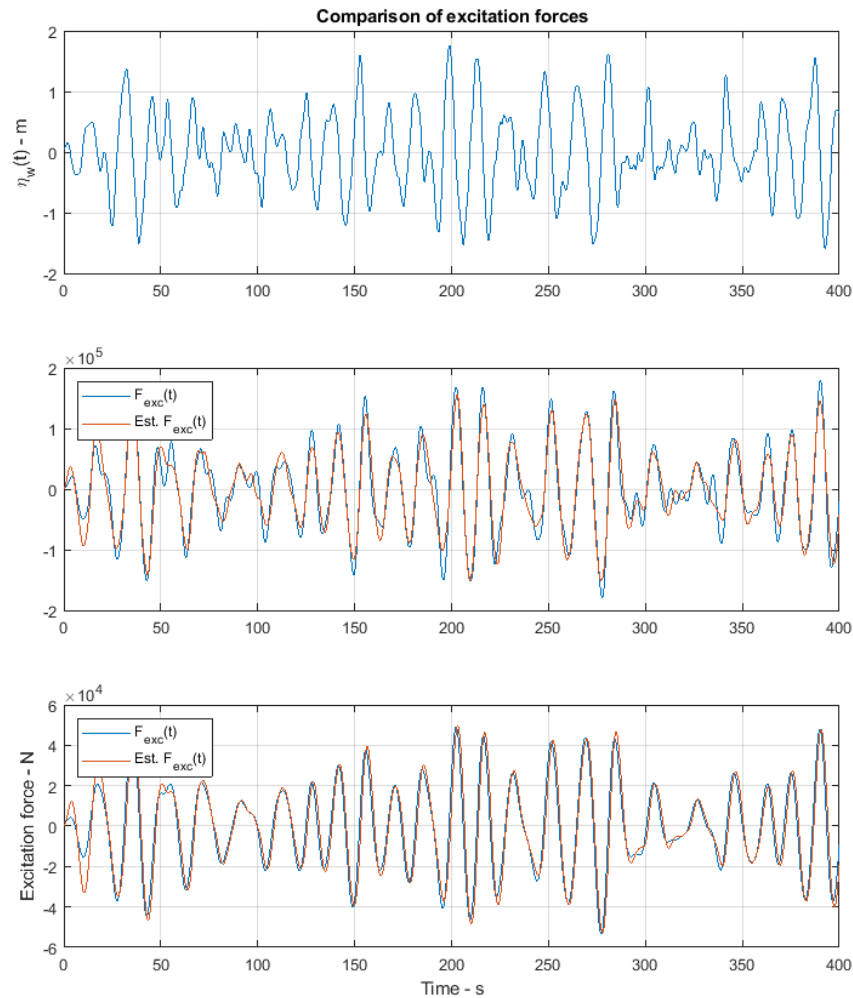
Fig. 6.4: Comparison of excitation forces and their estimations for the structure (middle) and the water column (bottom) using the wave elevation (top)

6.3 Dry PTO test rig validation

Around the world, full-scale multi-megawatt test benches for wind turbine nacelles have been built to accelerate and support the successful development of the sector. Two kinds of test facilities can be distinguished: mechanical dynamic test infrastructures and electrical grid emulators. On the one hand, the effect of the wind field on the drive train components (bearing, gearbox, generator, control system) can be tested. On the other hand, power quality and grid connection capabilities can be analysed for grid code compliance and international standards accreditation as stated in the IEC standard 61400-21 [IEC08]. Whether wind turbine manufacturers have dedicated facilities, a
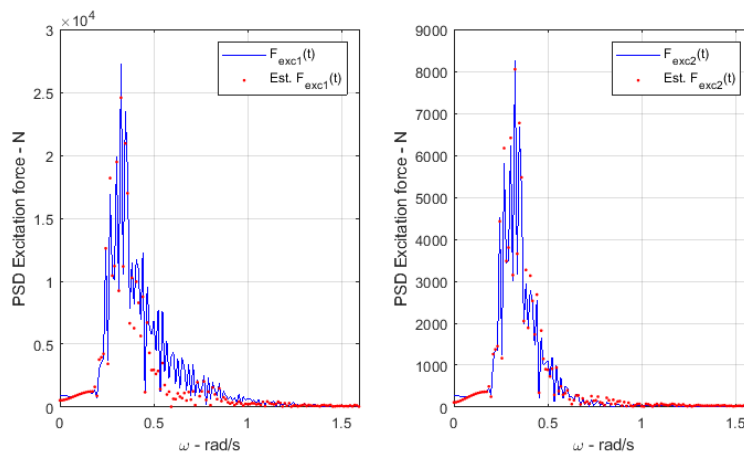
Fig. 6.5: FFT of excitation forces and their estimations

large variety of test facilities for research purposes on marine energy are available around the world with a wide range of rated capacity, from the kW to the multi-megawatt scale. The use of an electrical test infrastructure is crucial for developers to success in prototype testing. A clear advantage brought by these facilities is the ability to perform extensive tests in real dynamic operational conditions in a controllable and repeatable environment. In comparison, on-site testing is a more complex environment where the resource is not easy to deal with. In fact, these trials occur at a more advanced TRL once the technology is de-risked with extensive laboratory testing. In addition, bench testing offers the ability to experimentally validate control strategies that aim at increasing the power production while assuring the safe operation of the components.

6.3.1 Test benches for HIL testing

Infrastructures for marine technology development

Test facilities are available at full and small scale capacity depending on the needs of the developers and the TRL of the system to be tested. Multi-megawatt facilities typically hosts prime movers with ranges of rated power from 3 to 15 MW. The aim here is to dynamically reproduce the mechanical loads and stress the drive train is exposed to during its life cycle. Components like bearings, gearboxes and generators can be extensively analysed by applying forces in the 6 degrees of freedom in the emulated turbine rotor. Some of them include Hardware-In-the-Loop (HIL) grid emulators allowing

the certification for grid code compliance. This is the case of the 15 MW Wind Turbine Drivetrain Testing Facility associated to the Duke Energy eGrid at Clemson University (USA) [SF14], the 10 MW DyNaLab of Fraunhofer IWES in Bremerhaven (Germany) [Fis+16], and the 12 MW Lindoe Offshore Renewables Center in Munkebo (Denmark) [Ras16]. It is commonly used for the certification of wind turbine nacelles and obviously transferable to tidal energy. For example the ORE Catapult facility (UK) for turbine drive train testing hosted the 1MW tidal nacelles of Marine Current Turbine and Atlantis [Cat20]. Apart from these full scale test rigs, lower rated test infrastructures are also viable solutions for lower TRL to prepare the prototyping phase. At that stage, the testing of control strategies and the overall control framework that encapsulates them is mandatory. For example, small scale test rigs are available at SINTEF Renewable Energy Lab-SmartGrids, TECNALIA Electrical PTO Lab and UCC-MaREI Rotary Test Rig. Their characteristics are gathered in [Cav+16]. In this paper, Cavagnaro et al. used the three test rigs to perform a 'Round Robin' testing campaign. Their behaviour were compared through the implementation of the numerical model of the same tidal turbine and the test of the associated control strategies while using two scaling methodologies.

Objectives of HIL testing

Focusing on electrical infrastructures, they enable the profound study of each component that compose the electrical conversion chain. It is essential to understand the dynamic response of the system and gather data over a significant number of working hours during relevant conditions in both normal and extreme operation [Arm+15]. Indeed, part of the equipment composing the test bench is similar to the one embedded in the prototype deployed at sea. The power conversion components can be deeply studied from both mechanical and electrical perspectives. For example, the efficiency of the generator in different load conditions can be characterised; the peak values of torques and rotational speeds are measured. Limitations in voltages and currents that the power converter can handle are studied assuming the thermal behaviour of the equipment is known. As an example, in the wind industry, the most frequent component failure [Pér+13] – although associated to a minor turbine downtime – comes from the electronic components in the power converter.

Furthermore, another interesting application of a test bench is that it allows the programming and test of the SCADA and main control framework in the programmable logic unit. It is the central intelligence assuring the correct operation of the WEC, collects all the sensors data, process the control algorithms to generate the control action to be sent to the actuators. It is also the equipment that manages the auxiliary system. Nontheless, the major advantage of a HIL is its ability to experimentally validate control strategies that aim at increasing the power production, the overall performance and assure the safe operation of the components. These control laws are applied during the operation of the device and are developed in the Programmable Logic Controller (PLC) state machine. In the meantime, it leads to improvement in power quality when analysing the profiles of the voltages, currents and their harmonics at different steps of the power converter. Finally, grid integration can be investigated when a programmable power converter is employed. It is valuable to verify grid codes compliance when connected to a variable grid capable of emulating faults in both strong and weak electrical networks. In short, test infrastructure offer several ways to develop more cost-effective and reliable devices, and prepare them for trials at sea.

General HIL architecture

The HIL implies that at some point there is a feedback of data from measurements on the equipment to the model emulating the device which introduces a change in the modelled WEC. Figure 6.6 illustrates a general configuration of a HIL PTO rotary test bench where any device can be tested as long as the PTO mechanism supplies a rotational (mechanical) power suitable for feeding a generator. The basic components in a test rig are two electrical machines facing each other. On the one hand, the device emulator replicates the dynamics of the WEC, and on the other hand the real components to be tested are installed. From the emulator side, the frequency converter is supplied by the grid and connected to a motor drive. On the generator side, the real equipment installed in the device is composed of the generator connected to a power converter feeding the grid, or to a load bank to dissipate energy. The PLC centralises the sensors and process the control algorithm to operate the WEC. During the simulation, the numerical model runs in a computer containing the real time operating system and where the RT acquisition I/O board is installed. It receives the rotational speed from the test bench, resolves the set of differential equations of the numerical model
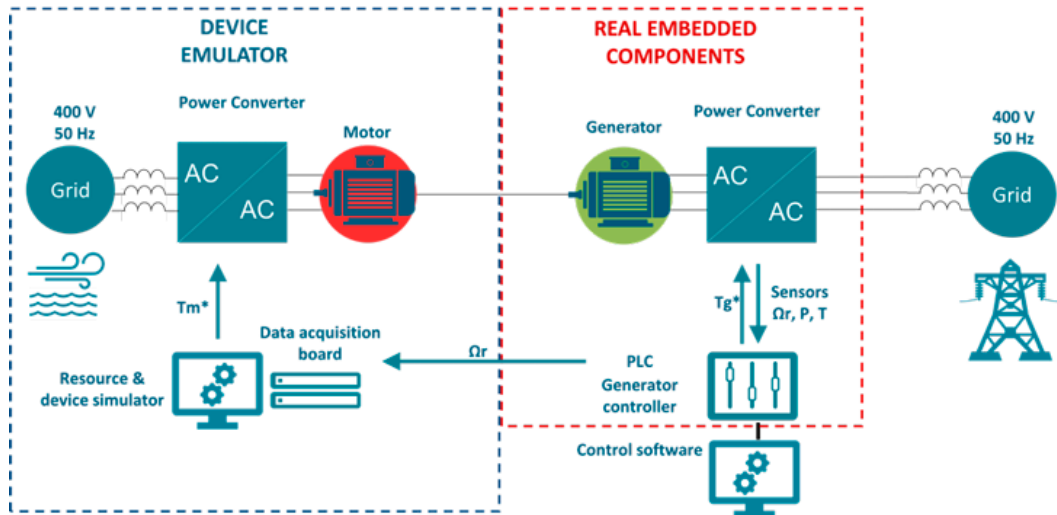
Fig. 6.6: General HIL architecture of a rotary test rig

that emulates the WEC in function of this measure, and computes the torque reference to be applied by the motor. The reference signal of torque is sent via analog signal to the drive which sets the motor in rotation consequently emulating the behaviour of the prime mover. Then, the control algorithm, coded in the PLC, reads the speed and the computes the resistive torque to be applied by the generator. The Back-to-Back power converter (B2B) treats this signal and controls the output current by an inner PI controller. This process is done at each sampling time along the experiment.

6.3.2 Scaling methodology from modelling to HIL experimentation

In order to perform a real time simulation and validate a control strategy, there are a series of adaptations to be made to get consistent relationship between the HIL and the model to be tested. The main reason is because the device at full scale is different from the ratings of the test bench equipment. To be valid, the experiment has to follow the principle of similitude between these different scales.

As the full scale device usually does not match the ratings of the equipment composing a test rig, a scaling method has to be employed. The choice of this technique depends on the most relevant forces in presence, and is related to the type of energy the device extracts. In wave energy, wave forces are strongly linked to gravitational forces so Froude scaling criterion [Fro68] is

used to maintain correct relationship between the prototype and the model [FH14]. Also, depending on the way the energy is transformed, there are specific considerations to be addressed. In the case of the OWC, the dynamics of the air chamber (compression and flow rate) would have to be scaled via the Reynolds rule [Rey86] to ensure the principle of similitude for the fluid viscosity. Though it is impossible to apply two scaling techniques in the same model scale. As a matter of fact, to avoid related issues, the whole numerical model is running in prototype scale and the inputs and outputs are scaled. The scale factor associated to each dimension of interest is presented in Table 6.1 where the scale factor is defined as the ratio of the device prototype and model diameters i.e. $\lambda = D_\mathrm{p}/D_\mathrm{m}$.

Tab. 6.1: Froude scaling for a selection of physical parameters

Physical parameters	Dimension	Scale factor
Time	s	$\lambda^{0.5}$
Length	m	λ
Force	N	λ^3
Power	W	$\lambda^{3.5}$
Torque	Nm	λ^4
Rotational speed	rad/s	$\lambda^{-0.5}$
Inertia	kg.m2	λ^5

There are three magnitudes of these quantities to take into account: the prototype at full scale denoted with the subscript p, the model scale of its reduced device m and the test bench scale composed of the physical equipment r. From now on, the subscripts p, m and r stand for the scales of the prototype, the model and the test bench real quantities respectively. Let us consider the turbo-generator set dynamics applying the 2nd law of Newton where the angular acceleration $\dot{\Omega}$ is defined for an ideal system without losses by:

$$\dot{\Omega} = \frac{T_\mathrm{t} - T_\mathrm{g}}{I} \tag{6.4}$$

Here the prime mover (turbine) and generator torques are respectively T_t and T_g, and the inertia is noted I. In order to match all of them and respect the system dynamics, especially to compensate the effect of the inertia, the Froude scaling law is applied to the rotational speed, torque and inertia as follows:

$$\Omega_\mathrm{m} = \Omega_\mathrm{p}/\lambda^{-0.5} \tag{6.5}$$

$$T_\mathrm{m} = T_\mathrm{p}/\lambda^4 \tag{6.6}$$

$$I_{\mathrm{m}} = I_{\mathrm{p}}/\lambda^5 \tag{6.7}$$

As it can be the case in scale testing, the ranges of rotational speed between the model scale and the test bench may not match so the equation to relate them is then:

$$\Omega_{\mathrm{r}} = \kappa\,\Omega_{\mathrm{m}} = \frac{\Omega_{\mathrm{nom,r}}}{\Omega_{\mathrm{nom,m}}}\,\Omega_{\mathrm{m}} \tag{6.8}$$

As explained previously, the rotational speed from the test bench is an input to the numerical model in the HIL simulation. It is set at the prototype scale by using Equation (6.5) and (6.8) so:

$$\Omega_{\mathrm{p}} = \Omega_{\mathrm{r}}\,\kappa\,\lambda^{-0.1}\,\Omega_{\mathrm{max,p}} \tag{6.9}$$

The term $\Omega_{\mathrm{max,p}}$ represents the prototype maximal speed and sets the speed ranges of the prototype.

Then, following Equation Eq. (6.4) with Eq. (6.8) and taking its time derivative:

$$\dot{\Omega}_{\mathrm{r}} = \kappa\,\frac{T_{\mathrm{t,m}} - T_{\mathrm{g,m}}}{I_{\mathrm{m}}} = \frac{T_{\mathrm{t,r}} - T_{\mathrm{g,r}}}{I_{\mathrm{r}}} \tag{6.10}$$

Multiplying by the test bench inertia:

$$I_{\mathrm{r}}\,\dot{\Omega}_{\mathrm{r}} = \kappa\,\frac{I_{\mathrm{r}}}{I_{\mathrm{m}}}\,(T_{\mathrm{t,m}} - T_{\mathrm{g,m}}) \tag{6.11}$$

Consequently, in order to match the test bench dynamics and emulate the effect of inertia, the turbine torque sent to the motor at the output of the numerical model is:

$$T_{\mathrm{t,r}} = K_{\mathrm{i}}\,T_{\mathrm{t,m}} \tag{6.12}$$

with the inertia compensation factor $K_{\mathrm{i}} = \kappa\,\frac{I_{\mathrm{r}}}{I_{\mathrm{m}}}$.

The same way, the resistive torque in the PLC is defined by:

$$T_{\mathrm{g,r}} = K_{\mathrm{i}}\,T_{\mathrm{g,m}} \tag{6.13}$$

Therefore, these quantities are in the test bench scale simulating a virtual inertia.

There are few adaptations to be made in order to compose with the particularities of any rig. As the drive train losses may not be known in the prototype at early stages, the effect of the specific test bench friction losses

are cancelled. To do so, these losses have to be measured along the range of rotational speeds and included in the model running in real time. They are cancelled by adding them to the mechanical torque. Also, in the simulated model run in parallel, the test bench dynamics are reproduced, along with the control strategy computed in the PLC, so the comparison and validation is feasible.

6.3.3 Experimental setup

The infrastructure used for the experiments is the **Tecnalia electrical PTO lab** presented in Fig. 6.7. It is composed of two electrical machines facing each other and mechanically attached by a shaft. The prime mover is a Leroy Somers LSES 160 LUR 4-pole SCIM with a rated power of 15 kW at 1460 rpm. The motor is controlled by a UMV4301 Leroy Somers drive following torque or speed reference provided by the analogue signals coming from the acquisition board NI PCI 6221 from National Instrument. The simulation is performed by an XPC target configuration which is the real-time architecture from Matlab/Simulink. The generator is an ABB M3BP200MLA 8-pole SCIG of 11 kW rated power for 768 rpm. As the motor, its frequency is 50 Hz and the voltage is 400 V connected in delta. The generator is grid connected via an ABB ACS800 B2B power converter. The PLC controller is a CX1020 from Beckhoff with a series of digital and analogue signal boards. The generator, B2B converter and the PLC are the equipment installed in the OE Buoy 4th scale prototype tested in Galway Bay as part of the CORES project [COR11] during which several control strategies were tested in this infrastructure. The total inertia of the system is raised at 1.2 kg.m^2 with a flywheel installed in the shaft.

A state machine algorithm is implemented the PLC. It is divided into 6 states describing the different necessary steps for the correct and safe operation of the system. At State 1, the system boots up and after a certain time goes directly to State 2 where some verifications are made to be sure that the sensors are operational and values are inside the requested ranges. For example, it will test the chamber pressure to know if it is within safe operation range. Then State 3 stands for the run up where the brake is released and the turbine starts rotating and then goes through State 4 where the control law is applied every sampling period. When an alarm is triggered by sensors or if an error is detected, the machine system enters in State 5 (low priority)

and the turbine slows down until breaking in State 6. If the error is critical, State 6 is directly engaged stopping the operation.
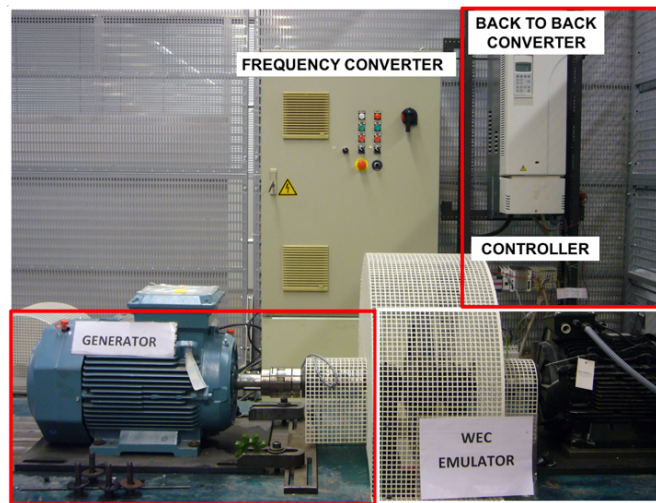
Fig. 6.7: Tecnalia PTO test bench

The methodology is applied to the numerical model of the OWC and the necessary adaptations are made to perform the experiment on the Tecnalia PTO test rig. During an experiment, two models are running simultaneously to allow comparison:

- The HIL one which has input and output signals coming from and going to the test bench with the required conversion blocks (scaling and speed/torque adapters), and the WEC numerical model. This model considers the energy conversion from the waves to the mechanical power.

- The fully simulated one, with the same WEC model, but in addition the control law and another model of the test bench to reproduce its dynamics. Without this block the comparison is not possible.

Both hydrodynamic models are set in motion by the same wave excitation forces. Figure 6.8 illustrates the general layout of the setup running in real time during the experiment.

The scale factor is calculated as the ratio of the rated powers of the generators from the prototype over the one of the test bench following the Froude scaling rules set in Table 6.1:

$$\lambda = \sqrt[3.5]{\frac{P_{g,nom}}{P_{r,nom}}} \tag{6.14}$$

The compensation factor to set the virtual inertia into the motor and the generator torques is defined such as:

$$K_i = \frac{\Omega_{nom,r}}{\Omega_{nom,m}} \frac{I_r}{I_m} \tag{6.15}$$

The friction losses to add to the torque sent to the turbine are not constant and higher in lower speeds. A look-up table assure the relation between the speed and the associated losses due to friction. Finally, the control law is applied every sampling time during State 4 in the PLC state machine corresponding to the normal operation.

Fig. 6.8: Simulink layout for the real time experimentation of the floating OWC

6.3.4 Case studies for the validation of control strategies

Two case studies are presented in this section where the scaling methodology developed earlier is applied for two OWC devices, with their specific PTO ratings. Each one has its control strategy and the validation tests are made using the same test rig:

- The first one relies on the implementation of a control law equivalent to the torque law CL2.2 developed in Section 5.3.3 and customised for the Sparbuoy. Its PTO is composed of a biradial turbine of 1.5 m diameter and a 90 kW generator with a nominal torque of 1159 Nm and speed 741 rpm. The drivetrain inertia is 200 kg.m^2. The offline optimisation resulted in the T-Ω curve of Fig. 6.9.

- The other experiment consists in the implementation of the predictive controller CL4.1 developed for the Mutriku plant in Section 5.3.4 with the PTO designed for OPERA (biradial turbine of 0.5 m diameter and a 30 kW generator).

These HIL tests are presented to understand the benefits of using this kind of infrastructures. They validate the implementation of the controllers in a real control environment. The scaling methodology detailed earlier is applied in order to prove its validity for various prototypes.

Adaptive controller based on a torque law

This section presents the results of the HIL experiment of the CL2.2 type controller in the test rig for three sea states. Although the results are presented here for three sea states, the full test campaign was done for 12 cases constituting the wave climate. Sea states SS5, SS8 and SS12 are characterised respectively by H_s of [2.0, 3.0, 4.9] m, and T_p of [8, 8, 12] s. They represent a variety of wave conditions from normal operation to extreme operation to capture the behaviour of the device and the PTO, and to know how the control reacts in the simulation and during the experiment. The data of the measured (plain blue line) and simulated (dashed red line) rotational speeds and generator torques are recorded during the experiments. They are in the test bench scale. The Figure 6.10 shows the fairly good match between measured and simulated data. Only some extreme waves during SS12 could not be tested in the test bench. As can be seen in this figure at the time 1280 s, the test bench equipment reach their limits and are not able to withstand that much power, using that scaling factor. The instantaneous generator power is $P_g = T_g \, \Omega = 100 \text{ x } 250 = 25 kW$, more than twice the nominal power that is 11 KW. In general, these experiments validate the methodology employed for testing control strategies.
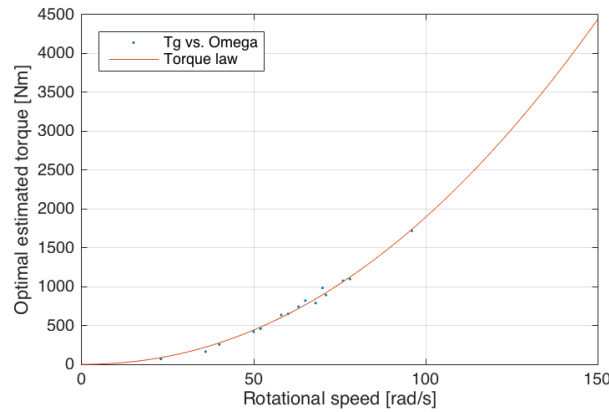
Fig. 6.9: Control law used in the HIL test

Non-linear predictive control algorithm

The second case study is focused on the validation of the NL-MPC algorithm using the Mutriku W2W model, see CL4 in Section 5.3.4 for its formulation. The challenge of the real time optimisation implementation resides in the correct time synchronisation. It has to be triggered at the very right instant for each replanning time in a parallel task while the experiment was running. The optimisation algorithm has to be optimised to reduce its duration. After code optimisation, the algorithm takes 3 sampling times (less than 0.3 sec) which is fair considered that this process happens once at each replanning period (between 10 and 20 sec) and not at each sampling times. There may be a small shift in time due to this delay and the control action may not be optimal for this short time period. In addition, in the specific case of the predictive controller, an additional computer linked to the target PC is necessary to compute the real time optimisation. The flow of data includes the state vector of the experimental model and the test rig rotational speed as inputs for the algorithm to initialise the system of equation. The outputs are the optimised control vector containing the new torque law parameters a and b. These parameters are then applied in the updated torque law during the next replanning period.

The test campaign with the rig was done for all the 14 sea states. However, SS7 SS10 and SS14 were chosen to highlight the test results. Indeed, SS7 represents the most frequent sea state, SS10 the most energetic one over a full year, and SS14 the most powerful one for the Mutriku site (see Fig. 5.5 for details on the wave climate). The sea conditions are characterised by H_s [1.5, 2.0, 4.0] m, and T_p of [14, 14, 18] s. Figure 6.11 shows time
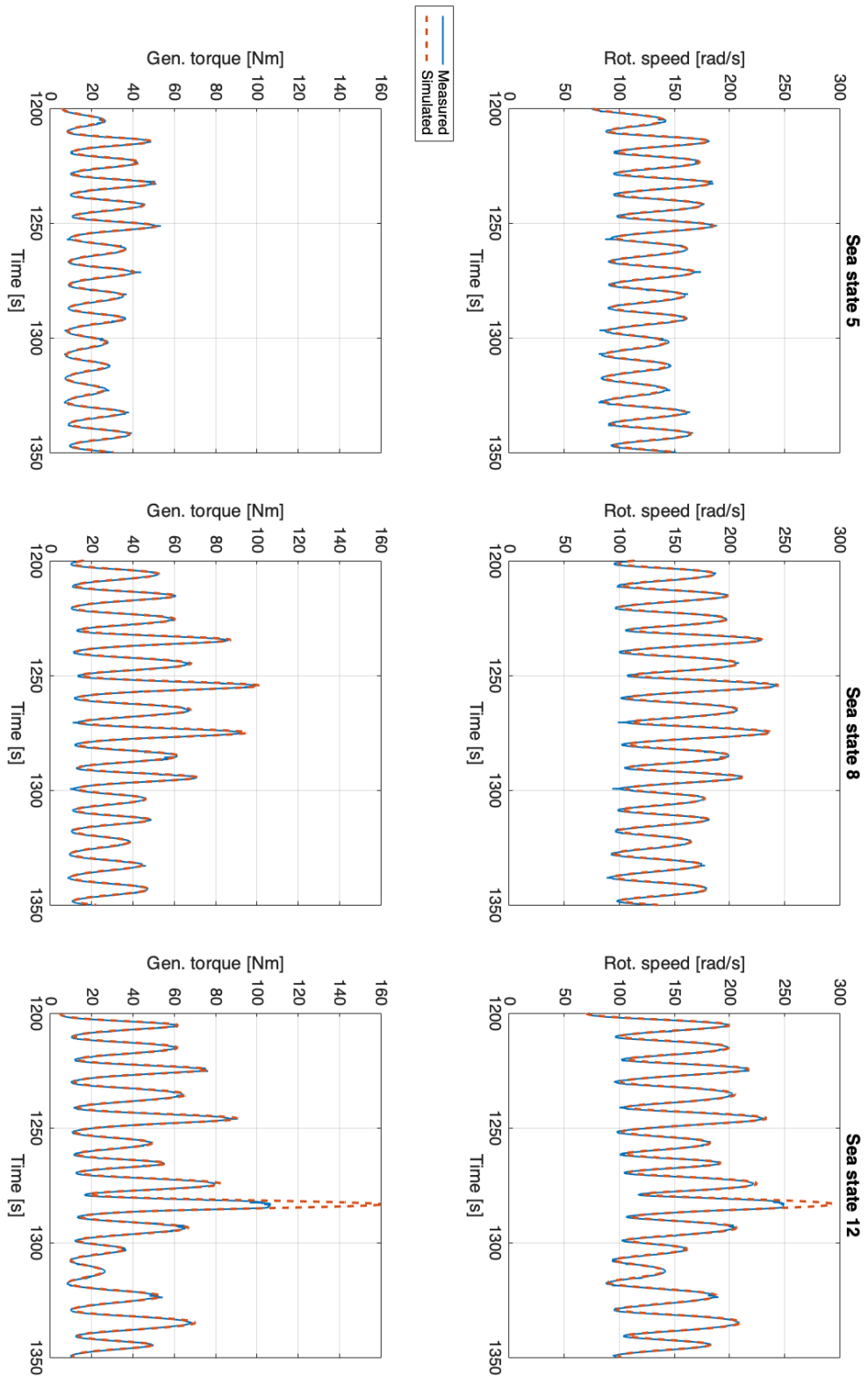
Fig. 6.10: Comparison of measured and simulated data of the motor rotational speeds and the generator torques in sea states 5, 8 and 12 for CL2.2 in the sparbuoy

series of the rotational speeds, turbine torques and generator powers for both the numerical model and the experimental results obtained during these three sea states. Note that the experimental values are presented back to the prototype scale to be compared with the numerical simulation results. The effects of applying the new calculated control parameters are visible in the time series of the generator power with the sudden changes in the power profile. It is meant to set a harder torque law when a future set of waves arrives and softer when the waves are calmer.

The quantities measured in the test bench are quite similar to the simulated model. Only some small misalignment appear, most of the time in speeds, but for several seconds and then the experimental and simulated curves meet again. As a consequence, the control law computes a generator torque a bit different. This produces a difference in the instantaneous output powers of few kilowatts. Given that the rated power is 30 kW this mean an error less than 10% only during few seconds and for the worst cases. Another reason for this small discrepancies can come from the small delay induced by the execution of the on-line optimisation. Anyway, this seems acceptable to validate both aspects of the correct implementation of the methodology for scaled tests and the correct implementation of the predictive algorithm.

Fig. 6.11: Experimental and simulated results for the validation of CL4.1 on Tecnalia PTO test lab during SS7, SS10 and SS14

6.4 Test campaign in the Mutriku OWC plant
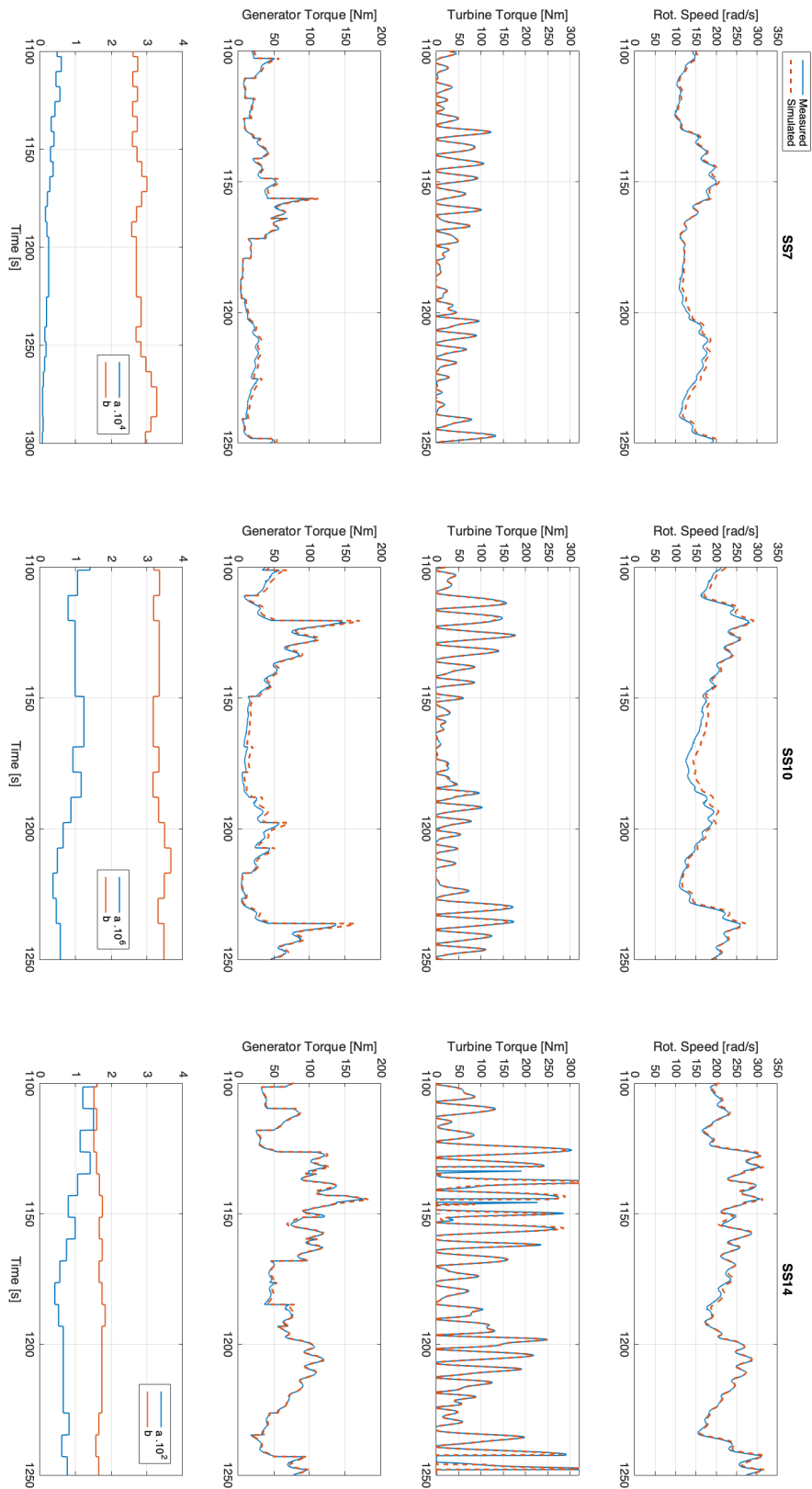
Following the correct implementation of the controllers using the dry PTO test rig, the opportunity to test some of them in real sea conditions was offered as part of the OPERA project. Although the Mutriku sea trial campaign allowed to deeply study the biradial turbine for over one year, along with several control algorithms, circumstances only offered the two remaining weeks of this campaign for the predictive control law. There was a delay in laying down the data cable from the wave elevation sensor ahead of the plant to the control room onshore. One of the project objectives for the sea trials consisted in comparing the torque law of CL2.1 with the predictive algorithm CL4.1 (following the naming of Section 5.3). Here they are denoted respectively CL2 and CL4 for ease. These trials allowed to test the correct implementation of these control laws in a real environment, and then to draw additional conclusions after comparing the simulation results obtained in Section 5.3.5. To do so, the test procedure was to switch automatically from one controller to the other. This section covers the context of these trials detailing the wave resource during the experiment, the necessary sensors for this type of test, and the control framework. Some proofs of the proper operation of the NL-MPC are presented and the obtained results are also compared.

6.4.1 Wave resource

As explained earlier, the knowledge of the excitation force from the incident waves is required to run the predictive algorithm. For the sea trials at Mutriku, an hydrostatic pressure sensor [Isu18] was used for both providing the wave climate, and sending the wave elevation measurements in real time to the controller. Figure 6.12 shows a top view of the plant with the bathymetry and location of the pressure sensor. It was located 200 m in front of Chamber #9 of the plant following the most frequent wave direction. During the sea trials, the wave elevation sensor measured various sea states but only 7 different ones had statistical relevance considering a number of tests for both control laws (see Fig. 6.13). These sea states are in the range of $H_s = [0.5 : 1]$ m and $T_e = [7 : 14]$ s. The two weeks in June 2018, during which the tests were performed, were poor in terms of variety of sea states but still 325 tests of half an hour each that fall into that wave climate could be done.
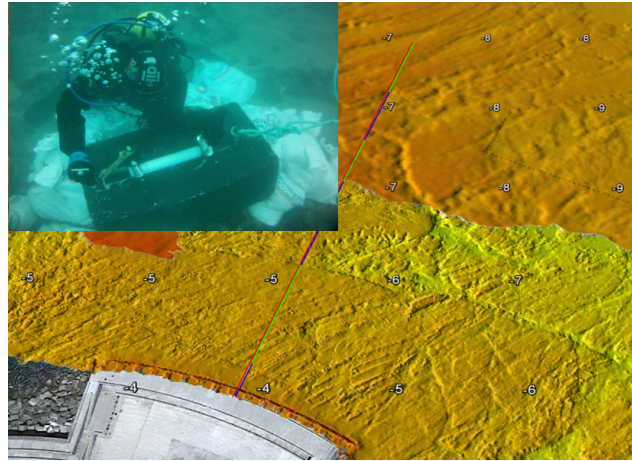
Fig. 6.12: Location of the pressure sensor in front of the Mutriku OWC plant
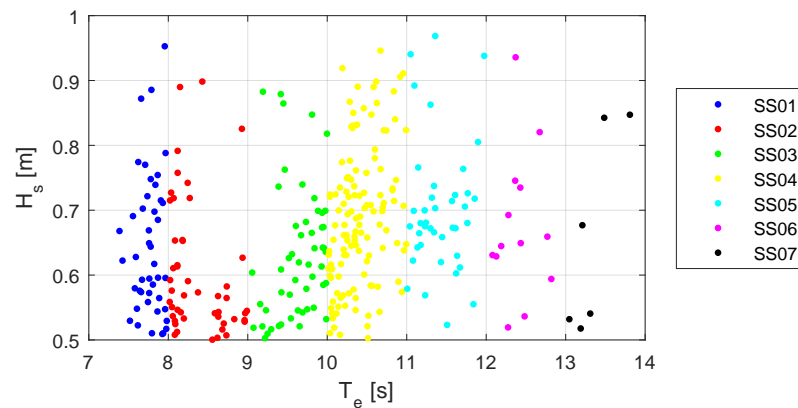
Fig. 6.13: Sea states during the test in the Mutriku plant

The real time wave measurement received by the control unit was sent as input to the predictive controller. The pre-processing included a tide cancellation to center the wave elevation to 0 and the excitation force estimator as detailed in Section 6.2. A moving vector containing the future excitation force, with a sliding window of the size of the prediction horizon, was filled in and sent to the predictive controller at the beginning of each replanning period. To remove some uncertainty in the synchronisation of the excitation force vector and the actual waves reaching the plant, the prediction time was variable and computed in function of the tide. Indeed, the water depth influences the travel speed of waves and thus the time between the measured wave until it reaches the plant. A correlation study was performed between the wave measured upwave by a previous installation of an offline pressure sensor [BT17] and plant operational data. As can be seen in Figure 6.14, the time delay (equivalent to the prediction time) was between 20 and 30s, and as for the simulation, the replanning time was half the prediction one.
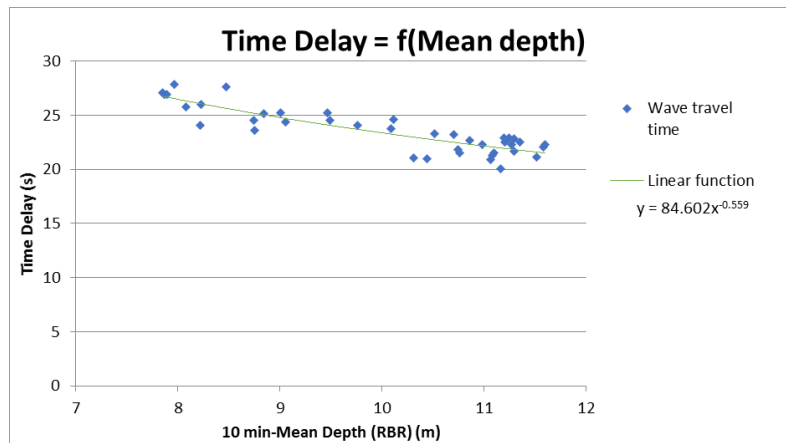
Fig. 6.14: Definition of the wave travel time in function of the tide level (water depth) using measured data

6.4.2 Instrumentation and control framework

All the plant sensors were centralised and processed in the PLC, a X20cCP1584 from B&R specially designed for harsh environmental conditions. Typical measurements included the motion of the IWS, both the butterfly valve and HSSV positions, pressures at different locations of the turbine, the drive train speed, rotor axial vibrations and generator winding temperature, electrical quantities at the generator and the grid side of the B2B power converter. All the operational data were sent by the PLC to a local database (DB) and replicated in a cloud web service for easy access and faster post processing.

The global advisory and control software was designed following a state-machine approach similar to the one of Tecnalia PTO test rig detailed in Section 6.3, with a security layer able to trigger different sorts of warnings or alarms. The hierarchy of alarms induced different safety actions to insure the plant and the PTO integrity. The real-time control of the turbine speed was done by simply computing the torque reference and sending it to the power electronics. This one follows the torque reference with its internal current and voltage control loops. The PLC cyclic time (the sampling time of a task) for the main control program was 100 ms. The test procedure was developed to assure autonomous operation, and to switch automatically the control laws between CL2 and CL4 each half an hour, the statistical duration of a sea state. To avoid issues from passing from one control law to the other, a safe transition procedure was coded. At the end of a 1/2h test, the butterfly valve between the air chamber and the turbine had to shut-off, and was allowed to open only after the speed came down to a certain threshold.

6.4.3 MPC implementation

To overcome the computation requirements of the on-line optimisation and the complexity in the implementation, it was decided to use an additional computer (named the control PC) and link it to the PLC via an OPC server. It is common communication protocol in industrial processes. Here, it allows the exchange of data between the PLC and the control PC. This computer released the PLC from the computation burden and run a Matlab/Simulink model for the experiment of CL4. This model is very similar to the one used in the test bench experimental phase (see Section 6.3). It received the wave elevation and the main plant operational data. At each time step, the excitation force moving vector was updated while the controller computed the radiation forces, as a virtual sensor would do, using the real water column velocity.

At the beginning of each replanning, the MPC algorithm received the state vector initialised with the last instantaneous plant data and the computed radiation forces components, plus the vector of estimated prediction forces. The MPC computed the best configuration of control parameters in a maximum of 3 PLC cyclic times and returned them to the PLC where they constituted the new torque law applied during a full replanning time. At the end of a CL4 test, the control parameters were saved so the next test could be initialised with the latest optimised parameters, after a CL2 test 1/2h later. The first time the predictive algorithm was used, the control parameters of CL4 where those of CL2.

During the implementation of the predictive algorithm, a 20-hour test was done to validate its autonomous and safe operation. The evolution of the control parameters in Fig. 6.15 is interesting in several ways. First it proves the controller was operational without interruption for a full day. In addition, at the beginning of this test, control parameters were set far from their optimal values to verify the algorithm could converge to a credible solution. Finally small variations of the a and b coefficients illustrates the fact the controller adapted to a short time changing wave conditions at each replanning period.

A comparison is made to validate the W2W model with the real plant measurement by showing the water column motion in frequency domain after applying a FFT and analyse the amplitudes along with the frequencies of
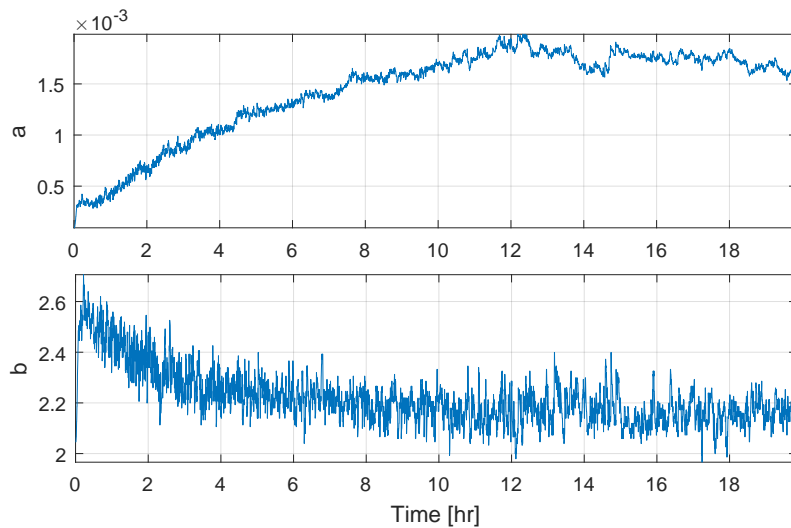
Fig. 6.15: Evolution of the control parameters during the large duration test of the predictive controller

motion. As it is difficult to synchronise both signals, given the estimated wave travel time, this approach allows a more visual comparison of both quantities (see Figure 6.16. The figure reveals the three main physical quantities of the system representing the differential equations. In all quantities, the frequencies are respected for both the model and the measurement, but the numerical model shows magnitudes lower than expected. The hydrodynamic model was tuned using real values and detailed in Section 3.1. But still, this one needs to be fully validated. This means there is still room for improvement for this predictive algorithm.
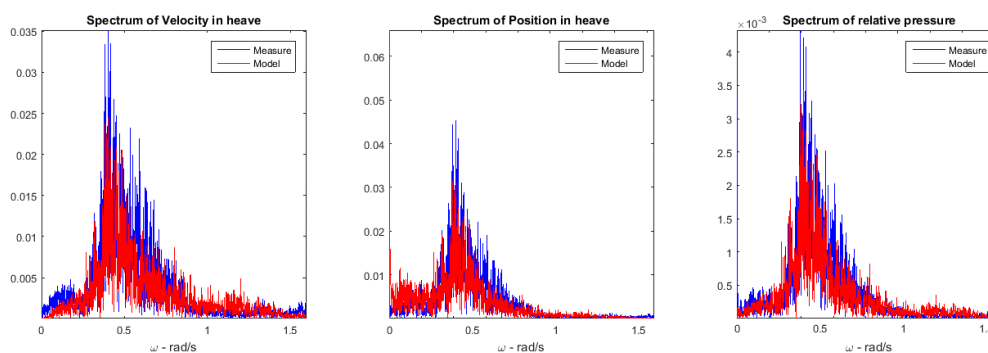
Fig. 6.16: Comparison in the frequency domain of measured and modelled water surface velocity, position and air chamber pressure of CL4 operation during $H_s = 0.73$ m AND $T_e = 11.43$ s

6.4.4 Comparative analysis of results

Power production performance

To ease the analysis and comparison of performance, the electrical power production is first presented for CL2 over the 7 studied sea states in Fig. 6.17. Because the controllers were operational several times during a same sea state, a boxplot is a convenient way to appreciate these test results. For each sea state, the mean of the averaged power production per sea state is shown with a star, the blue rectangle collects half of the tests between the quartiles 25% and 75%. The maximum and minimum are also represented at the extremities of the rectangles. The red crosses are outliers and thus not considered in the analysis. The dispersion of results is probably due to the fact that representing a sea state by H_s and T_e may not be the most appropriate for this case. Indeed, there are other criteria characterising a wave spectra such as the wave steepness or the peakedness of the spectrum. Also the wave direction and the tide level can influence the energy absorbed by the system. The first observation is that at sea states with significant wave height between 0.5 and 1 m, CL2 produces between 1-1.6 kW in average. For a generator nominal capacity of 30 kW this represents the region with more losses and thus the power production is little but still in the range of the numerical simulation results.
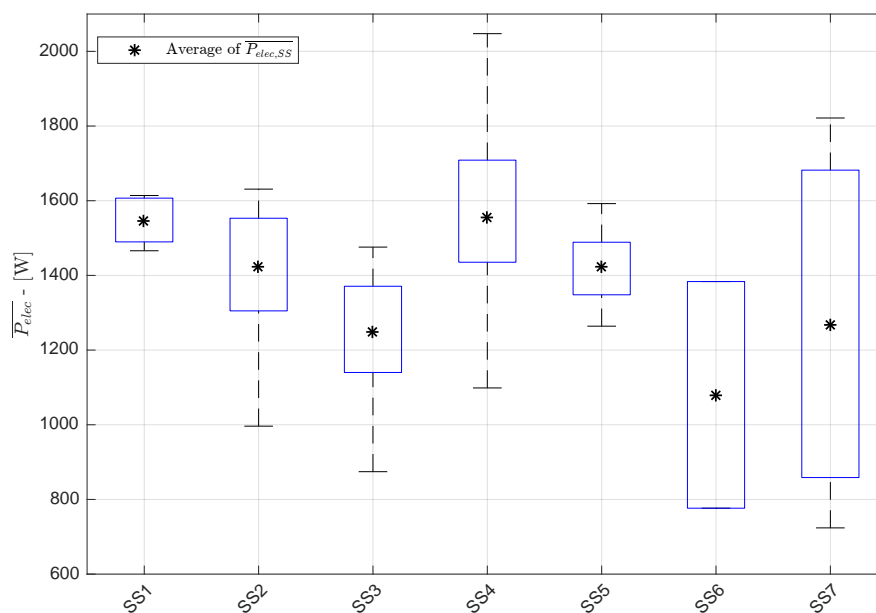
Fig. 6.17: Electrical power production of CL2 for the 7 sea states at Mutriku
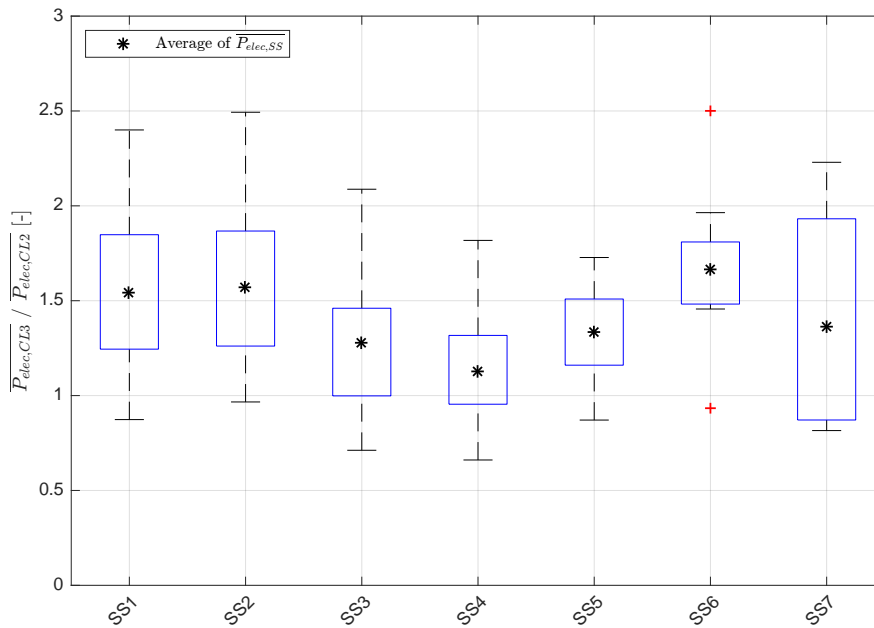
Fig. 6.18: Improvement on the average electrical power production of CL4 with respect to CL2 for the 7 sea states at Mutriku

The predictive controller results are presented in Fig. 6.18 linearised by the average of the mean electrical power productions of CL2 for each SS. CL4 presents an increase of electrical power in all the sea states between 13% and 65% in comparison with CL2. When taking into account the occurrence of each sea states, the weighted increase reaches 32%. The increase of power production can be explained by the fact that considerations are given to the entire PTO considering both the turbine and the generator during the optimisation.

In Fig. 6.19 the efficiencies of the turbine, the generator and the total PTO are shown for each test in function of the pneumatic power. The turbine efficiency is higher in CL2 but focusing on the overall PTO efficiency, CL4 highlights better performance. This validates the hypothesis raised in the analysis of numerical results that better consideration must be given to the generator behaviour. In addition, the efficiency of the PTO operating in CL2 during these low energetic wave conditions is around 30%, 35% for CL4. These scores are quite equivalent to the simulation results of Fig. 5.21, where the real sea states would correspond to those from SS1 to SS3. This means the numerical model is sufficiently well adjusted to predict the plant production under different environmental and control conditions.
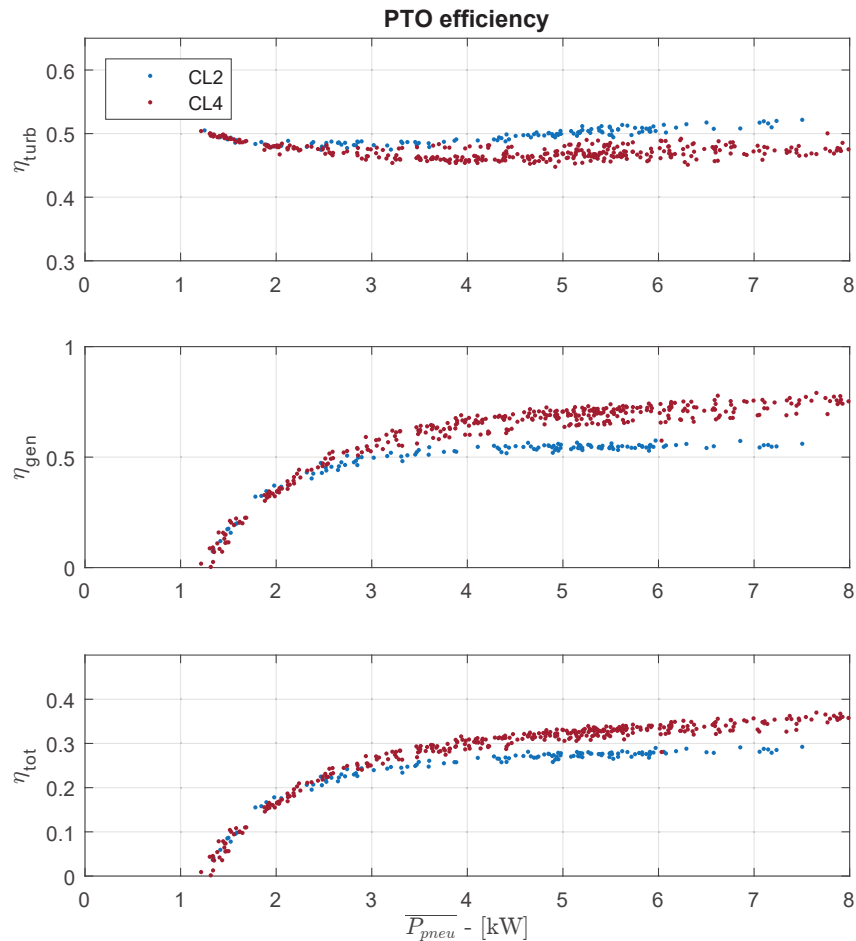
Fig. 6.19: Turbine efficiency (up), generator efficiency (mid) and overall PTO efficiency (low) at Mutriku for CL2 and CL4

Quality of power and PTO reliability

As for the numerical simulation case, an analysis of the quality of electrical power and the reliability of the component is done. Although only low energy sea states were experienced during the testing period, the values obtained allow a comparison of how the two controllers apprehend the power variations. Fig. 6.20 and Fig. 6.21 represent respectively the peak-to-average power ratio (Pk2av) and the standard deviation of the electrical power both with respect to the average of electrical power during all the tests. Globally, it appears CL2 shows little benefits with lower values both in peaks and in standard deviation of the electrical power. Concerning CL4, results show power peaks a bit higher and slightly more variability in the power production than CL2. This study is quite limited due to the low values of power experienced, average electrical power of 25% of the nominal capacity at most. Thus it is difficult to draw conclusions on the impact of the predictive

law on the power quality. As for the numerical results analysis, the predictive law captures more power in higher energetic group waves than the other control law studied here. There is clearly a lack of sea states and it should have been better to complete this analysis with higher energetic sea states to better understand how the predictive law deals with peaks of power in a larger variety of sea states and compare them to the assumptions formulated in the numerical analysis. As explained, these tests were done once the wave elevation sensor was installed which corresponding with the two remaining weeks when the turbine was available at the Mutriku plant.
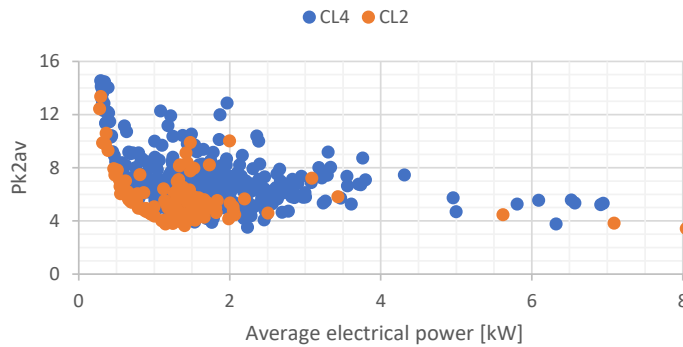
Fig. 6.20: Peak to average power ratio in function of the average electrical power for both controllers
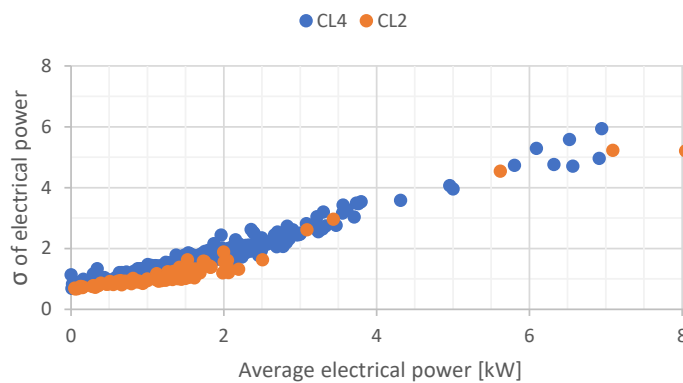
Fig. 6.21: Standard deviation in function of the average electrical power for both controllers

6.5 Test campaign in the Marmok-A-5 buoy in BiMEP

The opportunity to test the CL4 algorithm in the Marmok buoy presented itself at the end of the OPERA project and a 2-weeks test campaign was

done. In the test plan, which organised the schedule of the various control algorithms in the project, the predictive control law - the most complex and risky one - had to take place after the completion of the other control laws. The test duration was contractually decided with the authorities and could not be further extended. In comparison with the Mutriku testing, not all the results can be brought to light because of obvious intellectual property reasons upon the IDOM/Oceantec technology. The association between the wave resource and power production data was then not allowed. Instead, the results are presented in function of process variables. Nonetheless, experience related to the implementation is interesting to highlight here.

6.5.1 Prediction and estimation of the wave forces

In practice, the maximum time for the prediction depends on the wave propagation time from the measurement buoy to the WEC. To avoid over complicating the process, the propagation time was decided to vary in function of the distance between the two buoys and the wave period. Before each test, the wave buoy and the WEC sent their GPS coordinates and the propagation distance d_{T2M} was calculated. The wave velocity c can be computed knowing the wave period and the water depth following Figure 6.22 extracted from the DNV recommendation RP-C205 [DNV07].
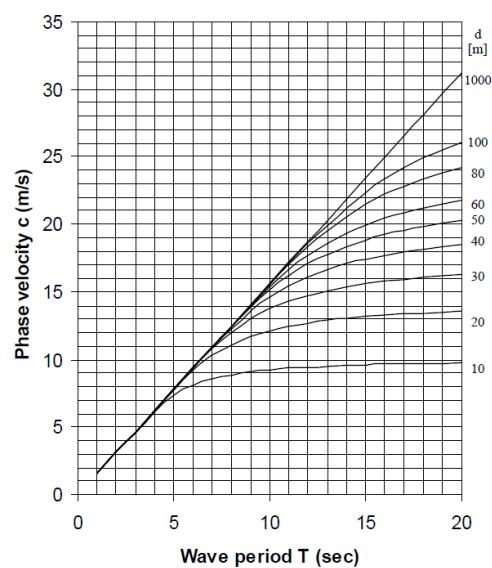
Fig. 6.22: Wave velocity in function of the period and depth – from [DNV07]

The water depth where the WEC was installed was around $d = 80$ m. The curve associated to this depth in the figure can be described as a polynomial function. The wave phase velocity is then calculated in function of the wave period T by the second order polynomial:

$$c = a_c T^2 + b_c T + c_c \qquad (6.16)$$

with the coefficients $a_c = -0.03972$, $b_c = 0.0863$ and $c_c = -1.2983$. Finally, the wave travel time, and thus the prediction horizon, was given by:

$$T_{ph} = d_{T2M}/c \qquad (6.17)$$

Before triggering the optimisation, the algorithm required a vector of the excitation forces of the incoming waves representing the wave forces exerted on both the buoy structure and the internal water column. The procedure to obtain them from the wave elevation measurement was detailed earlier in Section 6.2.

The wave elevation was measured by the wave buoy and sent to the control in real-time at 2 Hz. It was re-sampled at 10Hz, the frequency of the model, while filling a moving vector of the size of the prediction horizon. Figure 6.23 shows in practice the wave measured at the wave buoy and the equivalent wave forces estimated for a full 30-minutes test and zoomed in (500 s – 600 s) for a sea state $H_s = 1$ m, $T_e = 6$ s.

6.5.2 Predictive control requirements

Before running the MPC algorithm, a series of variables had to be initialised with a mix of measured and calculated quantities. The model state vector was composed of the 6 states resolving the differential equation and extended with the radiation terms:

$$x = [v_1 \ v_2 \ x_1 \ x_2 \ p \ \Omega \,|\, Rad] \qquad (6.18)$$

The first 6 states were given by local measurements from the PLC where v_1 and v_2 were respectively the buoy structure and the internal water surface
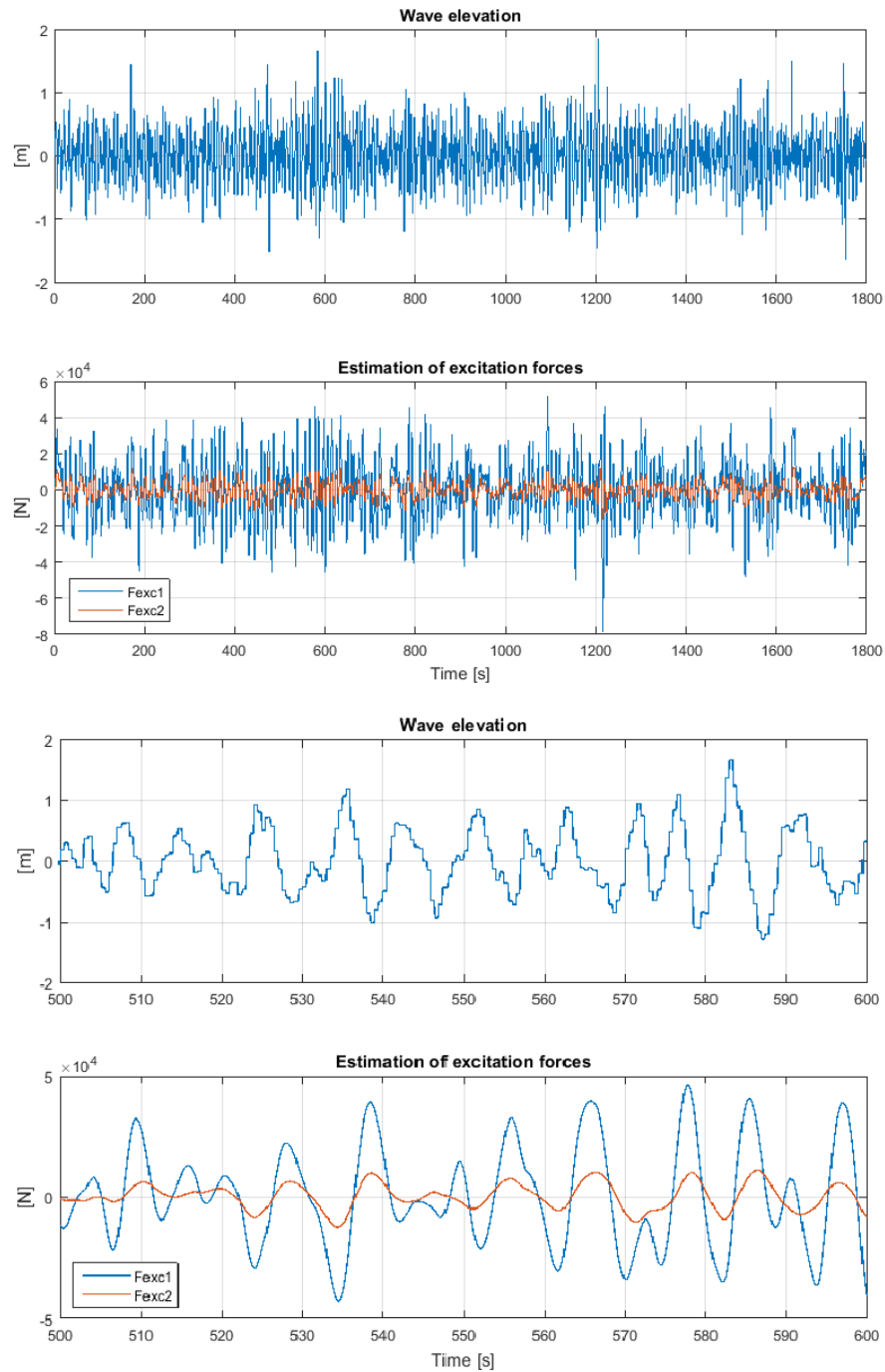
Fig. 6.23: Wave elevation from the wave buoy and excitation force estimation of the buoy structure (blue) and the water column (red)

heave velocity, x_1 and x_2 their positions, p is the internal chamber pressure and Ω the turbine rotational speed. The vector Rad represents the different radiation states used to compute the radiation forces. Similarly, to the excitation forces, these cannot be measured, and a virtual sensor estimating them had to be modelled, so the radiation forces are computed by the model.

At each moment, the instantaneous wave elevation was measured by the wave buoy, and the associated wave excitation forces filled in the sliding vector following a LIFO procedure (Last-In First-Out). That way when this wave reaches the WEC, the forces for each body are the first elements of the vector. As the waves propagate the vector is filled by the next wave forces passing over and constitute the future wave forces. Knowing the excitation forces, the buoy motion, the pressure and the turbine speed, the radiation forces were computed and so were the states Rad in the state vector which initialises the MPC.

This algorithm used both measurements from the Marmok and data from the wave buoy. The requirements are:

- Real-time measurements of the buoy structure and IWS motion in the chamber (position and speed), the internal chamber pressure, the turbine speed feedback;
- Real-time wave elevation from the wave buoy with minimum 1 wave period prediction;
- An accurate hydrodynamic model and a precise PTO characterisation

6.5.3 Implementation in the control framework

From one side, the wave data (sea state statistics and real time wave elevation) are sent to shore by the Triaxys wave buoy [Tec] via a VHF radio link (Very High Frequency). The antenna receiving these data is installed on-shore in the surveillance mast of BiMEP and linked to the onshore PC, located in the BiMEP offices, with fibre optics and then with a serial connection. From the other side, the PLC was located on-board in the Marmok buoy and connected to shore via the fibre optics wires of the electrical export cable.

There are two versions of the CL4 algorithm, one original version similar to the one used in the Mutriku, and another one customised in collaboration with colleagues of the PAIDI TEP-950 group from the University of Sevilla:

- CL4.1: the optimisation process is done by the onshore PC to avoid too many constraints on the PLC computation burden;
- CL4.2: the algorithm is lightened so the optimisation can run on the PLC directly.

For CL4.1, the onshore PC received data from both sides, executed the algorithm and sent back the control parameters to the PLC which applied the new control law. Figure 6.24 illustrates this control framework and the communications between the wave buoy, the control PC and the PLC. For CL4.2, the onshore PC received the data from the wave buoy and sent them to the PLC which computed the optimisation algorithm and applied the control law.
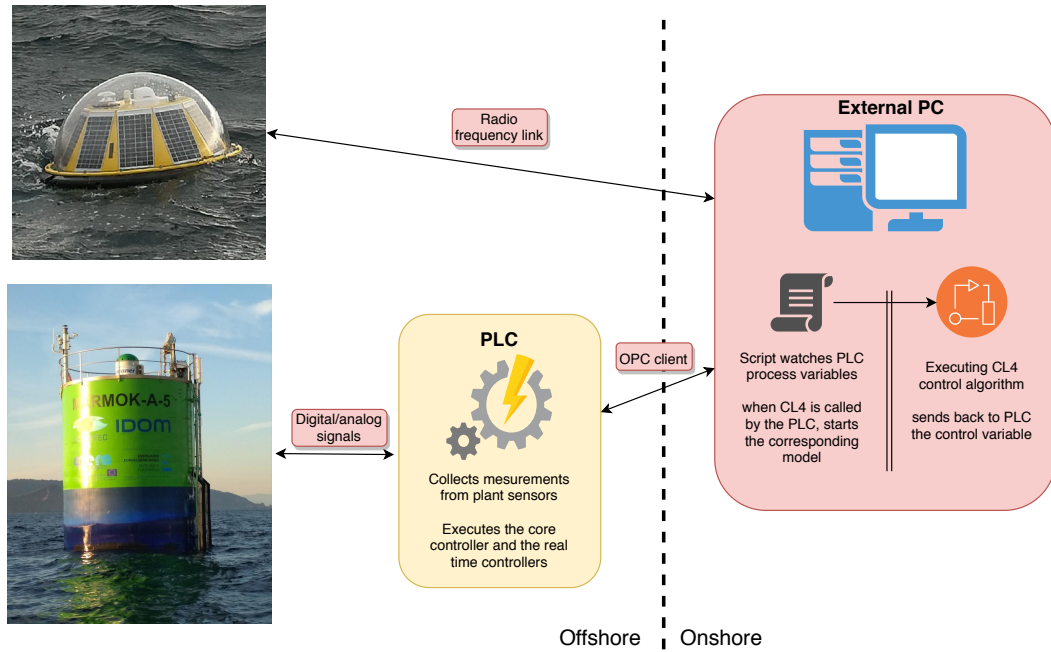
Fig. 6.24: Control framework at BiMEP site
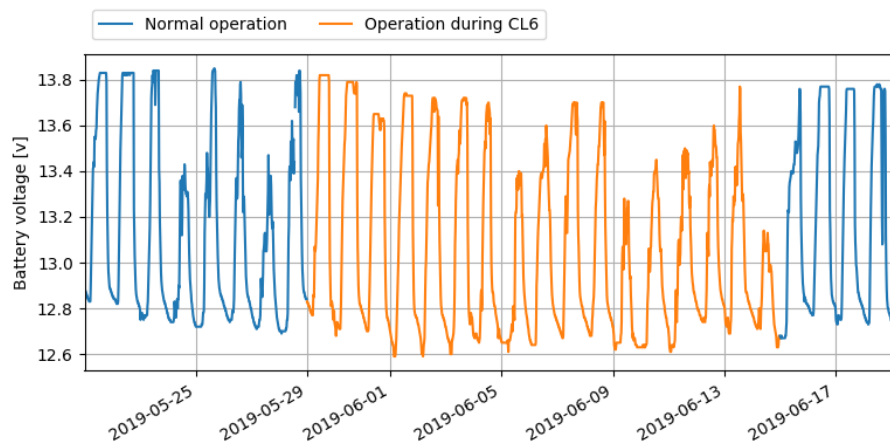
Fig. 6.25: Battery charge with and without the real time data transmission

When the real-time wave elevation transmission is activated, the stress on the batteries is more demanding than usual. To indicate the charge of the battery

pack and the effect of CL4 operation, Figure 6.25 presents the battery voltage in normal operation and during real time transmission for the predictive law. The batteries were powered by solar panels and the voltage variation was due to the solar irradiance, charging, and its operation mode, discharging. When operating with the real time transmission on, the voltage decreases day after day and the sun cannot fully charge them during day hours. However, it never falls below the threshold value of 80% of the full capacity, where the buoy enters in sleep mode.

The predictive controller computes online the best configuration of the $[a, b]$ parameters which ones characterise the torque law. The validation of both the implementation of the overall setup and the control algorithm were achieved by two convergence tests made on these control parameters. These tests are done to assure there is no unexpected events, like an interruption in the operation which can be characteristic of issues in the communication between the equipment, or a bug in the code execution. Figure 6.26 presents two long duration tests showing a continuous operation and allow to analyse the behaviour of the MPC. For both tests, the $[a, b]$ parameters were willingly set far from their optimal values, and their evolution is observed during 3 and 5 hours tests respectively. The sea states are reported in Table 6.2. The two tests were done during sea states quite similar. In both cases, the control parameters evolve in a short time period representing the local optimised parameters, and in a longer period are converging to the same values, oscillating close to $a \approx 2.10^{-4}$ and $b \approx 2.25$.
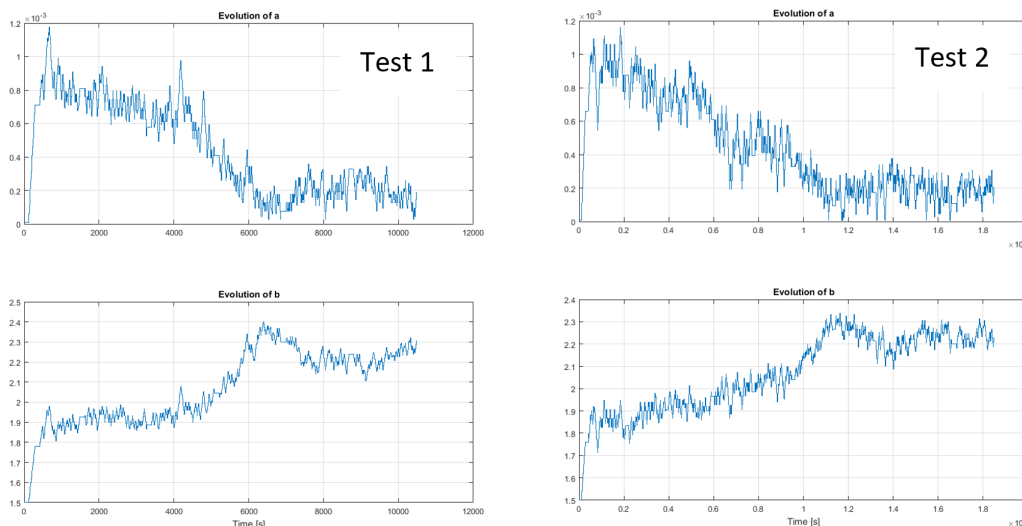
Fig. 6.26: Convergence tests of the control parameters to validate the MPC implementation

Tab. 6.2: Sea states during the convergence tests

Test #	H_s [m]	T_e [s]
1	0.75 to 1.00	7.5 to 8.5
2	0.65 to 0.80	6.5 to 7.5

In practice, a change of the [a,b] control parameters represents a new torque law curve. Within a same test, and depending on the environmental conditions, the combination of [a,b] may not vary – see Fig. 6.27a) the instantaneous torque values follow a unique trend, low energetic conditions – and on the opposite can present high variations – see Fig. 6.27b) the instantaneous torque values populate the entire figure. This could be witnessed for example in high energetic conditions when a set of big waves was followed by a set of calm waves, thus proving the ability of the control to adapt to these fast-changing conditions. This shows the versatility of the control and the constant adaptation to wave conditions.
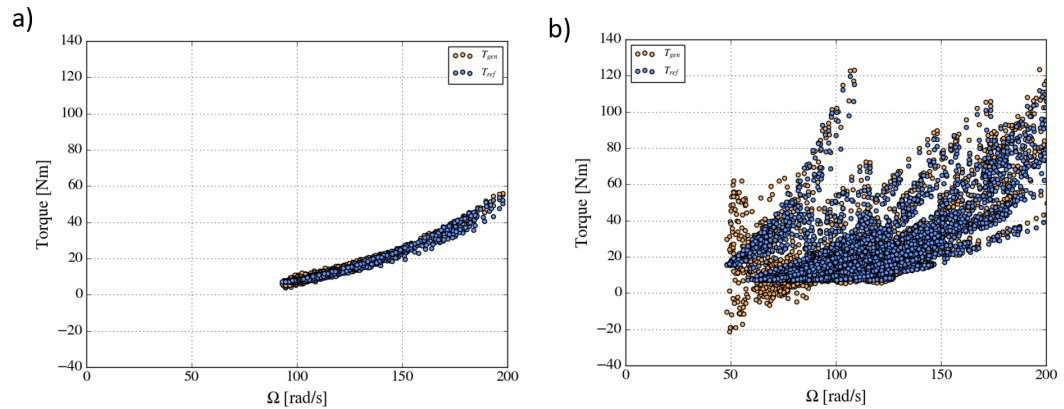
Fig. 6.27: Two cases with different behaviour of the predictive algorithm CL4: a) low energetic SS - b) high energetic SS

6.5.4 Controllers performance results

During the sea trials within the OPERA project, three main control laws were tested including the predictive one CL4. Due to the short testing period, the controllers were not tested sequentially as it was the case in Mutriku. A thorough comparison between all the controllers is therefore not possible. During the testing slot reserved for the predictive algorithm, the buoy was first operating with CL4.1 only, and then alternating between CL4.1 and CL4.2. Hence, there are more results for the first one than for the second. Operational data were collected covering a total of 200 hours of almost

uninterrupted operation combining both versions of CL4. The tests took place during the first weeks of June 2019, which is usually a period of calm sea conditions. The results presented in the following figures consider both the turbine and the generator performance. To respect the confidentiality established in the project consortium, the results are represented normalised and are not associated to any sea condition.

This section presents the PTO performance under the two versions of the predictive controller CL4. As explained earlier, the control strategy is the same and the optimisation algorithms are similar. The difference lies in the implementation techniques of the online optimisation inside the control system. One was executed in the additional control PC - CL4.1, and the other one directly in the PLC - CL4.2.

Focusing on the turbine power performance, a dimensionless analysis is proposed in Figure 6.28, where each point is a 1/2 h test. It considers the average turbine efficiency η_{turb} in function of the rms values of the dimensionless pressure head Ψ (see Eq. (4.28)). This variable is composed of two quantities affecting the controller or depending on it: the chamber pressure which gives an idea of the present sea condition; and the turbine speed - upon which the controlled torque is calculated. Let us recall the performance curve of the biradial turbine of the Figure 4.19 (turbine #6). The instantaneous peak efficiency occurs at $\Psi = 0.4$ and rounds 70% and when $\Psi = 1.0$ the efficiency is 60%. Both algorithms show outstanding results as the average efficiency is just few points below the efficiency curve obtained experimentally by Gato et al. [Gat+17].

Both versions of CL4 present overlapping results which confirms that both implementation techniques are consistent one another. The outer part of the graphic shows probability distributions functions (PDF) of the observed quantities for both controller versions. For example in 6.28, the curves at the top are the PDF of the pressure heads, and those at right side are related to the average turbine efficiencies. Most of the tests fall in the range 54-58% for values of Ψ centered around 1.1, a good score knowing the peak turbine efficiency is 70%. It can be seen that CL4.2 has more events in values of Ψ where the performance is higher. Again, CL4.1 operated alone for most of the time before CL4.2 was added. There is not as much statistical significance for CL4.2 than for CL4.1.
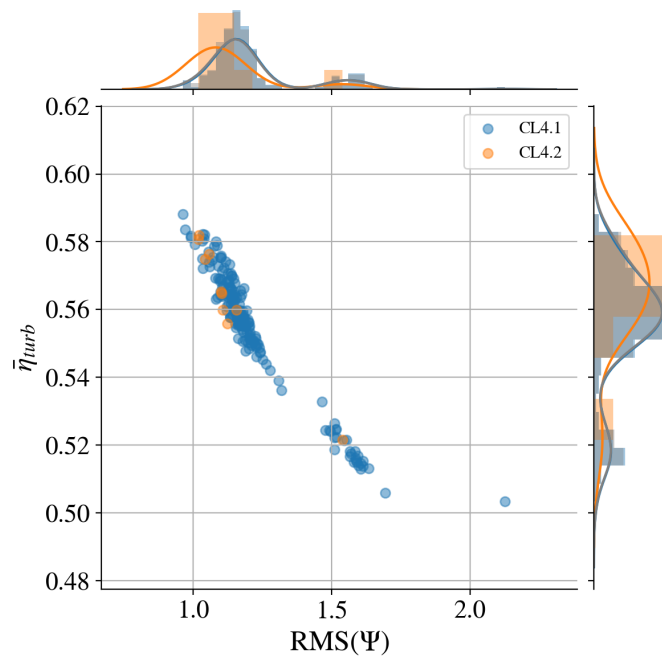
Fig. 6.28: Average turbine efficiency under CL4

The normalised average turbine power is presented in function of the rms value of the internal pressure in Figure 6.29. The PDF of the pressure informs that most of the tests were run in ranges of pressure between 2 and 5 kPa, which corresponds to low and mid-low sea conditions. During the overall test campaign of OPERA, the rms values of pressure could easily reach 9 kPa depending on the control law [Faÿ+18b]. This is why the results show average turbine powers of between 10 to 30% of the nominal turbine power. These performances may seem poor but in fact they depend a lot on the sea states. There were not enough cases to study the controllers in a wider variety of environmental conditions. Still, a linear trend can be seen and allow to extrapolate the results for sea states with higher energy and estimate the previsions for higher rms pressure values. The only test showing 50% of average turbine power would be in line with this trend.

The performance of the generator is now analysed. The average normalised generator efficiency is represented in Fig. 6.30 as a function of its load (the ratio of the generator average power and its nominal value, i.e. the normalised average generator power). The results are interesting in the sense they describe a typical generator efficiency curve, even if we are looking at efficiencies in average here. Most of the cases occur at low generator loads where the average efficiency is obviously reduced. However, at 10% of the load, the average efficiencies fall in the range between 40 and 50%. Again,
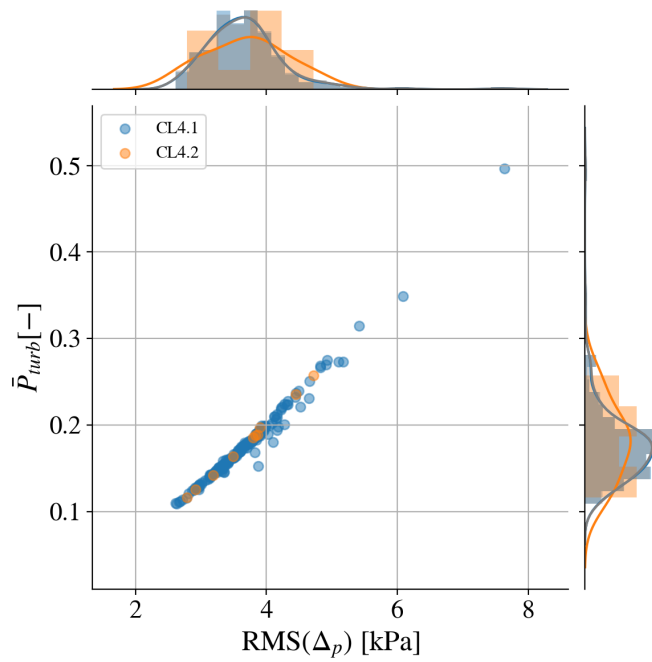
Fig. 6.29: Average turbine power under CL4

the low energetic sea states did not offer a way to explore the full potential of the PTO but still the control algorithms performed well. It is interesting
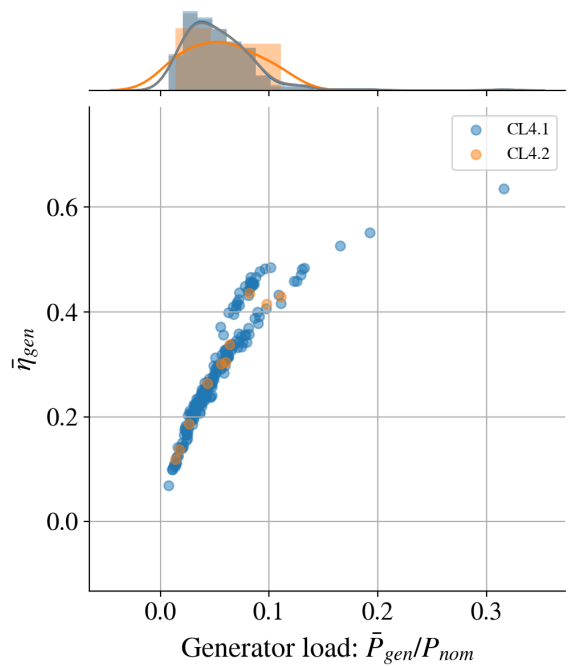
Fig. 6.30: Average generator efficiency under CL4

to see that there are 2 different clusters of points. The first cluster is in the range of generator loads from 0.01 to 0.2, and the another one from

0.05 to 0.1. In that area, the average efficiencies are 5 to 10% higher. The various areas are a consequence of the main characteristic of this predictive controller, that is to adapt the T-Ω curve in function of internal and external conditions. These two operation areas are also visible in Fig. 6.31. In this graphic, the generator average power is represented in function of the rms values of pressure. The generator was operating most of the time in ranges of average powers between 0 to 10%, again these sea trials lacked higher sea states to fully understand the effect of the controllers on the generator performance. Following the main trend, the beginning of an exponential curve can be observed.
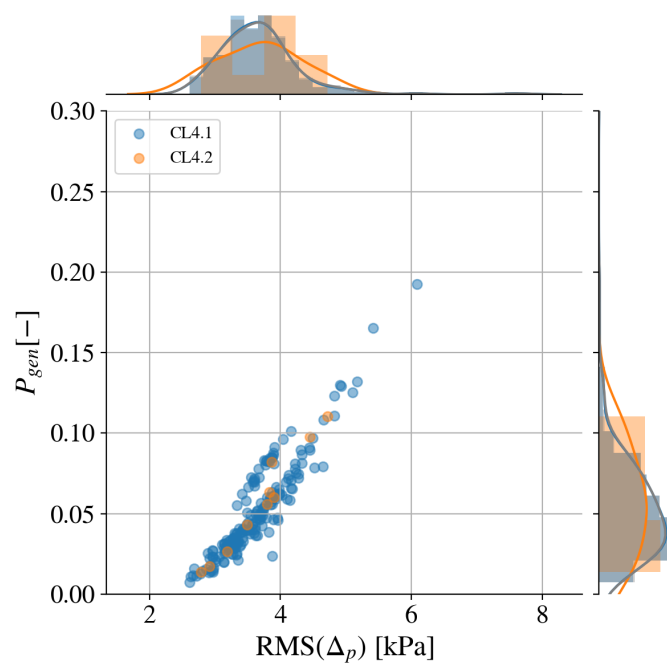
Fig. 6.31: Average generator power under CL4

6.6 Chapter conclusion

This section described the benefits of using an electrical test infrastructure for the development of control strategies and specifically at early stages in the technology development. Such infrastructures are useful to test the electrical components composing the PTO system of the device. The validation of two control strategies to control the rotational speed of the biradial turbine has been conducted. CL2 was a simple torque law whose control parameters were obtained offline, and CL4 was the NL-MPC that parametrises the torque law

online at each replanning period using future wave information. The methodology to adapt the numerical model to rotary test rig has been proposed where the scaling technique employed using Froude principle was detailed. The results of the HIL simulation following the presented methodology for scale tests at the Tecnalia electrical PTO test bench. The HIL testing campaign showed a perfect match between the simulation and experimental data, validating the correct implementation of the two tested control strategies. Results were presented in one conference paper [FX +16] and one journal paper [Faÿ+20b].

Tests in real sea conditions in the Mutriku Wave Power plant were performed for the adaptive controller CL2 and the predictive one CL4, being the first of its kind to be tested in a real environment for an OWC system. The tests lasted 2 weeks in the quiet wave conditions of June 2018. In the 7 sea states experienced during the testing period, the predictive law outran in average electrical power production the other one by 30%. The good performance of this CL offers promising results and could validate the implementation in a real control environment. Future work can be oriented to further investigate and tune the numerical model of Mutriku to better fit realistic conditions. Indeed, the MPC is as good as the numerical model. The implementation into the control framework can be improved by implementing the controller directly into the PLC. Although the predictive controller could only be tested in low energetic sea states, the presented results are encouraging and justify to go on with a deeper analysis during a wider variety of sea states. The experience collected during the sea trials was reported in a journal publication [Faÿ+20b].

The last testing phase under the framework of the OPERA project was to bring the best advanced control strategies tested in Mutriku and apply them to the Marmok-A-5 buoy installed in BiMEP, using the same PTO unit and in larger environmental conditions. The predictive controller could be implemented and tested during the calm sea states of June 2019. In fact two versions were tested, one performing the optimisation algorithm in an external PC linked to the PLC via OPC server, and the other where the optimisation code was written directly in the PLC. Although the test campaign was a success and proved the reliable operation of the controllers, the performance analysis is somehow penalised by the limitations brought by confidentiality concerns and could not be presented as deep as the case in the Mutriku plant. The performance results were satisfactory. Nonetheless, the overall OPERA project

allowed to advance the TRL of this predictive controller from TRL3 to TRL6. Upon what is publicly available and as far as the author knows, it is the first time a predictive controller is applied in wave energy conversion in a WEC operating at sea and being fed with wave elevation measured from an upwave buoy.

Conclusion

7.1 Thesis summary

Wave energy conversion has not yet succeeded in converging into a winning technology and the commercial viability is still questionable. Many challenges have to be addressed by the technology developers to bring to the market devices that are highly efficient and cost effective. Although the wave resource is quite significant worldwide, the sector has to compete with other renewable energy sources that are more mature and that have seen in the past years a significant decrease in their LCOE, like offshore wind for example. Policy makers also have a part to play in accelerating the development of this sector. Some of these challenges were identified at the beginning of this work and became the main focus of this thesis. Its global objective was to improve the knowledge around control strategies for OWC technologies, develop controllers able to increase the energy production while addressing practical implementation issues.

To analyse how would be the energy production, it is necessary to develop trusted W2W models. Among the challenges tackled in this research, let us cite **the lack of accuracy in W2W numerical models** and **the absence of considerations in some critical components**:

- **Hydrodynamics of Mutriku**: The hydrodynamic modelling part of one chamber of the Mutriku OWC plant was developed with close considerations brought by data collected on-site. This is to date the most advanced numerical model of this plant present in the literature.
- **Air chamber model**: The presence of non-linear phenomena makes the modelling part increasingly complex. In this research, the modelling of the air chamber was an important focus. The approach included a polytropic model that could be validated with real data measured at the Mutriku OWC plant.
- **Components of the PTO**: The power conversion equipment is in general not well detailed in the energy conversion chain. The present work included advances in the modelling of an induction generator for

the use in wave energy conversion. This is a specific application for a conventional equipment. Indeed, wave energy can induce sudden power peaks and force these components to operate in regions beyond the nominal values. The model was improved to include overloading operation and the flux weakening region. It is important to know the component limitations, and include appropriate restrictions in the control strategy to assure their reliable operation throughout their useful life.

The W2W models enabled several important areas of this research. This task was fundamental for:

- The **comparison of PTO alternatives** with different configurations of turbines and generators. Six different turbines were analysed including Wells type and impulse type turbines. The outcomes of the analysis led to the proper sizing of the electrical components.
- The **development of advanced control strategies** and analysis of simulation results for several sea states. These must be able to take into account restrictions of the main components that compose the PTO system and customised for a specific device. As a result, several control laws were assessed in simulation first, focusing on aspects like the performance, their effects on component reliability, and the ease for the future implementation in a real control system.
- The **laboratory testing campaign** where a selection of algorithms was validated comparing simulation results with others generated by an emulated part of the model. The verification of the correct implementation of the controllers is crucial before testing them in a device at sea.
- The **sea trials** that took place in the Mutriku OWC plant and the IDOM/OCEANTEC Marmok-A-5 buoy. These offered the possibility to test the variable speed controllers such as a version using a torque law and the predictive controller.

In line with the last point, **the insufficiency of publicly available experience sharing based on sea trials** was another challenge raised in this research. This was covered by the publication and the analysis of results based on operational data collected during field testing campaigns both at the Mutriku plant and the Marmok when installed in BiMEP. These sea trials allowed to test predictive scheme control algorithms in relevant environments, validate their practical implementation, justify the improvement in

the energy production and advance the technology to TRL6. One demonstrated feature of the predictive controllers is the ability to adapt best to the changing conditions of the ocean. In addition, they naturally include the PTO component restrictions. They are versatile in the sense it is possible to customise them to address the two main consideration for controllers: maximise power production or assure the useful life of the components. In fact, a fine tune will make them find the perfect balance between these two.

7.2 Significant contributions

The main contributions of this thesis are derived in three major aspects:

- **Improvements in W2W modelling of OWC systems.**

Because tests were to be performed in the Mutriku plant, an accurate W2W model of one of its air chamber was developed in the time domain. This one considered hydrodynamic parameters affected by its physical environment: the seabed slope in front of the wall plant, and the neighbour chambers. In the meantime, a more precise air chamber model was developed to consider the compressibility of air under a polytropic process. This model was adjusted with pressure levels of real measurements for a series of sea states.

Globally, progress have been brought in modelling PTO systems considering the electrical conversion with a more realistic approach. From one side, the development of a loss model for the generator contributed in assessing the electrical efficiency in a more detailed manner. It included the inclusion of the flux weakening region characterised by a reduction of the electromagnetic torque when the generator operated in regions above nominal values.

The development of an accurate W2W model for the Mutriku plant has proven to be useful for the preliminary assessment and sizing of various PTO components (air turbine and generator). Although all the steps could not be fully validated separately with operational data, a comparison of the main physical quantities (heave displacement, velocity and pressure in the chamber) between real plant measurements and variables provided during the test of the predictive control law offered quite realistic similarities. The full W2W model and the air chamber model were published in **Paper 1** in the *list of Publications* hereinafter.

- **Development and tests in simulation of several advanced control strategies.**

The full W2W model of the Mutriku OWC was used for the design, tuning and assessment of 4 control laws, with sometimes several versions of them, and in a variety of realistic sea states. The biradial turbine design for the H2020 OPERA project associated with its induction generator was selected for this task, having in mind the possibility of testing some controllers in a real environment in the framework of the project. **Paper 1** in the *list of Publications* presented a thorough comparison analysis of the main controllers of this work, including the predictive controller. Also, this one could be benchmarked against other control laws developed for the OPERA project in **Paper 4** and **Paper 5** and presented very interesting features.

CL1 used a fixed drive train speed approach with a reference speed defined for each sea state, and followed by a simple PI controller. It performed best in terms of AEP but had the most demanding operation conditions. This controller would be more likely to cause harmful effects to the components and reduce their useful life. Also, it was the only sea state dependant CL which would raise serious feasibility issues for its implementation in a real control framework. All the other laws were considering a variable speed scheme and thus were considered adaptive controllers.

The various versions of **CL2** were based in torque laws where the curve characterisation allowed to consider either the turbine best efficiency point, the highest mechanical power conversion, and the overall PTO with the turbine and the electrical generator. Depending on the versions, the AEP were very distinct. When considering only the turbine or the mechanical conversion, the power output was not optimal. The benefits of this control law surely came when considering the PTO as a whole in the torque law, with both efficiencies of the mechanical and the electrical conversion components. In terms of reliability, the first two torque laws assured a generator operation below the nominal capacity. However they needed the support of the shut-off valve to dissipate energy, and thus sacrificed part of the production. On the contrary, the third version of CL2 was allowed to overload the generator and thus presented high power peaks, especially in high energetic sea states. The main drawback would be in the end to reduce its service life. The CL2, with its versions, would be the easiest controller to implement in a real system as

it requires solely the rotational speed and applied the associated generator controlled torque.

CL3 was considered a quasi-fixed speed control strategy as it provided a variable reference speed for the PI controller. The reference was calculated using statistical value based on pressure variations. It produced one of the highest AEP but highlighted the drawbacks of presenting the highest power peaks at the generator in the highest sea states. The real implementation of this control law would be more complex than a torque law one, but would only require some additional computation steps and do not represent an overwhelming challenge.

CL4 was based on the torque law approach but with the particularity to change the parameters of the torque law in function of the incoming waves and the plant internal conditions, thanks to a non-linear model predictive control scheme. The online optimisation included both the turbine and the generator performance and restrictions. The AEP was one the highest, but presented the drawbacks of reliability concerns. That is the reason why another version was developed, with the additional feature to include harder constraints to avoid operating the generator in such highly demanding operation regimes. As a result, the AEP was a bit lower, but this more protectionist mode of the predictive controller allowed to obtain better reliability scores. The practical implementation of this control law represented a challenge that was later solved during the tests in the laboratory prior to the field testing campaigns.

Recommendations were given to state on the use of the various control laws. The predictive controller with the additional restrictions would be preferred when applicable (i.e. having a solution for the wave elevation measurement), and otherwise a combination of two control laws could be thought out to benefit from the highest power production in low to medium energetic sea states, and then switch to a more conservative controller in the most energetic ones.

Lately, the **latching control strategy** was applied for the Mutriku plant but was found to be inefficient due to the proper hydrodynamic characteristics of the plant. It was then customised for the W2W model of the sparbuoy. The additional degree of freedom inherent to this type of floating device and its motion response to waves did allowed to assess its performance. The

latching principle was achieved by actuating on the high-speed stop valve of the biradial turbine to block the air flow at the best moment which would create an overpressure able to act on the buoy relative motion and force an artificial resonance condition. The control law for the valve actuation was defined by defining values of 4 pressure thresholds ordering the valve to open or close. These thresholds were optimised by the same non-linear predictive control approach as the one used for the variable speed controller. Simulation results proved the increase in final power production from 5 to 25%, depending on the sea states, in comparison with a case without latching. In both cases, the same simple torque law was employed to the turbine speed in the same conditions for both. It was stated that the practical implementation of this control strategy was even more demanding than CL4 as it would need a perfect synchronisation of the valve actuation, which is difficult to achieve in a real environment. The predictive controller based on a pressure threshold latching strategy was assessed with simulation results in **Paper 3** present in the *Publications list* here below.

- Contribution to practical implementation of control algorithms

Prior to any implementation at sea, the control laws had to be validated in a dry test rig at a reduced scale using a HIL approach. This was a required step to assure the controllers were behaving as expected and reduce the risks associated with badly evaluated assumptions in the simulation phase. Two controllers - the torque law one CL2 and the predictive controller CL4 - were successfully tested in the lab and the issues related to the predictive algorithm were solved by running the online optimisation in an additional computer and transmitting the control parameters to the PLC which in the end applied the updated torque law. The synchronisation between both was assured by an OPC server. The methodology presented to validate the controllers in a HIL test rig has been developed throughout various works that are compiled in *the list of Publications* by **Paper 2**, **Paper 7**, **Paper 8** and **Paper 9**.

Both controllers were then tested in the Mutriku OWC plant for two weeks in the calm weather of June 2018. The estimation of the future wave force was made possible by a wirely connected pressure sensor measuring the wave elevation 200 m ahead of the plant. Although there were not a wide variety of sea states, the controllers performed as they should. Operational data were collected, processed and the results analysed both considering performance (PTO efficiencies and power production) and reliability issues (peaks of power

and standard deviation of powers). An improvement in the power production in the range of 13 to 65% was observed for the predictive controller with respect to the other one. In average, combining the occurrence of the sea states, the predictive algorithm outperformed the other law by 32%. Mainly it was found that the simple torque law provided a higher turbine efficiency and the MPC a higher generator efficiency. These results were quite encouraging for the innovative predictive controller but had to be contrasted by the fact that the PTO was producing at low regimes, where the losses are the highest. In addition, there is a large dispersion of results within the same sea state due to the proper characterisation of the sea states (H_s and T_e). The analysis could have gone deeper taking into account the tide level affecting the device response or also the wave propagation direction that also affects the plant reaction. These results are gathered in **Paper 1** from *the list of Publications*.

The last phase of the OPERA project led to the testing at sea of several control algorithms. They were implemented in the control framework of the Marmok-A-5 buoy of Oceantec/IDOM moored in BiMEP. The same PTO as the one tested in the Mutriku plant was installed in the buoy. The predictive control law could be tested in the last two weeks of the testing campaign between May and June 2019. In the area where the buoy was installed, a measurement buoy situated upwave was configured to send real-time wave elevation measurements to the control system on shore. That way, the estimated wave force could be known in advance and fed the predictive algorithm. Two implementation techniques were tested, one with the additional control PC performing the online optimisation and the other one where all the code was written in the PLC. Convergence tests of the control parameters were successfully done in several occasions to test the robustness of the controllers. Apart from validating their reliable operation, the performance results were satisfactory. The analysis of production results could not go as deep as in the trials at Mutriku because of IP issues. Still, the non linear predictive controller was the first of its kind to be tested in a real environment and could advance from TRL3 to TRL6.

7.3 Publications

In the following list are gathered the journal and conference publications related to the thesis and sorted by the main contributions.

Improvements in W2W modelling of OWC systems

- Paper 1 - **F.-X. Faÿ**, E. Robles, M. Marcos, E. Aldaiturriaga, and E. F. Camacho, 'Sea trial results of a predictive algorithm at the Mutriku Wave power plant and controllers assessment based on a detailed plant model', Renewable Energy, vol. 146, pp. 1725-1745, feb. 2020.

- Paper 2 - J.C. Henriques, L.M.C. Gato, A.F.O. Falcão, E. Robles, and **F.-X. Faÿ**, 'Latching control of a floating oscillating-water-column wave energy converter', Renewable Energy, vol. 90, pp. 229-241. 2016.

- Paper 3 - **F.-X. Faÿ**, M. Marcos, and E. Robles, 'Novel Predictive Latching Control for an Oscillating Water Column Buoy', presented at the 12th EWTEC, Cork, Ireland, 2017.

- Paper 4 - **F.-X. Faÿ**, J. Kelly, J. Henriques, A. Pujana, M. Abusara, M. Mueller, I. Touzon, and P. Ruiz-Minguela, 'Numerical Simulation of Control Strategies at Mutriku Wave Power Plant', presented at the ASME 37th International Conference on Ocean, Offshore and Arctic Engineering, Madrid, Spain, 2018.

- Paper 5 - **F.-X. Faÿ**, J.C. Henriques, J. Kelly, M. Mueller, M. Abusara, W. Sheng, and M. Marcos, 'Comparative assessment of control strategies for the biradial turbine in the Mutriku OWC plant', Renewable Energy, vol. 146, pp. 2766-2784, feb. 2020.

Development and tests of several advanced control strategies

- Paper 1 - **F.-X. Faÿ**, E. Robles, M. Marcos, E. Aldaiturriaga, and E. F. Camacho, 'Sea trial results of a predictive algorithm at the Mutriku Wave power plant and controllers assessment based on a detailed plant model', Renewable Energy, vol. 146, pp. 1725-1745, feb. 2020.

- Paper 2 - J.C. Henriques, L.M.C. Gato, A.F.O. Falcão, E. Robles, and **F.-X. Faÿ**, 'Latching control of a floating oscillating-water-column wave energy converter', Renewable Energy, vol. 90, pp. 229-241. 2016.

- Paper 3 - **F.-X. Faÿ**, M. Marcos, and E. Robles, 'Novel Predictive Latching Control for an Oscillating Water Column Buoy', presented at the 12th EWTEC, Cork, Ireland, 2017.

- Paper 4 - **F.-X. Faÿ**, J. Kelly, J. Henriques, A. Pujana, M. Abusara, M. Mueller, I. Touzon, and P. Ruiz-Minguela, 'Numerical Simulation of Control Strategies at Mutriku Wave Power Plant', presented at the ASME 37th International Conference on Ocean, Offshore and Arctic Engineering, Madrid, Spain, 2018.

- Paper 5 - **F.-X. Faÿ**, J.C. Henriques, J. Kelly, M. Mueller, M. Abusara, W. Sheng, and M. Marcos, 'Comparative assessment of control strategies for the biradial turbine in the Mutriku OWC plant', Renewable Energy, vol. 146, pp. 2766-2784, feb. 2020.

- Paper 6 - **F.-X. Faÿ**, J.C. Henriques, M. Marcos and E. Robles, 'Review of control strategies for oscillating water column wave energy converters', presented at the EWTEC2015, Nantes, France, 2015.

Contribution to practical implementation of control algorithms

- Paper 1 - **F.-X. Faÿ**, E. Robles, M. Marcos, E. Aldaiturriaga, and E. F. Camacho, 'Sea trial results of a predictive algorithm at the Mutriku Wave power plant and controllers assessment based on a detailed plant model', Renewable Energy, vol. 146, pp. 1725-1745, feb. 2020.

- Paper 2 - J.C. Henriques, L.M.C. Gato, A.F.O. Falcão, E. Robles, and **F.-X. Faÿ**, 'Latching control of a floating oscillating-water-column wave energy converter', Renewable Energy, vol. 90, pp. 229-241. 2016.

- Paper 7 - **F.-X. Faÿ**, E. Robles, J.C. Henriques, and M. Marcos, 'Best practices for the use of electrical test infrastructures to validate control strategies: a case study in wave energy conversion', presented at the Renew 2016 2nd International Conference on Renewable Energies Offshore, Lisbon, Portugal, 2016.

- Paper 8 - S. Armstrong, J. Rea, **F.-X. Faÿ**, and E. Robles, 'Lessons learned using electrical research test infrastructures to address the electrical

challenges faced by ocean energy developers', International Journal of Marine Energy, vol. 12, pp. 46–62, Dec. 2015.

- Paper 9 - N. Delmonte, E. Robles, P. Cova, F. Giuliani, **F.-X. Faÿ**, J. Lopez, P. Ruol, and L. Martinelli, 'An Iterative Refining Approach to Design the Control of Wave Energy Converters with Numerical Modeling and Scaled HIL Testing', Energies, vol. 13, n.º 10, p. 2508, May 2020.

7.4 Future works

This thesis covered a wide spectrum related to the development of control algorithms for OWC systems and the improvement of W2W time domain models accuracy. There are several aspects which could have been studied more thoroughly but were left apart, mainly due to time constraints imposed by the OPERA project and the impossibility to extend the testing period on site. The Mutriku W2W model, for example, could only be partially validated. The non-linearities introduced by the biradial turbine during its operation made it very difficult to accurately adjust the model. To complete the analysis, more tests were required, in the margins of the planned tests, using a Wells turbine controlled in fixed speed and during a wide variety of sea states. This is the equivalent to having a linear PTO damping and directly derive an accurate PTO force. Also with the installation of a humidity and temperature sensor inside the air chamber, the changes in the air density could have been captured and considered in the air compressibility model. Another aspect which could have strengthened the present work would have been to test the predictive controller in a larger diversity of sea states in Mutriku and in BiMEP. Indeed, the additional restrictions to avoid over-stressing the generator could not be tested on site. The sea conditions were simply too low during the field testing and the generator was rarely operating at nominal power. These two aspects had to be left for future tests if the opportunity shows itself, and center on the objectives previously established.

During the numerical simulation phases, the pros and cons of the fixed and variable speed control strategies were proposed. In the fixed speed approach, the production output is better but the power peaks are such that is can be risky for the components and reduce the quality of power injected to the grid. An analysis of energy storage systems installed at different stages of the energy conversion could be an attractive line of work for future

research. The present work focused on one device. However, when there is a high penetration of highly fluctuating energy, like in wave farms of multi-MW scale, the peaks of power can really generate negative impacts on power quality aspects, especially on weak electrical grids. With this approach, several power smoothing techniques can be thought out: from optimal spatial placement of the devices of the farm, to the use of variable inertia flywheels in the drive train of the PTO, or even storing electrical energy in batteries or supercapacitors. In this case, a cost versus benefits of an energy storage system will have to be drawn up. The wave energy technology is already suffering the slow decrease in LCOE, and adding expensive technologies can further delay its commercial deployment.

Another interesting approach for future works could be to use all the operational data and outputs of the predictive controller to train a control strategy that has learning capabilities. This one would be able to apply different combinations of torque law parameters in function of measurable data directly at the device (a Fuzzy Controller type or one based on some kind of Artificial Neural Networks). That way the uncertainties in the wave measurements or the estimation of future excitation forces would not be an issue.

The objective of the thesis was to improve the energy production with the development of advanced control algorithms. As a consequence, the LCOE is expected to decrease, motivated by the increase of income generated by the sale of the extra energy. On the other side, when components are operating above their rated capacity, they are expected to suffer higher failure rates and a reduction of their operation duration. The impact on the OPEX was mentioned but in any case was quantified. A future research focus can cover this gap by including a global LCOE reduction on the controller's objective function, capable of optimally computing the trade-off between maximising the energy production and extend the components service life.

References

[ABB04]   ABB. "ABB Catalogue: Low Voltage General Purpose Motors".
             2004. URL: https://library.e.abb.com/public/367c91cdc
             1dee017c1257b130057111e/Catalogue%20GenPurpMotors_GB_
             12_2004%20RevA.pdf (visited on Aug. 15, 2015) (cit. on pp. 93,
             94, 134).

[Alb+11a]   M. Alberdi, M. Amundarain, A. J. Garrido, I. Garrido, and F. J.
             Sainz. „Control for voltage dips Ride-Through of Oscillating
             Water Column-based wave power generation plant equipped
             with Doubly-Fed Induction Generator". In: Control & Automation
             (MED), 2011 19th Mediterranean Conference on. IEEE, 2011,
             pp. 371–377 (cit. on p. 55).

[Alb+11b]   M. Alberdi, M. Amundarain, A. J. Garrido, et al. „Complementary
             Control of Oscillating Water Column Based Wave Energy Conver-
             sion Plants to Improve the Instantaneous Power Output". In: *IEEE
             Transactions on Energy Conversion* 26.4 (Dec. 2011), pp. 1021–
             1032. ISSN: 0885-8969. DOI: 10.1109/TEC.2011.2167332 (cit.
             on pp. 55, 67).

[Alb+11c]   Mikel Alberdi, Modesto Amundarain, Aitor J. Garrido, Izaskun
             Garrido, and Francisco Javier Maseda. „Fault-Ride-Through
             Capability of Oscillating-Water-Column-Based Wave-Power-
             Generation Plants Equipped With Doubly Fed Induction Gener-
             ator and Airflow Control". In: *IEEE Transactions on Industrial
             Electronics* 58.5 (May 2011), pp. 1501–1517. ISSN: 0278-0046,
             1557-9948. DOI: 10.1109/TIE.2010.2090831 (cit. on pp. 55,
             69).

[Alb+12a]   Mikel Alberdi, Modesto Amundarain, Aitor J. Garrido, Izaskun
             Garrido, and Francisco Javier Sainz. „Control of Oscillating Water
             Column-based wave power generation plants for grid connec-
             tion". In: *Control & Automation (MED), 2012 20th Mediterranean
             Conference on*. IEEE, 2012, pp. 1485–1490 (cit. on p. 67).

[Alb+12b] Mikel Alberdi, Modesto Amundarain, Aitor Garrido, and Iza-skun Garrido. „Neural control for voltage dips ride-through of oscillating water column-based wave energy converter equipped with doubly-fed induction generator". en. In: *Renewable Energy* 48 (Dec. 2012), pp. 16–26. ISSN: 09601481. DOI: 10.1016/j.renene.2012.04.014 (cit. on p. 55).

[Alv+11] Marco Alves, Antonio Sarmento, Miguel Vicente, and Mathieu Guerinel. „Implementation and Verification of a Time Domain Model to Simulate the Dynamics of OWCs". en. In: 9th European Wave and Tidal Energy Conference (EWTEC). 2011, p. 10 (cit. on pp. 53, 72).

[Amu+10a]M. Amundarain, M. Alberdi, A. J. Garrido, and I. Garrido. „Control strategies for OWC wave power plants". In: *American Control Conference (ACC), 2010*. IEEE, 2010, pp. 4319–4324 (cit. on pp. 55, 67).

[Amu+10b]Modesto Amundarain, Mikel Alberdi, Aitor J. Garrido, Izaskun Garrido, and Javier Maseda. „Wave energy plants: Control strategies for avoiding the stalling behaviour in the Wells turbine". en. In: *Renewable Energy* 35.12 (Dec. 2010), pp. 2639–2648. ISSN: 09601481. DOI: 10.1016/j.renene.2010.04.009 (cit. on p. 55).

[Amu+11] Modesto Amundarain, Mikel Alberdi, Aitor J Garrido, and Iza-skun Garrido. „Modeling and Simulation of Wave Energy Generation Plants: Output Power Control". In: *IEEE Transactions on Industrial Electronics* 58.1 (Jan. 2011), pp. 105–117. ISSN: 0278-0046, 1557-9948. DOI: 10.1109/TIE.2010.2047827 (cit. on p. 67).

[ANS19] ANSYS. *AQWA - Hydrodynamics Simulation and Diffraction Analysis*. 2019. URL: https://www.ansys.com/products/structures/ansys-aqwa (visited on Dec. 12, 2019) (cit. on p. 49).

[Aqu12] AquaRET. *AquaRET text book - Chapter 4: Wave Energy*. Tech. rep. AQUARET, 2012, pp. 141–207 (cit. on pp. 25, 26).

[Arb12] Alain Arbouet. "Le bélier siphon maritime à chambre barométrique de Biarritz dans les années 30 : idée géniale ou chimère ?" 2012. URL: http://alainarb2.pagesperso-orange.fr/Conference_2012/conference2012texteb.htm (visited on Feb. 1, 2017) (cit. on p. 16).

[Are+18] Felice Arena, Alessandra Romolo, Giovanni Malara, Vincenzo Fiamma, and Valentina Laface. „Response of the U-OWC Prototype Installed in the Civitavecchia Harbour". en. In: Volume 10: Ocean Renewable Energy. Madrid, Spain: ASME, June 2018, V010T09A034. ISBN: 978-0-7918-5131-9. DOI: 10.1115/OMAE2018-78762 (cit. on p. 33).

[Arm+15] S. Armstrong, J. Rea, F.-X. Faÿ, and E. Robles. „Lessons learned using electrical research test infrastructures to address the electrical challenges faced by ocean energy developers". en. In: *International Journal of Marine Energy* 12 (Dec. 2015), pp. 46–62. ISSN: 22141669. DOI: 10.1016/j.ijome.2015.08.004 (cit. on p. 149).

[Bab15] A. Babarit. „A database of capture width ratio of wave energy converters". en. In: *Renewable Energy* 80 (Aug. 2015), pp. 610–628. ISSN: 09601481. DOI: 10.1016/j.renene.2015.02.049 (cit. on pp. 2, 25).

[BC06] A. Babarit and A.H. Clément. „Optimal latching control of a wave energy device in regular and irregular waves". en. In: *Applied Ocean Research* 28.2 (Apr. 2006), pp. 77–91. ISSN: 01411187. DOI: 10.1016/j.apor.2006.05.002 (cit. on p. 60).

[Ber18] Joannès Berque. *OPERA - DS Wave Mutriku: Wave resource at Mutriku (Spain)*. 2018. DOI: 10.5281/zenodo.1478564 (cit. on p. 108).

[BF77] K. Budal and J. Falnes. „A resonant point absorber of ocean-wave power". In: *Nature* 256.5517 (1977), pp. 478–479. DOI: 10.1038/256478a0 (cit. on pp. 48, 59).

[BiM19] BiMEP. *Biscaye Marine Energy Platform*. 2019. URL: https://bimep.com/ (visited on Nov. 12, 2019) (cit. on p. 4).

[Bla+12] Anne Blavette, Dara L. O'Sullivan, Antony W. Lewis, and Michael G. Egan. „Impact of a wave farm on its local grid: Voltage limits, flicker level and power fluctuations". In: *OCEANS, 2012-Yeosu*. IEEE, 2012, pp. 1–9 (cit. on p. 68).

[Boa+02] Cuan B. Boake, Trevor J. T. Whittaker, Matt Folley, and Hamish Ellen. „Overview and Initial Operational Experience of the LIMPET Wave Energy Plant". en. In: The Twelfth (2002) International Offshore and Polar Engineering Conference. Kitakyushu, Japan, May 2002, p. 9 (cit. on p. 33).

[Bol03]   M.H.J. Bollen. „What is power quality?" en. In: *Electric Power Systems Research* 66.1 (July 2003), pp. 5–14. ISSN: 03787796. DOI: 10.1016/S0378-7796(03)00067-1 (cit. on p. 68).

[BRB16]   Helen Bailey, Bryson R.D. Robertson, and Bradley J. Buckham. „Wave-to-wire simulation of a floating oscillating water column wave energy converter". en. In: *Ocean Engineering* 125 (2016), pp. 248–260. ISSN: 00298018. DOI: 10.1016/j.oceaneng.2016.08.017 (cit. on p. 54).

[Bri+01]   A. Brito-Melo, T. Hofmann, A. H. Clément, and G. Delhommeau. „Numerical Modelling of OWC Shoreline Devices Including the Effect of Surrounding Coastline and Non flat Bottom". In: *International Journal of Offshore and Polar Engineering* (2001) (cit. on pp. 32, 33, 53, 73, 74).

[Bro03]   John Brooke. *Wave Energy Conversion*. R. Bhattacharyya, M.E. McCormick. Elsevier Ocean Engineering Series, 2003. ISBN: 978-0-08-044212-9 (cit. on pp. 18, 33).

[BT17]   Joannès Berque and Iñaki Txarterina. *DS_Wave_Mutriku: Wave resource at Mutriku (Spain)*. July 2017. DOI: 10.5281/zenodo.832847 (cit. on p. 163).

[Bud82]   Budal K, Falnes J, Iversen LC, Lillebekken P, Oltedal G, Hals T, Onshus T,Hoy A. „The Norwegian wave-power buoy project". In: The Second International Symposium on Wave Energy Utilization. Trondheim, 1982, pp. 323–344 (cit. on p. 48).

[Cas10]   David P. Cashman. „Electrical machine characterisation and analysis for renewable energy applications". PhD thesis. University College Cork, 2010 (cit. on p. 33).

[Cat20]   ORE Catapult. *Powertrain facilities*. 2020. URL: https://ore.catapult.org.uk/testing-validation/facilities/powertrains/ (visited on Apr. 21, 2020) (cit. on p. 149).

[Cav+16]   Robert J. Cavagnaro, Jason C. Neely, François-Xavier Faÿ, Joseba Lopez Mendia, and Judith A. Rea. „Evaluation of Electromechanical Systems Dynamically Emulating a Candidate Hydrokinetic Turbine". en. In: *IEEE Transactions on Sustainable Energy* 7.1 (Jan. 2016), pp. 390–399. ISSN: 1949-3029, 1949-3037. DOI: 10.1109/TSTE.2015.2492943 (cit. on p. 149).

[Ceb+13]   Salvador Ceballos, Judy Rea, Iraide Lopez, et al. „Efficiency Optimization in Low Inertia Wells Turbine-Oscillating Water Column Devices". In: *IEEE Transactions on Energy Conversion* 28.3 (Sept. 2013), pp. 553–564. ISSN: 0885-8969, 1558-0059. DOI: 10.1109/TEC.2013.2265172 (cit. on pp. 55, 66, 67, 103, 112).

[Ceb+15]   Salvador Ceballos, Judy Rea, Eider Robles, et al. „Control strategies for combining local energy storage with wells turbine oscillating water column devices". en. In: *Renewable Energy* 83 (Nov. 2015), pp. 1097–1109. ISSN: 09601481. DOI: 10.1016/j.renene.2015.05.030 (cit. on pp. 55, 67).

[COR11]   CORES. *Final Publishable Summary Report*. Tech. rep. 2011 (cit. on pp. 28, 67, 103, 154).

[Cre+11]   Julien Cretel, Anthony W. Lewis, Gareth P. Thomas, and Gordon Lightbody. „A Critical Assessment of Latching as Control Strategy for Wave-Energy Point Absorbers". In: *Twenty-first International Offshore and Polar Engineering Conference*. Maui, Hawaii, USA, 2011, pp. 680–686. ISBN: 978-1-880653-96-8 (cit. on p. 64).

[Cre10]   Julien AM Cretel. *Control of a wave- energy point absorber: an approach based on model predictive control*. Oct. 2010. URL: http://www.eeng.nuim.ie/coer/doc/EV001_20101021_J_Cretel_presentation_NUIM_workshop.pdf (visited on July 22, 2014) (cit. on p. 61).

[CWS98]   R. Curran, T. J. T. Whittaker, and T. P. Stewart. „Aerodynamic conversion of ocean power from wave to wire". In: *Energy conversion and management* 39.16 (1998), pp. 1919–1929 (cit. on p. 52).

[DCC01]   Gaelle Duclos, Alain H. Clément, and Gontran Chatry. „Absorption of Outgoing Waves In a Numerical Wave Tank Using a Self-Adaptive Boundary Condition". In: *International Journal of Offshore and Polar Engineering* 11.3 (2001). ISSN: 1053-5381 (cit. on pp. 50, 76).

[Del+15]   Nicola Delmonte, Davide Barater, Francesco Giuliani, Paolo Cova, and Giampaolo Buticchi. „Review of Oscillating Water Column Converters". In: *IEEE Transactions on Industry Applications* (2015), pp. 1–1. ISSN: 0093-9994, 1939-9367. DOI: 10.1109/TIA.2015.2490629 (cit. on pp. 31, 52, 61).

[DH14]   S.L. Dixon and C.A. Hall. In: *Fluid Mechanics and Thermody-namics of Turbomachinery (Seventh Edition)*. Ed. by S.L. Dixon and C.A. Hall. Seventh Edition. Boston: Butterworth-Heinemann, 2014, pp. 1–37. ISBN: 978-0-12-415954-9. DOI: https://doi.org/10.1016/B978-0-12-415954-9.00001-2 (cit. on p. 86).

[DNV07]   DNV. *Recommended Practice DNV-RP-C205: Environmental Conditions and Environmental Loads*. Tech. rep. 2007 (cit. on pp. 20, 108, 119, 171).

[DPS09]   B. Drew, A. R. Plummer, and M. N. Sahinkaya. „A review of wave energy converter technology". en. In: *Proceedings of the Institution of Mechanical Engineers, Part A: Journal of Power and Energy* 223.8 (Dec. 2009), pp. 887–902. ISSN: 0957-6509, 2041-2967. DOI: 10.1243/09576509JPE782 (cit. on p. 25).

[DR19]   Donagh Cagney and Remi Gruet. *ETIP Ocean (2019), Powering Homes Today, Powering Nations Tomorrow*. Tech. rep. 2019 (cit. on p. 2).

[Dra14]   Wave Dragon. "The Wave Dragon Technology". 2014. URL: http://www.wavedragon.net/ (visited on Feb. 1, 2017) (cit. on p. 28).

[Dre15]   Dresser-Rand. *Brochure_HydroAir.pdf*. 2015. URL: https://www.all-energy.co.uk/__novadocuments/355054?v=636288145775300000 (visited on Sept. 15, 2017) (cit. on pp. 39, 40).

[Eva82]   D. V. Evans. „Wave-power absorption by systems of oscillating surface pressure distributions". In: *Journal of Fluid Mechanics* 114 (1982), pp. 481–499. DOI: 10.1017/S0022112082000263 (cit. on p. 73).

[Fal+14]   António F.O. Falcão, João C.C. Henriques, Luís M.C. Gato, and Rui P.F. Gomes. „Air turbine choice and optimization for floating oscillating-water-column wave energy converter". en. In: *Ocean Engineering* 75 (Jan. 2014), pp. 148–156. ISSN: 00298018. DOI: 10.1016/j.oceaneng.2013.10.019 (cit. on p. 54).

[Fal+19]   A.F.O. Falcão, L.M.C. Gato, A.J.N.A. Sarmento, and A. Brito-Melo. „The Pico OWC wave power plant: Its life from conception to closure 1986-2018". en. In: Proceedings of the 3rd International Conference on Renewable Energies Offshore (RENEW 2018). Lisbon, Portugal: Advances in Renewable Energies Offshore , Guedes Soares (Ed.), 2019, p. 9 (cit. on pp. 32, 33, 37).

[Fal00]   A.F.O. Falcão. „The shoreline OWC wave power plant at the Azores". In: *Fourth European Wave Energy Conference, Aalborg, Denmark, Dec*. 2000, pp. 4–6 (cit. on pp. 28, 52, 66).

[Fal02a]   A.F.O. Falcão. „Control of an oscillating water column wave power plant for maximum energy production". In: *Applied Ocean Research* 24 (2002), pp. 73–82 (cit. on pp. 66, 103, 113).

[Fal02b]   Johannes Falnes. *Ocean waves and oscillating systems*. Cambridge University Press, 2002 (cit. on pp. 48, 144).

[Fal07]   Johannes Falnes. „A review of wave-energy extraction". en. In: *Marine Structures* 20.4 (Oct. 2007), pp. 185–201. ISSN: 09518339. DOI: 10.1016/j.marstruc.2007.09.001 (cit. on pp. 2, 25).

[Fal08]   António F. de O. Falcão. „Phase control through load control of oscillating-body wave energy converters with hydraulic PTO system". en. In: *Ocean Engineering* 35.3-4 (Mar. 2008), pp. 358–366. ISSN: 00298018. DOI: 10.1016/j.oceaneng.2007.10.005 (cit. on p. 64).

[Fal10]   A.F.O. Falcão. „Wave energy utilization: A review of the technologies". In: *Renewable and sustainable energy reviews* 14.3 (2010), pp. 899–918 (cit. on pp. 2, 25, 29, 32, 37).

[Faÿ+18a]   François-Xavier Faÿ, James Kelly, João Henriques, et al. „Numerical Simulation of Control Strategies at Mutriku Wave Power Plant". en. In: *ASME 2018 37th International Conference on Ocean, Offshore and Arctic Engineering*. Madrid, Spain, 2018, p. 11 (cit. on p. 139).

[Faÿ+18b]   F.-X. Faÿ, A. Pujana, P. Ruiz-Minguela, et al. *OPERA D4.2 - Shoreline OWC wave power plant control algorithms*. 2018 (cit. on pp. 108, 179).

[Faÿ+20a]   François-Xavier Faÿ, João C. Henriques, James Kelly, et al. „Comparative assessment of control strategies for the biradial turbine in the Mutriku OWC plant". en. In: *Renewable Energy* 146 (Feb. 2020), pp. 2766–2784. ISSN: 09601481. DOI: 10.1016/j.renene.2019.08.074 (cit. on p. 139).

[Faÿ+20b]   François-Xavier Faÿ, Eider Robles, Marga Marcos, Endika Aldaiturriaga, and Eduardo F. Camacho. „Sea trial results of a predictive algorithm at the Mutriku Wave power plant and controllers assessment based on a detailed plant model". en. In: *Renewable Energy* 146 (Feb. 2020), pp. 1725–1745. ISSN: 09601481. DOI: 10.1016/j.renene.2019.07.129 (cit. on pp. 100, 139, 182).

[FB78]   J. Falnes and K. Budal. „Wave-power absorption by point absorbers". In: *Norwegian Maritime Research* 6.4 (1978), p. 211 (cit. on p. 60).

[FG12]   Antonio Falcao and L.M.C Gato. „Air Turbines". In: *Comprehensive Renewable Energy* Ch. 8.05 (Dec. 2012), pp. 111–149. DOI: 10. 1016/B978-0-08-087872-0.00805-2 (cit. on pp. 33, 37, 56).

[FGN13]   A.F.O. Falcão, L.M.C. Gato, and E.P.A.S. Nunes. „A novel radial self-rectifying air turbine for use in wave energy converters". en. In: *Renewable Energy* 50 (Feb. 2013), pp. 289–298. ISSN: 09601481. DOI: 10.1016/j.renene.2012.06.050 (cit. on p. 39).

[FH14]   António F.O. Falcão and João C.C. Henriques. „Model-prototype similarity of oscillating-water-column wave energy converters". en. In: *International Journal of Marine Energy* 6 (June 2014), pp. 18–34. ISSN: 22141669. DOI: 10.1016/j.ijome.2014.05. 002 (cit. on p. 152).

[FH16]   A.F.O. Falcão and J.C.C. Henriques. „Oscillating-water-column wave energy converters and air turbines: A review". en. In: *Renewable Energy* 85 (Jan. 2016), pp. 1391–1424. ISSN: 09601481. DOI: 10.1016/j.renene.2015.07.086 (cit. on pp. 15, 31, 33, 56).

[FH18]   A.F.O. Falcão and J.C.C. Henriques. „The Spring-Like Air Compressibility Effect in OWC Wave Energy Converters: Hydro-, Thermo- and Aerodynamic Analyses". In: *Proceedings of the ASME 37th International Conference on Ocean, Offshore and Arctic Engineering (OMAE2018)*. OMAE2018 Conference on Ocean, Offshore and Arctic Engineering. Madrid, Spain, 2018 (cit. on p. 84).

[FHG18]   António F.O. Falcão, João C.C. Henriques, and Luís M.C. Gato. „Self-rectifying air turbines for wave energy conversion: A comparative analysis". en. In: *Renewable and Sustainable Energy Reviews* 91 (Aug. 2018), pp. 1231–1241. ISSN: 13640321. DOI: 10.1016/j.rser.2018.04.019 (cit. on pp. 38, 56–58, 96, 97).

[Fin04]   Timothy Finnigan. „Development of a 300 kW ocean wave energy demonstration plant". In: *Proceedings of Pacific 2004 International Maritime Conference. Sydney*. 2004, pp. 187–196 (cit. on p. 33).

[Fis+16] Boris Fischer, Christian Mehler, Adam Zuga, and Martin Shan. „Control design for mechanical hardware-in-the-loop operation of dynamometers for testing full-scale drive trains". In: *Wind Energy* 19.10 (2016), pp. 1889–1901. DOI: `10.1002/we.1957`. eprint: `https://onlinelibrary.wiley.com/doi/pdf/10.1002/we.1957` (cit. on p. 149).

[FJ99] A.F.O. Falcão and P.A.P. Justino. „OWC wave energy devices with air flow control". In: *Ocean Engineering* 26.12 (1999), pp. 1275–1295 (cit. on pp. 52, 63, 86).

[FMR17] François-Xavier Faÿ, Marga Marcos, and Eider Robles. „Novel Predictive Latching Control for an Oscillating Water Column Buoy". In: EWTEC. Cork, Ireland, 2017 (cit. on p. 139).

[FR02] A.F.de O Falcão and R.J.A Rodrigues. „Stochastic modelling of OWC wave power plant performance". In: *Applied Ocean Research* 24.2 (2002), pp. 59–71. ISSN: 0141-1187. DOI: `https://doi.org/10.1016/S0141-1187(02)00022-6` (cit. on pp. 63, 92).

[FR10] Francesco Fusco and John V. Ringwood. „Short-term wave forecasting with AR models in real-time optimal control of wave energy converters". In: *Industrial Electronics (ISIE), 2010 IEEE International Symposium on*. IEEE, 2010, pp. 2475–2480 (cit. on p. 143).

[Fre79] M. J. French. „A generalized view of resonant energy transfer". In: *Journal Mechanical Engineering Science* 21.4 (1979) (cit. on pp. 48, 60).

[Fro68] William Froude. „Observations and suggestions on the subject of determining by experiment the resistance of ships". In: *Correspondence with the Admiralty, Chelston Cross, December* (1868), pp. 120–128 (cit. on p. 151).

[FX +15] F.-X. Faÿ, J.C.H. Henriques, M. Marcos, and E. Robles. „Review of control strategies for oscillating water column wave energy converters". In: Proceedings of the 11th European Wave and Tidal Energy Conference (EWTEC). Nantes, France, Sept. 2015 (cit. on p. 69).

[FX +16]   F.-X. Faÿ, E. Robles, J.C.C. Henriques, and M. Marcos. „Best practices for the use of electrical test infrastructures to validate control strategies: a case study in wave energy conversion". In: Proceedings of the 2nd International Conference on Renewable Energies Offshore (RENEW 2016). Lisbon, Portugal: Advances in Renewable Energies Offshore , Guedes Soares (Ed.), Oct. 2016 (cit. on p. 182).

[Gar+13]   I. Garrido, A. J. Garrido, M. Alberdi, M. Amundarain, and O. Barambones. „Performance of an ocean energy conversion system with DFIG sensorless control". en. In: *Mathematical Problems in Engineering* 2013 (2013), pp. 1–14. ISSN: 1024-123X, 1563-5147. DOI: 10.1155/2013/260514 (cit. on p. 67).

[Gar+15]   Aitor J. Garrido, Erlantz Otaola, Izaskun Garrido, et al. „Mathematical Modeling of Oscillating Water Columns Wave-Structure Interaction in Ocean Energy Plants". en. In: *Mathematical Problems in Engineering* 2015 (2015), pp. 1–11. ISSN: 1024-123X, 1563-5147. DOI: 10.1155/2015/727982 (cit. on p. 55).

[Gas+16]   José F. Gaspar, Mojtaba Kamarlouei, Ashank Sinha, et al. „Speed control of oil-hydraulic power take-off system for oscillating body type wave energy converters". In: *Renewable Energy* 97.January (2016), pp. 769–783. ISSN: 18790682. DOI: 10.1016/j.renene.2016.06.015 (cit. on p. 27).

[Gat+17]   L.M.C. Gato, A.A.D. Carrelhas, F.X Correia da Fonseca, and J.C.C. Henriques. *OPERA D3.2 - Turbine-generator set laboratory tests in variable unidirectional flow*. Tech. rep. June 2017 (cit. on pp. 33, 57, 58, 96, 97, 178).

[Gom+12]   R.P.F. Gomes, J.C.C. Henriques, L.M.C. Gato, and A.F.O. Falcão. „Hydrodynamic optimization of an axisymmetric floating oscillating water column for wave energy conversion". en. In: *Renewable Energy* 44 (Aug. 2012), pp. 328–339. ISSN: 09601481. DOI: 10.1016/j.renene.2012.01.105 (cit. on pp. 54, 78).

[GS12]   Kester Gunn and Clym Stock-Williams. „Quantifying the global wave power resource". en. In: *Renewable Energy* 44 (Aug. 2012), pp. 296–304. ISSN: 09601481. DOI: 10.1016/j.renene.2012.01.101 (cit. on p. 18).

[Guo+18]   Bingyong Guo, Ron J. Patton, Siya Jin, and Jianglin Lan. „Numerical and experimental studies of excitation force approximation for wave energy conversion". en. In: *Renewable Energy* (Mar. 2018). ISSN: 09601481. DOI: 10.1016/j.renene.2018.03.007 (cit. on p. 144).

[Hea07]   T. V. Heath. „The Development of a Turbo-Generation System for Application in OWC Breakwaters". In: *EWTEC 2007*. Porto, Portugal, 2007 (cit. on p. 53).

[Hea12]   T. V. Heath. „A review of oscillating water columns". en. In: *Philosophical Transactions of the Royal Society A: Mathematical, Physical and Engineering Sciences* 370.1959 (Jan. 2012), pp. 235–245. ISSN: 1364-503X, 1471-2962. DOI: 10.1098/rsta.2011.0164 (cit. on pp. 17, 31).

[Hen+12a]   J. C. C. Henriques, A. F. O. Falcão, R. P. F. Gomes, and L. M. C. Gato. „Latching control of an OWC spar-buoy wave energy converter in regular waves". In: *ASME 2012 31st International Conference on Ocean, Offshore and Arctic Engineering*. American Society of Mechanical Engineers, 2012, pp. 641–650 (cit. on pp. 64, 86).

[Hen+12b]   J.C.C. Henriques, M.F.P. Lopes, R.P.F. Gomes, L.M.C. Gato, and A.F.O. Falcão. „On the annual wave energy absorption by two-body heaving WECs with latching control". en. In: *Renewable Energy* 45 (Sept. 2012), pp. 31–40. ISSN: 09601481. DOI: 10.1016/j.renene.2012.01.102 (cit. on p. 54).

[Hen+14]   João C.C. Henriques, Juan C. Chong, António F.O. Falcão, and Rui P.F. Gomes. „Latching Control of a Floating Oscillating Water Column Wave Energy Converter in Irregular Waves". In: *ASME 2014 33rd International Conference on Ocean, Offshore and Arctic Engineering*. American Society of Mechanical Engineers, 2014 (cit. on p. 64).

[Hen+16a]   J.C.C. Henriques, L.M.C. Gato, A.F.O. Falcão, E. Robles, and F.-X. Faÿ. „Latching control of a floating oscillating-water-column wave energy converter". en. In: *Renewable Energy* 90 (May 2016), pp. 229–241. ISSN: 09601481. DOI: 10.1016/j.renene.2015.12.065 (cit. on pp. 41, 64, 86).

[Hen+16b]   J.C.C. Henriques, L.M.C. Gato, J.M. Lemos, R.P.F. Gomes, and A.F.O. Falcão. „Peak-power control of a grid-integrated oscillating water column wave energy converter". en. In: *Energy* 109 (Aug. 2016), pp. 378–390. ISSN: 03605442. DOI: 10.1016/j.energy.2016.04.098 (cit. on p. 67).

[Hen+16c]   J.C.C. Henriques, R.P.F. Gomes, L.M.C. Gato, et al. „Testing and control of a power take-off system for an oscillating-water-column wave energy converter". en. In: *Renewable Energy* 85 (Jan. 2016), pp. 714–724. ISSN: 09601481. DOI: 10.1016/j.renene.2015.07.015 (cit. on pp. 54, 67, 103, 113).

[Hen+16d] J.C.C. Henriques, J.C.C. Portillo, L.M.C. Gato, et al. „Design of oscillating water column wave energy converters with an application to self powered sensor buoys". en. In: *Energy* 112 (Oct. 2016), pp. 852–867. ISSN: 03605442. DOI: 10.1016/j.energy.2016.06.054 (cit. on pp. 40, 58).

[Hen06] Ross Henderson. „Design, simulation, and testing of a novel hydraulic power take-off system for the Pelamis wave energy converter". In: *Renewable Energy* 31.2 (2006), pp. 271–283. ISSN: 09601481. DOI: 10.1016/j.renene.2005.08.021 (cit. on p. 27).

[HFM11] Jorgen Hals, Johannes Falnes, and Torgeir Moan. „Constrained Optimal Control of a Heaving Buoy Wave-Energy Converter". en. In: *Journal of Offshore Mechanics and Arctic Engineering* 133.1 (2011), p. 011401. ISSN: 08927219. DOI: 10.1115/1.4001431 (cit. on p. 60).

[HG01] J.C.H. Henriques and L.M.C Gato. „Adaptive Control of the High-Speed Stop-Valve of the Azores Plant". In: Proceedings of the 4th European wave energy conference, Aalborg, Denmark. 2001, pp. 327–334. DOI: 10.13140/2.1.1544.0643 (cit. on p. 41).

[HKV13] Rico H. Hansen, Morten M. Kramer, and Enrique Vidal. „Discrete displacement hydraulic power take-off system for the wavestar wave energy converter". In: *Energies* 6.8 (2013), pp. 4001–4044. ISSN: 19961073. DOI: 10.3390/en6084001 (cit. on p. 27).

[HN86] R Hoskin and N.K Nichols. *Latching control for the point absorber wave power device*. 1986. URL: http://www.reading.ac.uk/web/FILES/maths/NA_Report_1-86.pdf (visited on Feb. 23, 2015) (cit. on p. 62).

[Hod+08] N. Hodgins, M. A. Mueller, W. K. Tease, and D. Staton. „Measurement and modelling of induction generator performance in an Oscillating Water Column wave energy converter". In: 4th IET Conference on Power Electronics, Machines and Drives. 2008, pp. 76–80 (cit. on p. 33).

[Hod10] N. Hodgins. „High Speed Electrical Power Takeoff for Oscillating Water Columns". PhD thesis. The University of Edinburgh, 2010 (cit. on p. 41).

[IEC08] IEC. *IEC standard 61400-21, Measurement and assessment of power quality characteristics of grid connected wind turbines*. Tech. rep. 2008 (cit. on p. 147).

[Int15] International Energy Agency. *World Energy Outlook - 2015 Special Report: Energy and Climate Change*. 2015 (cit. on p. 2).

[Int17]   International Energy Agency. *World energy outlook 2017*. Tech. rep. 2017 (cit. on p. 2).

[Isu18]   Isurki. *CNC4200-MT3 Captador de Nivel Cerámico 4-20 mA*. 2018. URL: http://www.isurki.com/images/fichas-tecnicas/nivel.pdf (visited on Mar. 30, 2018) (cit. on p. 162).

[JC07]   C. Josset and A.H. Clément. „A time-domain numerical simulator for oscillating water column wave power plants". en. In: *Renewable Energy* 32.8 (July 2007), pp. 1379–1402. ISSN: 09601481. DOI: 10.1016/j.renene.2006.04.016 (cit. on p. 53).

[Joh15]   Malcolm Johnson. *Oceanlinx*. 2015. URL: http://www.mountainculturegroup.com/for-whom-the-swell-tolls/ (visited on Feb. 1, 2017) (cit. on p. 34).

[JW01]   J.M.J. Journée and W.W. Massie. *Offshore Hydromechanics*. Delft University of Technology, Faculty of Civil Engineering and Geosciences, Delft University of Technology, Faculty of Mechanical, Maritime and Materials Engineering. Vol. 3. 2001 (cit. on pp. 20, 22, 23).

[KA14]   George C. Konstantopoulos and Antonio T. Alexandridis. „Full-Scale Modeling, Control, and Analysis of Grid-Connected Wind Turbine Induction Generators With Back-to-Back AC/DC/AC Converters". In: *IEEE Journal of Emerging and Selected Topics in Power Electronics* 2 (2014), pp. 739–748 (cit. on p. 45).

[Kel+14]   J. Kelly, D. O'Sullivan, W. M. D. Wright, R. Alcorn, and A. W. Lewis. „Challenges and lessons learned in the deployment of an offshore oscillating water column". In: *COMPEL: The International Journal for Computation and Mathematics in Electrical and Electronic Engineering* 33.5 (2014), pp. 1678–1704 (cit. on pp. 28, 32, 33, 67).

[Kih+]   Kazuyoshi Kihara, Yasushi Hosokawa, Kunihiko Kanaya, et al. „Design of a Middle Scale Wave Energy Convertor of a PW-OWC type for a Sea Test in Sakata Port". en. In: *the 9th International Workshop on Ship and Marine Hydrodynamics, 26-28 August 2015, Glasgow, UK*, p. 5 (cit. on pp. 33, 35).

[Kih+16]   Kazuyoshi Kihara, Kouichi Masuda, Tomoki Ikoma, et al. „Practical study on coupled analysis of the primary and the secondary wave energy conversion of PW OWC type device". In: *Journal of Japan Society of Civil Engineers, Ser. B3 (Ocean Engineering)* 72.2 (2016), pp. 802–807. DOI: 10.2208/jscejoe.72.I_802 (cit. on p. 33).

[Kof+04]   Jens Peter Kofoed, Peter Frigaard, Erik Friis-Madsen, and Hans
             Chr Sorensen. „Prototype testing of the wave energy converter
             wave dragon". en. In: *Proceedings of the 8th World Renewable
             Energy Congress: WREC VIII, Denver, USA*. 2004, p. 6 (cit. on
             p. 28).

[Kof15]   J.P. Kofoed. *Frequency-domain analysis, PhD short course on WEC
             modelling*. Tech. rep. Nantes, France, 2015 (cit. on pp. 21, 22).

[Kra13]   Peter Kracht. „Wave prediction and its implementation on control
             systems of wave-energy converters". In: *Fraunhofer IWES, EU
             MaRINet Infrastructure Access Report, Tech. Rep. MARINET-TA1-
             Adaptive WEC control* (2013) (cit. on p. 143).

[Kuo+17]   Yu-Shu Kuo, Chih-Yin Chung, Shih-Chun Hsiao, and Yu-Kai Wang.
             „Hydrodynamic characteristics of Oscillating Water Column cais-
             son breakwaters". In: *Renewable Energy* 103 (2017), pp. 439–
             447. ISSN: 09601481. DOI: 10.1016/j.renene.2016.11.028
             (cit. on p. 84).

[Lai17]   George Laird. *HydroAir Power Take Off System*. en. Feb. 2017.
             URL: https://www.energy.gov/sites/prod/files/2017/
             04/f34/hydroair-power-take-off-system.pdf (visited on
             Sept. 15, 2017) (cit. on pp. 39, 40).

[Lei+08]   Mats Leijon, Cecilia Boström, Oskar Danielsson, et al. „Wave En-
             ergy from the North Sea: Experiences from the Lysekil Research
             Site". en. In: *Surveys in Geophysics* 29.3 (May 2008), pp. 221–
             240. ISSN: 0169-3298, 1573-0956. DOI: 10.1007/s10712-008-
             9047-x (cit. on p. 29).

[Li+18]   Liang Li, Zhiming Yuan, Yan Gao, and Xinshu Zhang. „Wave
             force prediction effect on the energy absorption of a wave energy
             converter with real-time control". en. In: *IEEE Transactions on
             Sustainable Energy* (2018), pp. 1–1. ISSN: 1949-3029, 1949-3037.
             DOI: 10.1109/TSTE.2018.2841886 (cit. on p. 143).

[LK11]   John Lavelle and Jens Peter Kofoed. *Power production analysis
             of the oe buoy wec for the cores project*. Tech. rep. Department of
             Civil Engineering, Aalborg University, 2011 (cit. on pp. 28, 32,
             33).

[Lop+09]   M.F.P. Lopes, J. Hals, R.P.F. Gomes, et al. „Experimental and
             numerical investigation of non-predictive phase-control strate-
             gies for a point-absorbing wave energy converter". en. In: *Ocean
             Engineering* 36.5 (Apr. 2009), pp. 386–402. ISSN: 00298018. DOI:
             10.1016/j.oceaneng.2009.01.015 (cit. on pp. 63, 64).

[Lóp+13]   Iraide López, Jon Andreu, Salvador Ceballos, Iñigo Martínez de Alegría, and Iñigo Kortabarria. „Review of wave energy technologies and the necessary power-equipment". en. In: *Renewable and Sustainable Energy Reviews* 27 (Nov. 2013), pp. 413–434. ISSN: 13640321. DOI: 10.1016/j.rser.2013.07.009 (cit. on pp. 38, 41).

[MA13]   Giovanni Malara and Felice Arena. „Analytical modelling of an U-Oscillating Water Column and performance in random waves". en. In: *Renewable Energy* 60 (Dec. 2013), pp. 116–126. ISSN: 09601481. DOI: 10.1016/j.renene.2013.04.016 (cit. on p. 33).

[MA19]   Giovanni Malara and Felice Arena. „Response of U-Oscillating Water Column arrays: semi-analytical approach and numerical results". en. In: *Renewable Energy* 138 (Aug. 2019), pp. 1152–1165. ISSN: 09601481. DOI: 10.1016/j.renene.2019.02.018 (cit. on p. 33).

[mar17]   marineenergy.biz. "Ocean Energy ready for 500kW wave device build-out". 2017. URL: https://marineenergy.biz/2017/10/18/ocean-energy-ready-for-500kw-wave-device-build-out/ (visited on Oct. 18, 2018) (cit. on p. 33).

[Mec13]   Mecometer. *Electricity - installed generating capacity - by country.* 2013. URL: http://mecometer.com/topic/electricity-installed-generating-capacity/ (visited on May 3, 2018) (cit. on p. 18).

[Meh86]   Even Mehlum. „TAPCHAN". In: *Hydrodynamics of Ocean Wave-Energy Utilization: IUTAM Symposium Lisbon/Portugal 1985*. Ed. by David V. Evans and Antonio F. O. de Falcão. Berlin, Heidelberg: Springer Berlin Heidelberg, 1986, pp. 51–55. ISBN: 978-3-642-82666-5. DOI: 10.1007/978-3-642-82666-5_3 (cit. on p. 28).

[Mig18]   Borja de Miguel. „Operating experience of Marmok-A-5 owc wave energy converter at BiMEP". In: International Conference on Ocean Energy (ICOE). Cherbourg, France, June 2018 (cit. on pp. 28, 32, 33).

[Mon+13]   Kieran Monk, Daniel Conley, Miguel Lopes, and Qingping Zou. „Pneumatic Power Regulation by Wave Forecasting and Real - Time Relief Valve Control for an OWC". In: *10th European Wave and Tidal Energy Conference*. Aalborg, Denmark, 2013 (cit. on pp. 32, 33, 41, 67).

[Mon15]   Kieran Monk. „Simulations and Field Test s of Pneumatic Power Regulation by Valve Control Using Short-term Forecasting at the Pico OWC". In: *Proceedings of 11th EWTEC Conference*. Nantes, France, 2015 (cit. on p. 33).

[Mor+10]   Gunnar Mork, Stephen Barstow, Alina Kabuth, and M. Teresa Pontes. „Assessing the global wave energy potential". In: *ASME 2010 29th International Conference on Ocean, Offshore and Arctic Engineering*. American Society of Mechanical Engineers, 2010, pp. 447–454 (cit. on p. 59).

[Mur+12]   D. B. Murray, J. G. Hayes, D. L. O'Sullivan, and M. G. Egan. „Supercapacitor Testing for Power Smoothing in a Variable Speed Offshore Wave Energy Converter". In: *IEEE Journal of Oceanic Engineering* 37.2 (Apr. 2012), pp. 301–308. ISSN: 0364-9059, 1558-1691. DOI: 10.1109/JOE.2012.2188157 (cit. on p. 68).

[Mur13]   D. B. Murray. „Energy storage systems for wave energy converters and micro-grid". PhD thesis. University College Cork, 2013 (cit. on p. 4).

[MWL18]   Kieran Monk, Victor Winands, and Miguel Lopes. „Chamber pressure skewness corrections using a passive relief valve system at the Pico oscillating water column wave energy plant". en. In: *Renewable Energy* (Apr. 2018). ISSN: 09601481. DOI: 10.1016/j.renene.2018.04.037 (cit. on pp. 32, 33, 53).

[Nan19]   Ecole Centrale de Nantes. *NEMOH-Presentation*. 2019. URL: https://lheea.ec-nantes.fr/logiciels-et-brevets/nemoh-presentation-192863.kjsp (visited on Dec. 12, 2019) (cit. on p. 49).

[Nic96]   N.K Nichols. *Optimal strategies for the control of wave energy converters with various PTO mechanisms*. 1996 (cit. on p. 62).

[NM10]   K. E. Nielsen and M. Molinas. „Superconducting Magnetic Energy Storage (SMES) in power systems with renewable energy sources". In: *2010 IEEE International Symposium on Industrial Electronics*. July 2010, pp. 2487–2492. DOI: 10.1109/ISIE.2010.5637892 (cit. on p. 68).

[NT18]   Hoai-Nam Nguyen and Paolino Tona. „Short-term wave force prediction for wave energy converter control". en. In: *Control Engineering Practice* 75 (June 2018), pp. 26–37. ISSN: 09670661. DOI: 10.1016/j.conengprac.2018.03.007 (cit. on p. 143).

[Nun+11]   Guilherme Nunes, Duarte Valério, Pedro Beirão, and José Sá da Costa. „Modelling and control of a wave energy converter". en. In: *Renewable Energy* 36.7 (July 2011), pp. 1913–1921. ISSN: 09601481. DOI: 10.1016/j.renene.2010.12.018 (cit. on p. 63).

[OA17]   Emre Ozkop and Ismail H. Altas. „Control, power and electrical components in wave energy conversion systems: A review of the technologies". en. In: *Renewable and Sustainable Energy Reviews* 67 (Jan. 2017), pp. 106–115. ISSN: 13640321. DOI: 10.1016/j.rser.2016.09.012 (cit. on p. 61).

[Oce16]   Ocean Energy Forum. *Ocean Energy Strategic Roadmap*. Tech. rep. 2016 (cit. on p. 2).

[Oce19]   Oceantec. *Oceantec*. 2019. URL: http://www.oceantecenergy.com/ (visited on Dec. 1, 2019) (cit. on p. 4).

[OL11]   Dara L. O'Sullivan and Anthony W. Lewis. „Generator Selection and Comparative Performance in Offshore Oscillating Water Column Ocean Wave Energy Converters". In: *IEEE Transactions on Energy Conversion* 26.2 (June 2011), pp. 603–614. ISSN: 0885-8969, 1558-0059. DOI: 10.1109/TEC.2010.2093527 (cit. on pp. 41, 57).

[OLD13]   M. O'Connor, T. Lewis, and G. Dalton. „Techno-economic performance of the Pelamis P1 and Wavestar at different ratings and various locations in Europe". In: *Renewable Energy* 50 (Feb. 2013), pp. 889–900. ISSN: 09601481. DOI: 10.1016/j.renene.2012.08.009 (cit. on p. 27).

[OPE19]   OPERA. *H2020 OPERA Project*. 2019. URL: http://opera-h2020.eu/ (visited on Oct. 19, 2019) (cit. on p. 4).

[Pér+13]   Jesús María Pinar Pérez, Fausto Pedro García Márquez, Andrew Tobias, and Mayorkinos Papaelias. „Wind turbine reliability analysis". In: *Renewable and Sustainable Energy Reviews* 23 (2013), pp. 463–472. ISSN: 1364-0321. DOI: https://doi.org/10.1016/j.rser.2013.03.018 (cit. on p. 149).

[Per+15]   Bruno Pereiras, Iván López, Francisco Castro, and Gregorio Iglesias. „Non-dimensional analysis for matching an impulse turbine to an OWC (oscillating water column) with an optimum energy transfer". en. In: *Energy* 87 (July 2015), pp. 481–489. ISSN: 03605442. DOI: 10.1016/j.energy.2015.05.018 (cit. on p. 56).

[PF07]   Tristan Perez and Thor Inge Fossen. „Kinematic Models for Ma-
           noeuvring and Seakeeping of Marine Vessels". en. In: *Modeling,
           Identification and Control: A Norwegian Research Bulletin* 28.1
           (2007), pp. 19–30. ISSN: 0332-7353, 1890-1328. DOI: 10.4173/
           mic.2007.1.3 (cit. on pp. 50, 78).

[PF09]   Tristan Perez and Thor I. Fossen. „A Matlab toolbox for paramet-
           ric identification of radiation-force models of ships and offshore
           structures". In: *Modeling, Identification and Control* 30.1 (2009),
           pp. 1–15. DOI: 10.4173/mic.2009.1.1 (cit. on p. 81).

[PG16]   G Parisella and T P Gourlay. *Comparison of open-source code
           Nemoh with Wamit for cargo ship motions in shallow water*. en.
           Tech. rep. 2016, p. 39 (cit. on p. 49).

[PK17]   Arthur Pecher and Jens Peter Kofoed. *Handbook of Ocean Wave
           Energy*. English. OCLC: 950953302. Springer Verlag, 2017. ISBN:
           978-3-319-39888-4 (cit. on p. 27).

[Quo16]   Quoceant. *WES knowledge Capture - Pelamis - Power Take-Off:
           Non-Confidential Summary Report*. Tech. rep. Apr. 2016 (cit. on
           p. 27).

[R P95]   R. Prony. „ESSAI EXPÉRIMENTAL ET ANALYTIQUE Sur les lois
           de la Dilatabilité des fluides élastiques et sur celles de la Force
           expansive de la vapeur de l'eau et de la vapeur de l'alkool, à
           différentes températures". In: *Journal de l'École Polytechnique
           Floréal et Plairial* 1.22 (1795), pp. 24–76 (cit. on p. 50).

[Ram17]   Andreas Ramberg. „Ocean waves estimation - an Artificial intelli-
           gence approach". en. PhD thesis. Mälardalen University School
           of Innovation Design and Engineering Västerås, Sweden, 2017
           (cit. on p. 23).

[Ras16]   Lars Stylsvig Rasmussen. „LORC Nacelle Testing Realistic indoor
           nacelle testing using grid emulation". en. In: *3 rd Workshop grid
           simulator testing*. Tallahassee, FL, 2016, p. 22 (cit. on p. 149).

[RB96]   S. Raghunathan and W. C. Beattie. „Aerodynamic Performance
           of ContraRotating Wells Turbine for Wave Energy Conversion".
           In: *Proceedings of the Institution of Mechanical Engineers, Part A:
           Journal of Power and Energy* 210.6 (1996), pp. 431–447. DOI:
           10.1243/PIME_PROC_1996_210_071_02. eprint: https:
           //doi.org/10.1243/PIME_PROC_1996_210_071_02 (cit. on
           p. 37).

[RBF14a]   John V. Ringwood, Giorgio Bacelli, and Francesco Fusco. „Control, forecasting and optimisation for wave energy conversion". In: *World Congress*. Vol. 19. 2014, pp. 7678–7689 (cit. on p. 59).

[RBF14b]   John V. Ringwood, Giorgio Bacelli, and Francesco Fusco. „Energy-Maximizing Control of Wave-Energy Converters: The Development of Control System Technology to Optimize Their Operation". In: *IEEE Control Systems* 34.5 (Oct. 2014), pp. 30–55. ISSN: 1066-033X. DOI: 10.1109/MCS.2014.2333253 (cit. on p. 61).

[Rea+11]   J. Rea, J. Kelly, R. Alcorn, and D. O'Sullivan. „Development and operation of a power take off rig for ocean energy research and testing". In: *Eur. Wave Tidal Energy Conf., Southampton, UK*. 2011 (cit. on p. 33).

[Rey86]   Osborne Reynolds. „XXVIII. On the flow of gases". In: *The London, Edinburgh, and Dublin Philosophical Magazine and Journal of Science* 21.130 (1886), pp. 185–199 (cit. on p. 152).

[Rob+19]   Eider Robles, Marta Haro-Larrode, Maider Santos-Mugica, Agurtzane Etxegarai, and Elisabetta Tedeschi. „Comparative analysis of European grid codes relevant to offshore renewable energy installations". In: *Renewable and Sustainable Energy Reviews* 102 (2019), pp. 171–185. ISSN: 1364-0321. DOI: https://doi.org/10.1016/j.rser.2018.12.002 (cit. on pp. 4, 68).

[Sal74]   S. H. Salter. „Wave power". en. In: *Nature* 249.5459 (June 1974), pp. 720–724. ISSN: 0028-0836, 1476-4687. DOI: 10.1038/249720a0 (cit. on p. 48).

[SF14]   Ryan F. Schkoda and Charles Fox. „Integration of mechanical and electrical hardware for testing full scale wind turbine nacelles". In: *Power Systems Conference (PSC), 2014 Clemson University*. IEEE, 2014, pp. 1–8 (cit. on p. 149).

[She19]   Wanan Sheng. „Power performance of BBDB OWC wave energy converters". In: *Renewable Energy* 132 (2019), pp. 709–722. ISSN: 09601481. DOI: 10.1016/j.renene.2018.07.111 (cit. on p. 32).

[Shi+17]   Kenichiro Shimosako, Taro Arikawa, Masahide Takeda, et al. „Model experiment and field test of PW-OWC type wave power extracting breakwater". en. In: *Coastal Engineering Proceedings* 1.35 (June 2017), p. 2. ISSN: 2156-1028, 0589-087X. DOI: 10.9753/icce.v35.structures.2 (cit. on p. 33).

[Sim+18]   I. Simonetti, L. Cappietti, H. Elsafti, and H. Oumeraci. „Evaluation of air compressibility effects on the performance of fixed OWC wave energy converters using CFD modelling". In: *Renewable Energy* 119 (2018), pp. 741–753. ISSN: 09601481. DOI: 10.1016/j.renene.2017.12.027 (cit. on p. 84).

[SRA14]   Wanan Sheng, Alcorn Ray, and Lewis Anthony. „Hydrodynamics of OWC wave energy converters". en. In: *the 1st International Conference on Renewable Energies Offshore (RENEW2014), Lisbon, Portugal, 24-26 November 2014*. Nov. 2014. DOI: 10.1201/b18973 (cit. on p. 78).

[ST06]   Toshiaki Setoguchi and Manabu Takao. „Current status of self rectifying air turbines for wave energy conversion". en. In: *Energy Conversion and Management* 47.15-16 (Sept. 2006), pp. 2382–2396. ISSN: 01968904. DOI: 10.1016/j.enconman.2005.11.013 (cit. on p. 56).

[ST96]   Stephen Salter and Jamie Taylor. „The design of a high-speed stop valve for oscillating water columns". In: Proceedings of the 2nd European Wave Energy Conference. Vol. 3. Jan. 1996, pp. 195–202 (cit. on p. 41).

[Ste07]   AK Steel. *'Selection of electrical steels for Magnetic Cores'*. 2007. URL: https://www.brown.edu/Departments/Engineering/Courses/ENGN1931F/mag_cores_dataAKSteel-very%5C%20good.pdf (visited on Aug. 16, 2018) (cit. on p. 93).

[TD03]   T. Finningan and D. Auld. „Model Testing of a Variable -Pitch Aerodynamic Turbine". English. In: *The proceedings of the thirteenth (2003) international offshore and polar engineering conference.* 2003 (cit. on pp. 33, 38, 39).

[Tec]   Axys Technologies. *TRIAXYS Directional Wave Buoy*. URL: https://axystechnologies.com/products/triaxys-directional-wave-buoy/?open_cat=40 (visited on Jan. 5, 2017) (cit. on pp. 143, 174).

[Ted+11a] E. Tedeschi, M. Santos, P. Ricci, M. Molinas, and J. L. Villate. „Control strategies for the grid integration of wave energy converters at the biscay marine energy platform". In: *Proceedings of the European Wave and Tidal Energy Conference,(EWTEC2011), Southampton, UK*. 2011, pp. 5–9 (cit. on p. 69).

[Ted+11b] Elisabetta Tedeschi, Matteo Carraro, Marta Molinas, and Paolo Mattavelli. „Effect of Control Strategies and Power Take-Off Efficiency on the Power Capture From Sea Waves". In: *IEEE Transactions on Energy Conversion* 26.4 (Dec. 2011), pp. 1088–1098. ISSN: 0885-8969. DOI: 10.1109/TEC.2011.2164798 (cit. on p. 44).

[Ted07] James Tedd. „Testing, analysis and control of the wave dragon wave energy converter". PhD thesis. Aalborg University, Department of Civil Engineering, 2007 (cit. on p. 28).

[The05] The Carbon Trust. *Marine Energy Challenge - Oscillating Water Column Wave Energy Converter Evaluation Report*. Tech. rep. 2005 (cit. on pp. 32–34).

[Thi+11] F. Thiebaut, P. O'Sullivan, S. Ceballos, et al. „Testing of a floating OWC device with movable guide vane impulse turbine power take-off". In: *Proceedings of the 9th European Wave and Tidal Energy Conference, Southampton, UK*. 2011 (cit. on pp. 28, 67, 103, 113).

[Tho95] T W Thorpe. *An assessment of the ART OSPREY wave energy device. Final report*. Dec. 1995 (cit. on p. 33).

[TLH07] W. K. Tease, J. Lees, and A. Hall. „Advances in oscillating water column air turbine development". In: Proceedings of the 7th European Wave and Tidal Energy Conference, Porto, Portugal. 2007 (cit. on pp. 32, 53, 56, 58, 96, 97).

[TM10] E. Tedeschi and M. Molinas. „Impact of control strategies on the rating of electric power take off for Wave Energy conversion". en. In: *2010 IEEE International Symposium on Industrial Electronics*. Bari, Italy: IEEE, July 2010, pp. 2406–2411. ISBN: 978-1-4244-6390-9. DOI: 10.1109/ISIE.2010.5637522 (cit. on p. 57).

[TM12a] Elisabetta Tedeschi and Marta Molinas. „Tunable Control Strategy for Wave Energy Converters With Limited Power Takeoff Rating". en. In: *IEEE Transactions on Industrial Electronics* 59.10 (Oct. 2012), pp. 3838–3846. ISSN: 0278-0046, 1557-9948. DOI: 10.1109/TIE.2011.2181131 (cit. on p. 57).

[TM12b] Elisabetta Tedeschi and Marta Molinas. „Tunable Control Strategy for Wave Energy Converters With Limited Power Takeoff Rating". In: *IEEE Transactions on Industrial Electronics* 59.10 (Oct. 2012), pp. 3838–3846. ISSN: 0278-0046, 1557-9948. DOI: 10.1109/TIE.2011.2181131 (cit. on p. 128).

[TML10]   Y. Torre-Enciso, J. Marques, and L. I. Lopez de Aguileta. „Mutriku: Lessons learnt". In: *Proceedings of the 3rd International Conference on Ocean Energy, Bilbao, Spain*. 2010 (cit. on pp. 28, 33, 73).

[Tor+09a]   Y Torre-Enciso, I Ortubia, L I de Aguileta, et al. „Mutriku wave power plant: from the thinking out to the reality". In: *Proc 8th European Wave Tidal Energy Conf, Uppsala, Sweden*. 2009, pp. 319–329 (cit. on pp. 33, 37, 41).

[Tor+09b]   Y. Torre-Enciso, I. Ortubia, L. I. Lopez de Aguileta, and J. Marques. „Mutriku Wave Power Plant: from the thinking out to the reality". In: *Proceedings of the 8th European Wave and Tidal Energy Conference*. 2009, pp. 319–329 (cit. on p. 32).

[VGA14]   Sadegh Ghani Varzaneh, G.B. Gharehpetian, and Mehrdad Abedi. „Output power smoothing of variable speed wind farms using rotor-inertia". en. In: *Electric Power Systems Research* 116 (Nov. 2014), pp. 208–217. ISSN: 03787796. DOI: 10.1016/j.epsr.2014.06.006 (cit. on p. 68).

[VSR15]   M. Vieira, A. Sarmento, and L. Reis. „Failure analysis of the guide vanes of the Pico Wave Power Plant Wells turbine". en. In: *Engineering Failure Analysis* (Apr. 2015). ISSN: 13506307. DOI: 10.1016/j.engfailanal.2015.04.004 (cit. on pp. 28, 33).

[WAM16]   WAMIT. *User Manual Version 7.2*. 2016. URL: http://www.wamit.com/manualupdate/v72_manual.pdf (visited on Apr. 15, 2018) (cit. on pp. 49, 73, 75).

[Wav17]   Wave Energy Scotland. *Control Systems Competition Specification and Guidance Document Entry to Stage 1*. 2017 (cit. on p. 3).

[Wel+]   S D Weller, D Parish, T Gordelier, et al. „Open sea OWC motions and mooring loads monitoring at BiMEP". In: *Proceedings of the 12th European Wave and Tidal Energy Conference (EWTEC2017), Cork, Ireland* (cit. on p. 32).

[WF12]   T. Whittaker and M. Folley. „Nearshore oscillating wave surge converters and the development of Oyster". In: *Philosophical Transactions of the Royal Society A: Mathematical, Physical and Engineering Sciences* 370.1959 (2012), pp. 345–364. ISSN: 1364-503X. DOI: 10.1098/rsta.2011.0152 (cit. on p. 28).

[Whi+02]   T. J. T. Whittaker, W. Beattie, M. Folley, et al. *The LIMPET wave power project: the first years of operation*. Tech. rep. 2002 (cit. on pp. 28, 33, 37, 52).

[WL13]   Dong Wang and Kaiyuan Lu. „Energy Storage Systems, SDWED D3.1". In: (2013) (cit. on p. 93).

RESUMEN

Durante las últimas décadas, un creciente interés en la extracción de energía de fuentes renovables fomenta las actividades de Investigación y Desarrollo de tecnologías innovadoras para producir energía limpia de manera sostenible, sin emisiones de CO2. Hoy en día, las energías eólica y solar son las industrias más maduras y su participación en la producción de energía está aumentando rápidamente. El Escenario Bridge del informe de la Agencia Internacional de Energía predice un aumento en la producción mundial de electricidad de estas fuentes del 4 al 14% entre 2017 y 2030.

Las energías renovables marinas aprovechan la energía disponible en los mares y todavía están en sus primeras etapas de desarrollo. Entre ellos, la eólica flotante, la mareomotriz, la undimotriz, la energía térmica oceánica y el gradiente de salinidad son formas innovadoras de producir electricidad a partir de los océanos. Se dice que la energía oceánica, la que se centra principalmente en la energía de las olas y las mareas, tiene un potencial de mercado global de 337 GW de capacidad instalada en 2050 y alimentaría el 10% del consumo de energía de Europa.

Para ser asequible, el sector de la energía de las olas requiere innovaciones y avances en varias disciplinas para reducir el *Levelised Cost Of Energy* (LCOE). Los principales desafíos que enfrentan los desarrolladores están relacionados con el entorno hostil donde se implementarán los dispositivos. De hecho, un *Wave Energy Converter* (WEC) tiene que sobrevivir a las tormentas, su estructura está sujeta a corrosión y *biofouling* y las actividades de operación y mantenimiento son procesos complejos y costosos en instalaciones en alta mar. Hay que superar muchas barreras tecnológicas para aumentar la fiabilidad de los WECs y reducir los riesgos relacionados con su desarrollo. Los altos costes relacionados con el desarrollo de tales tecnologías y el alto riesgo percibido tienden a retrasar la aparición de un mercado sostenible

para la conversión de energía de las olas. Las instituciones públicas apoyan la idea de que, para alcanzar el mercado, los desarrolladores de tecnología deben seguir un proceso de etapa altamente competitivo para reducir los costes de producción.

Entre los varios conceptos existentes, el basado en una columna de agua oscilante, *Oscillating Water Column* (OWC), parece proporcionar una solución bien equilibrada con el objetivo de reducir la complejidad y, por lo tanto, el coste de un dispositivo. Su estructura puede ser costera unida a un acantilado o un rompeolas, cerca de la costa en aguas poco profundas, o incluso flotando integrada en una boya. El OWC se basa en un principio simple: en una estructura abierta en ambos extremos, el movimiento de una ola entrante por donde pasa el flujo de agua de mar en el fondo de la estructura, crea una oscilación del nivel del agua en una cámara de aire y, por lo tanto, una diferencia de presión que convierte la energía de las olas en energía neumática. En la parte superior de la cámara, el aire fluye a través de una turbina que convierte la energía neumática en una mecánica de rotación que luego se convierte en electricidad gracias a un generador eléctrico convencional. Finalmente, el convertidor de potencia asegura el control de la conversión de potencia y la compatibilidad de la red.

El campo de control aplicado a los WEC ofrece muchas ventajas. La primera, y obvia, es la optimización de la producción de energía, que aumenta directamente los ingresos al vender una mayor cantidad de energía. Una estrategia de control eficiente permite la conversión óptima de la energía disponible y aprovecha todo el potencial de la energía de las olas. Además, el control desempeña un papel fundamental en la mejora de la fiabilidad del dispositivo y alarga la vida útil de los componentes del tren de potencia.

Algunas plantas de demostración se han construido y probado en un entorno marino real, y solo unos pocos prototipos están realmente funcionando durante varios años. Todavía se debe investigar en diversas áreas para convertir los demostradores en dispositivos comerciales que sean rentables, eficientes en términos de energía, fiables y que puedan soportar tormentas de invierno. La provincia del País Vasco en España ofrece oportunidades reales para el desarrollo de dicha tecnología. El EVE (Ente Vasco de la Energía), la institución pública local de energía, administra la Plataforma Vizcaína de Energía Marina, *Biscay Marine Energy Plateform* (BiMEP), y sus dos sitios de prueba de la Costa Vasca: la planta de Mutriku situada en el nuevo dique

del puerto, y el área de prueba en alta mar frente a Armintza. La planta de energía de las olas de Mutriku está alimentando la red desde 2011 y, cuando se puso en servicio, fue el primer WEC en Europa en conectarse a la red. Desde entonces ha generado más de 2 GWh de electricidad limpia. Este demostrador tiene una capacidad máxima de 300 kW y está compuesto por 16 cámaras de aire equipadas con turbinas Wells. El sitio de ensayos en mar de Armintza se inauguró en julio de 2015. Es un centro de pruebas en mar abierto con toda la infraestructura (4 cables de exportación de 5 MW cada uno) y servicios (vigilancia 24/7) para que los desarrolladores de dispositivos marinos renovables puedan probar prototipos a gran escala y avanzar en el *Technology Readiness Level* (TRL) de sus soluciones. Además, Oceantec, creado por TECNALIA e Iberdrola y ahora parte de la consultora de ingeniería IDOM, está desarrollando una boya flotante tipo spar llamada Marmok. La versión Marmok-A-5 es una boya de escala reducida de diámetro y se instaló durante un año y medio entre octubre de 2016 y julio de 2018 y se volvió a instalar en septiembre de 2018 en el marco del proyecto H2020 OPERA financiado por la Comisión Europea y coordinado por TECNALIA. El objetivo de este proyecto es dividir entre 2 el coste de las tecnologías de energía de las olas mediante la integración de cuatro innovaciones principales al MarmokA-5. Antes de la instalación en la boya, dos de ellas se probaron y validaron en la planta Mutriku OWC.

El objetivo general de esta tesis es optimizar la producción de energía y reducir el LCOE, el coste de la producción de energía, mediante el dimensionamiento apropiado de los componentes y estrategias de control avanzadas. Esto también es necesario para mejorar la fiabilidad y robustez para asegurar la operación del dispositivo bajo cualquier condición de mar. Su objetivo es mejorar la precisión de los modelos numéricos*Wave-to-Wire* (W2W) de los sistemas OWC y, especialmente, enfocarse en el lado del *Power Take-Off* (PTO), desde la cámara de aire hasta la conversión de energía eléctrica. Algunas herramientas que cubren ciertos aspectos ya están disponibles en la literatura para estudiar el comportamiento de tales sistemas en el océano, pero los efectos de la compresibilidad del aire pueden mejorarse y los componentes eléctricos a menudo se dejan de lado. El trabajo desarrollado cubre toda la cadena de conversión de energía al integrar el rendimiento y las limitaciones de cada componente (turbina, generador y electrónica de potencia) teniendo en cuenta el objetivo general de proponer estrategias de control avanzadas que tengan en cuenta sus diferentes limitaciones. El W2W proporciona información útil sobre la producción de energía detallada con preocupación

sobre la calidad de la energía enviada a la red. Además, el campo de control para WEC hoy en día se entiende bastante bien, pero la falta de aplicaciones prácticas es lamentable.

En cuanto a las contribuciones de este trabajo, se propone una metodología para desarrollar modelos numéricos W2W teniendo en cuenta la dinámica de toda la cadena de conversión de energía: primero lineal en el dominio de frecuencia; y luego en el dominio del tiempo que se utiliza para incluir no linealidades de la cámara de aire y el sistema de la PTO. La metodología se aplica para dos dispositivos:

- Una planta fija de OWC integrada en un dique con el ejemplo de la planta OWC de Mutriku;
- Una boya OWC flotante tipo spar.

Los modelos incluyen las diferentes etapas de conversión de energía, desde las olas hasta la energía eléctrica, incluyendo todos los componentes de la PTO. Las pruebas de campo en la planta de Mutriku realizadas durante el proyecto OPERA ofrecieron la posibilidad de mejorar la precisión del modelo W2W basado en datos operativos. Se ajustó el modelo hidrodinámico y se mejoró el modelo de compresibilidad del aire para la cámara de aire utilizando estos datos experimentales. Las variables de proceso obtenidas por este modelo muestran una mejor coincidencia con los datos operativos medidos en la planta en comparación con los modelos numéricos de última generación. Además, la conversión de energía eléctrica está mejor representada por medio de un nuevo modelo de pérdidas de generador que también incluye la operación en diferentes regiones y el efecto del debilitamiento del flujo cuando se opera en rangos más allá de los valores nominales.

El W2W del OWC fijo se utiliza para comparar diferentes tecnologías de turbinas junto con una estrategia simple de control de velocidad. La herramienta permite la optimización del tamaño de los componentes de la PTO, como el tipo de turbina, su diámetro y el tamaño del generador. El estudio incluye la comparación de tres turbinas Wells y tres de impulso. El diámetro óptimo de la turbina se obtiene para cada turbina y esto permite seleccionar con mayor precisión la potencia nominal del generador. Los resultados mostraron que la turbina de dos planos Wells instalada en Mutriku no era necesariamente la mejor opción al analizar la potencia de salida mecánica promedio. Los resultados de este análisis están estrechamente vinculados con

las curvas características de la turbina utilizadas en la optimización. Algunas curvas se pueden obtener teóricamente y pueden sesgar los resultados, mientras que otras son más precisas, ya que se obtuvieron por experimentación. No obstante, esta metodología puede ser útil para seleccionar los componentes óptimos de la PTO, si se utilizan curvas características fiables de la turbina.

Otra contribución relevante de esta tesis se centra en el desarrollo, la simulación y la comparación de varias estrategias de control de velocidad de la turbina entre sí y con la turbina biradial utilizando el modelo W2W de Mutriku en varios estados marítimos. Este marco común permite una comparación rápida y basada en resultados entre estos algoritmos que son:

- Un control de velocidad fijo usando un controlador PI;
- Varias versiones de controladores de velocidad variable basados en un enfoque de *Torque Law* que utilizan parámetros de control sintonizados;
- Uno que combina los beneficios de la velocidad fija y variable y utiliza la desviación estándar de presión para establecer la velocidad de referencia, seguido por el controlador PI;
- Varias versiones de un controlador predictivo de horizonte de retroceso no lineal que utiliza el enfoque de *Torque Law* de la ley de control de velocidad variable.

Los resultados obtenidos son la base para una evaluación de eficiencia y fiabilidad que resalta las ventajas y desventajas de cada uno. Como resumen, cuando el controlador tiende a maximizar la potencia de salida, generalmente sobrecarga el generador reduciendo de hecho su fiabilidad. Se destaca que los controladores que funcionan mejor tienen en cuenta de manera equilibrada la eficiencia tanto de la turbina como del generador. Las restricciones adicionales impuestas en una versión del algoritmo predictivo mostraron resultados bastante equilibrados aliando un buen rendimiento y una operación más fiable. Un controlador predictivo no lineal aplicado a una estrategia de control llamada *latching* en el OWC flotante completa el análisis. El objetivo del *latching* es inmovilizar la estructura de un WEC hasta que llegue una ola y liberarla para que la fuerza de la ola sea en fase con la velocidad del cuerpo. Así se consigue un fenómeno de resonancia y un aprovechamiento mayor de energía. En este estudio, el efecto de *latching* se logra mediante la implementación de una válvula de accionamiento de alta velocidad ubicada en serie con la turbina biradial. Los resultados de la simulación se obtienen

con y sin aplicar *latching,* con la misma ley de control de velocidad de la turbina. Esa estrategia aumenta la potencia mecánica promedio en un 20 a 30%, dependiendo del estado del mar, y entre un 10 y un 25% en la producción de energía eléctrica promedio.

La última contribución de la tesis aborda los problemas relacionados con la implementación en tiempo real de controladores y especialmente el control predictivo no lineal, siendo el primero de su tipo en ser probado en una plataforma de prueba en las instalaciones de Mutriku y en el Marmok-A-5. Los desafíos relacionados con la estimación de la predicción de la fuerza de las olas se superan utilizando mediciones en tiempo real de la elevación de las olas por delante de las plantas. Otro problema relacionado con el cálculo en tiempo real de la optimización predictiva también se resuelve sin penalizar la precisión de la solución óptima. Al comparar los resultados del controlador predictivo en Mutriku con una Torque Law simple, se obtiene un aumento en la producción de energía de alrededor del 30%. Esto se debe al hecho de que la ley predictiva incluye la eficiencia general de la PTO durante la optimización en tiempo real, mientras que la otra ley de control se basa en una optimización 'offline', donde el objetivo es establecer solo la turbina en su mejor punto de eficiencia. Finalmente, el algoritmo predictivo se implementa con éxito en la boya Marmok cuando estaba fondeada en BiMEP, siendo el primero de su tipo en operar un WEC en condiciones reales del mar.

Declaration

I hereby declare that this thesis is my own work and effort and that is not been submitted anywhere for any award. Where other sources of information have been used, they have been acknowledged.

Bilbao, May, 2020

François-Xavier Faÿ